

Final Design Review Report

Partner Beamline NYX

19-ID

NYSBC Microdiffraction Beamline

Beamline Development Team Leadership

Joseph P. Lidestri
NYSBC Project Manager for NYX

Wayne A. Hendrickson
NYSBC Project Director for NYX

Howard Robinson
NSLS-II Project Manager for NYX

Andrew Broadbent
NSLS-II Partner Beamlines Portfolio Manager

Table of Contents

1. EXECUTIVE SUMMARY.....	4
2. SCIENTIFIC OBJECTIVE.....	5
2.1 SCIENTIFIC BACKGROUND.....	5
2.2 SCIENTIFIC AIMS.....	6
2.3 BEAMLINE PERFORMANCE REQUIREMENTS.....	7
3. BEAMLINE OVERVIEW.....	8
4. STRAIGHT SECTION AND INSERTION DEVICE.....	10
4.1 19-ID STRAIGHT SECTION	10
4.1 REFURBISHMENT OF X25 IVU	12
4.3 SEGMENTED ADAPTIVE GAP UNDULATOR (SAGU) OPTION.....	16
4.4 SPECTRAL FLUX FOR UNDULATOR OPTIONS.....	20
5. FRONT END.....	21
5.1 GENERAL LAYOUT.....	23
5.2 DESCRIPTION OF MAJOR COMPONENTS.....	23
5.3 FRONT END RAY TRACINGS.....	39
5.4 FINITE ELEMENT ANALYSIS	40
6. RADIATION AND VACUUM CONTAINMENT.....	42
6.1 BEAMPATH COMPONENT PACKAGES.....	42
6.2 BEAMLINE PHOTON SHUTTER	47
6.3 WHITE-BEAM TRANSPORT AND SHIELDING VALIDATION.....	48
6.4 RADIATION ENCLOSURES.....	50
6.5 BEAMLINE RAY TRACING.....	58
6.6 VACUUM SYSTEM.....	63
7. PHOTON DELIVERY SYSTEM	66
7.1 OPTICAL CONFIGURATION	66
7.2 MONOCHROMATOR.....	66
7.2.1 High energy resolution concept.....	67
7.2.2 Implementation of the NYX energy-resolving monochromator.....	70
7.2.3 Vertical bending mechanism.....	71
7.2.4 Sagittal bending mechanism for horizontal focusing.....	73
7.2.5 Cryogenic cooling system.....	73
7.3 VERTICAL FOCUSING MIRROR	74
7.3.1 Mirror specifications.....	76
7.3.2 Mirror bending system.....	77

7.4 BEAMLINE ANALYSIS.....	78
7.3.1 Ray tracing.....	78
7.3.2 Heat load estimates.....	82
7.3.2 Beamlne efficiency estimates.....	83
7.5 DIAMOND DETECTOR BEAM POSITION MONITORS.....	84
8. END STATION INSTRUMENTATION.....	85
8.1 MICRODIFFRACTOMETER SYSTEM.....	85
8.2 ROBOTIC SAMPLE CHANGING.....	90
8.3 PIXEL ARRAY DETECTOR SYSTEM.....	95
8.4 DATA ACQUISITION SYSTEM AND COMPUTING.....	111
9. BEAMLINE CONTROLS.....	112
9.1 GENERAL DESCRIPTION.....	112
9.2 MAJOR HARDWARE COMPONENTS	113
9.3 NYX BEAMLINE CONTROL SYSTEM	116
9.4 LOCAL CONTROL CABINETS	125
9.4 EQUIPMENT RACKS	127
9.6 CABLES AND INTERCONNECTIVITY	128
10. BEAMLINE SAFETY SYSTEMS	129
10.1 PERSONNEL PROTECTION SYSTEM (PPS).....	130
10.2 EQUIPMENT PROTECTION SYSTEM (EPS).....	133
11. UTILITIES	135
11.1 MECHANICAL.....	135
11.2 ELECTRICAL	137

1. Executive Summary

The NYX Microdiffraction Beamline aims to provide scientists from the New York Structural Biology Center (NYSBC), and also General Users, with convenient access to x-rays from NSLS-II for macromolecular crystallography. This beamline has the scientific objective of providing a state-of-the-art source for a wide spectrum of crystallographic experiments and a cutting-edge source for optimized anomalous diffraction experiments.

NYSBC has led a Participating Research Team (PRT) at the National Synchrotron Light Source (NSLS) for many years, maintaining, upgrading and operating beamlines X4A and X4C. The X4 beamlines were developed originally with support from the Howard Hughes Medical Institute (HHMI). That project began in 1987, and X4A began operations in 1991. NYSBC took over in 2003 and completed major upgrades of X4A and X4C in 2004.

In anticipation of its continued presence in macromolecular crystallography at NSLS-II, NYSBC submitted a Type-II Beamline Development Proposal (BDP) for the NYSBC Microdiffraction Beamline NYX, with Wayne Hendrickson as spokesperson, and this proposal was approved in 2010. NYX features exceptional energy resolution for the optimization of anomalous signals from resonance features. Subsequently, the NYSBC team also submitted a BDP in 2011 for the Low-energy Anomalous X-ray Diffraction Beamline LAX, and this was approved in 2013 and an update LAX proposal is under consideration. Low- β straight section 19-ID has been allocated for the NYX beamline. Funding for NYX is in place from the National Science Foundation, including matching funds from NYSBC and the New York State Office of Science, Technology and Academic Research (NYSTAR), and from the Army Research Office (ARO) of the Department of Defense (DoD). The LAX beamline is not yet funded, but it is anticipated that it will share the 19-ID straight with beams from the NYX and LAX undulators separated by canting magnets. Thus, the designs for NYX are taking into account the eventual accommodation of LAX.

NYX features several innovations giving it best-in-class performance. These include a novel monochromator design for providing exceptional energy resolution in order to assure maximal anomalous scattering signals from sharp resonant features. The ultimate NYX undulator will be an adaptation of a Segmented Adaptive Gap Undulator (SAGU) proposed by Oleg Tchoubar of NSLS-II; however, the undulator formerly used at NSLS X25 will be adopted as the initial source. NYX also includes a novel pixel array detector, co-developed by the Area Detector Systems Corporation and NYSBC, to match performance requirements for detector speed and dynamic range. The beamline is designed throughout to be a stable and versatile resource for macromolecular crystallography.

2. Scientific Objective

2.1 Scientific Background

Knowledge of biological structure at the atomic level has informed, indeed formed, modern biology since the discovery of the double helical structure of DNA. Nearly all enzymology is now structural enzymology; how transcription factors recognize their DNA targets is understood in the detail of atomic interactions; and fundamental processes of replication, transcription and translation are now all richly founded in atomic-level descriptions of polymerases, ribosomes and cofactors. There are structures for impressively large and often pathogenic viruses; structure often leads the way in the study of protein kinases and other signaling molecules; several ribozymes are structurally characterized, and the new biology of micro RNAs has quickly succumbed to structural analysis. Structure is well integrated into drug development; degradative systems, molecular chaperones, and other homeostatic mechanisms now have structural underpinnings; and ion channels and membrane receptors are increasingly amenable to structural analysis. These developments derive predominantly from x-ray crystallography (89% of > 115,000 current PDB entries). This science is vibrant; half of all known structures were determined in the past six years, and increasing numbers of these more recent structures are challenging subjects – mammalian proteins, large multi-component complexes, and integral membrane proteins. Synchrotron radiation plays a huge part now (88.0 % of crystal structures recorded into the PDB in the last five years), and we anticipate that enhancements at NSLS-II will provide new advantages for structural analyses in increasing numbers and at ever increasing complexity.

At its beginning, all macromolecular crystal structures (then only proteins) were determined by the method of multiple isomorphous replacement (MIR) using heavy-atom derivatives for the needed phase evaluation. Subsequently, the method of multiwavelength anomalous diffraction (MAD) provided an effective alternative for solving novel macromolecular crystal structures, and the method of molecular replacement (MR) grew into predominance as the repertoire of structural homologs provided templates for this approach. Truly new information about biological structure continued to depend on *de novo* structure determination, such as from MIR and MAD. The innovation of selenomethionine as a particularly efficient and effective agent for MAD phasing provided an important impetus to the MAD method, but so too did the introduction of beamlines specialized for MAD phasing, most notably the X4 beamlines at NSLS. Ultimately, advances in methods for density modification effected an efficient resolution of phase ambiguities, which then spurred adoption of the method of single-wavelength anomalous diffraction (SAD). At present, over 70% of all *de novo* crystal structures are determined by SAD phasing (Hendrickson, *Quart. Rev. Biophys.* **47**, 49-93, 2014).

The X4 beamlines at NSLS, developed initially by HHMI and taken over in 2003 by NYSBC, led the way in advances for optimized anomalous diffraction experiments. Beamline X4A was particularly instrumental, but effective tunability with maintenance of energy resolution was also demonstrated with a single-crystal monochromator at X4C (Lidestri & Hendrickson, *Nucl. Instr. Meth. A.* **599**, 289-300, 2009; Moore & Hendrickson, *Structure* **20**, 729-741, 2012), and this development is the basis for the NYX monochromator.

In relatively recent experiments at X4A and also at LCLS, we have demonstrated the special effectiveness of lower than usual x-ray energies for SAD phasing based on elements intrinsic to virtually all biological macromolecules, notably sulfur and phosphorous (Liu *et al.*, *Science* **336**, 1033-1037, 2012; Liu *et al.*, *Acta Crystallogr. D* **69**, 1314-1332, 2013; Liu *et al.*, *Acta Crystallogr. D* **70**, 2544-2557, 2014). These developments affect our plans for beamline development. In particular, NYX is being developed with its undulator canted such that in sector 19-ID will accommodate a second undulator to serve a partner beamline for Low-energy Anomalous X-ray Diffraction (LAX)

2.2 Scientific Aims

The primary scientific aim for NYX is focused on the needs of users from the nine member institutions of the New York Structural Biology Center (NYSBC) and also those of its DoD sponsor, but the beamline must also meet needs of NSLS-II General Users. Investigators from the NYSBC community include many pre-eminent structural biologists working on challenging problems at the forefront of the field. Challenges come from the size and complexity of systems under study. Moreover, as technological advances make it possible to deal with new challenges, such as those that come from very small samples, demand grows for the technical capability to meet these challenges. Micron-sized x-ray beams are readily feasible at NSLS-II, and we expect substantial demand for this capability. Micron-sized crystals are commonplace for many problems, and they are intrinsic to the lipidic cubic phase (LCP) methods from crystallization of membrane proteins. To achieve the desired brilliant x-ray microbeams, it is essential to take advantage of the enhancements that come best from undulator sources at a low-emittance synchrotron such as NSLS-II.

A second major emphasis for NYSBC beamlines, and a significant focus of research for NYSBC scientists, concerns the optimization for anomalous diffraction experiments. NYX is an intellectual successor to NSLS beamline X4A, which was designed in part for the testing of multiwavelength anomalous diffraction (MAD). While moving to incorporate microbeams, we also want to preserve the versatility of optimized anomalous scattering experiments across a broad spectrum of atomic resonances from different elements and we propose to capitalize on the intrinsic brightness of NSLS-II to optimize anomalous signals by improving energy resolution. In light of the overwhelming success of SAD phasing, such optimization has two aspects: one concerns the maximization of on-resonance anomalous scattering at the absorption edges, and the other concerns the off-resonance optimization of anomalous scattering signals in light of complications for diffraction experiments at low energy (long wavelengths).

Recognizing that many problems may not require *de novo* phase evaluation, we would not want to compromise generic performance of NYX to optimize anomalous diffraction experiments. With these considerations in mind, we focus for NYX on the kind of science that will benefit from three attributes that have motivated our proposed beamline design: (1) we aim to provide stable, high brightness beams at the level of cross sections from 50-micron down to 5-micron; (2) we aim to preserve the inherent spectral flux from a monochromator crystal (typically Si 111) within a bandpass down to energy resolution of $\Delta E/E = 5 \times 10^{-5}$; and (3) we aim to support efficient diffraction experiments in the range of x-ray energies from 5 to 17.5 keV. The NYX energy range covers all conventional phasing elements from the uranium L_{III} edge (17.17 keV) down to the cesium L_{III} edge (5.01 keV) with expected emphasis on the Se K edge (12.66 keV). Because low energy experiments encounter several special technical requirements, we have decided to limit the lower reach of NYX to approximately 5 keV, which includes transition metals through the manganese K edge ($Z= 25$, 6.54 keV) and accommodates demonstrably effective sulfur SAD experiments, and to develop LAX as a separate beamline dedicated to experiments at energies that can reach the potent uranium M_V edge (3.49 keV) and the biologically prevalent phosphorous and sulfur K edges (2.15 and 2.47 keV).

2.3 Beamline Performance Requirements

To meet the Scientific Objective that we have set, NYX will need to provide reliable operation for macromolecular crystallography experiments, including those without the need for a specific x-ray energy and those that require tuning to the energy of a specific resonance feature. This operation will also need to address crystallographic challenges of small crystals, large unit cells, radiation damage effects and sundry crystal pathologies. To be effective, it must also be designed to take full advantage of the high photon fluxes that the optics will be able to deliver.

The following are among the most salient of beamline characteristics needed to address the Scientific Objective and its specific aims:

- Accommodation of LAX as a companion beamline from a second canted undulator in the same straight section.
- Accommodation of the SAGU as the eventual NYX undulator, which will produce a greater heat load for the optics.
- Precision energy tuning (within 0.1 eV) over the range of energies from 5 keV to 17.5 keV.
- X-ray energy resolution to the level of $\Delta E/E = 5 \times 10^{-5}$ at the Se K-edge.
- X-ray beam focusing with uniform intensity across the illuminated spot for beam from 5 μm to 50 μm with differential control horizontally and vertically.
- Beam position control to deliver the beam stably centered on the target position (within 1 μm).
- Visualization optics and raster scanning options for sample orientation and positional control.
- Sample control to maintain crystal centering (within 1 μm) and reliable rotations at high scanning speeds (>600 deg/sec).
- Sample exchange robotics to accommodate current sample delivery systems, anticipating that new procedures may develop.
- X-ray detector designed to cope with anticipated fluxes and lattices with Bragg spacings as great as 2000 Å.

3. Beamline Overview

The x-ray source for NYX will be an undulator in the low- β straight section of NSLS-II sector 19, which will be laid out to accommodate two insertion devices (IDs), an upstream (U1) in the electron beam as the source for NYX and, ultimately, a second downstream undulator (U2) as the source for LAX (Figure 3-1). The ID source for the NYX beamline has two options, starting with the repurposed 1-meter X25 IVU and then upgraded to a 2-meter SAGU undulator. The X25 device is provided as a temporary option until the SAGU option can be produced. The straight section will incorporate appropriate canting magnets from the outset so that both the NYX and LAX beamlines can be accommodated without any future displacements. The 19-ID Front End is designed to handle the radiation from both undulators.

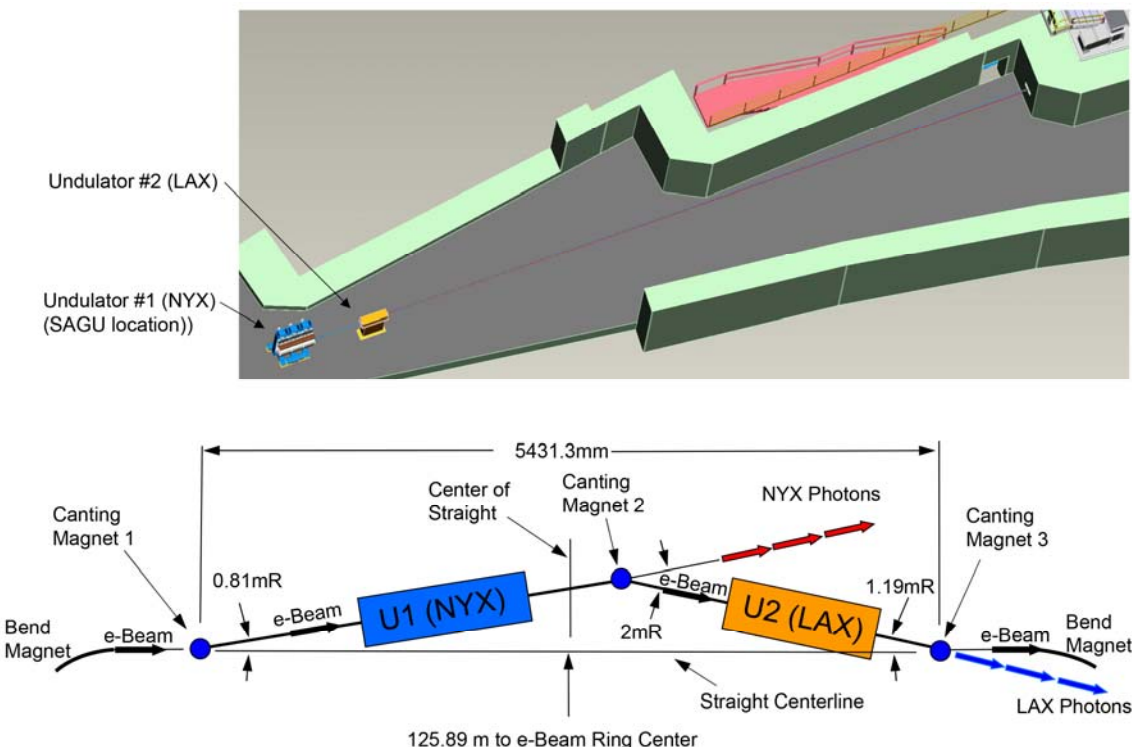


Figure 3-1. Straight-section geometry. Two undulators will be placed as shown without accelerator components in the 19-ID straight section (above), and as shown schematically to detail the separation of beampaths by canting-magnet deviations (below).

The NYX beam will be delivered through the front end components into a radiation and vacuum containment system as shown in Figure 3-2. Radiation enclosure hutch A, which abuts directly to the shield wall, will include the future LAX monochromator (Mo1). The NYX monochromator (Mo2) and vertical focusing mirror (VFM) will be enclosed in white-beam hutch C, which is contiguous with the NYX endstation hutch D. Hutch B is reserved for the eventual endstation radiation enclosure for LAX. A shielded white beam transport will pass the NYX beam from hutch A to hutch C. The entire NYX beam will be in vacuum through to its delivery into the environment at the sample crystal position (Xtl).

A fully developed CAD layout of the beamline has been generated that includes accurate 3D representation of all synchrotron beam apertures, bremsstrahlung collimators, vertically adjustable beam slits, beam filters, beam position monitors and beam optics components. The NYX beam optics components include the double crystal monochromator (DCM), and a Vertical Focusing Mirror (VFM) that deliver a focused monochromatic beam to the sample positioning point of the end station. The end station consists of a sample positioning goniometer, robotic sample handler, a sample dewar and x-ray

detector system. The first optical element in the white beam is the DCM, which is designed to accommodate the full strength from the SAGU without sacrifice of energy-resolution performance. The overall beamline and the experimental floor beamline component layout is shown in Figure 3-3.

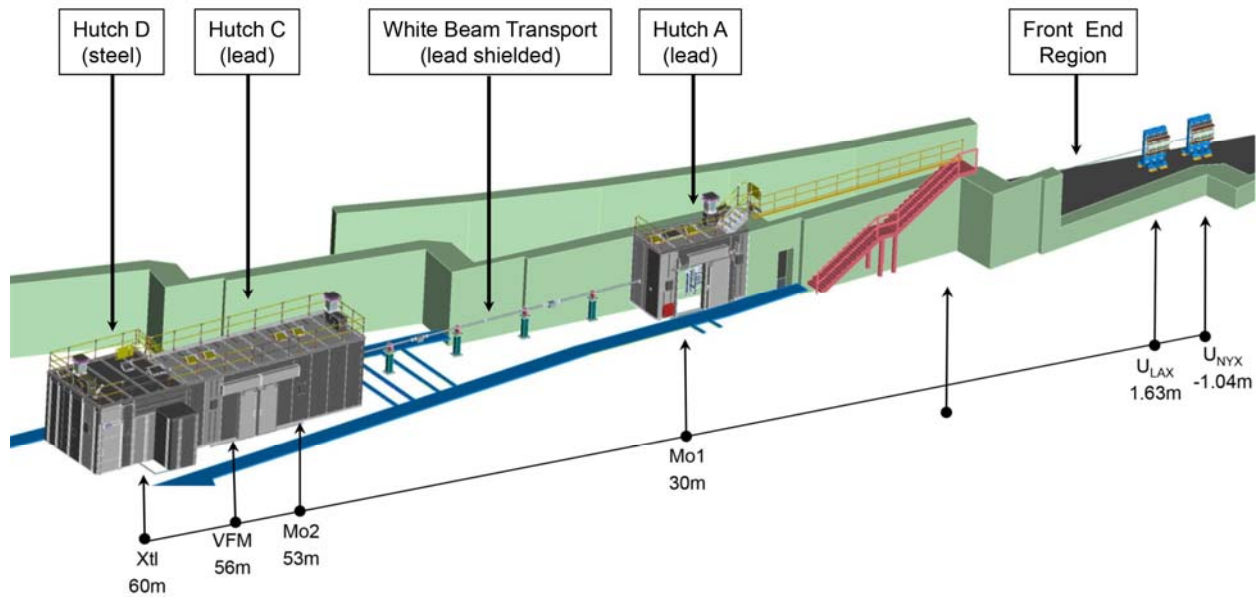


Figure 3-2. Isometric view of the radiation and vacuum containment system of the NYX beamline. This view is from outside shieldwall and toward the accelerator ring, opposite to that in Fig. 3-1.

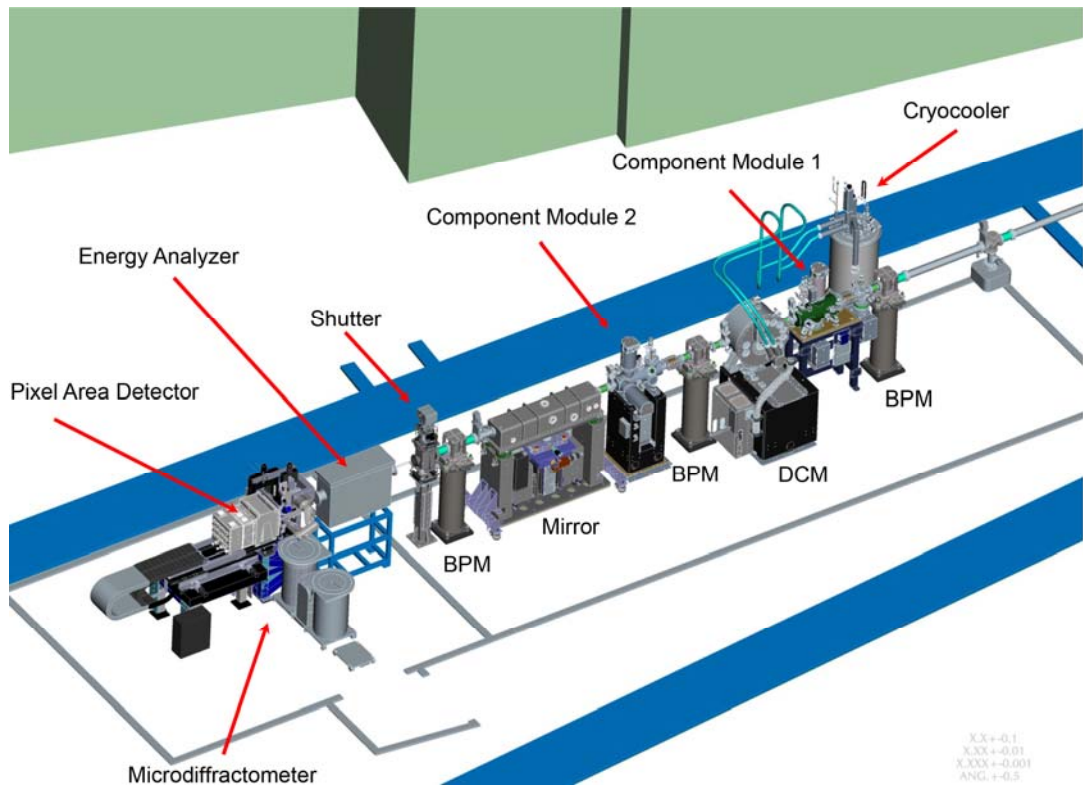


Figure 3-3. Layout of photon delivery system (C hutch) and endstation (D hutch) components of the NYX beamline. Floor footprints of the C and D hutch walls are shown in gray.

4. Straight Section and Insertion Device

4.1 19-ID Straight Section of Accelerator

4.1.1 General Description

The canting magnets in the 19-ID short straight are to be located so that a future 2 m undulator may be installed in the upstream section and a 1 m device in the downstream section. The upstream section will be used for the NYX source and will utilize a refurbished 1 m undulator acquired from NSLS X25. The 1 m X25 IVU will be placed with its downstream magnet location to coincide with the downstream magnet location of the future 2 m IVU as shown in Figure 4-1.

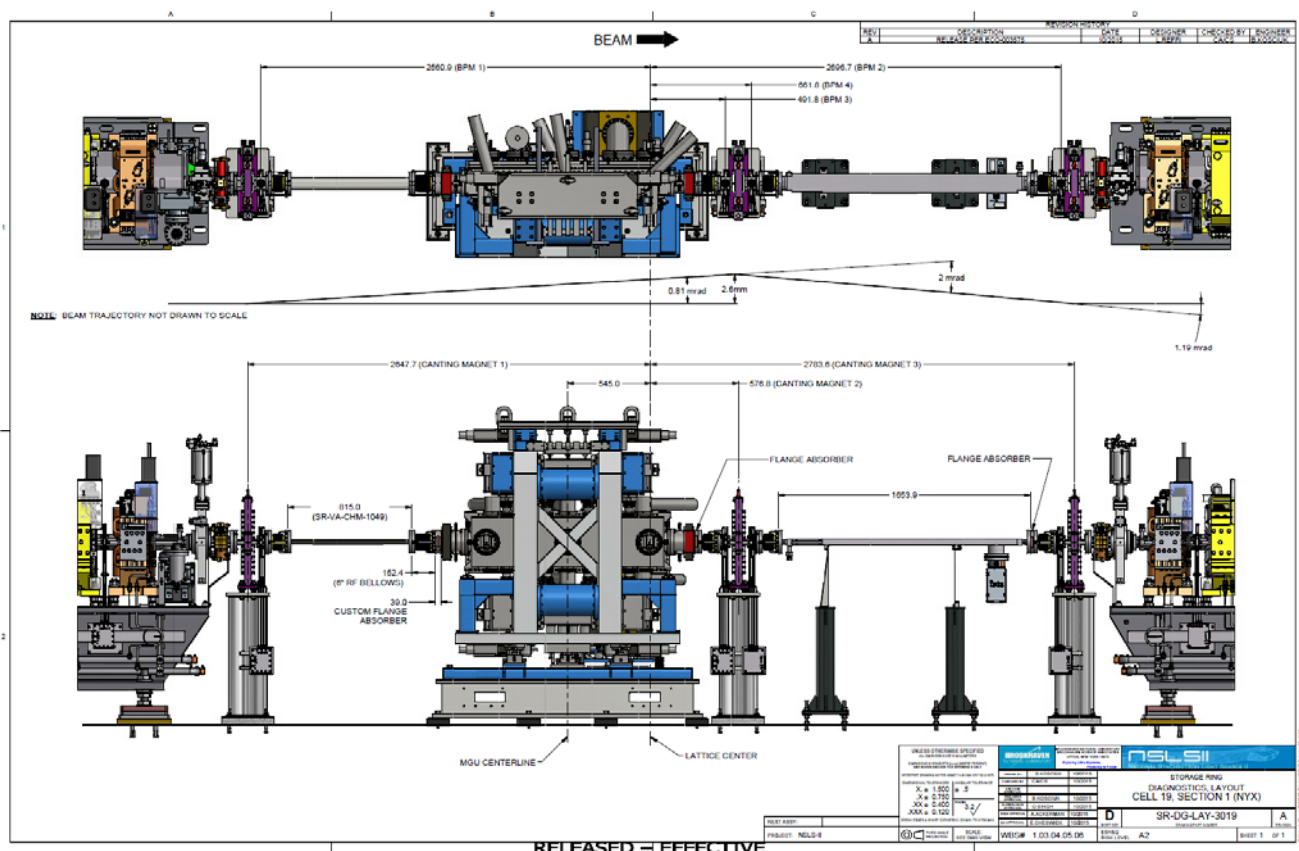


Figure 4-1. Straight section 19 ID layout with 1 m X25 IVU and asymmetric canting.

4.1.2 Requisition, Specification and Interface (RSI)

The following table summarizes the ID options for 19-ID beamlines NYX and LAX. There are two options for NYX: the IVU X25 repurposed from NSLS and the Segmented Adaptive Gap Undulator (SAGU), quoted in parentheses.

Table 4.1: Insertion devices for 19-ID beamlines.

Beamline	NYX	LAX
Type	X25 IVU (SAGU) ^{*4}	IVU
Length	1.0 (2.07) m ^{*5}	~1 m
Usable photon energy range	6.5 (1.4) – ~20 keV	~3 – 7 keV
Canted	Y (asymmetric)	
Canting angle	2.0 mrad NYX: -0.79 mrad outwards ring LAX: -1.21 mrad towards ring	
Period	18 (17.7 – 21.9) mm	~25 mm, TBD
Minimum magnetic gap ^{*1}	5.6 (3.5 – 6.3) mm	~6.6 mm
Peak magnetic field	0.95 (~0.98 – 1.43) T	~0.94 T
K _{eff} ^{*2}	1.55 (~1.90 – 2.23)	~2.2
Power total	2.43 (~7.6) kW	~2.5 kW
On-axis power density	22.6 (~55) kW/mr ²	~16.3 kW/mr ²
Straight section type	Short (low beta)	
Lowered horiz. beta desired	N/A	N/A
Device center	U/S 0.5 (~1.04) m	D/S ~1.63 m
Fan angle ^{*3} (mrad H)	0.75/1.36 (0.91/1.50)	~0.97/-1.57
Fan angle ^{*3} (mrad V)	0.80/1.26 (0.82/1.30)	~0.83/-1.32
Gap scanning and other requirements	Gap scanning speed 30 eV/sec or greater, over usable photon energy range.(?)	

Note 1: Vertical stay-clear aperture for in-vacuum devices (e.g. IVU, SAGU)

Note 2: In the general case of an ellipsoidal insertion device with non-sinusoidal periodic magnetic field:

$$K_{eff} = \frac{e\lambda_u}{2\pi m c} \left(\sum_{n=1}^{\infty} \frac{B_{hn}^2 + B_{vn}^2}{n^2} \right)^{1/2} = 0.0954 \frac{\lambda_u [\text{mm}]}{c} \left(\sum_{n=1}^{\infty} \frac{B_{hn}^2 + B_{vn}^2}{n^2} \right)^{1/2} [\text{T}]$$

where e and m are charge and mass of electron, λ_u is period, B_{hn} and B_{vn} are amplitudes of n -th harmonics of the horizontal and vertical magnetic field components. In cases where detailed magnetic design of an insertion device has not yet been performed, only fundamental harmonics of the vertical and/or (where applicable) horizontal magnetic field components were used to estimate emission characteristics.

Note 3: Fan angles of the radiation quoted here are as seen at 16 m from ID center, and take into account the effect of ID length. The two values quoted for each case correspond to the points where the power density falls to values that are 1% and 0.1% of the central value. These values are accurate to within 5%. Designs of the XBPM and fixed mask entrance shall take into account these fringe power loads.

Note 4: Two options of the NYX undulator: X25 IVU (from NSLS) and a Segmented Adaptive Gap Undulator (SAGU), are considered.

Note 5: Prior to finalizing the designs of these insertion devices, the length specification may vary by up to ±15%.

For 2 mrad canting, the ID positions should assume a ~1.0 m gap along the beam direction to allow for the canting magnets and beam position monitors, etc.

4.2 Refurbishment of X25 IVU

4.2.1 Assessment of X25 IVU

The X25 IVU (950 mm, 53 periods of 18 mm) was procured from ADC and delivered to the NSLS on January 10, 2005 (Figure 4-2) and removed from the NSLS accelerator tunnel on February 15, 2015. (Figure 4-3).

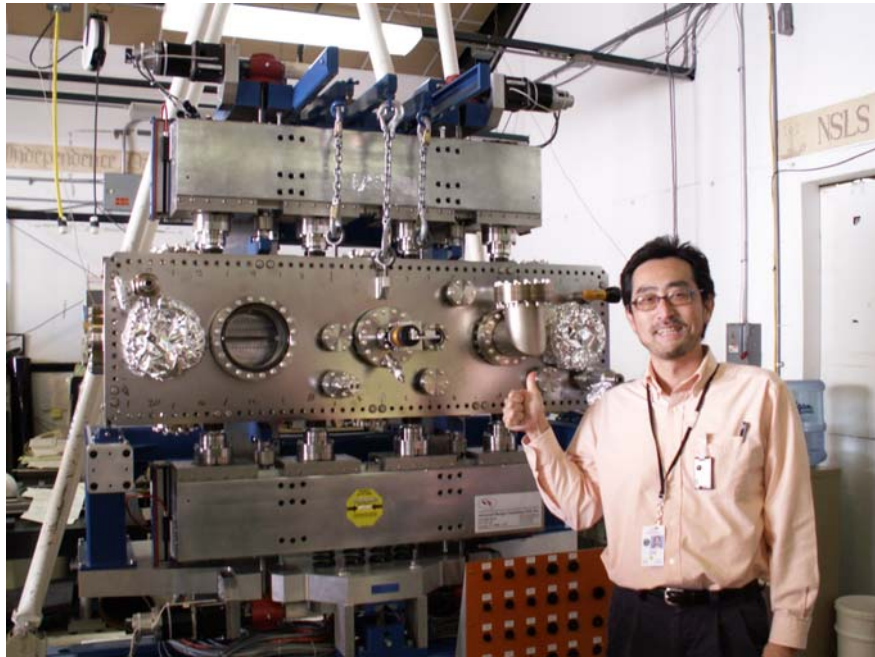


Figure 4-2. Arrival of the X25 IVU at NSLS from ADC on January 10, 2005

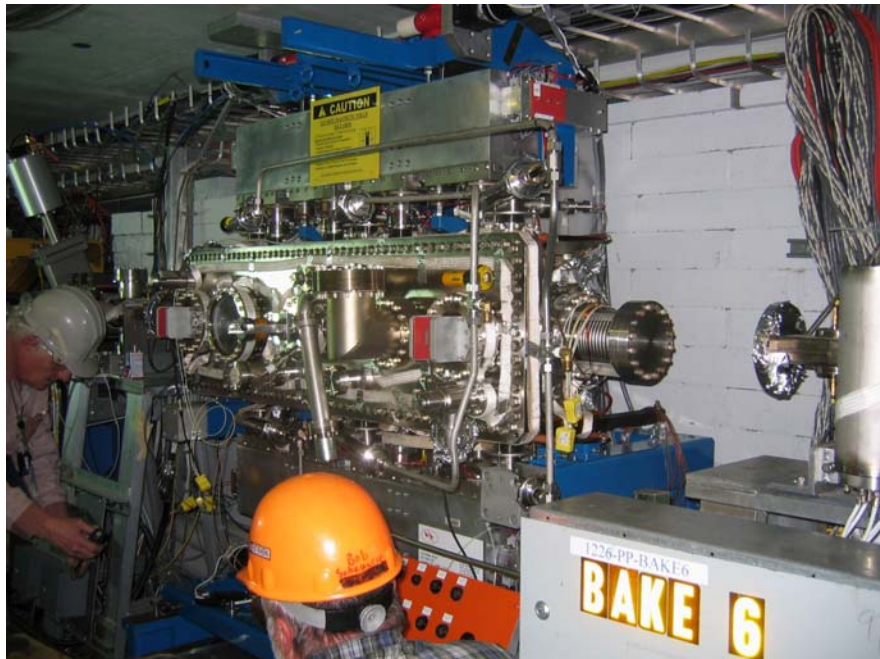


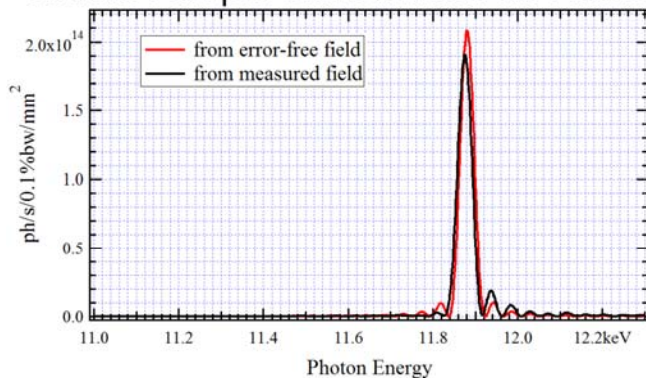
Figure 4-3. Removal of the X25 IVU from the NSLS accelerator tunnel on February 15, 2015

Magnetic field mapping of the X25 IVU was performed in November 2015 and calculations of Undulator Radiation (UR) spectral flux per unit surface and through a fixed collection aperture were made, using SRW code, for the recent X25 IVU magnetic measurements data provided by the ID group. Three different types of calculations were performed for 50.7 m observation distance (i.e. for the longitudinal position of first optical elements of the NYX beamline), for the real measured magnetic field of X25 IVU and for the corresponding “error-free” (ideal) periodic magnetic field. The calculations were performed for 6 mm IVU gap (the value for which one of the Hall probe measurements was performed), for 5th UR harmonic that peaks at ~11.85 keV photon energy Figure 4-4.

First, the on-axis spectral flux per unit surface for a filament electron beam (i.e. beam with zero transverse emittance and energy spread) was calculated for the two magnetic field cases (measured and error-free). This calculation showed only ~10% reduction of the flux per unit surface in the case of the measured magnetic field as compared to the error-free field case. Next, the on-axis spectral flux per unit surface was calculated taking into account the NSLS-II electron beam emittance and energy spread. This calculation showed only ~7% reduction of the spectral flux per unit surface in the case of the measured magnetic field compared to the error-free field case. Finally, the spectral flux of UR was calculated taking into account the electron beam emittance, energy spread, and a finite collection aperture (~6 mm (h) x 4 mm (v) at 50.7 m) that may be used at the NYX beamline. That calculation demonstrated <~4% reduction of the flux in the measured magnetic field case compared to the error-free case.

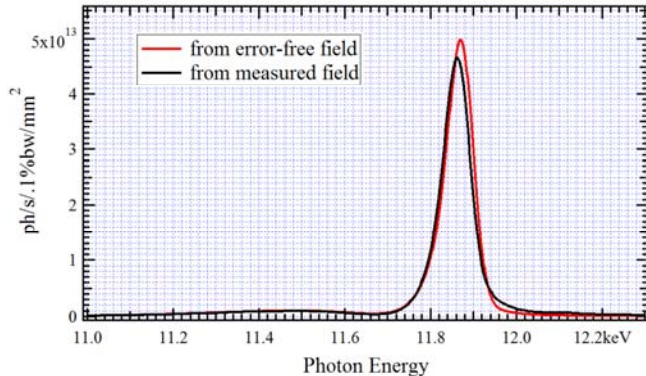
On-Axis Flux per Unit Surface from Filament E-Beam

December 2015



E-Beam Current: 0.5 A
Undulator Gap: 6 mm
UR Harmonic: #5
Observation Distance: 50.7 m

On-Axis Flux per Unit Surface from Finite-Emittance E-Beam



Flux from Finite-Emittance E-Beam within 6 mm (h) x 4 mm (v) Aperture

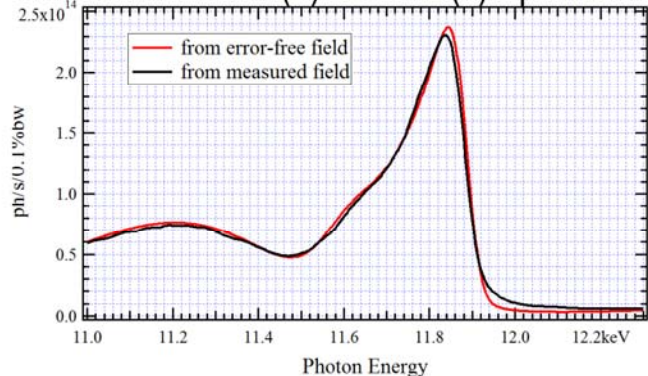


Figure 4-4. X25 undulator radiation spectra calculated from measured magnetic field compared to error-free field.

These spectral calculations confirm the good quality of the X25 IVU magnetic field (that even exceeds that of some of the recently-purchased IVU), which makes it possible to use this IVU at the NYX beamline without extra “spectral shimming”. It should be noted, however, that some “multipole shimming” of the X25 IVU may still need to be done using the “magic finger” technique, to minimize its potential effect on the electron beam at NSLS-II (especially at a small gap).

4.2.1 X25 IVU Installation Design at NYX

The X25 IVU is integrated into the NSLS accelerator with the standard bellows, custom absorber and custom taper transition, as shown in Figure 4-5.

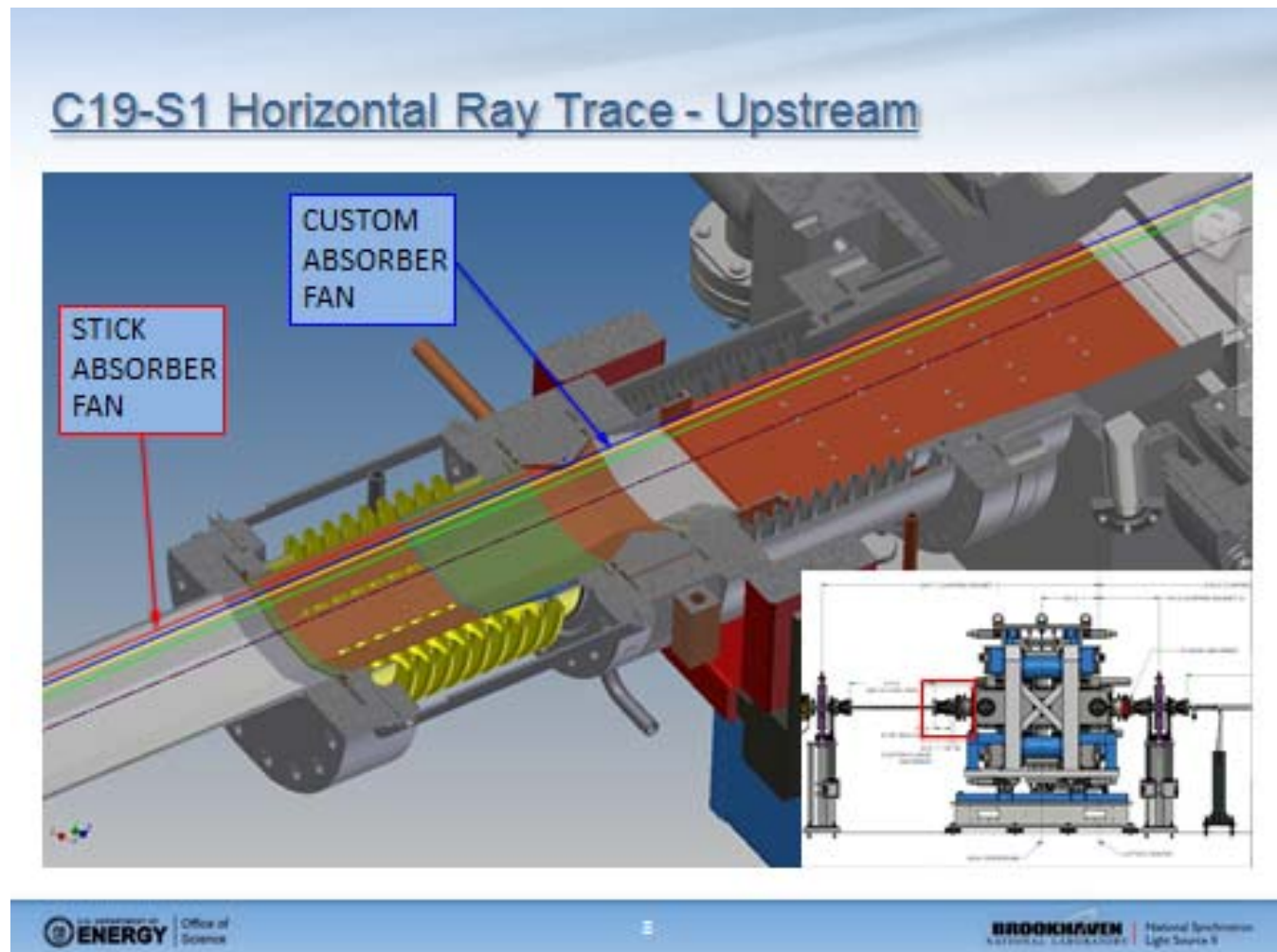


Figure 4-5. Upstream bellows, absorber and transition for the X25 installation into the NSLS-II accelerator at NYX.

Cooling for the taper transition (which must flex to accommodate the 5.6 mm to 20 mm magnet gap) will be provided by thermal straps to avoid a water leak in the accelerator if water cooling had been used (Figure 4-6).

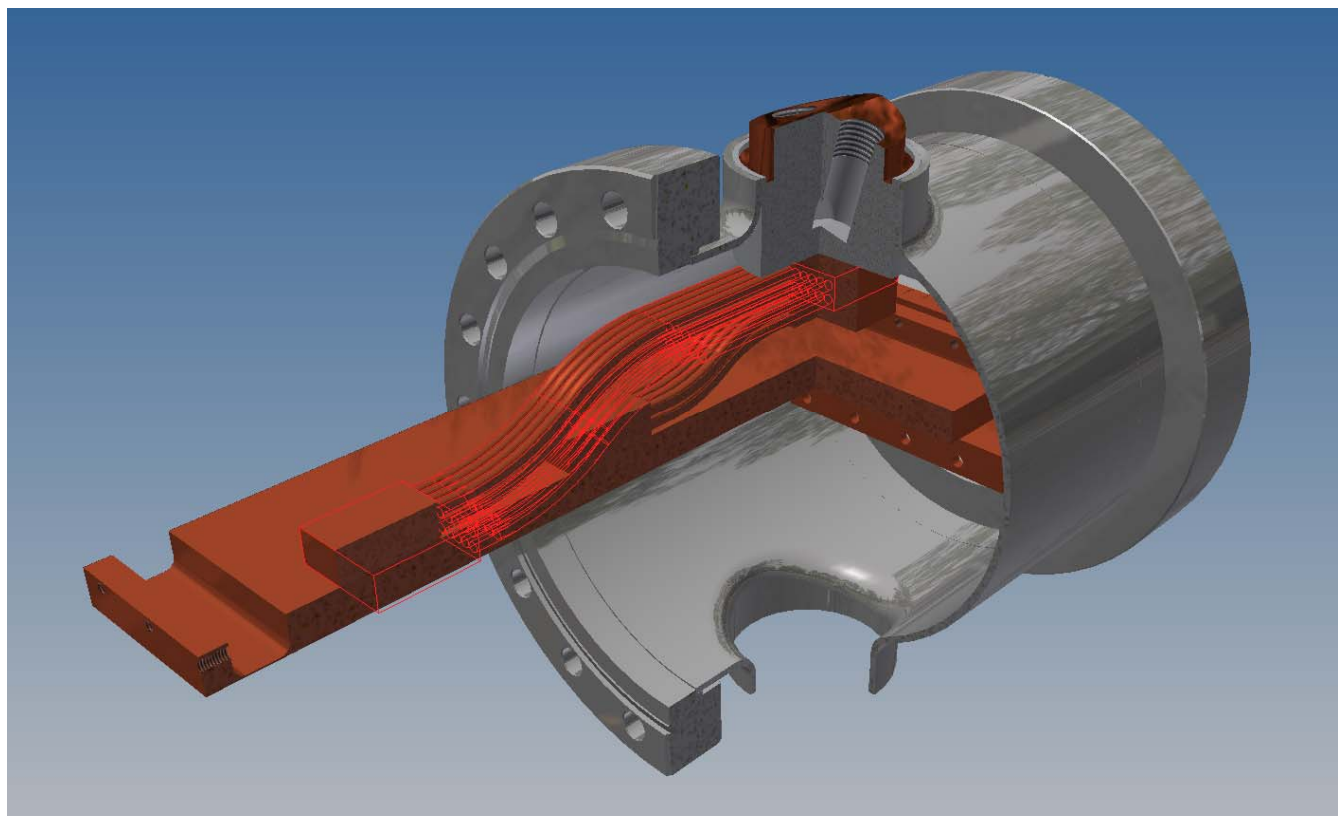


Figure 4-6. Thermal straps for cooling of the taper transition.

4.3 Segmented Adaptable Gap Undulator (SAGU) Option

4.3.1 General Description

The SAGU utilizes different gaps and magnetic periods in short segments to produce high flux and brightness hard X-rays that cannot be obtained with a standard IVU of similar length. The original concept (S.C. Gottschalk *et al.*, *AIP Conf. Proc.* **521**, 348, 2000) would have had many rather short segments; however, calculations demonstrate excellent performance from with longer segments (O. Chubar *et al.*, Spectral Performance of Segmented Adaptive-Gap In-Vacuum Undulators for Storage Rings", *Proc. of IPAC2012*, MOPPP090, 765-767, 2012), and the design for implementation at NYX was reported at SRI 2015 (T. Shea *et al.* Mechanical Systems for Segmented Adaptive-Gap In-Vacuum Undultator, *Proceedings of the 12th International Conference on Synchrotron Radiation 2015*)

Our SAGU implementation will have a total magnetic length of 2.07m in three independet segments each 660mm long. Vertical gaps in each segment are adjusted to satisfy "Stay-Clear" and impedance constraints and all segments are tuned to the same resonant photon energy by varying the magnet period. Undulator period will vary from segment to segment, however constant within each segment. Figure 4-7 below shows the conceptual design of the SAGU. A concept was created that only needs two motors, one for gap and one for vertical offset – taper would be provided manually. This was the preferred approach because it reduces the perceived complexity for three segments. Each segment will be mounted on a robust base plate. The below figure shows the three-segment concept for the SAGU. This is based on a two-motor design where one motor controls the gap and another motor controls the vertical offset. A double set of vertical rails is used to accomplish the gap and vertical offset. The inner rails mounted to the strong back that carries a plate which is moved vertically by the offset motor. Rails mounted to this plate support the outer girders which are driven by a single left/right hand threaded ball screw to produce the gap motion.

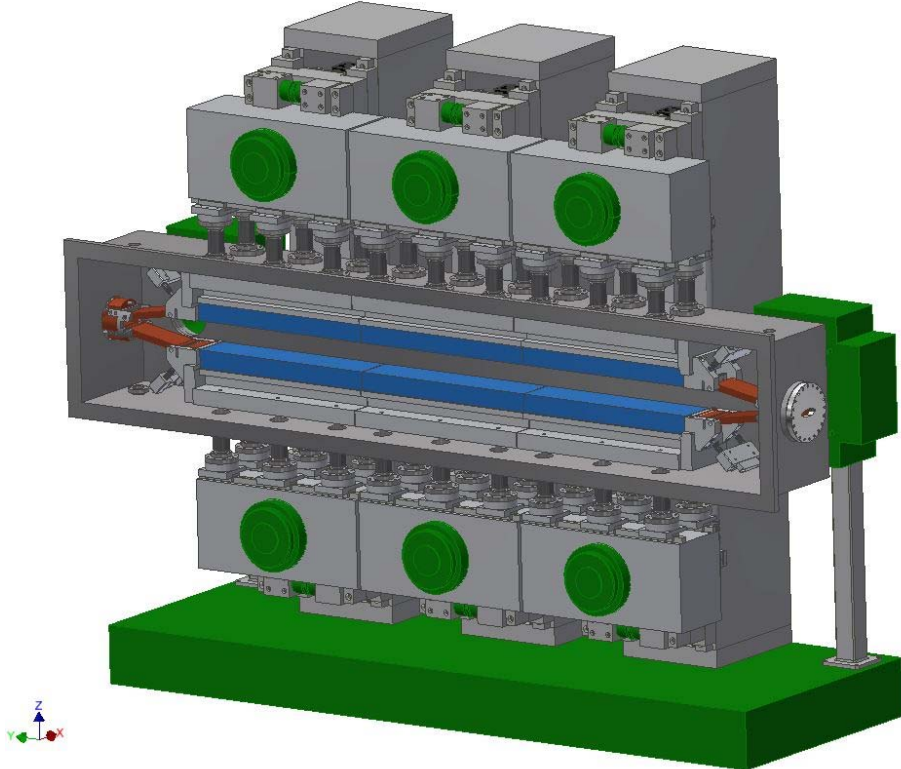


Figure 4-7. Conceptual design of the SAGU for NYX

4.3.2 Power Density Distributions for NYX IVU Options

Figure 4-8 shows the power density distributions at 56m, which will be the location of the NYX monochromator. The total power ranges from 4.9kW - 7.6 kW depending on the IVU option. This range of power is well below the power limits of the front end components (at 16m) . The details of the power limiting aperture upstream of the monochromator will be discussed in the photon delivery section of this report.

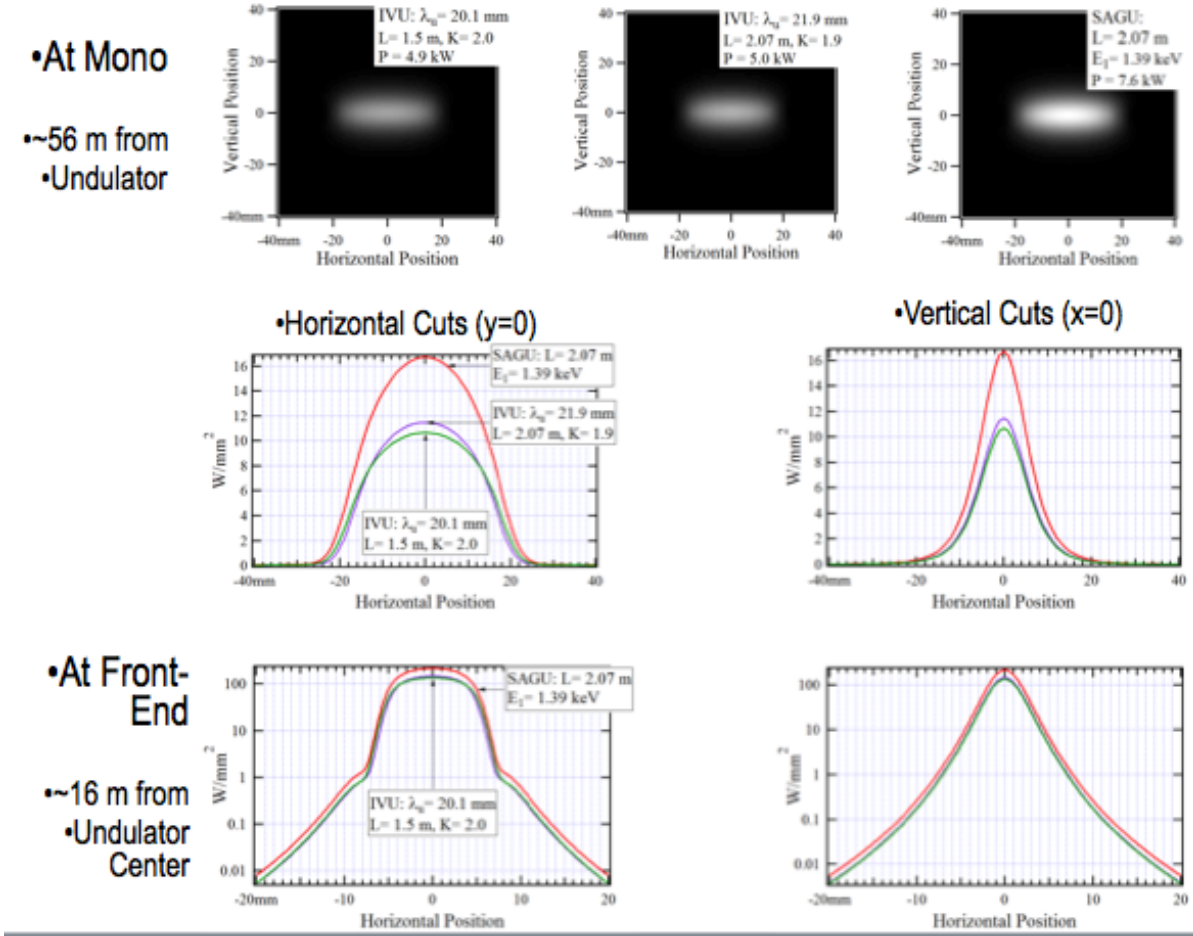


Figure 4-8. Power density distributions.

4.3.3 Tapered Transition

A tapered transition from the liner foil of an in-vacuum undulator (IVU) to the beam pipe in the NSLS-II synchrotron storage ring has been developed to provide a continuous conduction path for the image current induced by the passing electron bunches. Figure 4-9 shows a tapered transition concept developed by NYSBC, ADC & AES, which was intended as a common design for both the X25 and SAGU.

The criteria for the above tapered transition design were defined by Alexei Blednykh of BNL from longitudinal wake-potential calculations. Figure 4-10 shows an example wakepotential calculation that determines a maximum allowable step of 0.5mm in the transition.

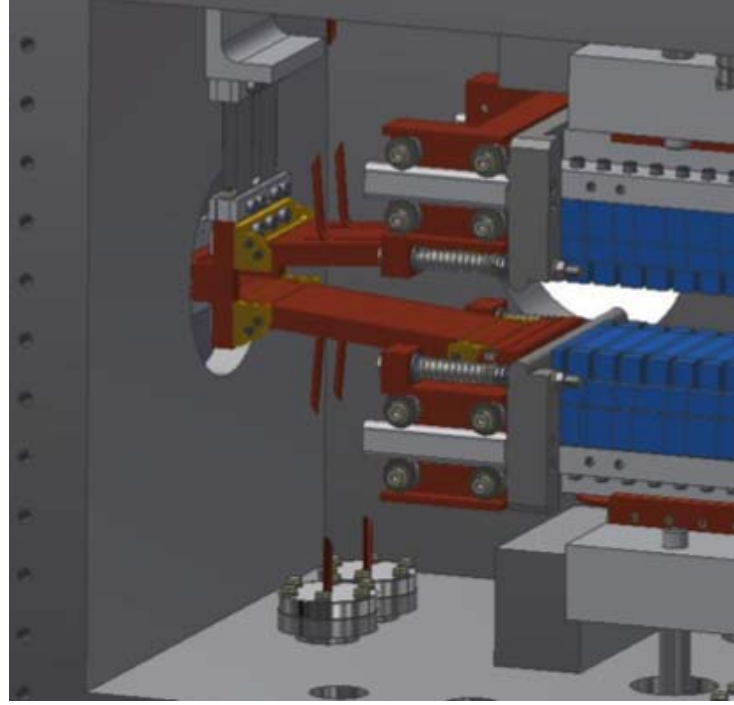


Figure 4-9. Tapered transition concept.

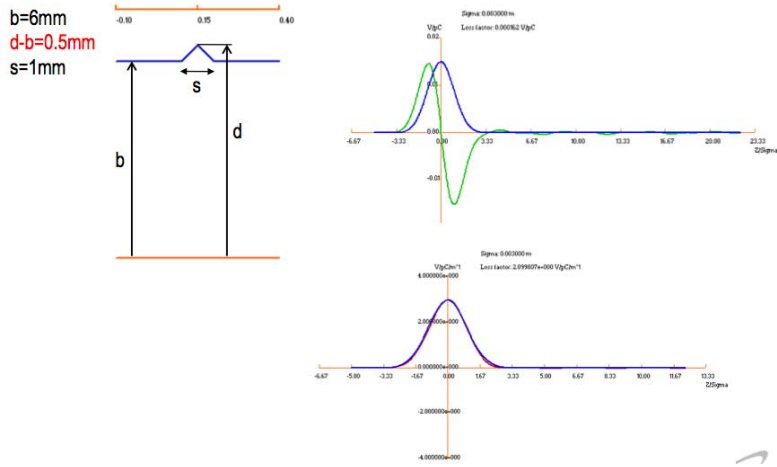


Figure 4-10. Example wake-potential calculation.

Current Density Estimates. The RF tapered transition design shown in Figure 4-8 takes advantage of beryllium copper flexures to provide good current contact and shield the RF wake fields generated by the high frequency electron bunch. Beryllium copper (BeCu), also known as copper beryllium (CuBe), beryllium bronze and spring copper, is a copper with 0.5–3 beryllium and is an industry standard for creating RF-tight electronic seals due to its excellent electrical conductivity and ability to be cold-formed before tempering into spring copper. Given the SAGU gap range of 3.5 -40mm it is important that the flexure operate within the elastic range well before plastic deformation occurs therefore CuBe spring copper is superior to many other metals. Also given the electrical resistivity of 7.8E-6 ohm-cm for BeCu an simple transient analysis can be done to estimate the maximum current density at the BeCu contact. First, given the actual risetime of the passing electron bunch at NSLS-II the RF skin depth can be calculated assuming a bunch frequency of 33GHz. The estimated skin depth

at this frequency and resistivity is $0.774\mu\text{m}$. The lateral extent of the image current can be estimated as a current filament over a plane where most of the current is within 6mm; therefore the resulting current density is estimated to be 108A/mm^2 given a maximum synchrotron current of 500mA. The RF tapered transition developed for the SAGU is well suited for the small emittances of NSLS-II and has the following advantages:

1. A pivoting rigid bridge design with BeCu shields provides durability and simplicity over flexing bridge tapered transitions.
2. Modularity allows the bridge alone to be incorporated into an IVU, or allows the axial compliance assembly or liner foil tensioner to be used with the bridge.
3. The taper transition cooling lines are simplified by the use of a rigid bridge.
4. Adapter plates can be made to connect the tapered transition with any IVU girders (X25 or SAGU).
5. Axial compliance section can be adapted to various chambers and beam pipes.
6. The number of sliding contacts is minimized and all steps or valleys are kept to 0.5 mm or less to minimize wake potential.
7. UHV compatible materials used throughout: C10100 Copper, 6061 Aluminum, 304 or 316 Stainless Steel.

4.3.4 Controls for Insertion Device

A complete and comprehensive definition of the control system requirement for the SAGU is provided in document ID: CSL-RSP-15-115440. Cosylab generated this document under contract to NYSBC by aggregating the BNL guidelines and criteria defined in 15 separate references listed in CSL-RSP-15-115440.

The simplified controls architecture (Figure 4-11) will be in compliance with the platform defined by NSLS-II. The motion controllers will be based on the NSLS-II preferred Delta-Tau Geobrick-LV. This will consist of two motors per segment, for gap and vertical offset, and five encoders per segment.

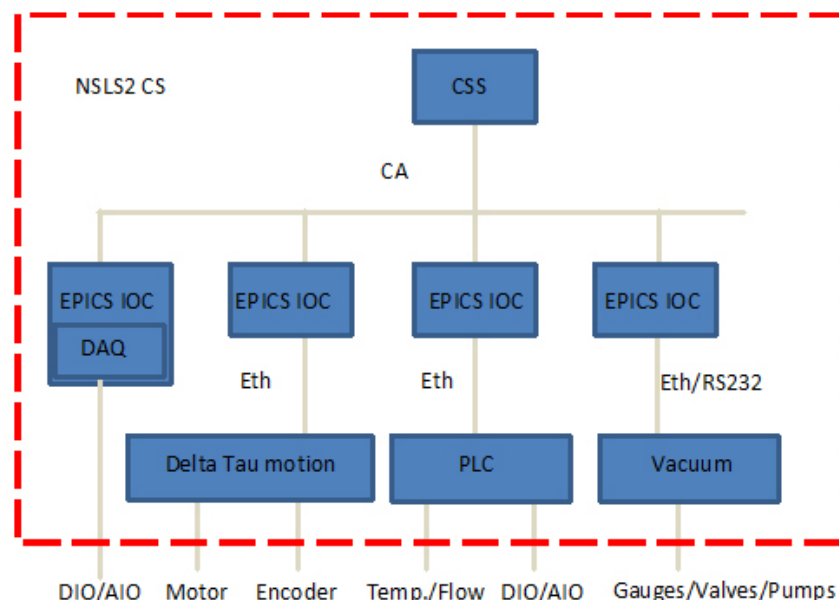


Figure 4-11. SAGU controls architecture.

4.4 Spectral Flux Comparisons

Figure 4-12 shows the calculated flux for the X25 IVU at the short straight NSLS II 19-ID (odd harmonics only) compared to SAGU options for the future upgrade to a 2 m device for NYX.

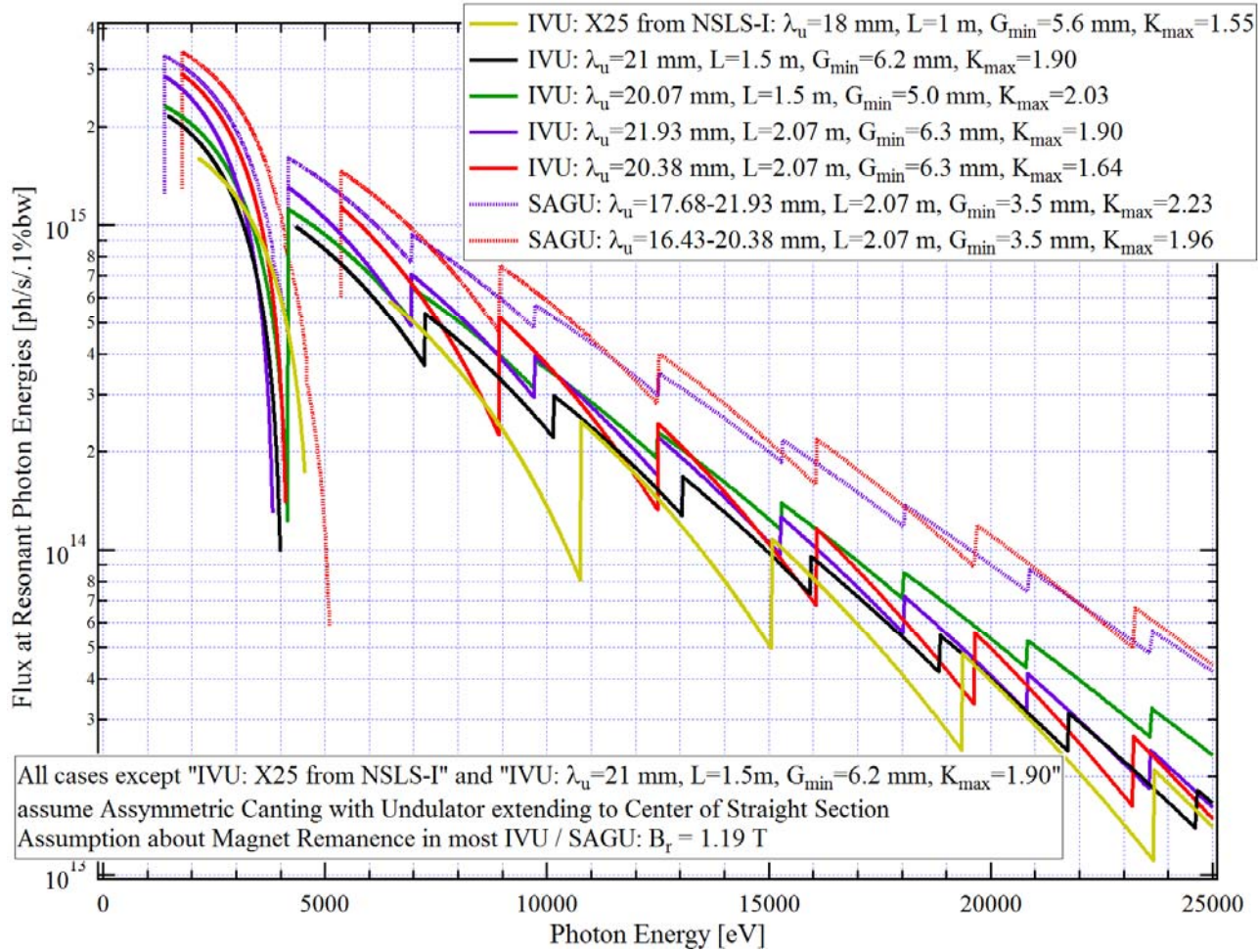


Figure 4-12. Spectral flux for odd harmonics for IVU devices at the NYX section of canted sector 19-ID at NSLS II.

5. FRONT END

Contents

5.1	GENERAL LAYOUT OF THE FRONT END (FE)
5.2	BRIEF DESCRIPTION OF THE MAJOR COMPONENTS OF THE FRONT END.....
5.2.1	Photon Shutter (BMPS) and Absorber
5.2.2	Slow Gate Valve (SGV).....
5.2.3	Beam Position Monitor 1 (XBPM1)
5.2.4	Beam Position Monitor 2 (XBPM2)
5.3.5	Fixed Aperture Mask (FAPM)
5.2.6	Bremsstrahlung Collimator (CO1)
5.2.7	4-Y Slits.....
5.2.8	Photon Shutter (PSH).....
5.2.9	Fast Gate Valve (FGV)
5.2.10	Bremsstrahlung Collimator (CO2).
5.2.11	Safety Shutter (SSH)
5.2.12	Ratchet Wall Collimator
5.2.13	Gate valve downstream of Ratchet Wall
5.3	FRONT END RAY TRACINGS
5.3.1	General Guidelines for Ray Tracings
5.4	FINITE ELEMENT ANALYSIS FOR THE FRONT END.....

Acronyms

BMPS	Bending Magnet Photon Shutter/Absorber
CO1, CO2	Lead Collimators 1 and 2
FEA	Finite Element Analysis
FGV	Fast Gate Valve
MSK	Fixed Aperture Mask
PLC	Programmable Logic Controller
PSH	Photon Shutter
RCO	Ratchet Wall Collimator
SGV	Slow Gate Valve
SR	Storage Ring
SS	Safety Shutter

Figures

5-1	Typical front end configuration at NSLS-II, canted.....
5-2	Principle of the Glidcop absorber
5-3	Design for the bending magnet photon shutter
5-4	Design for the slow gate valve
5-5	Fixed-aperture mask
5-6	Fixed-aperture mask assembly
5-7	Storage ring front end mask.....
5-8	Mask mounted in the assembly.....
5-9	Front end lead collimator
5-10	Burn through device.....
5-11	Photon shutter assembly
5-12	Closer view of the photon shutter.....
5-13	Photon shutter assembly detail
5-14	Design for the safety shutter
5-15	Safety shutter.....
5-16	Safety shutter bellows.....
5-17	Ratchet wall collimator
5-18	Slow gate valve in cell 28 (XPD beamline).....
5-19	Thermal calculations on the Glidcop mask and photon shutter.....

Tables

5-1	FEA for the front end.....
-----	----------------------------

5.1 General Layout of the NYX Front End (FE)

Layouts of the standard NSLS-II undulator beamline front ends (non-canted and canted) are shown in Figures 5-1. Constituent subassemblies include: Bending Magnet Photon Shutter/Absorber (BMPS), Slow Gate Valve (SGV), Fixed Aperture Mask (MSK), Lead Collimator (CO1), Fast Gate Valve (FGV); Photon Shutter (PSS), Lead Collimator (CO2), Safety Shutters (SSH), and Ratchet Wall Collimator (RCO, burn through device omitted for NY4.

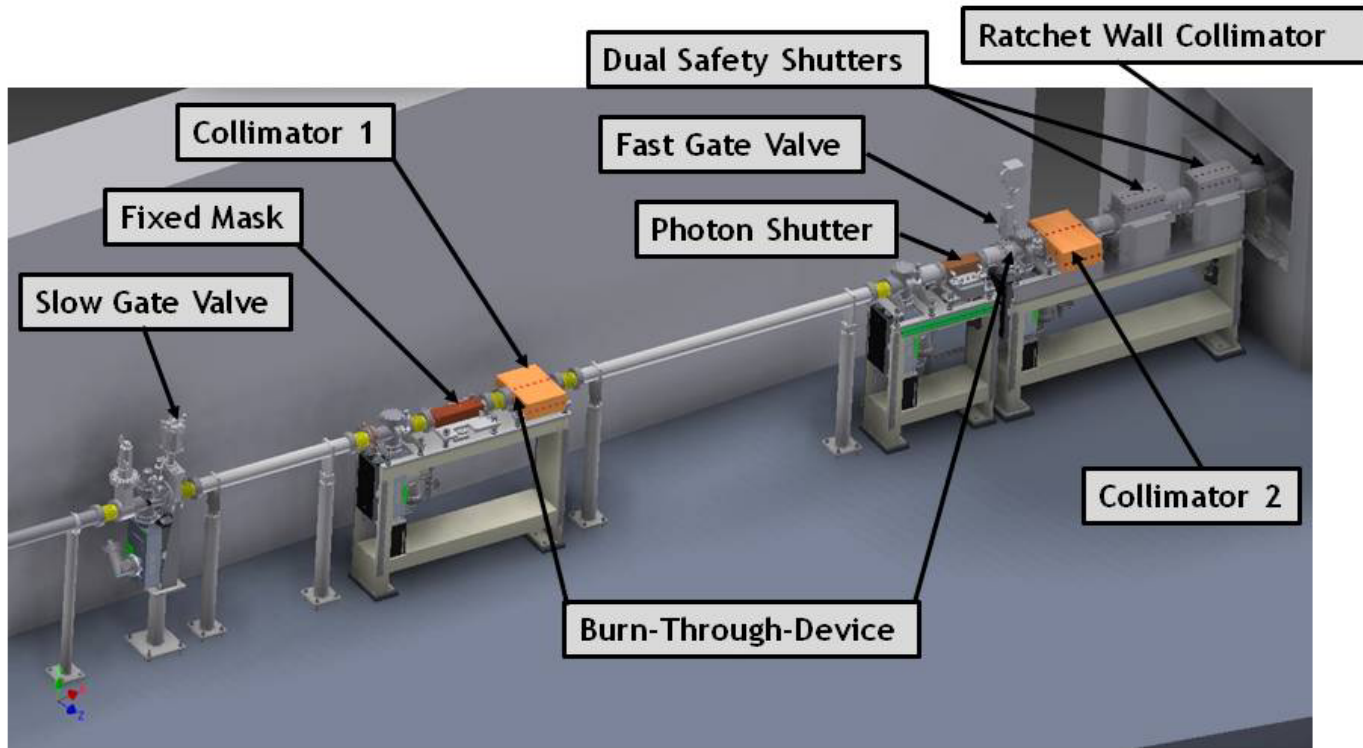


Figure 5-1. Typical front end configuration at NSLS-II, canted.

5.2 Brief Description of the Major Components of the Front End

5.2.1 Photon Shutter (BMPS) and Absorber

An absorber capable of trimming the sides of the insertion device beam will be mounted on the outlet of the bending magnet vacuum chamber immediately upstream of the front end. This absorber is required, to trim the beam in order to allow it to pass the sextupole and quadrupole magnets at the upstream end of the storage ring section four girder assembly. A maximum drift pipe size of 1.875 in. OD centered on the beam axis is allowable in this area.

The absorber is cantilevered from the upstream flange to allow thermal expansion during bakeout. A formed bellows will be mounted on the downstream flange of the absorber to allow for alignment and thermal movement during bakeout.

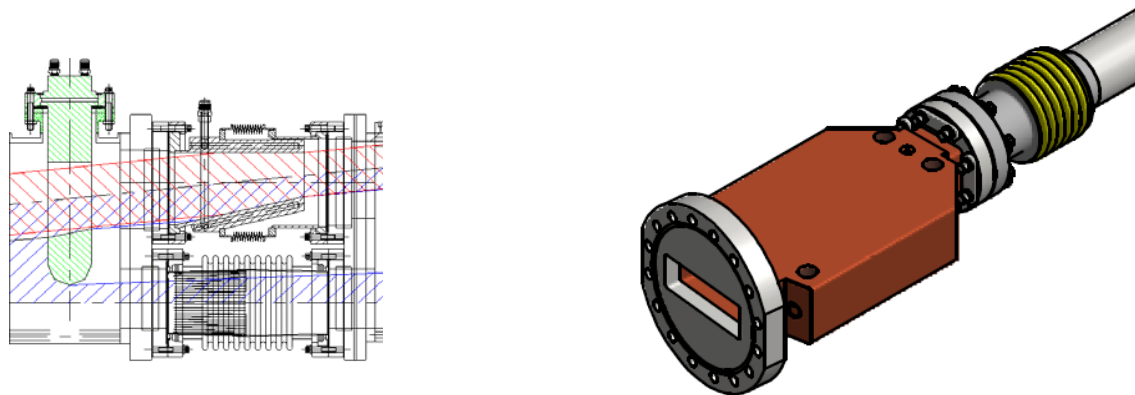


Figure 5-2. Principle of the Glidcop absorber.

The BMPS will be used to protect the SGV from bending magnet radiation if the completed front end needs to be isolated from the machine. If the SGV is required to close during machine operation, the ID power will first be reduced, followed by closing the BMPS and then the SGV.

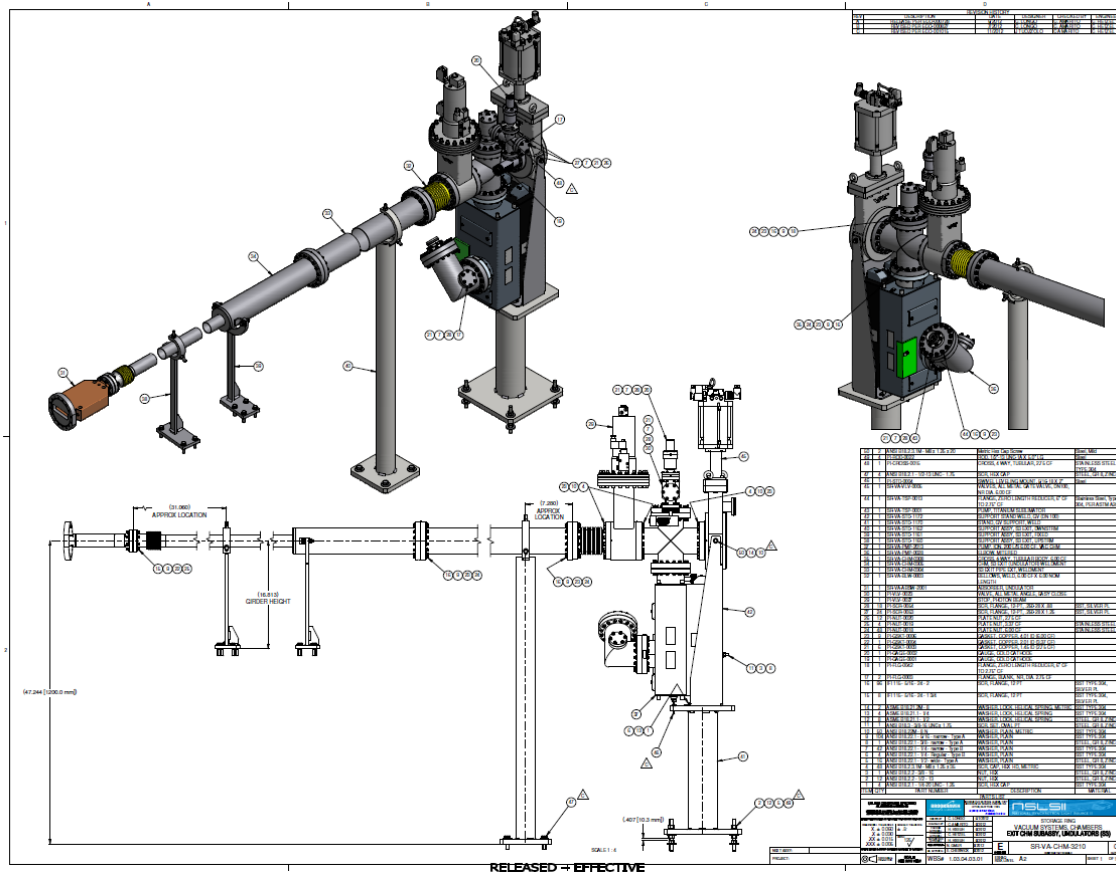


Figure 5-3. Design for the bending magnet photon shutter.

4.2.2 Slow Gate Valve (SGV)

The Slow Gate valve is part of the storage ring vacuum system and is included to isolate the machine and FE, but will not withstand white beam from IDs, or BM radiation. The SGV is controlled and monitored by storage ring vacuum PLC using a voting scheme with inputs from vacuum sensors at both sides of the valves and position of BMPs.

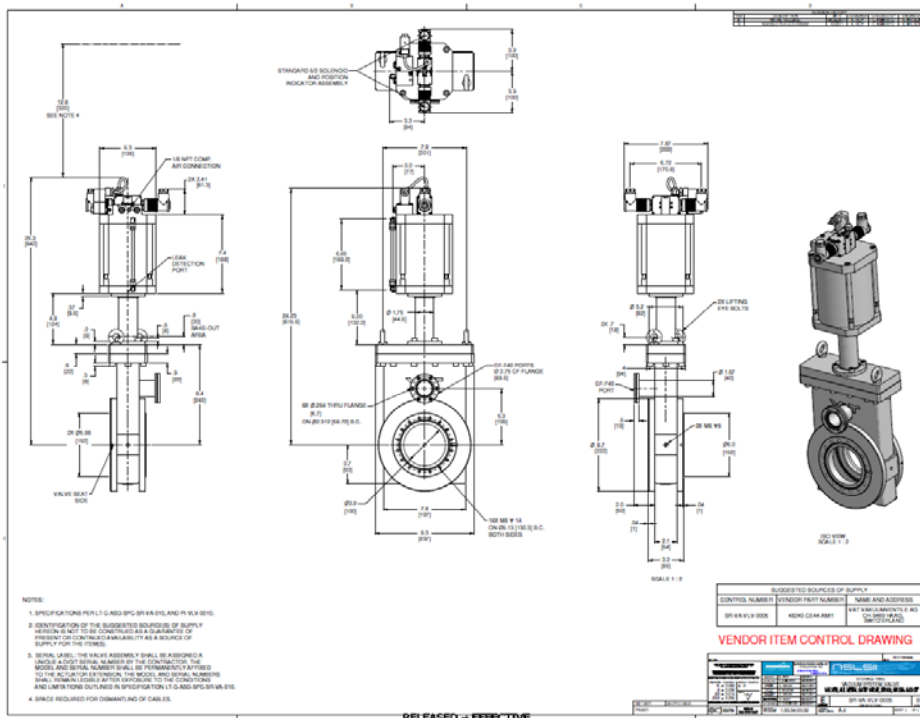


Figure 5-4.

5.2.3 Beam Position Monitor 1 (XBPM1)

The NYX Front End design has omitted the XBPM1.

5.2.4 Beam Position Monitor 2 (XBPM2)

The NYX Front End design has omitted the XBPM2.

5.3.5 Fixed Aperture Mask (FAPM)

The fixed aperture mask shall provide radiation fans to the FOE. No tolerance shall be added to the mask for mis-positioning; however, a manufacturing tolerance of ± 0.2 mm for the aperture (at the downstream end of the mask) shall be included in the downstream fan definition.

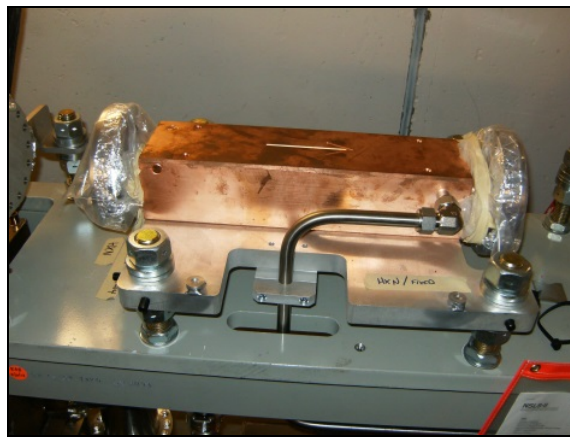
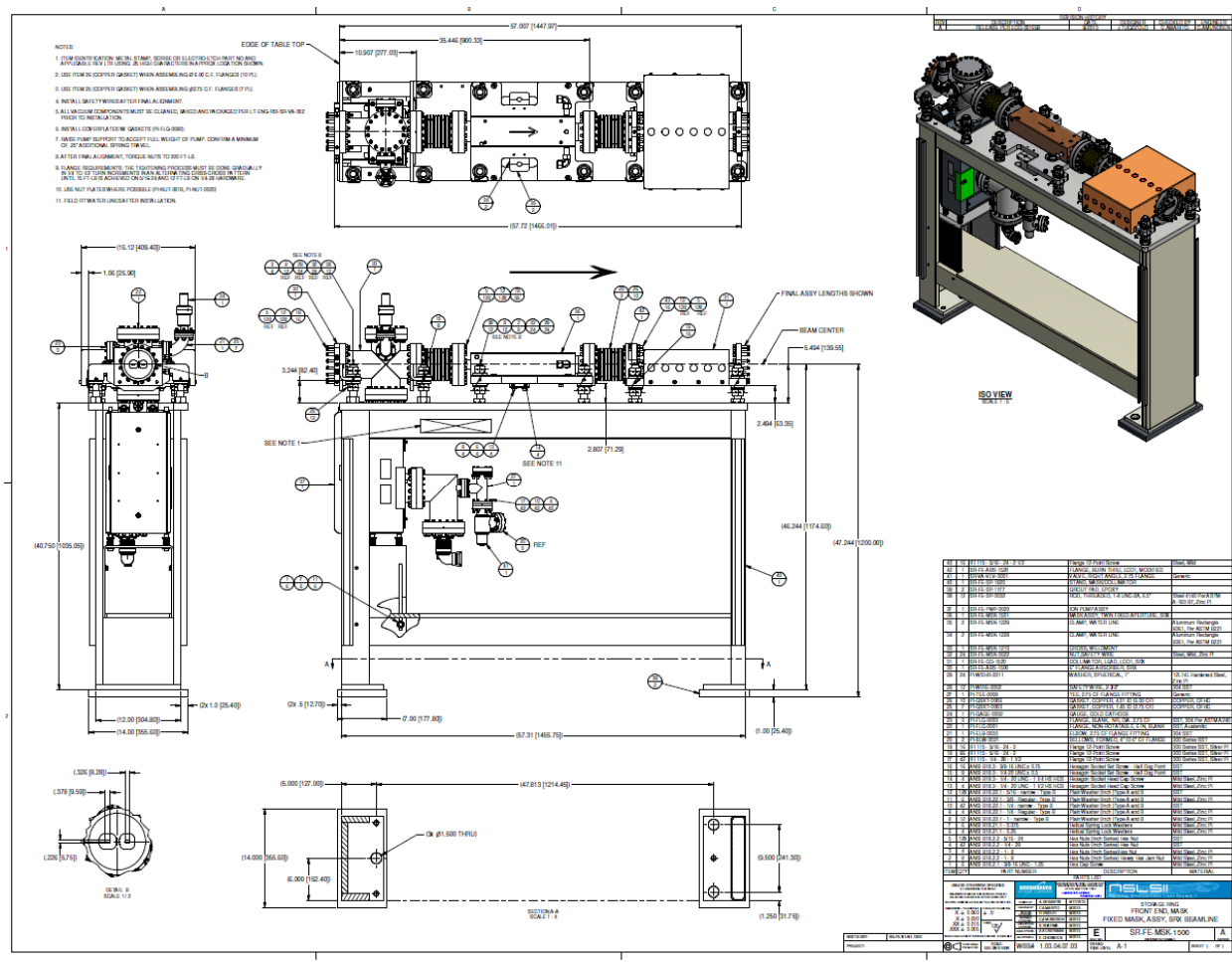
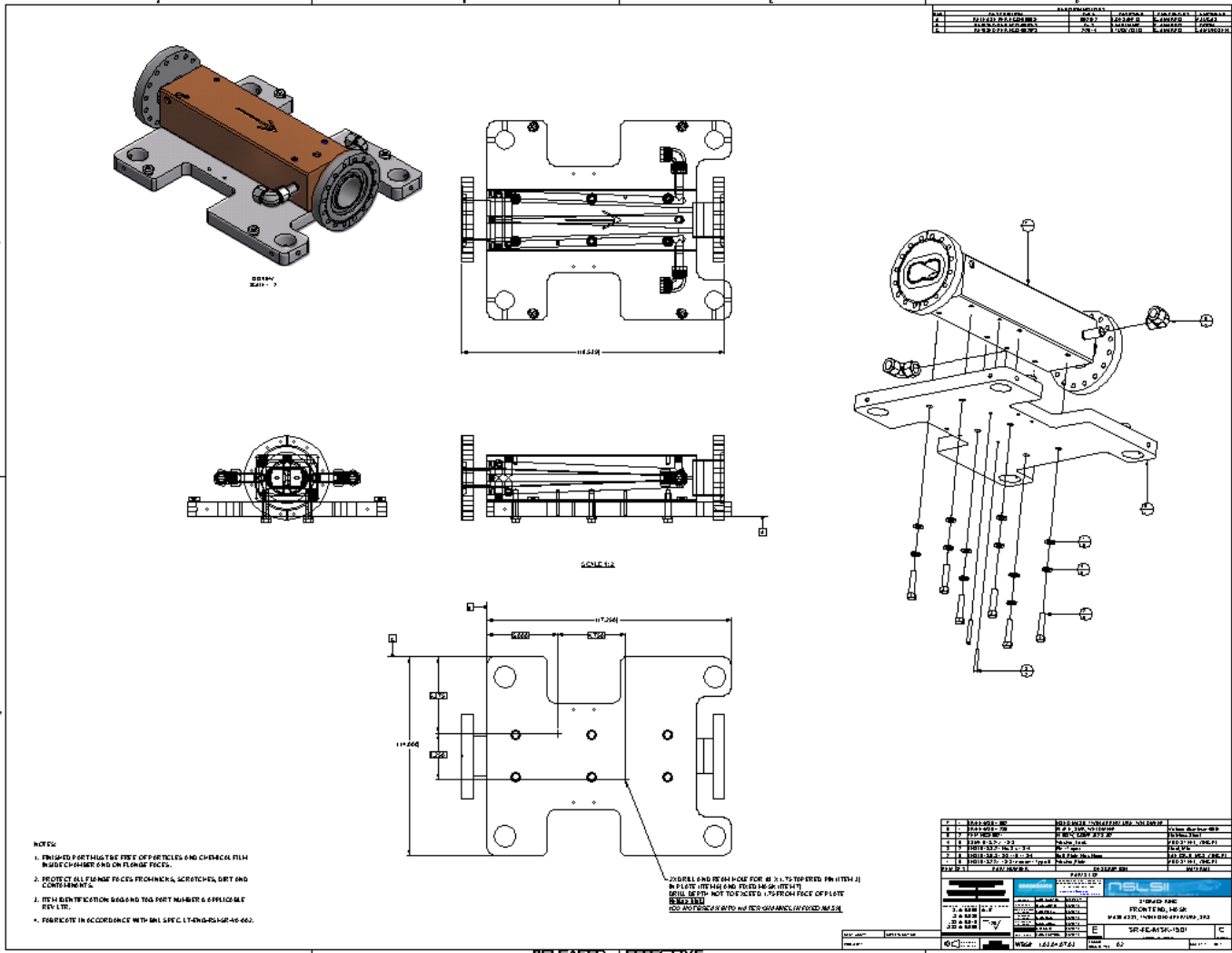


Figure 5-5. Fixed-aperture mask.





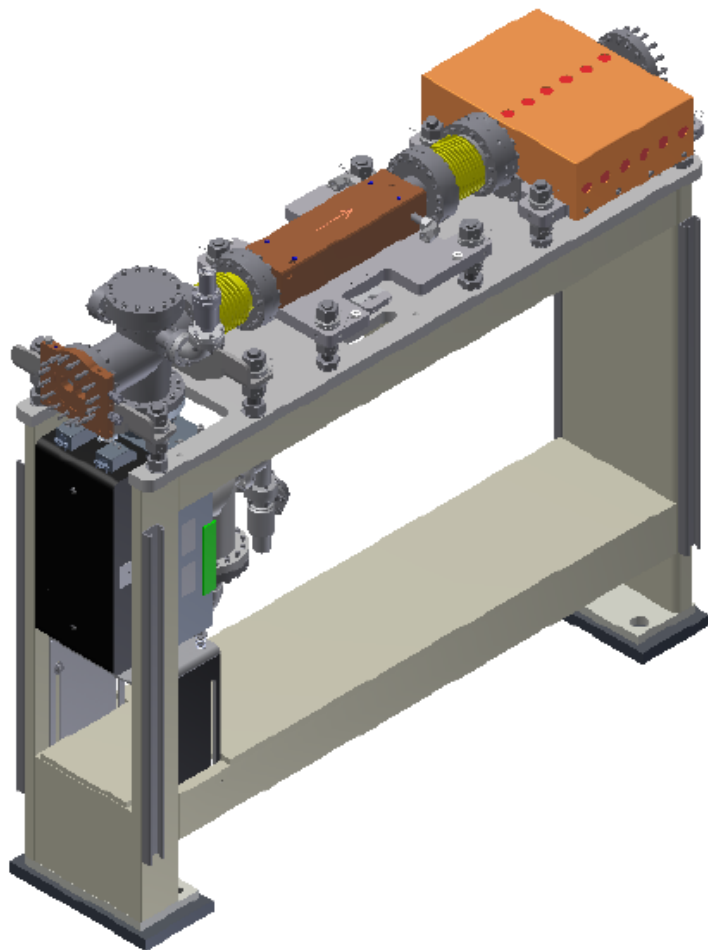


Figure 5-8. Mask mounted in the assembly.

5.2.6 Bremsstrahlung Collimator (CO1) and "Burn Through" Device

The bremsstrahlung collimator restricts the bremsstrahlung radiation fan exiting the shield wall. This should be as tight to the beam as is reasonable without undue mechanical tolerances or alignment difficulty.

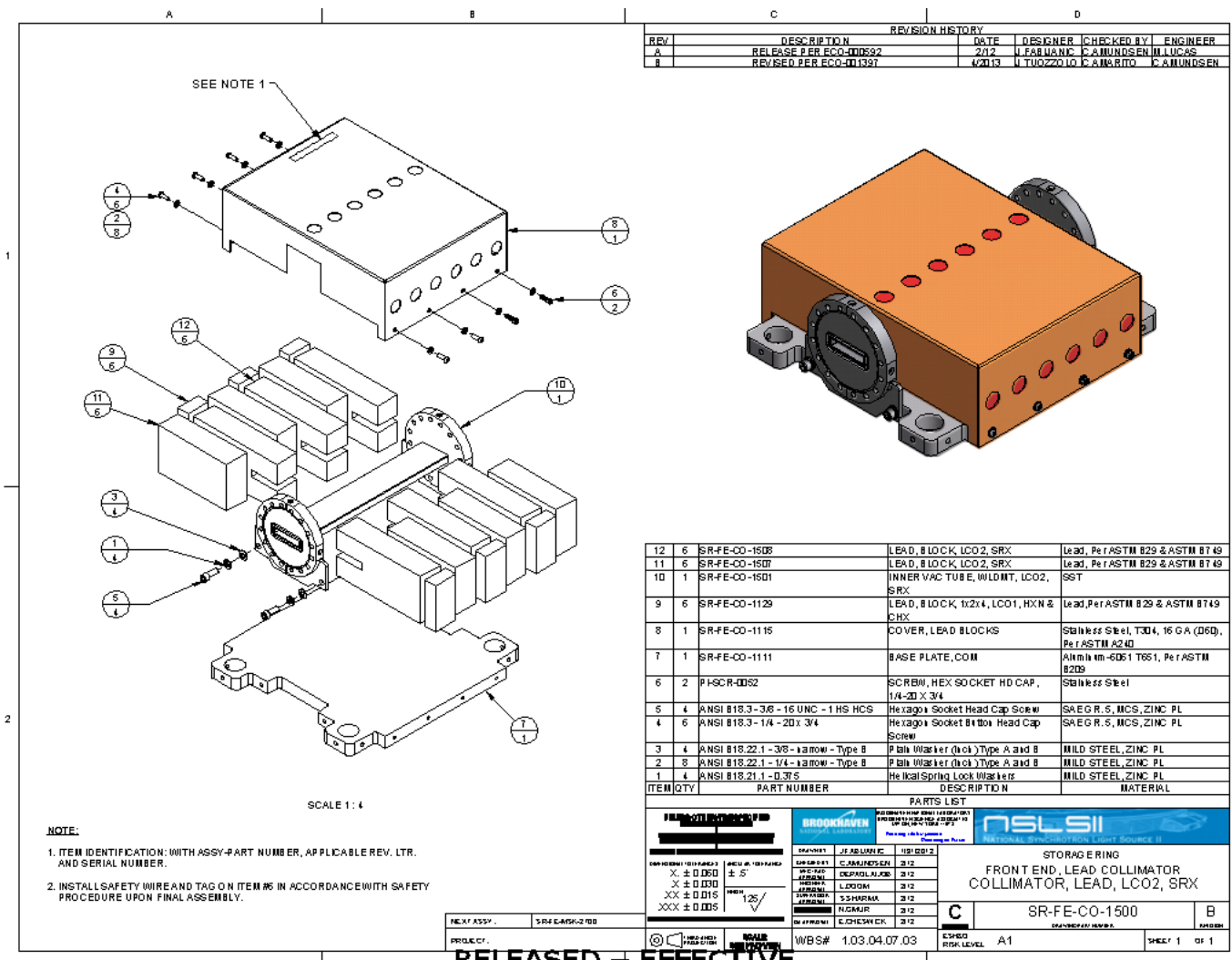


Figure 5-9. Front end lead collimator.

A Front End Personnel Protection System Task Force was assembled to review and make recommendations regarding the risks of stored electron beam excursions beyond the Active Interlock Envelopes. The Task Force recommendation being implemented is to add Burn Through Devices upstream of the lead collimators to protect the lead from melting in the case of an Equipment Protection System failure. The Burn Through Devices are designed to have apertures outboard of the maximum synchrotron fan defined by the Active Interlock Envelope. The Burn Through device will shadow the downstream lead collimator in case of beam excursions outboard of the Active Interlock Envelope or a Fixed Mask Failure. If the Burn Through Device intercepts Insertion device synchrotron beam it will vent the storage ring.

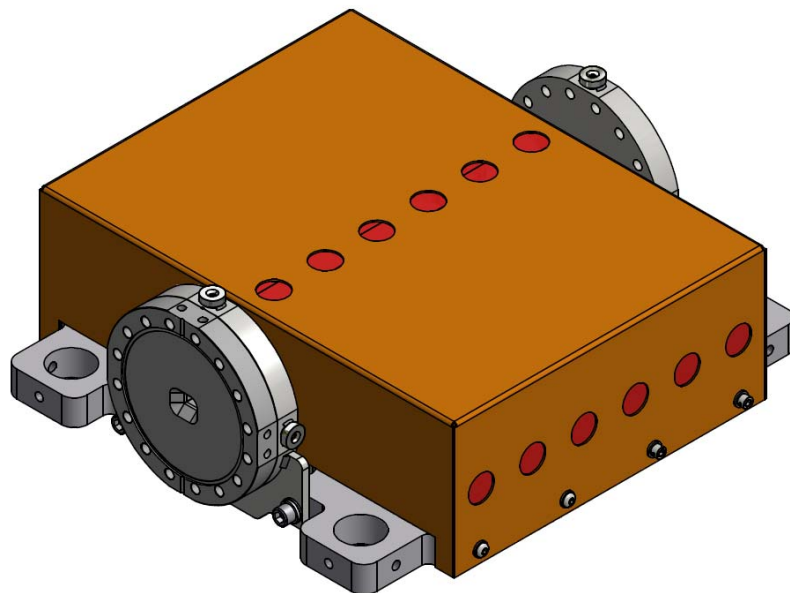
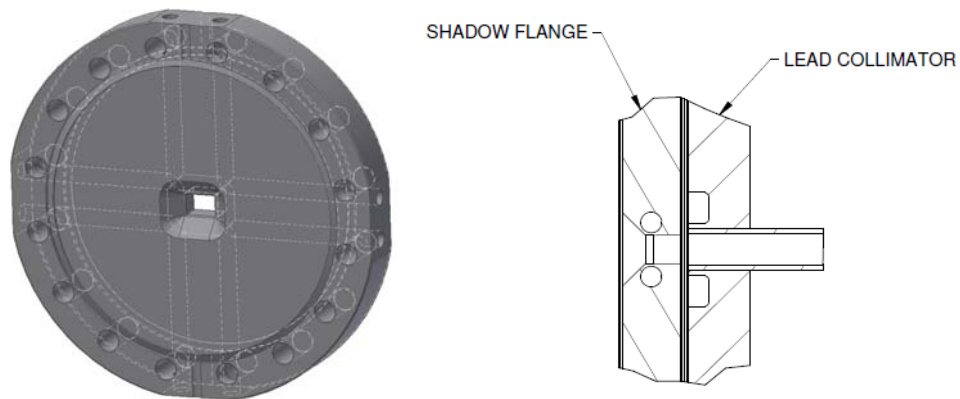
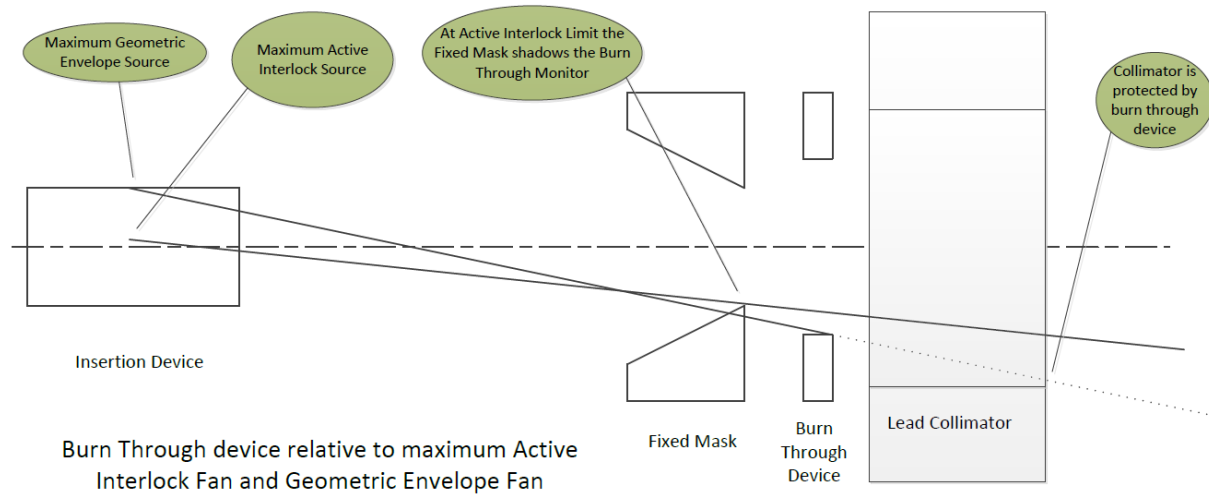


Figure 5-10. Burn Through Device Ray Tracing, Burn Through Device, Burn Through Device mounted on Lead Collimator

5.2.7 4-Y Slits

White-beam 4-Y slits usually located immediately downstream of the first lead have been omitted from the NYX Front End design, however, this space has been retained for future needs.

5.2.8 Photon Shutter (PSH)

The photon shutter is required to stop full white beam. For IDs this is a water-cooled Glidcop assembly with a grazing incidence angle.

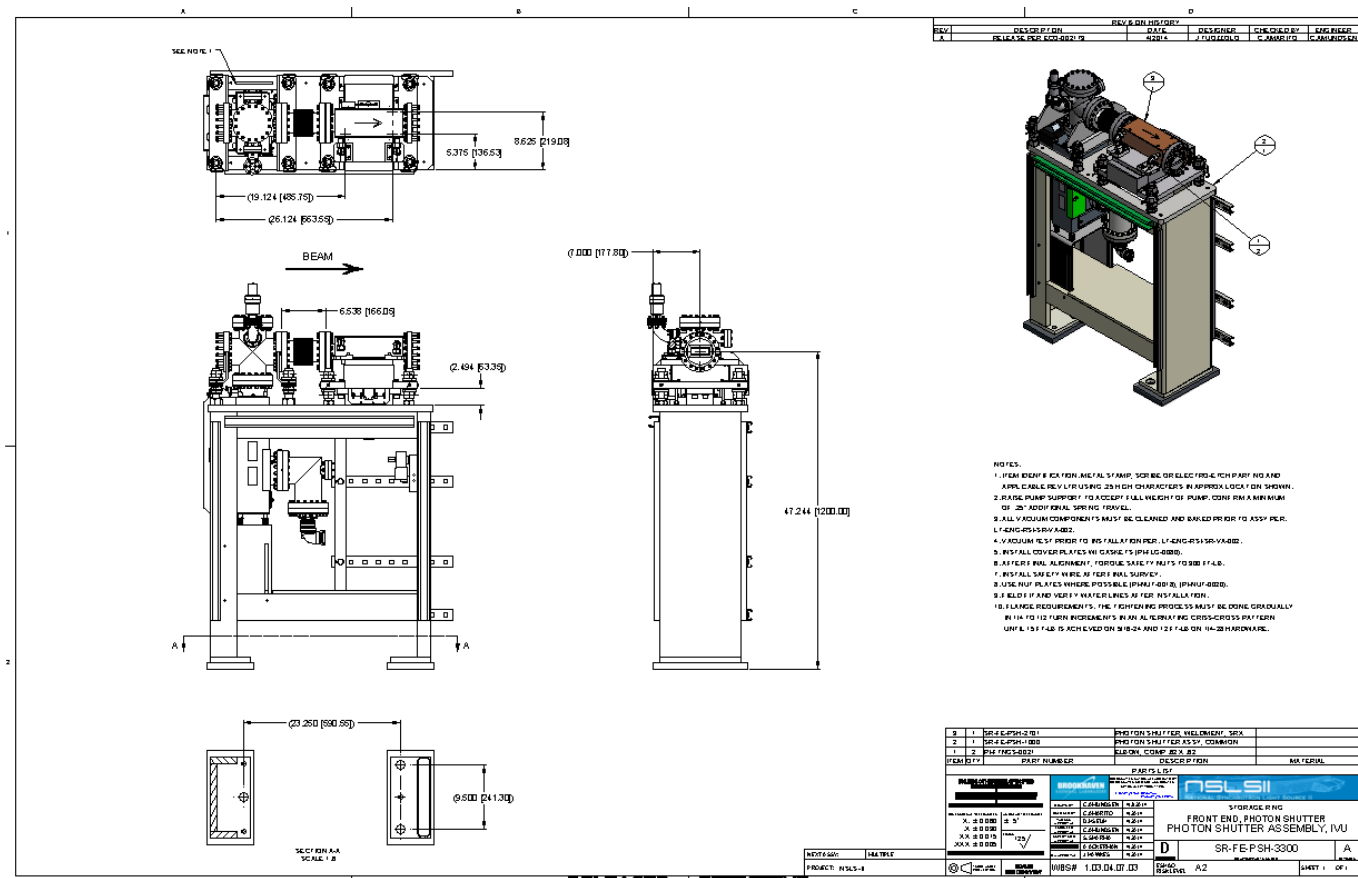


Figure 5-11. Photon Shutter Assembly

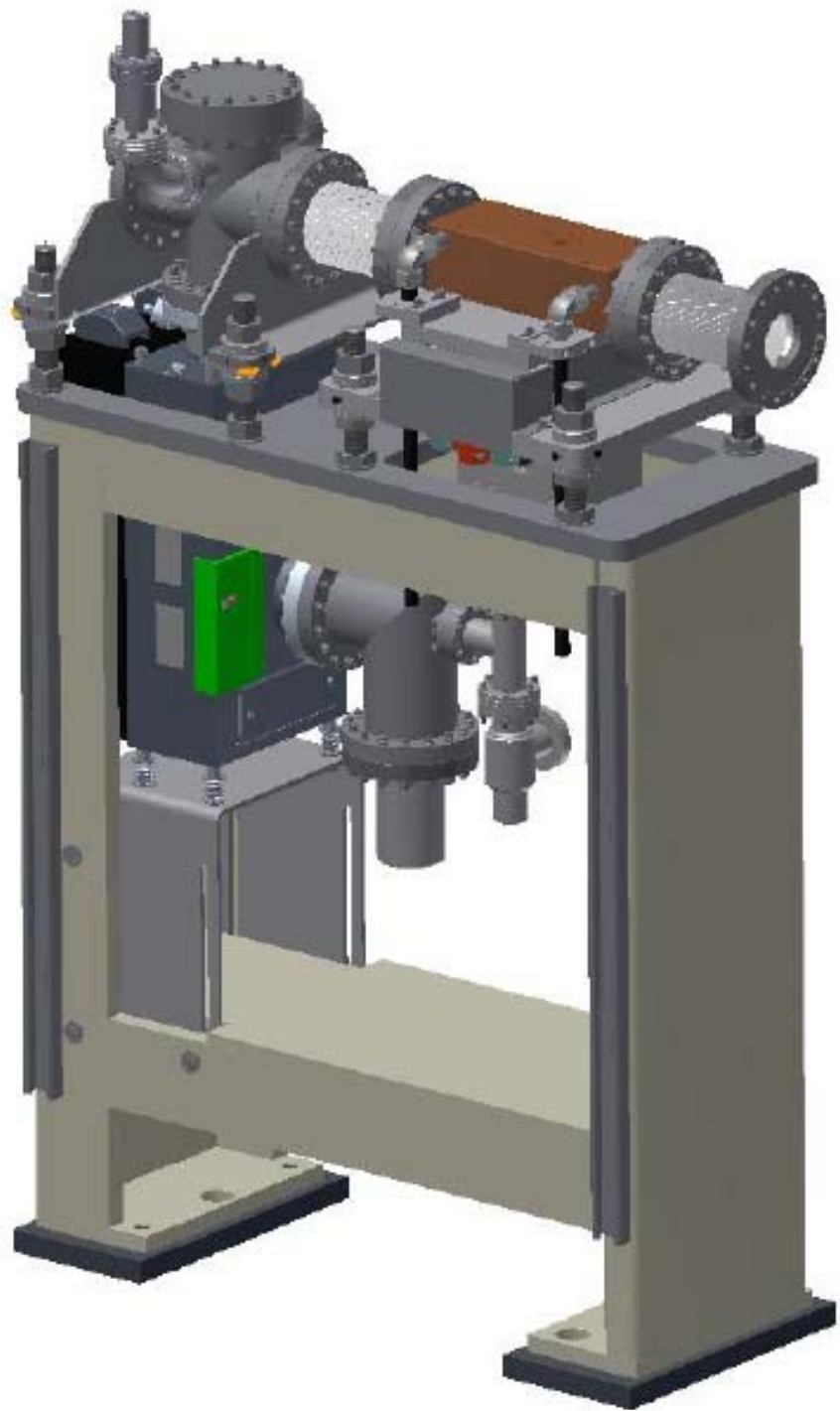


Figure 5-12. Closer view of the photon shutter.

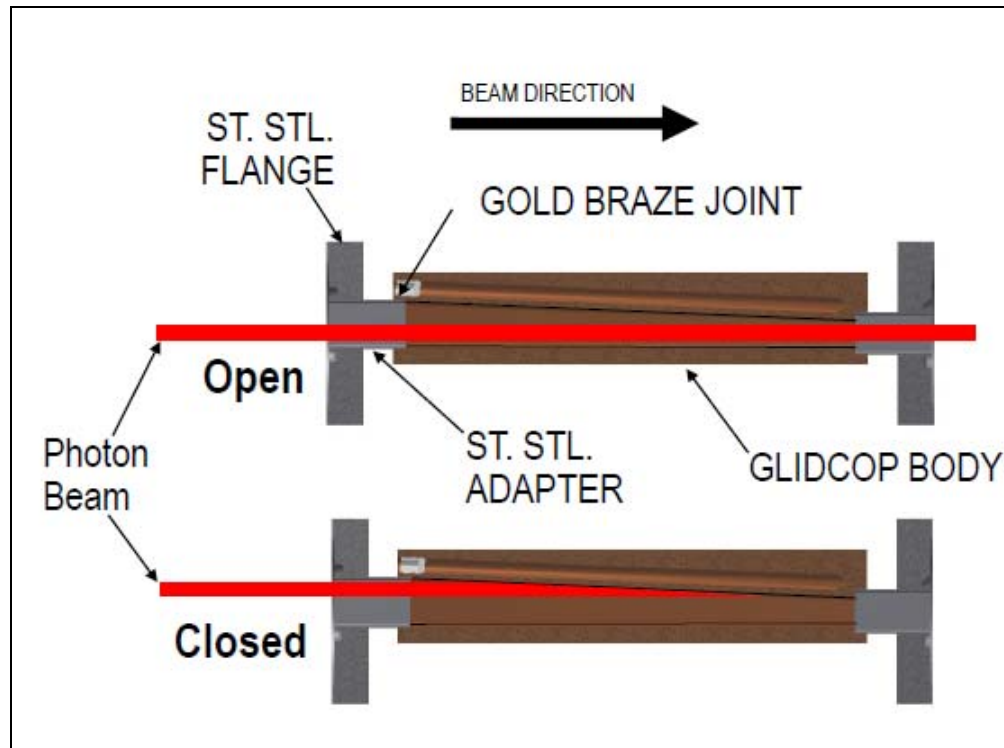


Figure 5-13.

5.2.9 Fast Gate Valve (FGV)

The fast gate valve is to shut within 12 milliseconds, once triggered by FGV sensors located in the FE and beamline whenever there is a sudden increase of pressure of a few decades. The stored beam has to be dumped prior to the FGV closing, and the cause then investigated and mitigated.

5.2.10 Bremsstrahlung Collimator (CO2).

Bremsstrahlung collimators 1 and 2 are of similar design.

5.2.11 Safety Shutter (SSH)

The safety shutter is actually a pair of shutters, required for redundancy, air actuated with independent redundant and diverse position sensing. An external lead design is being used, as shown below.

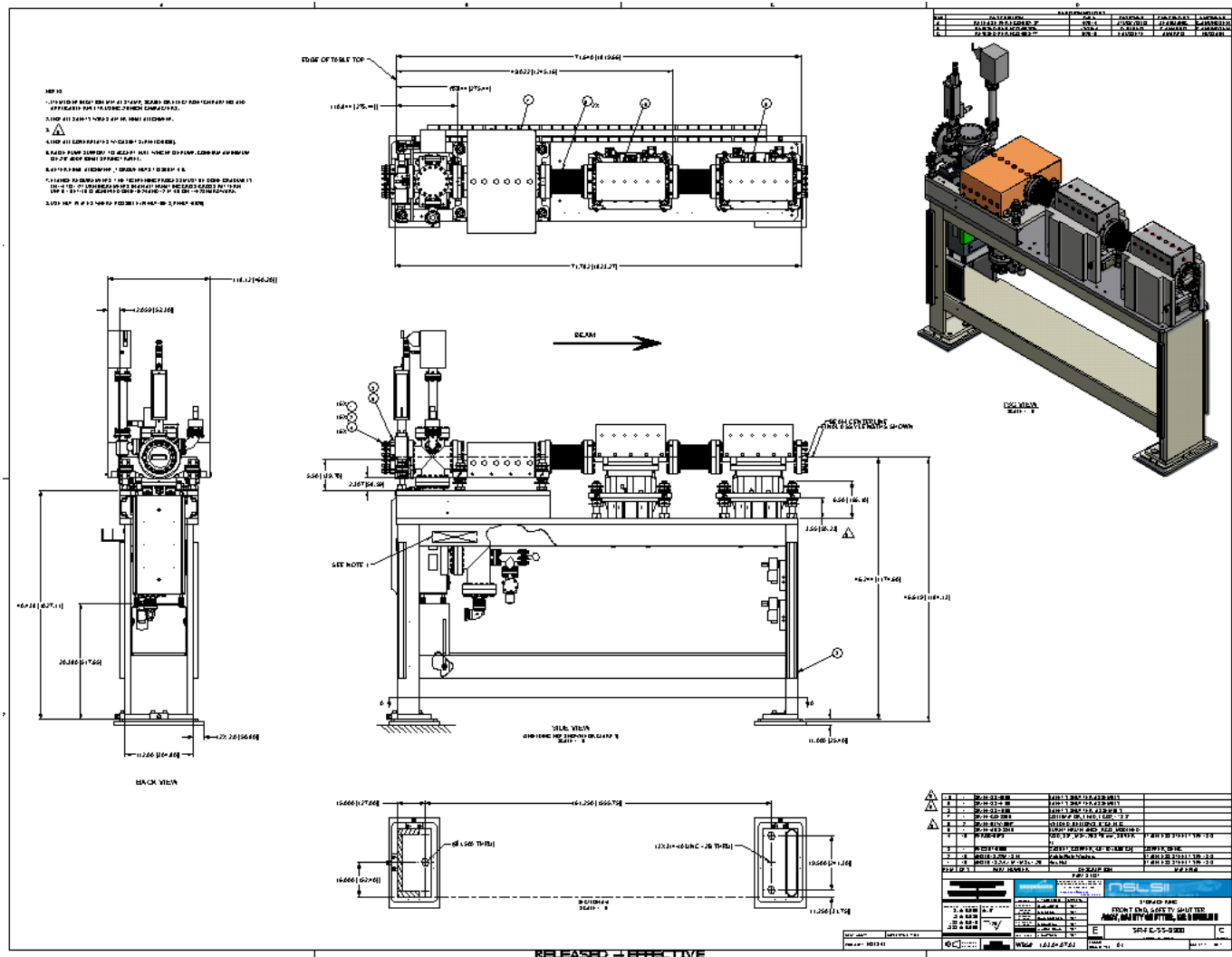


Figure 5-14. Design for the safety shutter.

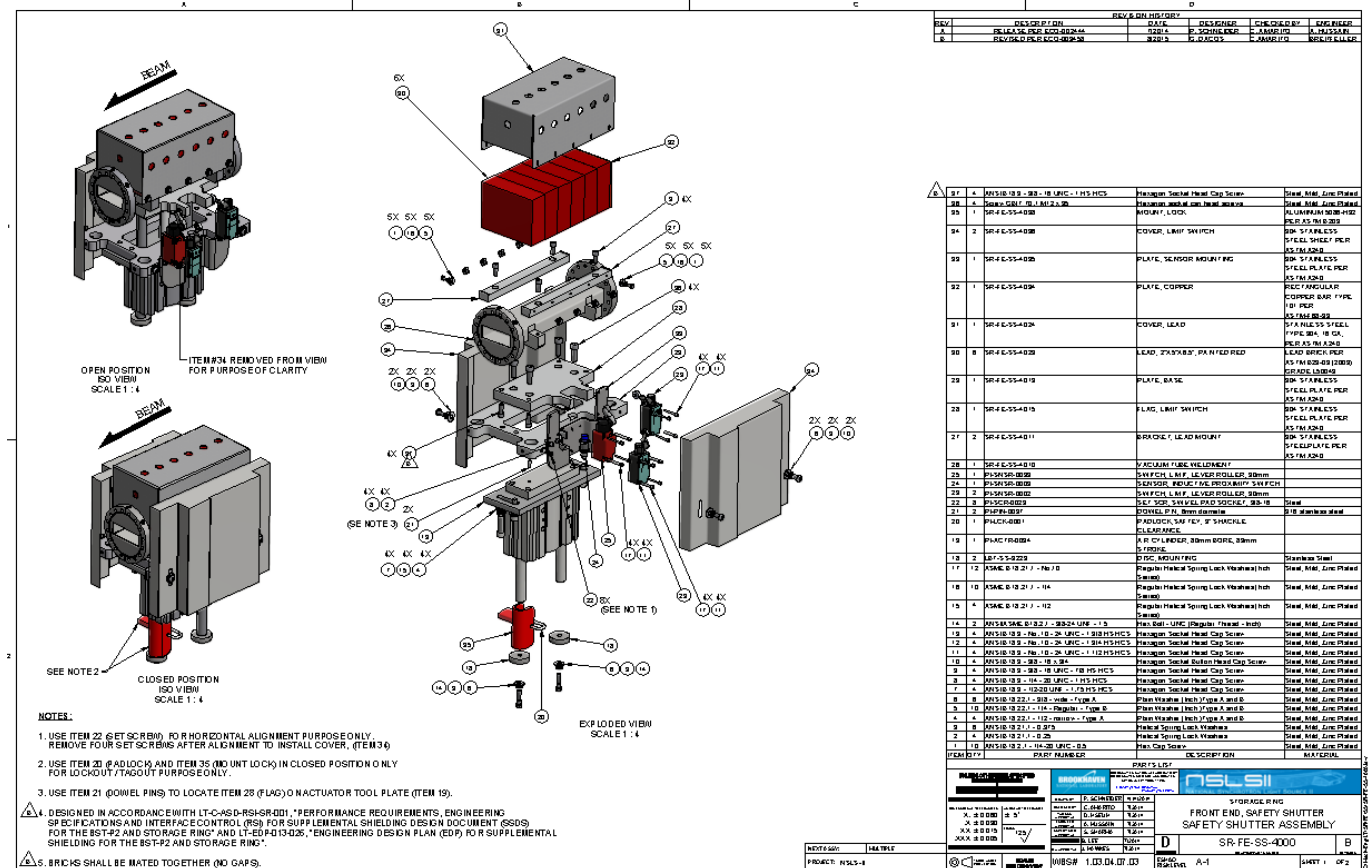


Figure 5-15. Safety Shutter

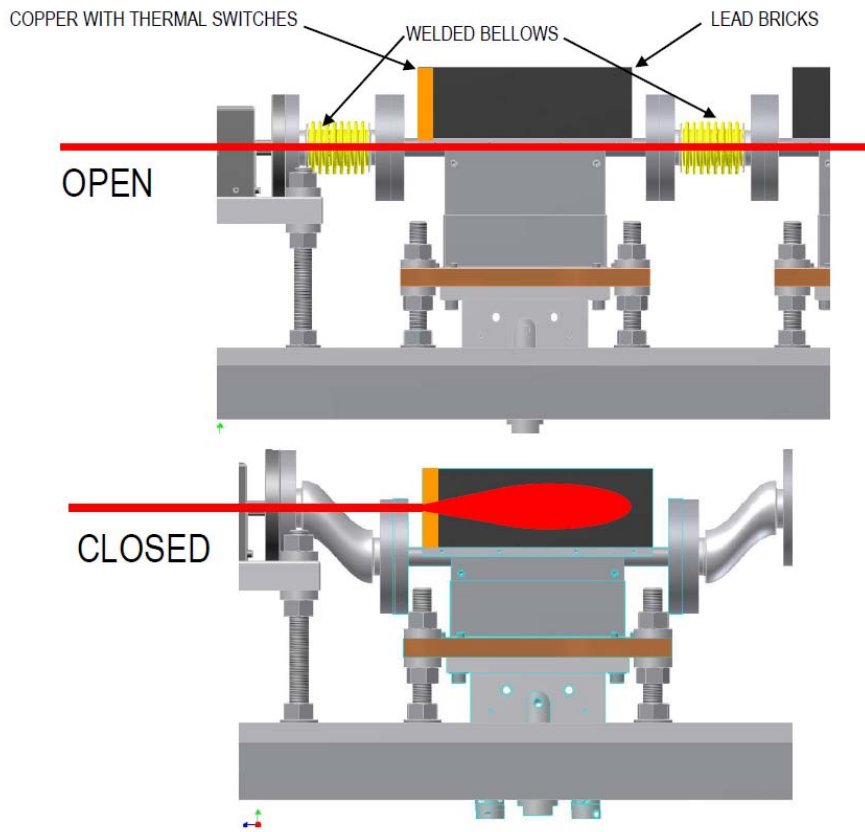
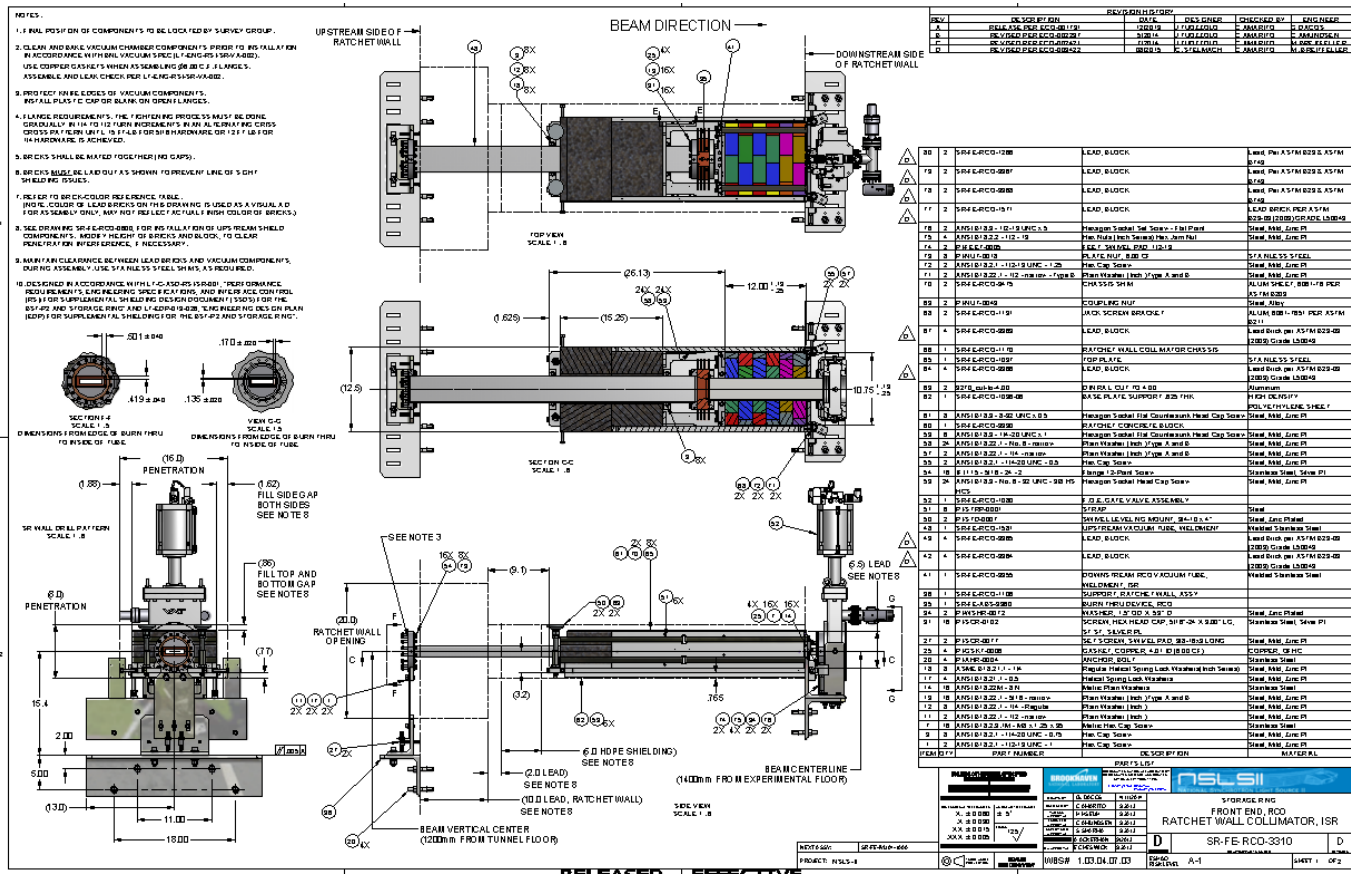
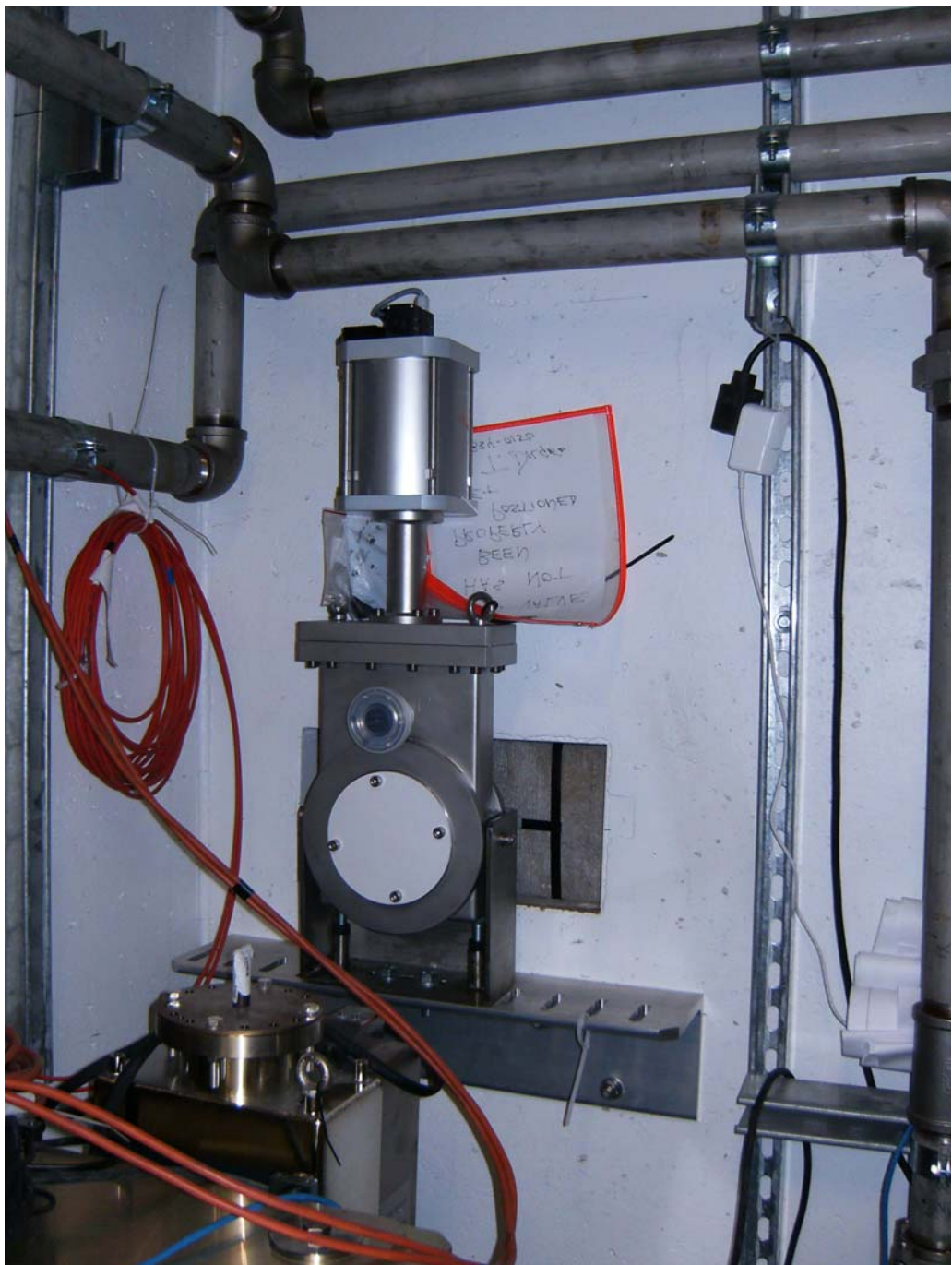


Figure 5-16. Safety Shutter Bellows Test Apparatus

5.2.12 Ratchet Wall Collimator

The design of the ratchet wall collimator is shown below. The upstream end of the collimator assembly includes 12" of lead and 6" of high density polyethylene surrounding the upstream beam pipe. The downstream beam pipe and lead provide the final Bremstrahlung collimation. The slow gate valve is mounted on the downstream flange of the beam pipe and includes a cold cathode gauge as well as a thermocouple gauge.





Note-1: This valve cannot be removed after commissioning.

Note-2: This gate valve must be protected from any exposure to beam.

Figure 5-18. Slow Gate Valve in cell 28 (XPD).

5.3 Front End ray Tracings

The NYX front end ray trace has been performed by the NSLS II accelerator group, approved by the NSLS II Radiation Safety Committee and deposited in the NSLS II drawing vault as drawing SR-FE-IVU19-1001. The pdf version of the NYX front end ray trace is available from the NYX FDR web site.

5.3.1 General Guidelines for Ray Tracings

- The origin for the dimensional convention is at the center of the straight section for the ID beamlines.
- The direction of the beam is taken as +Z direction. Beam direction is from left (upstream) to right (downstream).
- X is the direction transverse to the beam, with (+X) towards the outboard direction with respect to the storage ring, and (-X) towards the inboard direction.
- Y is the vertical direction with (+Y) as up and (-Y) as down.
- The typical scale used for synchrotron ray tracings is X:Z = 1:200 and Y:Z = 1:200.
- The typical scale used for bremsstrahlung ray tracings is X:Z = 1:50 and Y:Z = 1:50.
- All components shall be labeled with unique identifying names.
- The stopped external bremsstrahlung ray should not be closer than 3 Moliere Radii (3R) from the lateral edge of the collimator or stop. (Moliere Radius for lead is 12.5 m and for tungsten is 8 mm.)
- Lead thickness of >30 cm and tungsten thickness of >20 cm is required as stops/shutters/collimators at NSLS-II beamlines.
- Bremsstrahlung source locations for the ID beamlines (long straight) is +4 meters; for the ID beamline (short straight) is +2.5 meters.

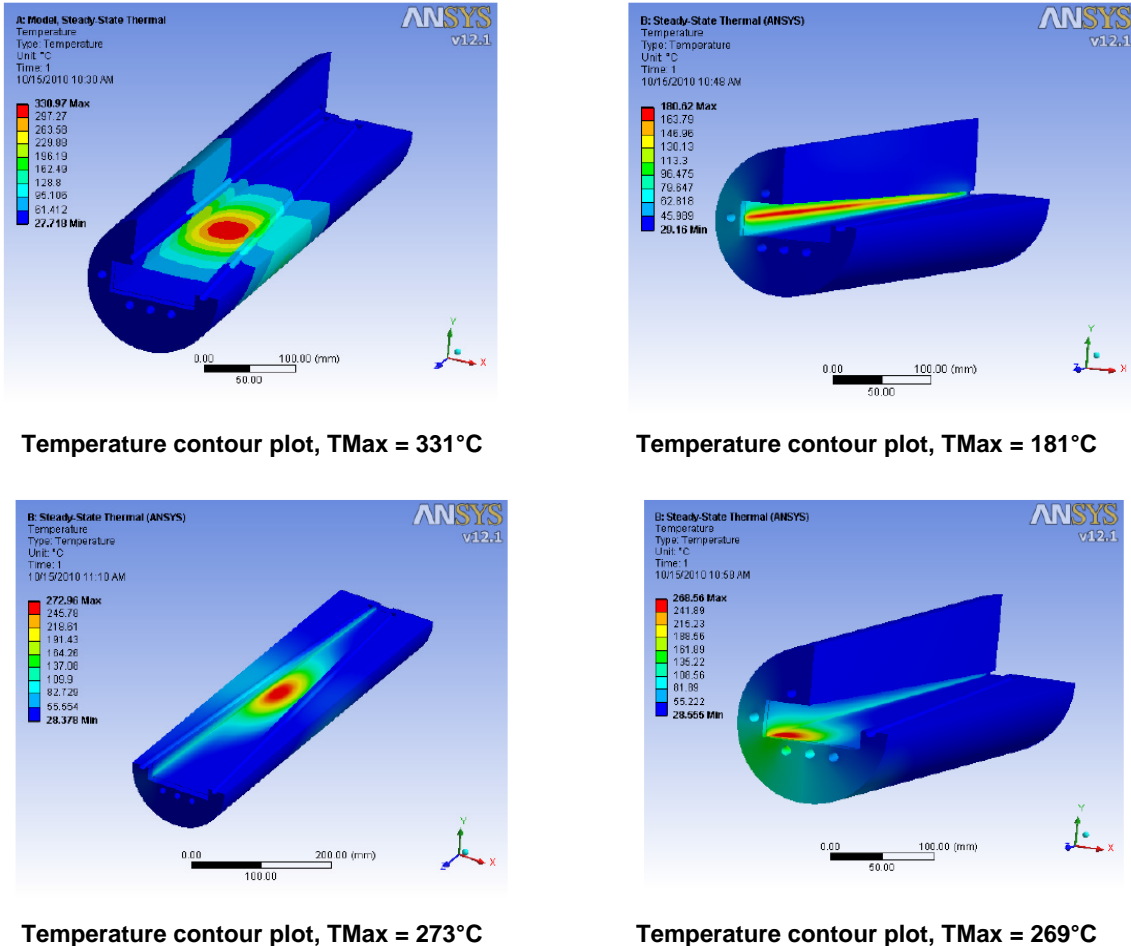
References: NSLS-II Technical Note No. 00014 and 00020.

5.4 Finite Element Analysis for the Front End

Table 5-1 Finite Element Analysis for the Front End

ID	EPU49 (CSX)		IVU22 (IXS)		DW100 (XPD)	
Total power (kW)	10		9.4		60	
Peak angular power density (kW/mrad^2)	33.4		89.8		55.5	
Components	Fixed mask	Photon shutter	Fixed mask	Photon shutter	Fixed mask	Photon shutter
Location (m)	18.93	21.63	20.19	22.88	20.19	22.88
Fixed mask exit aperture (mrad)	0.6(h) x 0.6(v)		0.5(h)x0.3(v)		1.1(h) x 0.15(v)	
P_Absorbed (W)	5	5	2.4	7	52	8
Peak power density (W/mm^2))	93	73	220	172	136	107
Horizontal taper angle (°)	4.5		3		4	
Vertical taper angle (°)	4.5	7	.2.7	3.5	2	3
Peak temperature (°C)	344	258	265	257	331	268
Peak von Misses Stress (MPa)		352		425		424

FIXED MASK



PHOTON SHUTTER

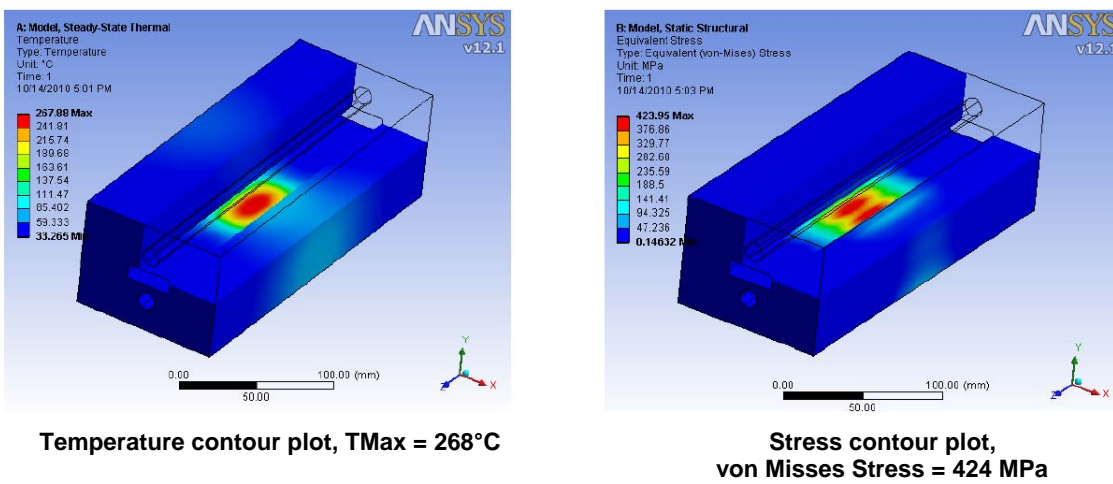


Figure 5-19. Thermal calculations on the Glidcop mask and photon shutter.
(Courtesy of V. Ravindranath)

6. Radiation and Vacuum Containment

Conventional vacuum tubulation, pumping and gauging will contain the beam path from the front end through the optical elements and into the experimental end station. This vacuum beam path passes through three radiation containment enclosures that contain all beamline components (Figure 6-1).

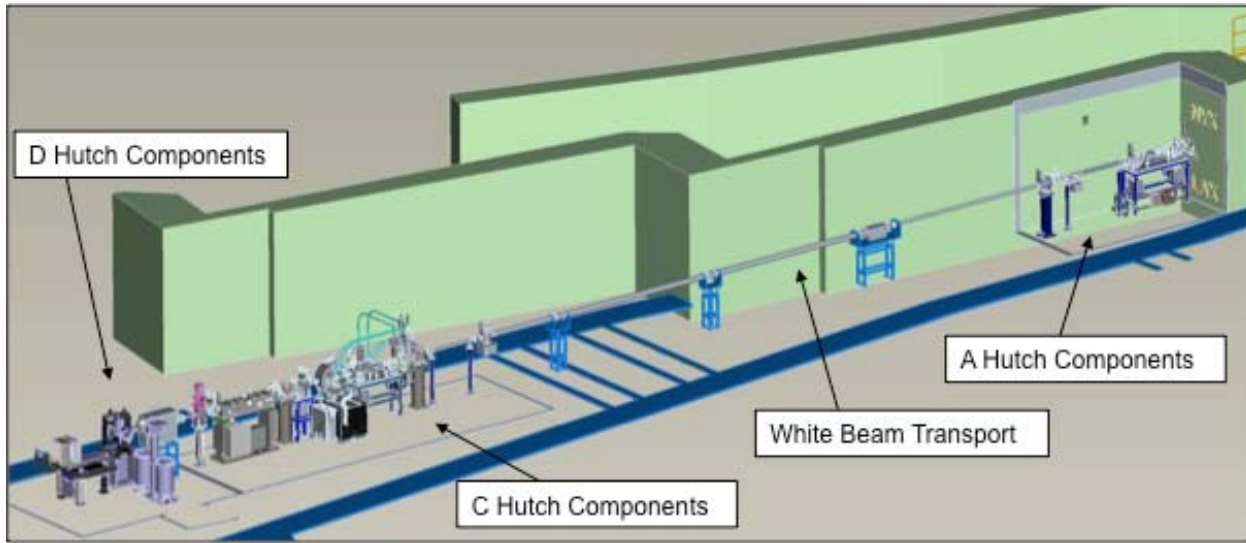


Figure 6-1. Beamline layout in radiation containment elements

6.1 Beampath Component Packages

The NYX beamline components are organized into two major groups, which contain either optical elements or non-optical elements. Details of the optical elements, such as diffracting and reflecting elements, will be described in Section 7 of this document on the photon delivery system. The non-optical elements, which are described in this section, have the primary purpose of passing the useful synchrotron radiation to the Photon Delivery System while restricting the undesirable portion of the synchrotron radiation as well as restricting the passage of bremsstrahlung radiation. These components primarily condition the beam for the downstream NYX beamline. The various elements are grouped into “Component Modules” that are described in this section: “LAX Hutch Components”, “White Beam Transport”, “Diagnostic Module 1” and “Diagnostic Module 2”. “Diagnostic Module 1” intercepts the white beam upstream of the monochromator and “Diagnostic Module 2” intercepts the vertically offset monochromatic beam downstream from the monochromator. The “LAX Hutch Components” are located in Hutch A. Both “Diagnostic Module 1” and “Diagnostic Module 2” are located in Hutch C. The component packages “LAX Hutch Components”, “Diagnostic Module 1” and “Diagnostic Module 2” contain water-cooled masks, apertures and collimators that are designed to manage the expected heat load from the 2-meter long IVU described Section 4 above. These three component packages will be manufactured by FMB-Oxford, who have produced the detailed Finite Element Analysis (FEA) that is deposited at the FDR website.

6.1.1 LAX Hutch Components

The “LAX Hutch Components” (Figure 6-2) are designed to accept the incoming canted undulator beams, separated by 2mrad, provide a space for a future, large-offset monochromator off the inboard beam and allow the outboard beam to pass downstream to the NYX hutch.

Ports are provided for mounting diagnostic elements, however the diagnostic elements themselves are not included.

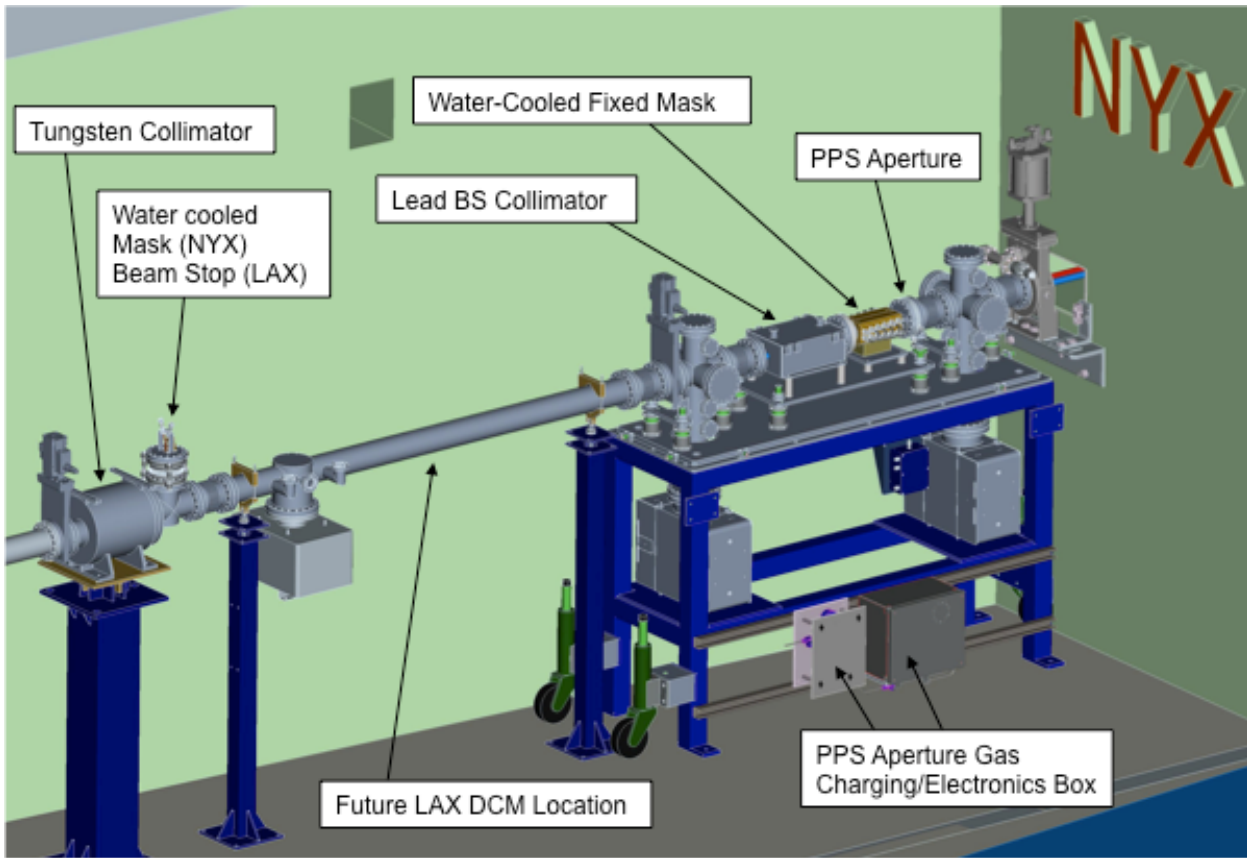


Figure 6-2. LAX hutch components. The LAX hutch is also known as Hutch A.

6.1.2 Beamlne Component Module 1

Beamlne Component Module 1 is located immediately upstream of the DCM and includes a single aperture mask, BS collimator, cooled filter unit and a cooled Fluorescent Screen (complete with camera) on a mild steel support frame.

White Beam Filter Assembly. The filter materials are mounted on a water-cooled OFHC copper filter holder. Each filter holder has provision to mount 4 filters up to 2mm thick. The unit also accommodates an out of beam position. The filter material is clamped against a lapped copper surface using a sprung loaded clamping plate.

The filter system is based on FMB's proven filter mechanism which is already installed at various facilities on undulator beamlines including NSLS II, ANKA and Soleil. The filter system comprises two independently actuated filter holders (Figure 6-3) mounted on the same DN200CF flange. The filters can be actuated to allow for any combination of two filters.

The filter holders move along external and in-vacuum guides to ensure that they remain parallel to each other. A stepper motor and gearbox driven precision actuator moves each filter holder. The actuator operates through a bellows assembly mounted on the flange.

Each actuator has two limit switches at each end of the travel. These switches are to stop the motor driving the actuator into the end stops. The limit switch actuators are adjustable to set the end of

travel position. The first switch acts as a soft limit while the second acts as a “kill switch” which actuates if the system travels through the soft limit

Each independent filter holder is directly encoded by attachment of a Renishaw TONIC encoding system, which allows for repeatable positioning for different filter combinations.

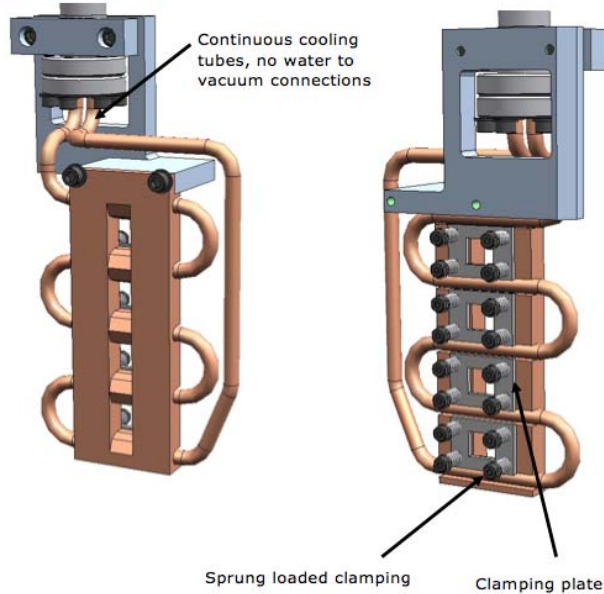


Figure 6-3. Front and rear views of the filter holder

Fluorescent Screens. The white-beam screen, FS1, uses a doped CVD diamond foil mounted on a water-cooled copper absorber block to image the beam (Figure 6-4).

The monochromatic beam screens, FS2 and FS3, use YAG crystals to image the beam.



Figure 6-4. YAG Fluorescent Screen Assembly. The white-beam water-cooling block is not shown.

Fluorescent Screen Actuation. The pneumatically-actuated fluorescent screen is mounted onto a Conflat and the camera/lens unit is mounted to the viewport to image the beam.

The Actuator consists of two fixed Conflats joined via edge welded bellows. A hollow shaft is welded to the top Conflat and travels through the inside of the bellows. Attached to each Conflat of the bellows are the actuator plates. The top plate is where the slide rods are fixed. Roller switches are attached to each end of travel to give 2 end of travel feedback.

Cameras. Prosilica CCD cameras in accordance with NSLS-II specifications are fitted to each fluorescent screen (Figure 6-5).

A CCD camera is mounted on a viewport so that it has a clear view of the CVD diamond foil. The CCD camera allows positional and spatial information about the X-ray beam to be viewed remotely.

The camera mount is designed to clamp onto a DN63 4 1/2"CF. The mount provides adjustment to help in the setup of the system.

EPICS drivers for the cameras produced by FMB-Oxford will be delivered to NYX.



Figure 6-5. GC-Series Camera

6.1.3 Beamline Component Module 2

Beamline Component Module 2 (Figure 6-6) is located immediately downstream of the DCM and includes a white beamstop, BS stop and Fluorescent Screen FS2 (complete with camera) on a mild steel support frame.

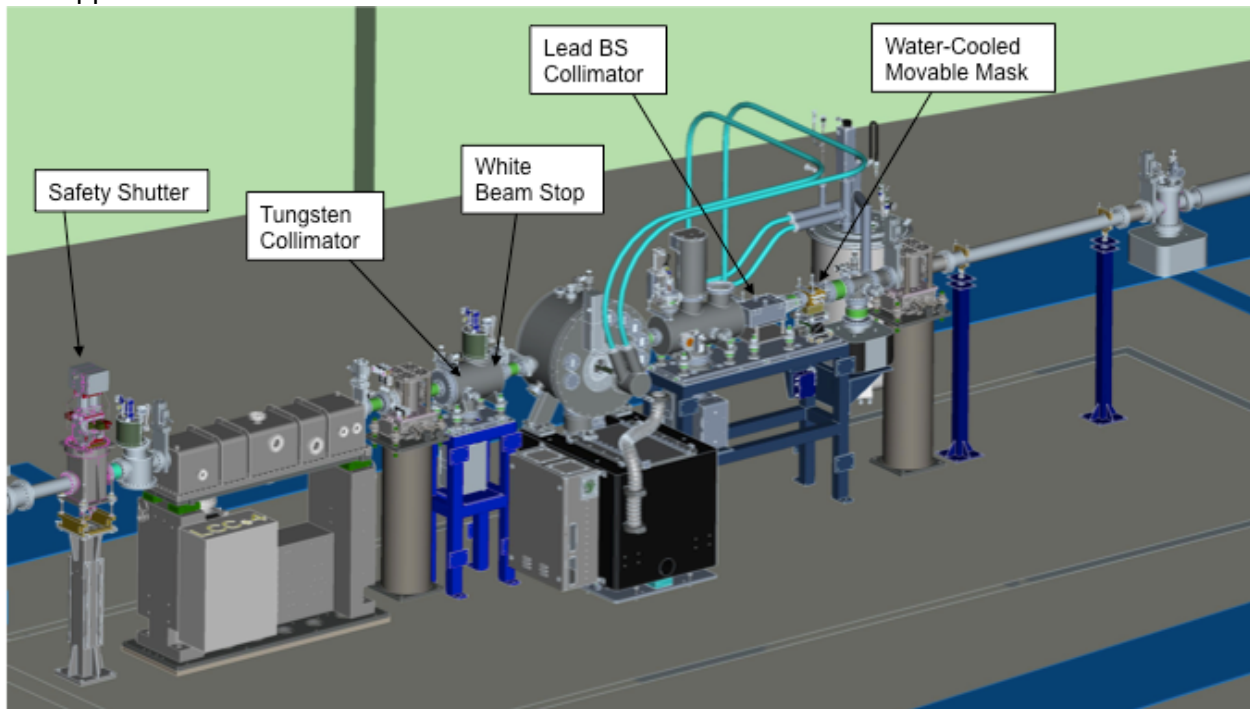


Figure 6-6. Beamline Component Module 2

6.1.4 4-Jaw Slits

A set of 4-jaw slits is located on the exit port of the 2nd diagnostic stand and is used to aperture the beam entering the Vertically Focussing Mirror.

The four blade in flange slit unit comprises of two pairs of horizontal and vertical beam slits. Each slit unit consists of two slit blades and defines either the horizontal or vertical dimension of the beam. The slits are able to close in both directions. The slit blades move along in-vacuum guides to ensure that they remain parallel to each other. Each slit blade is moved by a stepper motor with two limit switches and encoder.

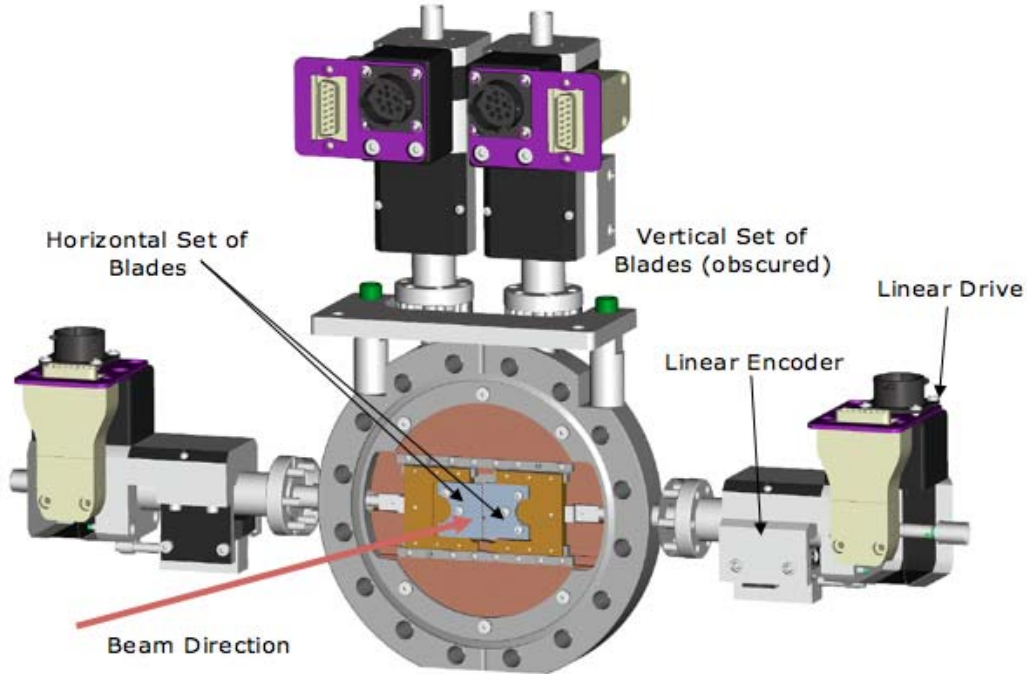


Figure 6-7. 4-Jaw Slit

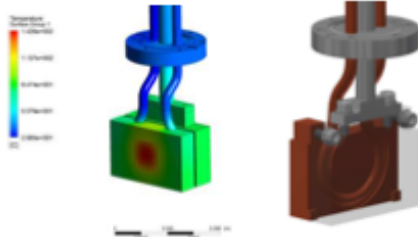
6.1.5 Fluorescent Screen 3 (FS3)

A third motorized, uncooled Fluorescent Screen is mounted onto a flange of the Diagnostic Stand downstream of the VFM to image the beam exiting either the VFM or directly from the DCM. Details of the FS are contained in the relevant previous section.

6.2 Beampath Photon Shutter

Johnsen Ultravac has successfully developed a dual-shutter style photon shutter for various beamlines operating in state of the art synchrotron facilities, some of the advantages of our photon shutter are listed below:

1. The beamline photon shutter assembly (see right) consists of an Ultra-High Vacuum (UHV) vessel with two aperture blocks and two water-cooled shutters that are controlled by two independent actuators.



2. The overall shutter block provides sufficient thermal protection: The photon shutter blocks are designed and fabricated for a minimum of 1.15KW of heat energy incident upon either shutter block applied over an area of 25mm x 25mm centered vertically and horizontally on the shutter block face with a maximum heat density of 2.7W/mm². One formed 5/16" OD x 0.035" wall OFHC copper tubing is vacuum brazed into the groove of Glidcop block to eliminate the direct water-to-vacuum joints. The maximum temperature on Glidcop block is under 150°C with 2.52L/min water flow rate (see left).

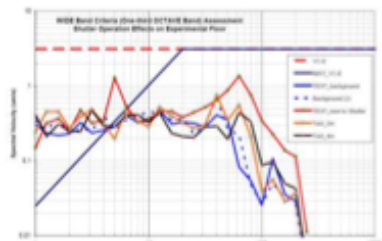


3. Tungsten alloy ≥95% W, for radiation protection, detailed specifications are: Shutter Block: 80 W x 50 H x 19.05 T (mm); Aperture Plate: 125 W x 150 H x 19.05 T (mm) with a 40 W x 25 H (mm) aperture in the center. The thickness of tungsten shutter can be increased upon customer's request.

4. Two identical actuators with 2.5" bore and 2" stroke are used to independently move each shutter block. The actuators are designed to be fail-safe; the shutters are fully closed upon loss of actuator supply power (e.g., loss of air pressure and/or electrical power). When the shutter is commanded to close or when a loss of actuator power/ air pressure occurs, both shutter blocks will fully close with sufficient overlap – 10mm and keep the minimum gap (less than 1.0mm) between the aperture plates at all times, so that no radiation leakage downstream of the shutter occurs.

5. The all-metal CF flange structure allows repeated bake-out of all in-vacuum components at 200C max.

6. Our compact design, with 300mm overall length from upstream to downstream, provide maximum space for other beamline components which may be located on either end.



7. The overall structure of the photon shutter is designed & manufactured to minimize shock and vibration transfer to the supporting beamline as well as the experimental floor resulting from opening or closing of the shutter blocks. The First Item Tests were performed and the vibration levels transmitted to the experimental floor were much lower than the VC-E curve criteria (see left) The provisions of shock/vibration in actuator, chamber support and stand are optional features.

8. Competitive both on pricing and delivery due to the proficient design, excellent QA system, outstanding workmanship and zero failure rate of our products.

9. The redundant PPS interlock, provisions for safety and tamper-resistance will satisfy all synchrotron facility requirements globally. All materials, coating and finishes are capable of withstanding prolonged exposure to x-ray radiation.

6.3 White-beam Transport and Shielding Validation

6.3.1 White-beam Transport

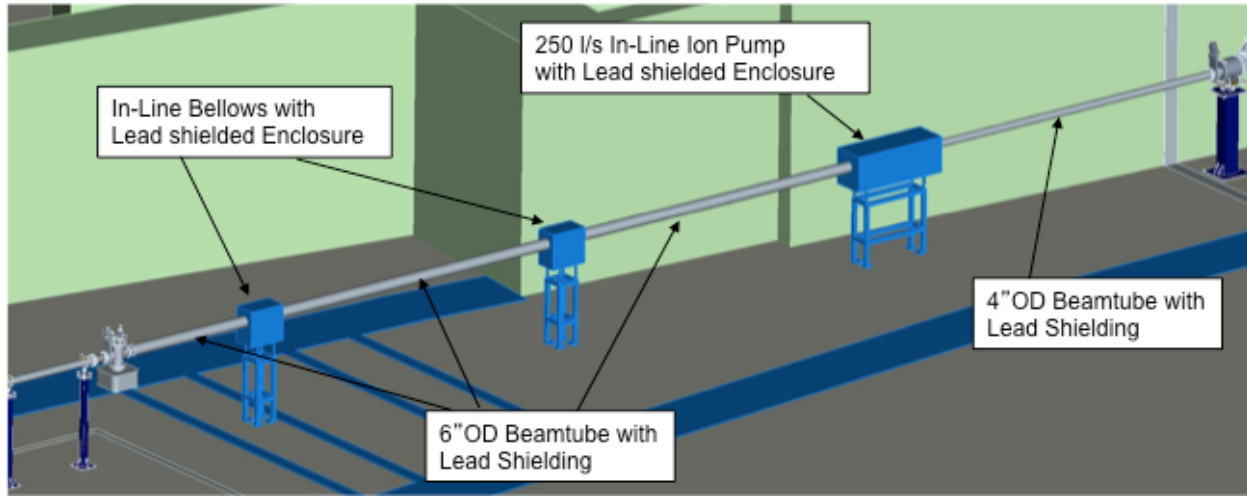


Figure 6-8. White-beam transport vacuum and radiation containment components.

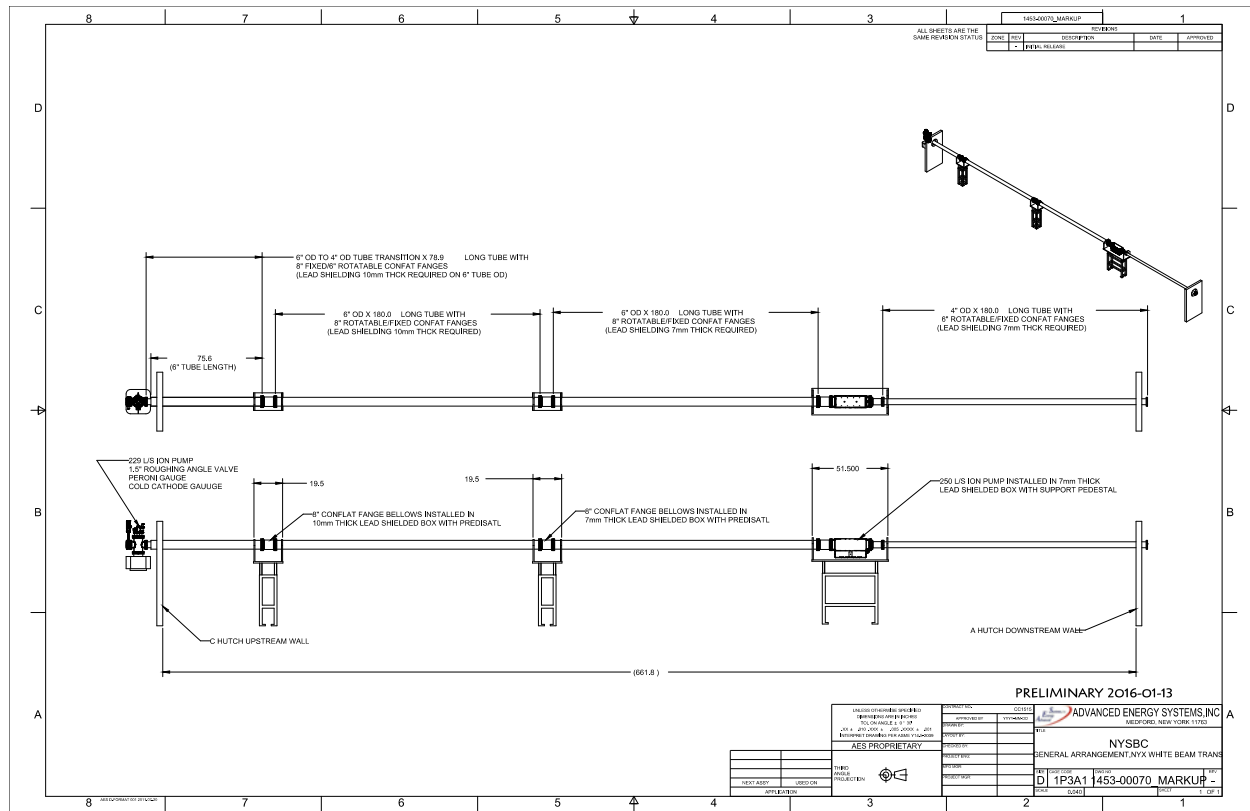


Figure 6-9. White-beam transport vacuum layout.

6.3.2 Shielding validation.

The 19-ID hutches and white-beam transport have been designed following the “*Guidelines for Beamline Radiation Shielding Design at the National Synchrotron Light Source II*” however shielding validation is required to insure that proper radiation protection has been provided in full compliance with NSLS-II standards. Radiological risks need to be analyzed in the following specific areas:

- 1) The stay-clear region of gas-Bremsstrahlung in the last section of the white-beam transport.
- 2) Shielding required to reduce the dose from secondary radiation (electromagnetic shower and photoneutrons) produced by the gas-Bremsstrahlung encountering the transition from 6” to 4” dia. tube at the downstream end of hutch 19-ID-C.
- 3) Shielding required to reduce the dose from secondary radiation (electromagnetic shower and photoneutrons) produced by the gas-Bremsstrahlung encountering the high-Z material in the slits upstream of the monochromator.
- 4) Shielding required to reduce the dose from secondary radiation (electromagnetic shower and photoneutrons) produced by the gas-Bremsstrahlung encountering the 1st crystal of the monochromator.
- 5) Shielding required to reduce the dose from secondary radiation (electromagnetic shower and photoneutrons) produced by the gas-Bremsstrahlung encountering the high-Z material of the white-beam stop at the exit of the monochromator.

The NYX beamline design includes accommodations for additional shielding as described in the above NSLS-II guideline; however, further validation is required before actual shielding can be implemented.

6.4 Radiation Enclosures

6.4.1 General Description

NYX has three radiation enclosures (Figure 6-10): Hutch A, which will also serve as the first optical enclosure for the eventual LAX beamline and Hutch B, which is the first optical enclosure for NYX are lead shielded. Hutch C encloses the end station is shielded with steel. Hatches C and D are contiguous. The eventual enclosure for LAX will be called Hutch B.

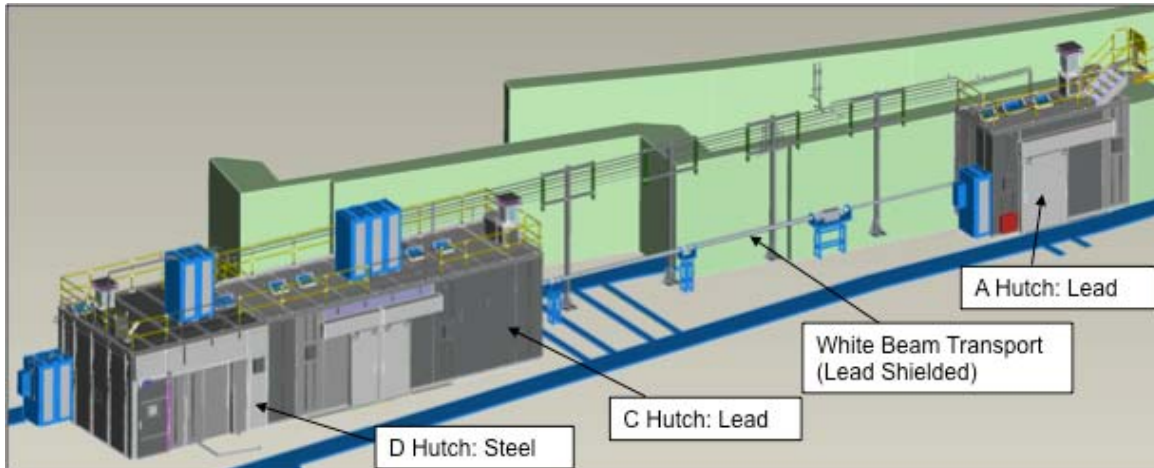


Figure 6-10. Bealine layout the hutch identifications

Beamline hatches for NYX are being implemented throughout the beamlines' WBS areas; the technical aspects of the hatches are described in this section. The hatches have been contracted with GPS by NYSBC and installation is complete at NSLS II with final acceptance expected by the end of January 2016.

The beamline hatches are provided to contain all harmful x-ray radiation and prevent personnel exposure during operation. The First and Secondary Optics Enclosures (FOE, SOE), constructed from thick lead panels of a standard 1 m width and calculated thickness, to contain not only the white x-ray beam, but also the very-high-energy bremsstrahlung x-ray radiation. Experimental stations for monochromatic beam will be constructed from steel (typically, $\frac{1}{4}$ -in. thick). The NYX FOE during utilities installation is shown in Figure 6-11.

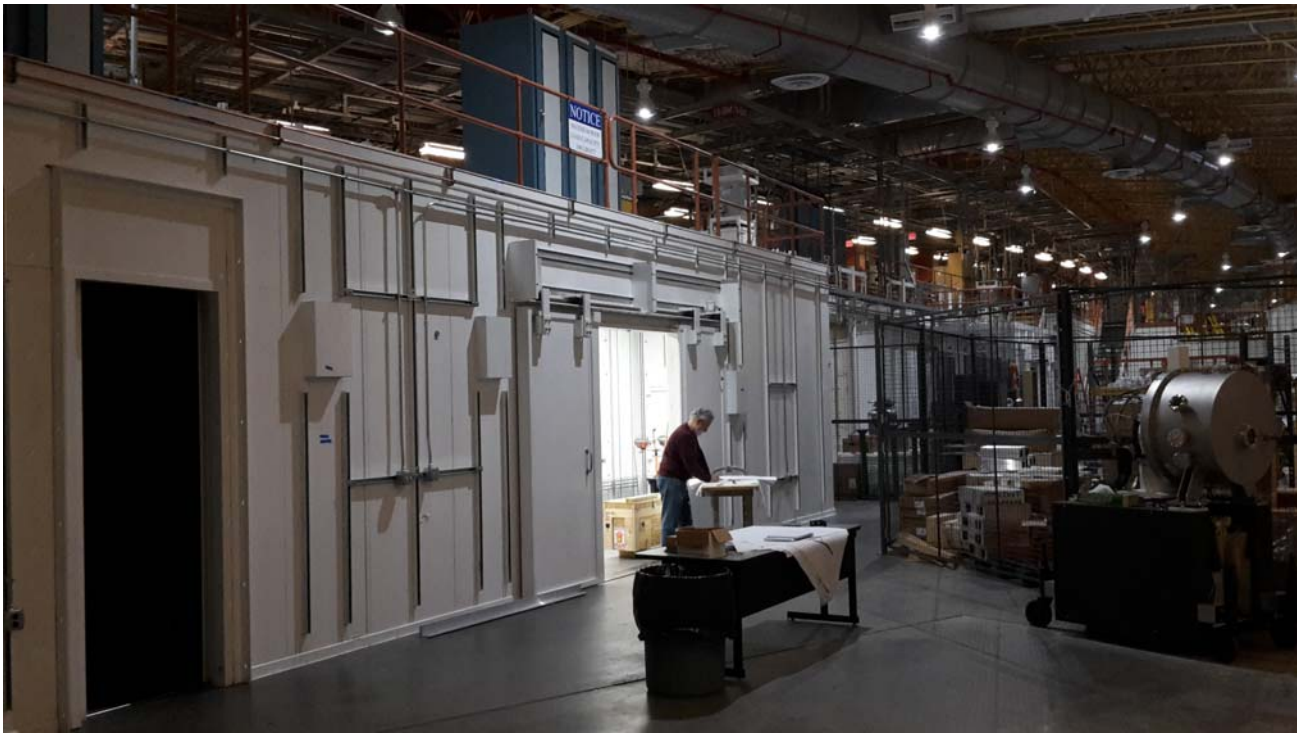


Figure 6-11. View of an FOE hutch (18 mm lead sidewall thickness) after completion.

Calculations have been performed on the lead thickness requirements for sidewalls, roofs, and downstream walls of FOE, SOE, white beam transport between the FOE and SOE the and experimental station for an IVU source; these are documented in “Guidelines for NSLS-II Beamlines and Front End Radiation Shielding Design,” LT-ESHDES-08-003-Rev 001, and summarized in Table 6-1, below.

Table 6-1. First Optics Enclosure (FOE) and Experimental End Station shielding thickness requirements, in mm. The first dimension is for sidewalls, then roof, then downstream wall.

Source	FOE Shielding*	End Station Shielding*
IVU	18/6/50 Pb	6/3/6 Fe

- Shielding given is for sidewalls/roof/downstream wall, in mm.

6.4.2 Hutch Labyrinths

All hutches will be provided with labyrinths for allowing passage through the shielding walls of the following services:

- Control cabling
- Mains electricity
- PPS cabling
- Liquid nitrogen
- Ventilation air (in and out)
- Exhaust gas (from hoods ,etc. to the facility extraction system)
- Chilled water

Note that Low Conductivity Water and compressed air will enter the FOE through the concrete ratchet wall from the accelerator tunnel.

Labyrinths will be fitted with Personnel Protection System (PPS) locks and/or safety switches, as needed, to inhibit beamline operation when a labyrinth is not closed and secured.

A typical labyrinth is shown in Figures 6-12.



Figure 6-12. Typical NYX roof labyrinths.



Figure 6-13. NYX endstation hutch and SOE, hutches C and D.

Hutches will be fitted with standard doors, either swinging single door or sliding single/door as needed (Figure 6-13). One door per hutch will be pneumatically actuated. These will be fitted with PPS magnetic locks, switches, etc. Generally, windows are discouraged on FOEs due to the extreme thickness of lead glass needed. Experimental station windows are more reasonable in thickness and will be used where desirable. The image below (Figure 6-14) shows the typical lead lined floor groove cross section.



Figure 6-14. Typical hutch floor showing groove, steel insert, and the lead shielding.

6.4.3 Hutch Electrical Equipment

The hutch will be fitted with standard ventilation fans and lights within the hutch contract. Wiring to this equipment (and all other electrical wiring) will be performed under the beamline utilities scope.

6.4.4 Hutch Roof Access

The hutches are all designed for roof access (except in the case of any small “doghouse type” hutches); features include load ratings compatible with human loads, as well as equipment and utilities, handrails and kick-plates, and swing gates to restrict access to hutch roofs from the mezzanine floor (storage ring tunnel roof) to just beamline staff and other authorized staff (Figure 6-15).



Figure 6-15. Personnel access gate and railing for the 19-ID-C&D hutches.

Table 6-2. Specification Sheet for Enclosure 19-ID-A

Specification Sheet for Enclosure 19-ID-A

Enclosure designation	19-ID-A
Enclosure type	IVU (LAX)
Enclosure description	LAX White Beam Optics Enclosure
Shielding material	Lead
AES Drawing reference	1453-00100
Dimensions (m)	
Height max	3.5 m
Width max	2.3 m
Length max	5 m
Shielding	
Side (lateral) panels	18 mm lead
Roof panels	10mm lead
Downstream wall panels	50mm lead
Guillotine	2 required, Single aperture-downstream, One supplied with lead shielding plug
Beam pipe penetration door	(alignment window): Not required
Entry 1	
Position	Outboard side
Size (m)	2.4 H x 1.2 W (minimum)
Type	Sliding single door, Manual operation
Floor groove	yes
PPS Interfaces	Mounting plates for magnetic lock and dual position switches.
Window	Not required
Strip Curtain (internal)	No
Hoist	Not Required
Labyrinths	Positioned as on drawing, sealed with anti-tamper screws except where locks/interlocks specified.
Fluids labyrinth	(on roof): Qty 1
Electrical labyrinth	(on roof): Qty 1
Air inlet labyrinth, with fan and filter	(on roof): Qty 1
Air outlet labyrinth	(base of sidewall): Qty 1
Exhaust labyrinth	(on roof): N/A
User access labyrinth	(on sidewall): Qty 1, with interlock switch provisions
Liquid nitrogen labyrinth	(on roof): Qty 1
Bridges	Not required
Lighting	Fluorescent
Other	Attachment points for adjacent enclosures: Not required
Drawings	Number of full sized prints required of all drawings: Qty 3
Manuals	Number of copies required of all manuals: Qty 3

Table 6-3. Specification Sheet for Enclosure 19-ID-C

Specification Sheet for Enclosure 19-ID-C

Enclosure designation	19-ID-C
Enclosure type	IVU (NYX)
Enclosure description	NYX White Beam Optics Enclosure
Shielding material	Lead
AES Drawing reference	1453-00101
Dimensions (m)	Height max 3.5 m Width max 3.25 m Length max 10.0 m
Shielding	Side (lateral) panels 18 mm lead Roof panels 10 mm lead Upstream panels 18 mm lead Downstream wall panels 50 mm lead Guillotine 2 required, Single aperture- upstream and downstream Beam pipe penetration door (alignment window): Not required
Entry 1	Position Outboard side Size (m) 2.4 H x 2.0 W Type Sliding double, Manual Operation Floor groove PPS Interfaces Window Yes Mounting plates for magnetic lock and dual position switches. Strip Curtain (internal) Not required No
Holst	Not Required
Labyrinths	Positioned as on drawing, sealed with anti-tamper screws except where locks/interlocks specified. Fluids labyrinth (on roof): Qty 2 Electrical labyrinth (on roof): Qty 2 Air inlet labyrinth, with fan and filter (on roof): Qty 1 Air outlet labyrinth (base of sidewall): Qty 1 Exhaust labyrinth (on roof): N/A User access labyrinth (on sidewall): Qty 2, (Qty 1 with interlock switch provisions, Qty 1 with padlock provisions for PPS) Liquid nitrogen labyrinth (on sidewall): Qty 1
Bridges	Not Required
Lighting	Fluorescent
Other	Attachment points for adjacent enclosures: Required for attachment to 19-ID-C (see AES drawing 1453-00103)
Drawings	Number of full sized prints required of all drawings: Qty 3
Manuals	Number of copies required of all manuals: Qty 3

Table 6-4. Specification Sheet for Enclosure 19-ID-D

Specification Sheet for Enclosure 19-ID-D

Enclosure designation		19-ID-D
Enclosure type		IVU (NYX)
Enclosure description		NYX Endstation 1
Shielding material		Steel
AES Drawing reference		1453-00102
Dimensions (m)	Height max	3.5 m
	Width max	4.25 m
	Length max	5.0 m
Shielding	Side (lateral) panels	6 mm steel
	Roof panels	3 mm steel
	Upstream wall panels	6 mm steel on 1.1m wide segment, Open area attaches to downstream wall of Endosure 19-ID-B
	Downstream wall panels	6 mm steel
	Gillotine	None Required
Beam pipe penetration door		(alignment window): Not required
Entry 1 & 2	Position	Entry #1 Inboard side, Entry #2 Outboard side
	Size (m)	2.4 H x 1.0 W
	Type	Entry #1 Sliding Single, Entry #2 Hinged Single, Both Manual Operation
	Floor groove	Entry #1 Yes, Entry #2 No
	PPS Interfaces	Mounting plates for magnetic lock and dual position switches.
	Window	Not required
Strip Curtain (internal)		No
Hoist	N/A	
Labyrinths	Positioned as on drawing, sealed with anti-tamper screws except where locks/interlocks specified.	
	(on roof): Qty 1	
	(on roof): Qty 1	
	(on roof): Qty 1	
	(base of sidewall): Qty 1	
	(on roof): Qty 1	
	(on sidewall): Qty 2 (Qty 1 with interlock switch provisions, Qty 1 with padlock provisions for PPS)	
	(on sidewall): Qty 1	
Bridges	Not Required	
Lighting	Fluorescent	
Other	Attachment points for adjacent enclosures: Required for attachment to 19-ID-B (see AES drawing 1453-00103). Required for attachment to future load lock vestibule around perimeter of Entry #1	
Drawings	Number of full sized prints required of all drawings: Qty 3	
Manuals	Number of copies required of all manuals: Qty 3	

6.5 Beamline Ray Tracing

The latest revision of the NYX Beamline Ray Trace drawing, dated 12-23-2015, has been tentatively approved by the BNL Radiation Safety Committee (RCS). This ray trace drawing specifies the synchrotron beam water cooled mask aperture geometry and synchrotron beam stops, the high energy bremsstrahlung collimator geometry and bremsstrahlung beam stops as well as the white beam transport beam tube shielding. The axial location of all components and aperture geometry is accurately represented in this layout. Aperture geometry is sized to assure delivery of the total synchrotron beam fan angle that can be captured and focused by the tangentially bent first crystal and sagittally bent second crystal set planned for the Double Crystal Monochromator (DCM). Table 6-5 below outlines the beamline aperture and collimator location and sizes. Figures 6-16 through 6-19 below depict the four-sheets of the Ray Trace drawing submitted for review by the RSC on 12-23-2015.

Table 6-5. NYX Beamline Apertures/Collimators

Position	Beamline Component	from X25 center	from SAGU center	Aperture Horz	Aperture Vert	Aperture Diag	Fan Angle $\mu\text{rad H}$ (from SAGU)	Fan Angle $\mu\text{rad V}$ (from SAGU)	Fan Angle $\mu\text{rad Diag}$ (from SAGU)	from Cant Mag #1	Transvers offset from center of straight to NYX
-1035	Center of Source IVU (SAGU)	-490	0							1612.70	
-545	Center of Source IVU (X25)	0	490							2102.70	
0	Center of Straight	545	1035							2647.70	
17892.75	Fixed Mask-Front End (water cooled)	18438	18928	9.4	5.4	10.8	496.6	285.3	572.7	20540.45	16.638
26224	Fixed Mask (water cooled)	26769	27259	4.3	2.2	4.8	157.7	80.7	177.2	28871.60	23.386
26224	Rev 12 Fixed Mask (water cooled)	26769	27259	4.0	2.0	4.5	146.7	73.4	164.1	28871.60	23.386
26424	(aperture exit location)									29071.60	23.548
26540	Lead Collimator	27085	27575	round	round	9.0			326.4	29187.70	23.642
26540	Rev 12 Lead Collimator	27085	27575	round	round	5.0			181.3	29187.70	23.642
26840	(aperture exit location)									29487.70	23.885
29670	White Beam Mask (NYX) & Beamstop (LAX)	30215	30705	5.0	3.0	5.8	162.8	97.7	189.9	32318.18	26.178
29670	Rev 12 White Beam Mask (NYX) & Beamstop (LAX)	30215	30705	5.0	3.0	5.8	162.8	97.7	189.9	32318.18	26.178
29710	(aperture exit location)									32358.18	26.210
29850	Rev 12 BS Collimator (tungsten)	30395	30885	8.2	5.8	10.0	265.5	187.8	325.2	32497.70	26.323
30050	(aperture exit location)									32697.70	26.485
50655	Single Aperture White Beam Mask (water cooled)	51200	51690	8.0	4.0	8.9	154.8	77.4	173.0	53302.70	43.175
50855	(aperture exit location)									53502.70	43.337
51000	BS Collimator (Lead)	51545	52035	round	round	17.0			326.7	53647.70	43.455
51300	(aperture exit location)									53947.70	43.698
52697	DCM	53242	53732							55344.70	44.829
53477	White Beam Stop (water cooled)	54022	54512							56124.70	45.461
53594	Tungsten Collimator	54139	54629							56241.70	45.556
53794	(aperture exit location)									56441.70	45.718
55400	VFM	55945	56435							58047.70	47.019
56833	Photon Shutter	57378	57868							59480.70	48.179
59400	Microdiffractometer (goniometer)	59945	60435							62047.70	50.259
62245	Beam Stop - Downstream Wall	62790	63280							64892.70	52.563

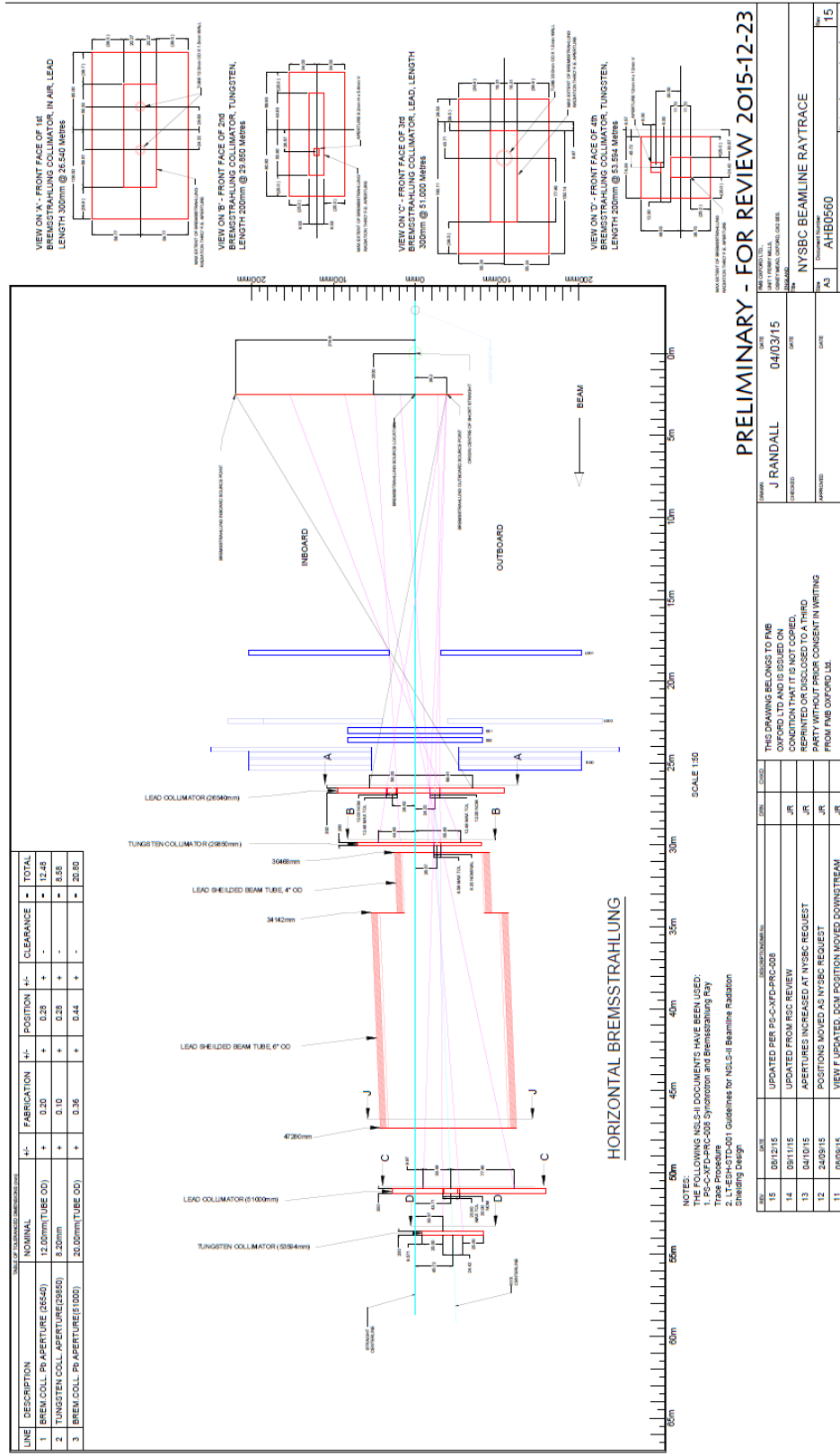


Figure 6-16. Horizontal Bremsstrahlung Ray Trace (Sheet 1)

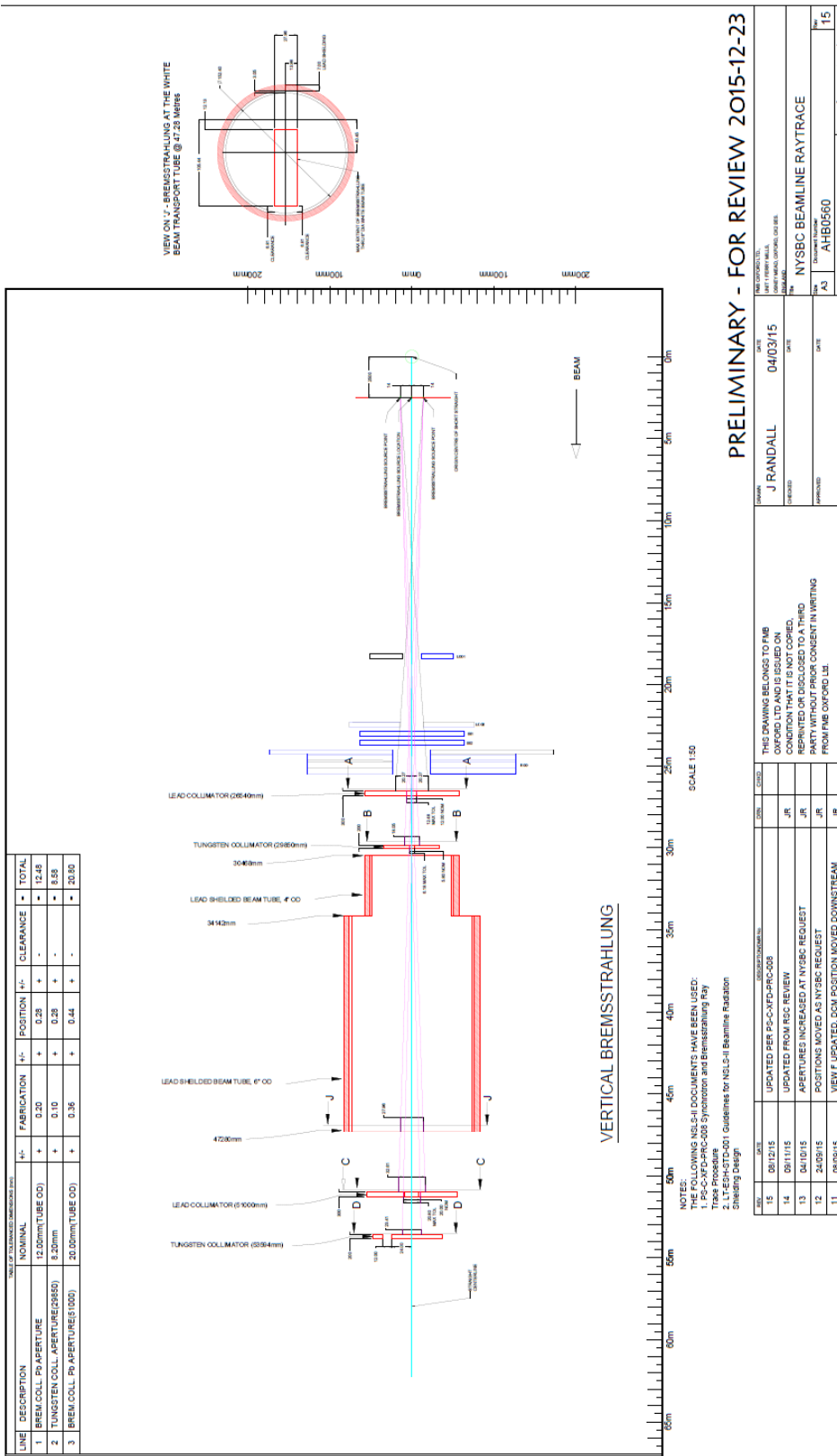


Figure 6-17. Vertical Bremsstrahlung Ray Trace (Sheet 2)

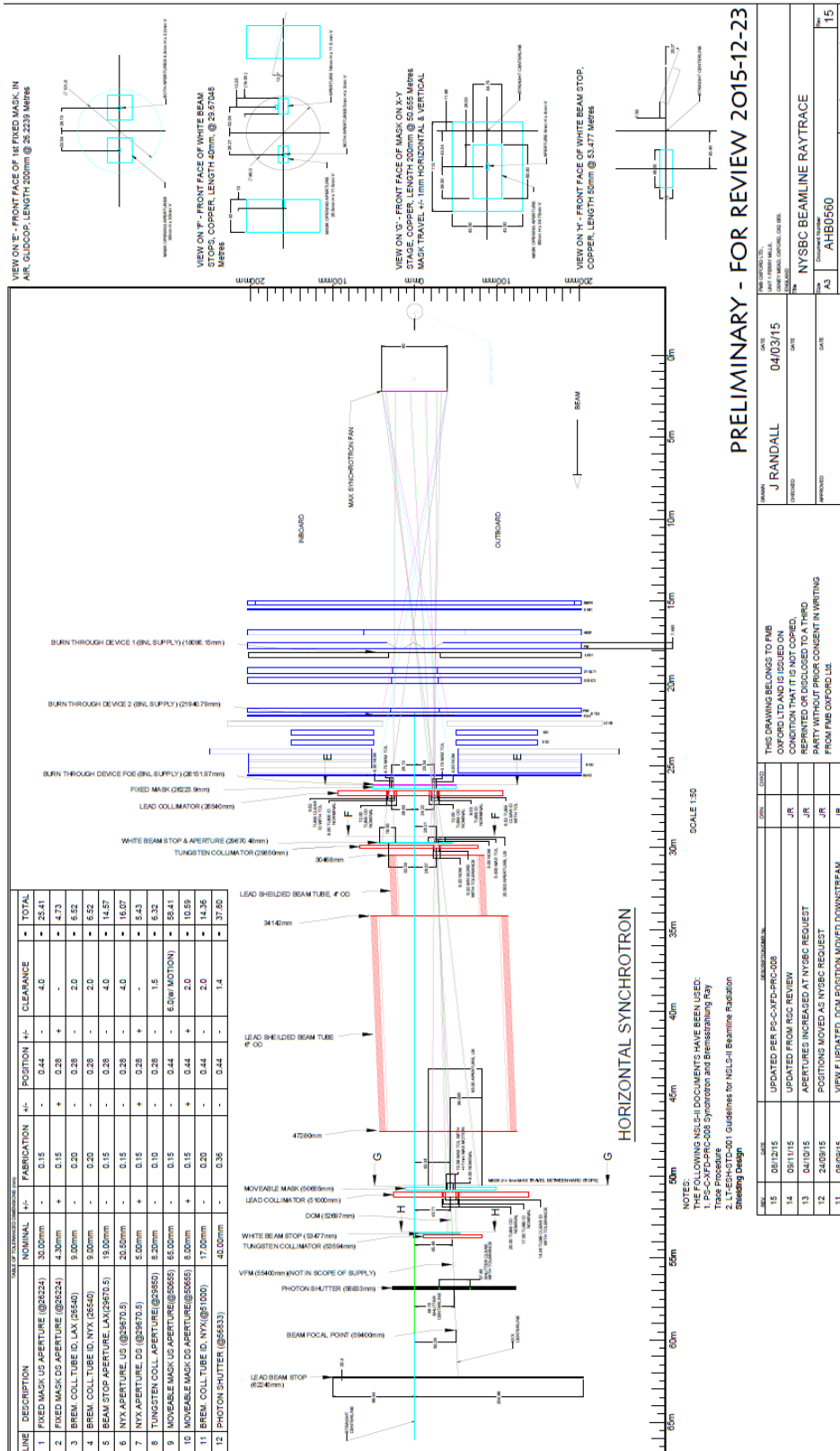


Figure 6-18. Horizontal Synchrotron Ray Trace (Sheet 3)

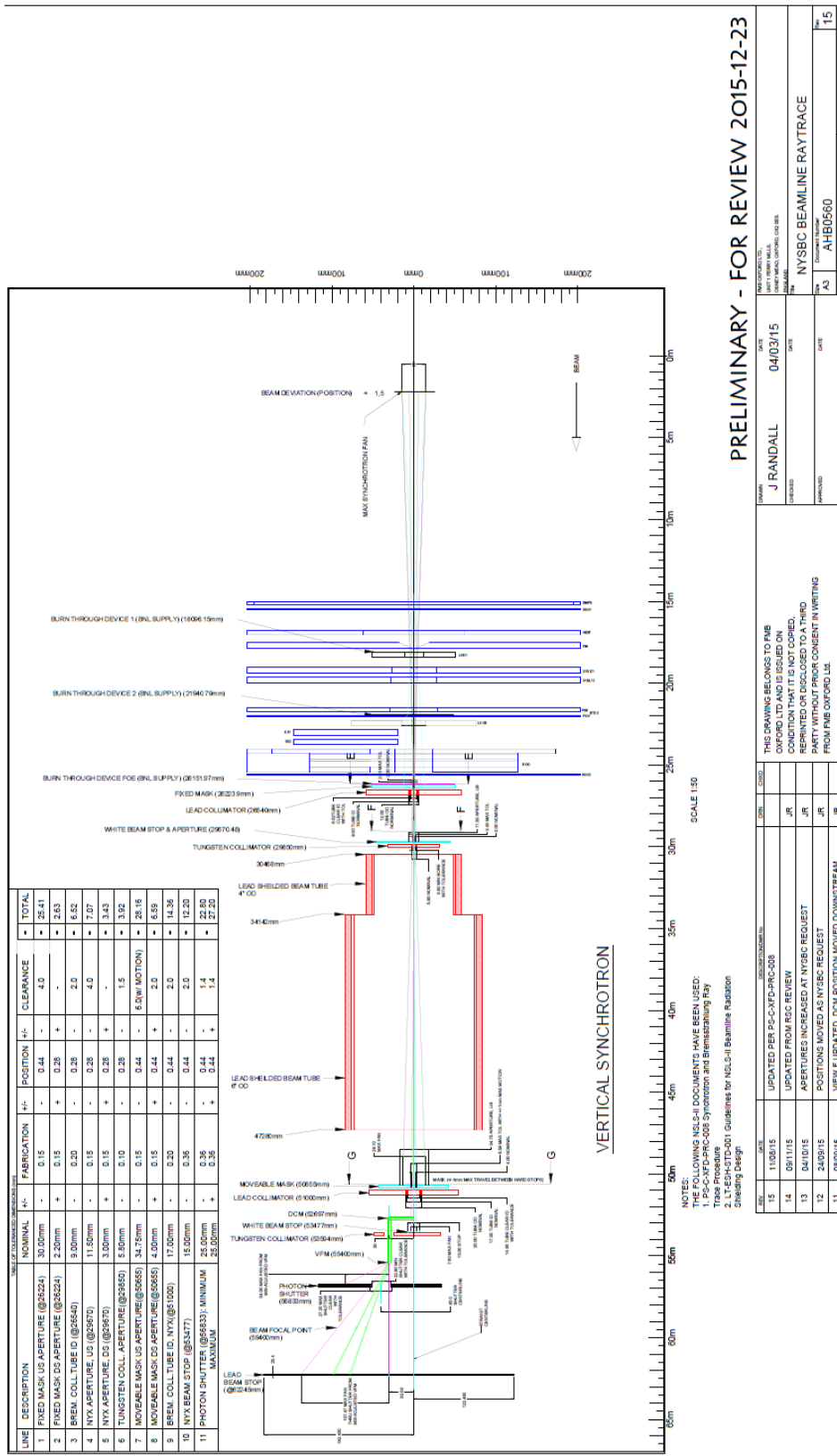


Figure 6-19. Vertical Synchrotron Ray Trace (Sheet 4)

6.6 Vacuum System

NYX vacuum system was developed following the guidelines in “Standard Technical Specifications for NSLS-II Beamline Components” and involved acquiring new equipment along with repurposing viable equipment from our prior beam line efforts on NSLS.

The Beamline will be UHV (NSLS-II ring vacuum) from the front end isolation valve located at the ratchet wall to the beginning of the end station hutch where a Beryllium window will isolate the vacuum system for the remainder of the photon transport. This vacuum system includes nine VAT series 10 and series 48 gate valves, sizes DN63 and DN100, along the beamline transport resulting in nine individual vacuum sections that can be independently isolated. The beamline is serviced by thirteen ion pumps ranging in size from 30 l/s to 500 l/s making up a mix of conventional and differential style pumps. Seven Gamma Vacuum Digital MPC’s are used for Ion Pump control and monitoring. Vacuum instrumentation includes ten convection enhanced Pirani series 317 gauges for pressure reading from atmospheric pressure down to 1×10^{-3} Torr and seven cold cathode series 422 gauges for pressure measurements from 10^{-3} Torr to $<10^{-10}$ Torr. MKS series 937b gage controllers are used to display and transmit vacuum status. Beamline vacuum integrity will be verified with the Hiden Residual Gas Analyzer model HAL101. A total of six MDC 420035 burst disks are included for incorporation in all vacuum sections housing water and or LN2 cooled components to mitigate over pressure scenarios due to possible coolant-to-beamline vacuum leaks. All metal 1.5" right angle valves are incorporated in each vacuum section between gate valves for rough vacuum pumping of the isolated sections in preparation for the start of ion pump operation. Table 6-6 summarizes the assortment of ion pumps and VAT valves used throughout the beamline.

Table 6-6. Ion Pump and Gate Valve List

Ion Pumps			Vat Gate Valves		
Qty.	Size	Type	Qty.	Size	Type
2	30 l/s	differential	1	DN 63	series 10
1	120 l/s	differential	2	DN 63	series 48
1	150 l/s	conventional	5	DN 100	series 10
3	220 l/s	differential	1*	DN 100	series 48
1	250 l/s	conventional			
3	300 l/s	conventional			
2	500 l/s	conventional		*Ratchet Wall Valve	

The vacuum system components described in this section are distributed throughout the beamline in the A hutch, white beam transport section and C hutch component systems. The first two vacuum sections reside in the A hutch, illustrated in the following Figure 6-20. The very first vacuum section includes a Residual Gas Analyzer as well as the more standard Pirani and Cold Cathode vacuum gauges to verify vacuum integrity prior to opening the

beamline ratchet wall gate valve to the NSLS-II ring vacuum. The white beam transport section is next, extending into the C hutch as shown in Figure 6-21.

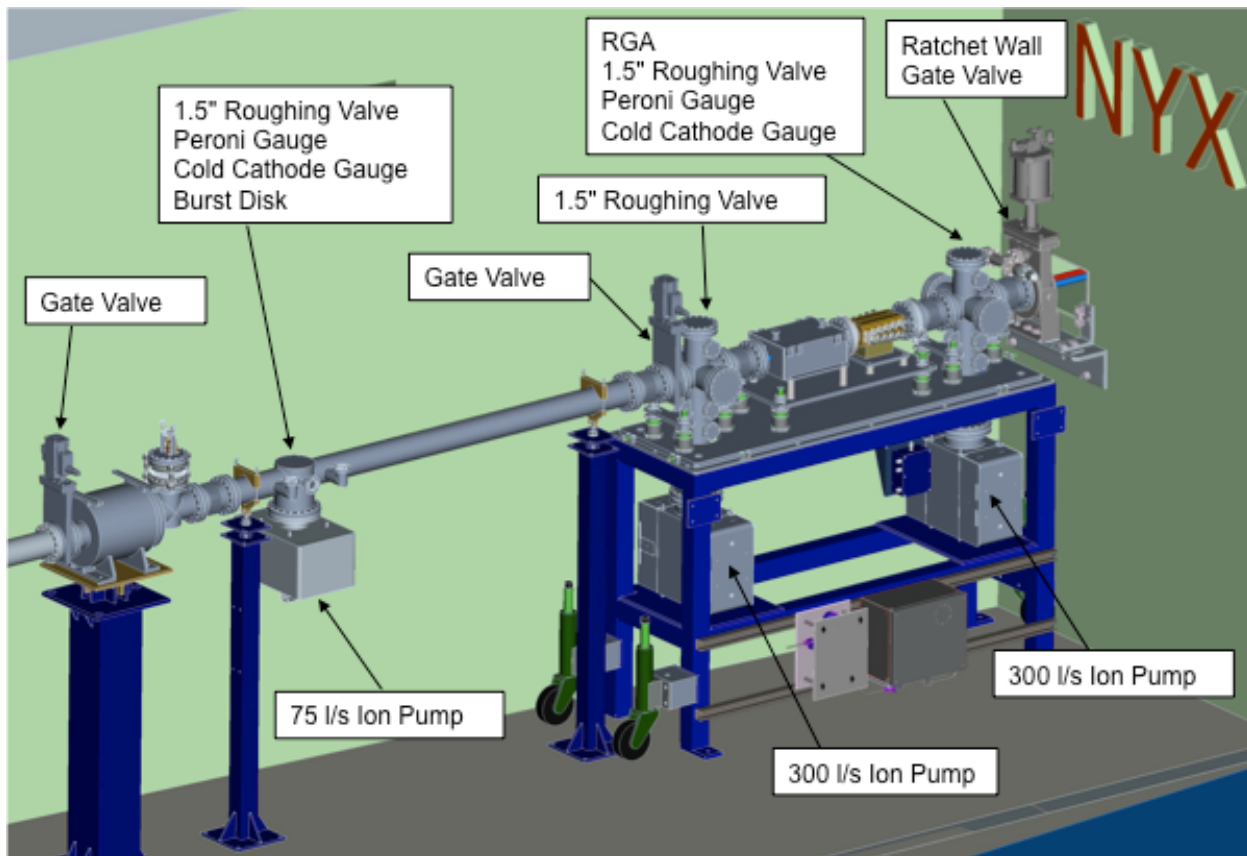


Figure 6-20. A Hutch vacuum components

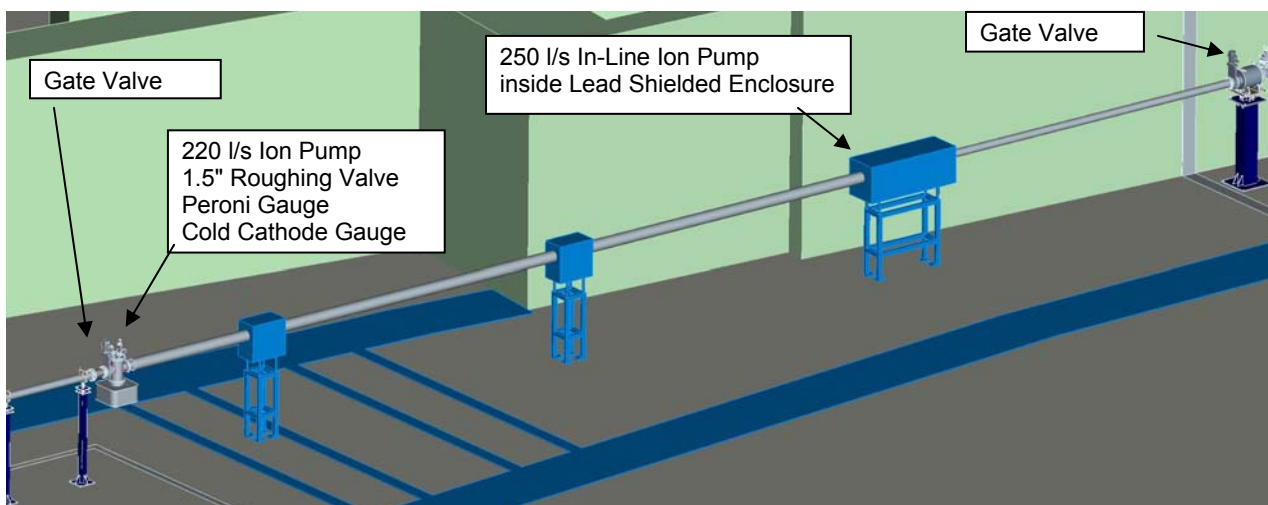


Figure 6-21. White-beam transport vacuum components

The remaining six vacuum sections serviced by the components outlined in this section reside in the C hutch. As indicated in Figure 6-22, the components are distributed throughout the sections enabling the isolation, venting and pumping of each section independently.

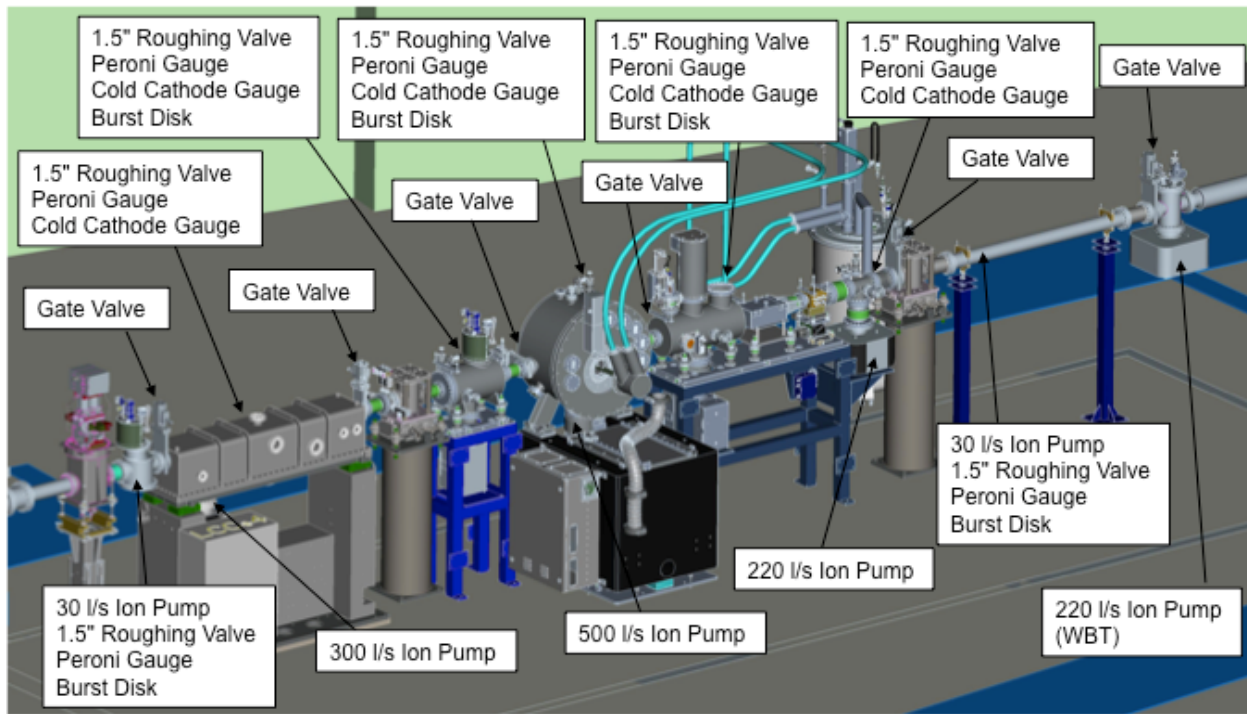


Figure 6-22. C Hutch Vacuum Components

7. Photon Delivery System

The unique brilliance of the NSLS-II storage ring provides great opportunities to address the science needs in macromolecular crystallography that we identify above. NSLS-II was designed to produce and store electrons with extremely low beam emittance. The low emittance results in a small source size with low divergence which contribute to an extraordinarily confined phase space, and both properties contribute to produce photon beams with exceptional opportunities for focus into microbeams and also exceptional opportunities for energy resolution.

7.1 Optical Configuration

The monochromator is the heart of the NYX beamline and its novel design will define the energy resolution, pre-focus the beam vertically, and focus the beam horizontally. A downstream vertical mirror will complete the vertical focus and also provide harmonic rejection. The overall beamline view is shown in Figure 7-1 where the a double crystal monochromator (DCM) is positioned before a vertical focusing mirror (VFM).

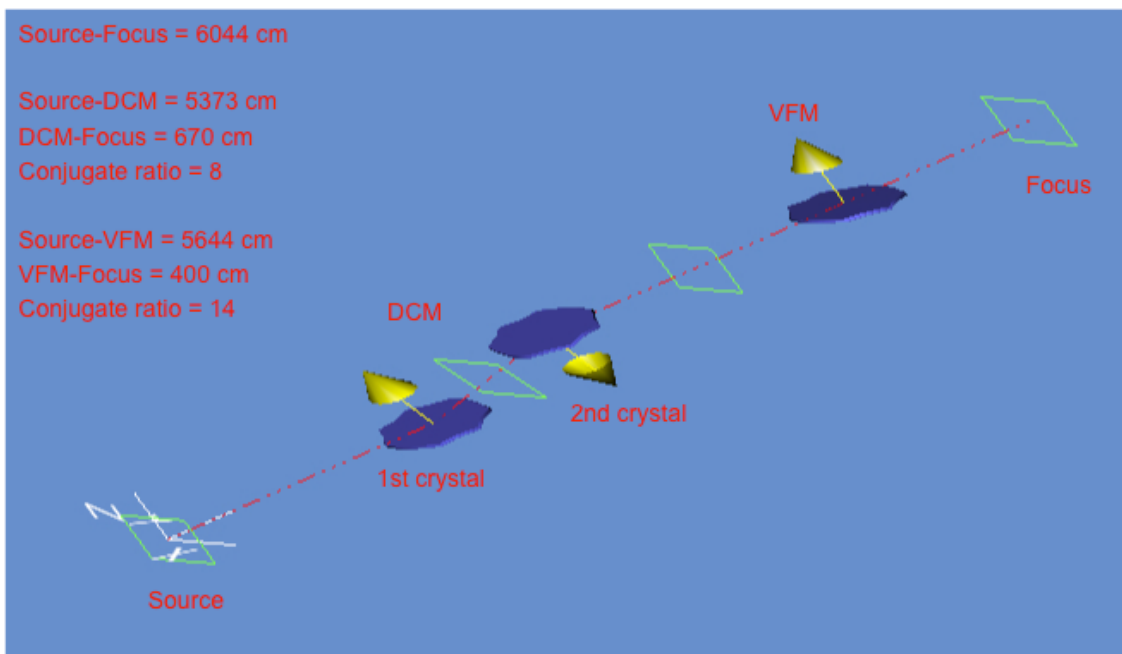


Figure 7-1. Shadow BL View

We have designed x-ray optics that will capture the full spectral brilliance passed by a Si(111) monochromator but focused into a beam of less than 10 micron cross-section and while achieving an energy resolution under 6×10^{-5} in $\Delta E/E$ (0.8 eV at 12 keV). Beams can readily be defocused to 50 micron cross section, with differential control for the vertical and horizontal directions.

7.2 Double Crystal Monochromator

The purpose of the DCM is to select and transmit X-ray radiation of the desired photon energy from an incident white synchrotron beam. The monochromator will employ a set of Si[111] crystals to cover the energy range 5 – 17.5 keV. It is possible to translate the 2nd crystal relative to the 1st in order to achieve the fixed offset and fixed reflection point of the monochromatic beam with respect to the white beam. This requires a translation of the 2nd crystal in a direction perpendicular and parallel to its diffracting surface to ensure that the beam is always centered on the 2nd crystal. The 1st crystal will reflect upwards and the 2nd crystal will reflect downwards. The desired energy is selected by rotating the crystal set, thereby varying the Bragg angle (θ), whilst keeping the crystals parallel to one

another. The axis of rotation passes through the centre of the 1st crystal diffracting surface and perpendicular to the beam axis so that the incident white beam is always centred on the axis of rotation. The beam will exit the monochromator parallel to the input beam but at a 30mm offset (upwards) and tracking the 2nd crystal will achieve a fixed monochromatic beam within the operational energy range. The DCM is designed for a nominal beam height of 1400mm.

7.2.1 High Energy Resolution Concept

Although energy resolution is not intrinsic to synchrotron radiation, the contracted phase space resulting from relativistic effects at synchrotron light sources does make high energy resolution achievable, and with low emittance as for NSLS-II this is more readily accomplished. Typically, the monochromator is configured to exploit that the smallest phase plane to achieve satisfactory energy resolution. A defined energy resolution can be realized by matching the angular acceptance of the monochromator to the Darwin width of the monochromator crystal. A common monochromator geometry at synchrotron beamlines uses a flat, unbent crystal oriented to diffract in the vertical plane. The vertical plane is chosen most often because of its much smaller phase plane relative to the horizontal; nevertheless, as the incident beam divergence typically exceeds the monochromator rocking curve width, usually this still requires reduction of angular acceptance by limiting slits or a collimating mirror. The use of slits necessarily results in an overall reduction of flux; pre-monochromator collimation may not achieve perfection and, depending on mirror length, there may be flux losses in this approach as well. Alternatively, without such conditioning of the incident beam, the energy resolution intrinsic to a given monochromator will be spoiled. A perfect and perfectly matched Si(111) monochromator will produce an energy resolution of $\Delta E/E = \Delta\lambda/\lambda = 1.3 \times 10^{-4}$; however, if the incident beam divergence is greater, then the Si(111) acceptance then $\Delta E/E$ is degraded.

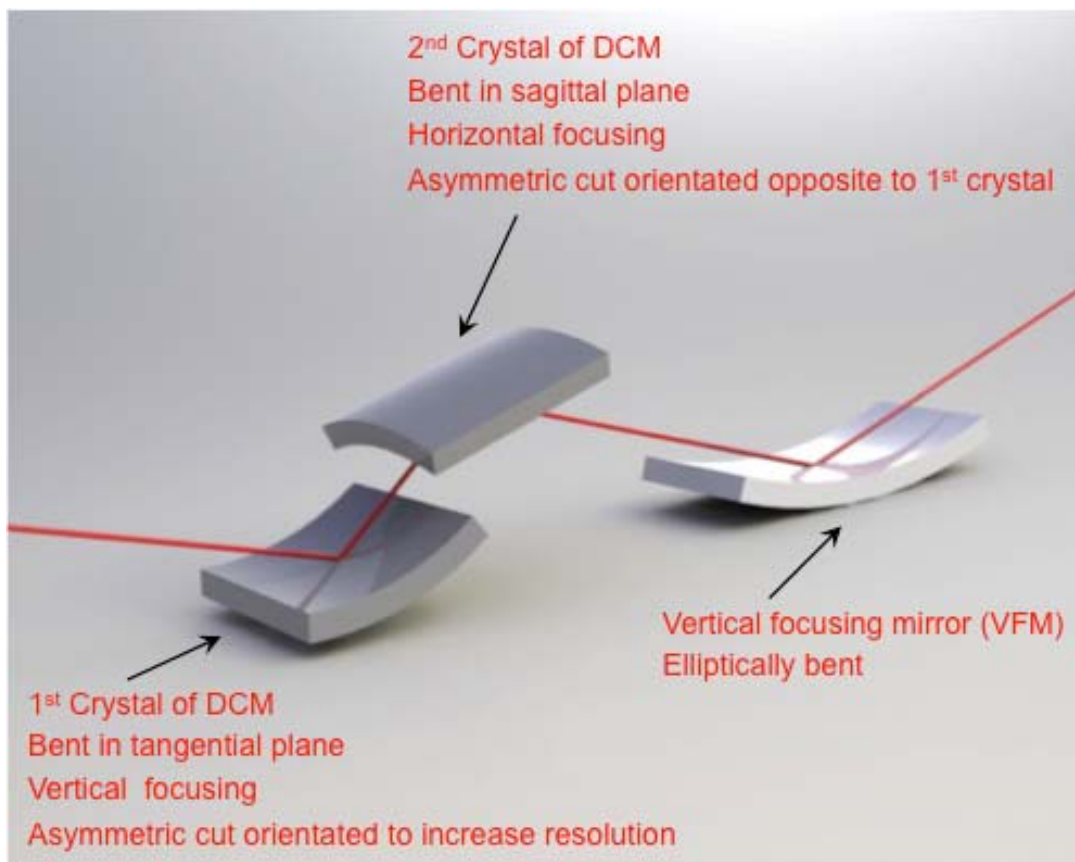


Figure 7-2. Schematic diagram of NYX optics.

Alternatively if the monochromator is bent to match the opening angle of the x-ray source in such a way that all rays in the diffracting plane satisfy the Bragg condition, then the energy resolution can be optimized without slitting or the need of a collimating mirror. This can be accomplished by exploiting the condensing effect of an asymmetric cut, as introduced by Fankuchen (1937); and, with Rowland-circle bending (Lemonnier et al., 1978; Schildkamp, 1988), such cylindrically bent asymmetric crystals have been effective for horizontally diffracted monochromators. We have used such a crystal at NSLS beamline X4C, and we recently analyzed the energy resolution properties of this monochromator (Lidestri & Hendrickson, 2009). Here, we plan to implement such bending in the vertical plane as illustrated in Figure 7-2. We have developed a novel geometry double-crystal geometry in which the first crystal is bent tangentially and second crystal is bent sagittally. This geometry can only be made to work efficiently by using an asymmetric cut crystal in the second position with its orientation reversed to favor increasing the acceptance angle facing the first crystal. The energy band pass is definable by selection of the asymmetric angle, α . Here, emergence of the diffracted beam at the 17.5 KeV extreme constrains α to 6° . This energy-resolving double-crystal configuration is illustrated in Figure 7-3, and the rocking curves generated for crystals with $\alpha = 6^\circ$ is shown in Figure 7-4.

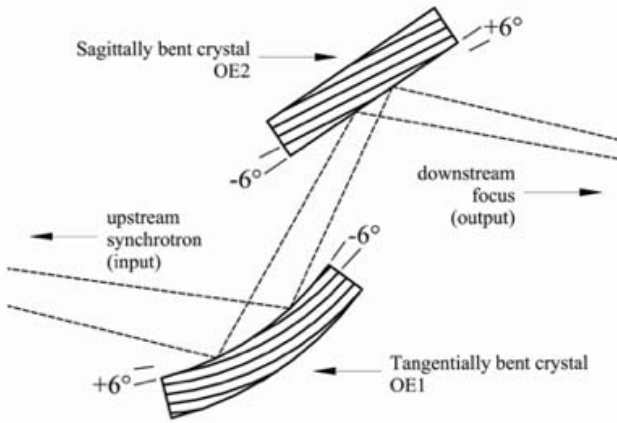


Figure 7-3. Monochromator schematic. The bent asymmetrically cut first crystal defines the energy resolution. The sagittally bent second crystal focuses horizontally and has a reversed asymmetric cut to fully accept the convergent beam from the first crystal.

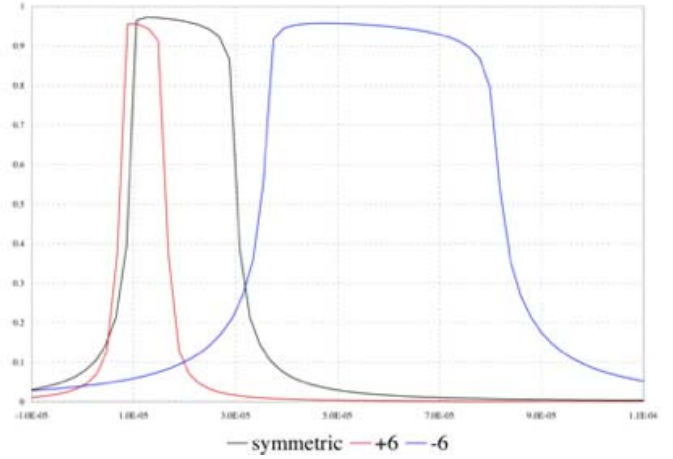


Figure 7-4. Rocking curves. Profiles are shown for Si(111) crystals at the Se K-edge (12658 eV), including the case for symmetric geometry (black) and for asymmetric cuts of both $+6^\circ$ (red) -6° (blue).

By examination of the rocking curves (Fig. 7-4), we noted the narrowing and broadening of the rocking curves when compared to the symmetric case. The full width of the narrowed rocking curve incident on the first crystal defines the improved energy resolution and the width of the broadened curve incident on the second crystal results in increased angular acceptance in the second crystal. This increased angular acceptance in the second crystal is essential because of the mismatch in the diffracting planes caused by tangentially bending the first crystal to the radius of curvature that satisfies the condition of diffraction along the entire length of the crystal. The primary feature of this novel monochromator geometry is the monochromatic match to the finite angular divergence of the x-ray beam while still allowing the second crystal to be sagittally bent for horizontal focusing. Since diffracted rays from the bent first crystal are convergent, the second crystal must have an asymmetric cut oriented in oppositely to permit full acceptance. A secondary feature is to eliminate reliance on vertical slits, which introduce stability issues associated with maintaining alignment of a slit between the source and the DCM.

With the low emittance of NSLS-II, the source divergence is dominated by that from the undulator emission. The component due to electron beam divergence, $\sigma'_x^e = 2.7\mu\text{rad}$, is small compared to that due to the undulator, σ'_x^U . The relevant overall divergence seen by the monochromator is then $\sigma'_x^{\text{overall}} = (2\pi [(\sigma'_x^e)^2 + (\sigma'_x^U)^2])^{1/2}$, which we have computed for selected energies including extremes of the NYX design and used to evaluate energy resolution. Further estimates of the source divergences were made given vertical beam slices from the computer code SRW (Choubar). Monochromator performance is calculated for both the X25 and SAGU undulators and summarized in Tables 7-1 and 7-2 using source divergences derived from SRW.

Table 7-1. Monochromator Performance at Selected Relevant Energies with the X25 Undulator
H = harmonic order of the undulator

Energy (eV)	H	Source $\sigma'_x^{\text{overall}}$ (μrad)	Si(111) Darwin Width		Energy Resolution Si(111), $\alpha=0$ flat		Energy Resolution Si(111), $\alpha=6^\circ$ bent		Flux (ph/s/0.1%)
			$\alpha=0$ (μrad)	$\alpha=6^\circ$ (μrad)	$\Delta E/E$	$\Delta E(\text{eV})$	$\Delta E/E$	$\Delta E(\text{eV})$	
4000	1	71	77.5	64.3	1.9×10^{-4}	0.7	1.1×10^{-4}	0.5	5.5×10^{14}
12658	5	43	21.0	9.5	3.1×10^{-4}	3.9	6.0×10^{-5}	0.8	1.5×10^{14}
17500	7	35	15.1	3.0	3.4×10^{-4}	5.9	2.6×10^{-5}	0.5	4.5×10^{13}

Table 7-2. Monochromator Performance at Selected Relevant Energies with the SAGU Undulator
H = harmonic order of the undulator

Energy (eV)	H	Source $\sigma'_x^{\text{overall}}$ (μrad)	Si(111) Darwin Width		Energy Resolution Si(111), $\alpha=0$ flat		Energy Resolution Si(111), $\alpha=6^\circ$ bent		Flux (ph/s/0.1%)
			$\alpha=0$ (μrad)	$\alpha=6^\circ$ (μrad)	$\Delta E/E$	$\Delta E(\text{eV})$	$\Delta E/E$	$\Delta E(\text{eV})$	
4000	1	53	77.5	64.3	1.7×10^{-4}	0.7	1.1×10^{-4}	0.5	1.0×10^{15}
12658	7	43	21.0	9.5	3.1×10^{-4}	3.9	6.0×10^{-5}	0.8	3.5×10^{14}
17500	9	35	15.1	3.0	3.4×10^{-4}	5.9	2.6×10^{-5}	0.5	1.7×10^{14}

We have also compared the performance anticipated from the above-described energy-resolving DCM as based on a bent asymmetric 1st crystal with the performance expected from the alternative design for enhanced energy resolution based on symmetric ($\alpha = 0^\circ$) flat crystals and having a slit to limit incident divergence to the Darwin width of the monochromator crystal. Calculations were made for flat Si(220) and Si(311) crystals as well as for Si(111), and those at the Se K-edge energy (12.658 keV) are shown in Table 7-3 in comparison with values for the bent, asymmetric ($\alpha = 6^\circ$) case. The actual energy resolution from a flat crystal in an x-ray beam with divergence greater than the Darwin width is smeared from the optimized resolution that can be achieved when the slit-limited beam divergence is matched to the Darwin width. The bandpass-limited flux for the case of a flat crystal with no slit is the product of the spectral flux and the energy resolution. Optimized energy resolution that is achieved by slit limitation of divergence comes at the price of reduced bandpass-limited flux. The alternative of an optimally bent asymmetric crystal has the advantage that each ray diverging from the source is kept within the limited bandpass of the asymmetric Darwin width; thus, as for a parallel incident beam, all diffracted rays will have energies defined by the intrinsic bandpass of the perfect monochromator crystal. For a bent Si111 crystal cut with $\alpha = 6^\circ$, we obtain an energy resolution ($\Delta E/E = 6 \times 10^{-5}$) like that achieved from a flat Si220 crystal with slit limitation of beam divergence; however, the flux is nearly three times greater with Rowland-circle bending than with slit limitation.

Table 7-3. Comparison of Energy-resolution Optimizations at the Se K-edge (12.658 keV)

IVU	Si (hkl)	α	σ'_x overall (μrad)	----- Flat, No Slit -----				----- Optimized -----			
				Darwin Width (μrad)	Spectral Flux (ph/s/0.1%)	Energy Resolution $\Delta E/E$	Bandpass Limited Flux (ph/s)		Energy Resolution $\Delta E/E$	Bandpass Limited Flux (ph/s)	Flux Factor
							Limited	Flux			
X25	111	6	43	9.5	1.5×10^{14}				6.0×10^{-5}	9.0×10^{12}	0.08
SAGU	111	6	43	"	3.5×10^{14}				"	2.1×10^{13}	0.19
SAGU	111	0	"	21.0	"	3.1×10^{-4}	1.1×10^{14}		1.3×10^{-4}	2.2×10^{13}	0.20
SAGU	220	0	"	15.4	"	1.7×10^{-4}	6.0×10^{13}		5.8×10^{-5}	7.2×10^{12}	0.07
SAGU	311	0	"	8.8	"	1.4×10^{-4}	4.9×10^{13}		2.8×10^{-5}	2.0×10^{12}	0.02

Optimization for the cases with $\alpha=6^\circ$ is by Rowland-circle crystal bending. Optimization for the three cases with $\alpha=0$ is by slit limitation of beam divergence. Flux reduction factors (last column) are given relative to values (in bold) for the case of an unbent symmetric Si111 crystal without slit limitation.

7.2.2 Implementation of the NYX Energy-resolving DCM

Optical parameters for the actual NYX monochromator are summarized in Table 7-4. The radius of the 1st crystal bent in the tangential plane and the radius of the 2nd crystal bent in the sagittal plane are listed at the relevant energy of 12.658 keV as well as for the upper and lower operational range. The intermediate conjugate distances are listed with the matching bend radii to satisfy the Rowland condition given Si(111) crystals with a 6° asymmetric cut. Also listed in Table 7-4 are the reflectivities and asymmetric factors. All the details of the calculations listed are explained in the below reference (Lidestri & Hendrickson, 2009).

Lidestri, Joseph P., and Wayne A. Hendrickson. "Optimization of X-ray energy resolution from a horizontally focused single-crystal monochromator." *Nuclear Instruments and Methods in Physics Research Section A: Accelerators, Spectrometers, Detectors and Associated Equipment* 599.2 (2009): 289-300.

Table 7-4. Optical Parameters for the NYX DCM at Selected Relevant Energies

Energy (eV)	Reflectivity Si(111) ASC=6°	Asymmetric-factor Si(111) ASC=6°	Distance Source-DCM Tangential-Plane	Bend-radius 1 st Crystal (intermediate)	Conjugate-distance 1 st Crystal Sagittal-Plane	Bend-radius 2 nd Crystal	Distance DCM-Focus (cm)
			(cm)	(cm)	(cm)	(cm)	(cm)
4000	80%	1.45	5374	9225	3697	571	670
12658	97%	4.96	5374	20778	1083	180	670
17500	90%	25.45	5374	24849	212	130	670

The actual layout of the optical elements in the NYX beamline is shown in Figure 7-5 where the monochromator is positioned at 5374 cm from the source and 670 cm from the point of focus. All of the optical elements are located in Hutch 19-ID-C as shown in Section 6.

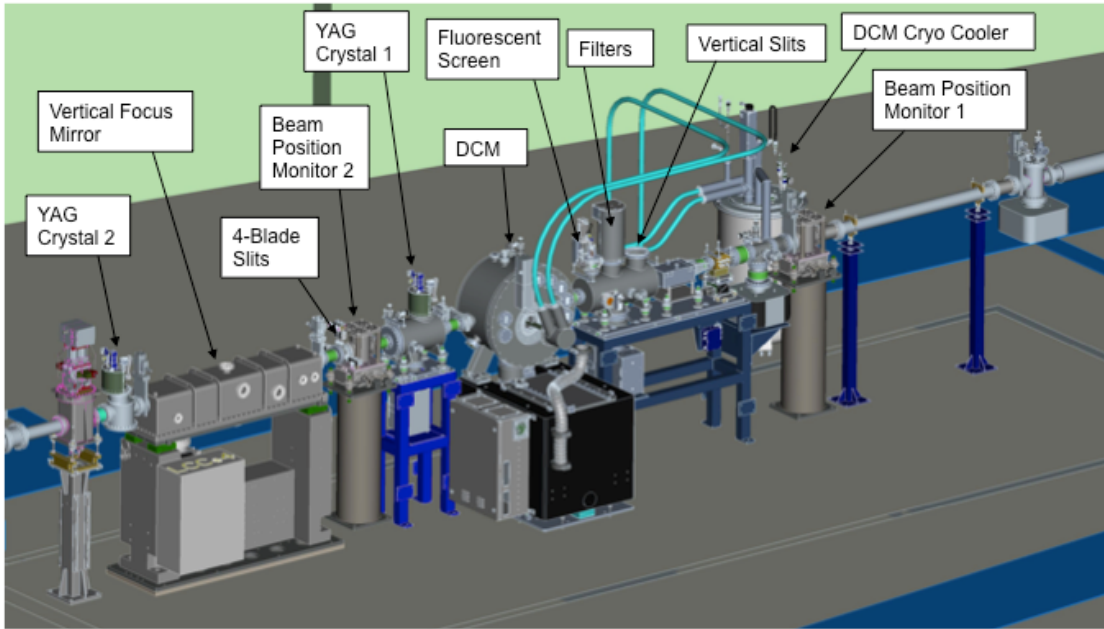


Figure 7-5. Layout of the optical elements in the NYX beamline.

7.2.3 Vertical Bending Mechanism

The 1st crystal in the DCM will be dynamically bent to achieve the Rowland condition at the various operational energies. The 1st crystal will be cylindrically bent in the tangential plane to the required radius to achieve the Rowland condition at varying energies. A prototype for such a bender was designed, installed and tested at beamline X4A prior to the shutdown of NSLS. This prototype is shown in Figure 7-6 and was internally water cooled. The prototype was tested along with a 6° asymmetric cut crystal positioned downstream and bent in the sagittal plane, successfully demonstrating the concept described above.

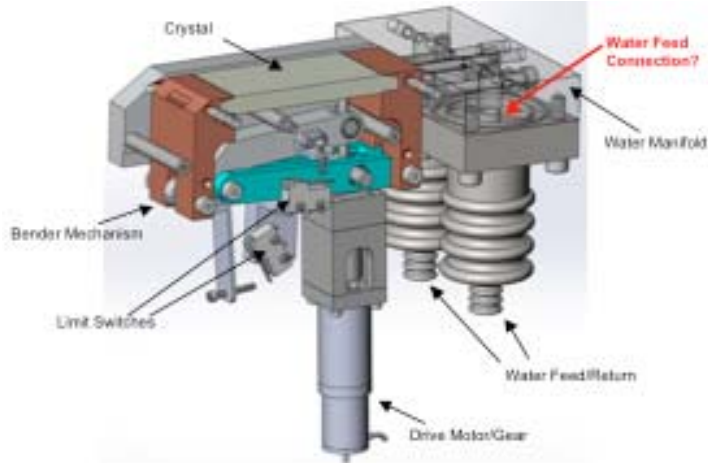


Figure 7-6. Prototype tangential bending mechanism tested at NSLS beamline X4A.

The tangential bending mechanism for NSLS-II beamline NYX will require integration of liquid N₂ cooling to manage the high heat loads associated with the IVU. The original bending mechanism proposed by FMB-Oxford is shown in Figure 7-7 and assumed a heat load similar to that produced by the X25 IVU.

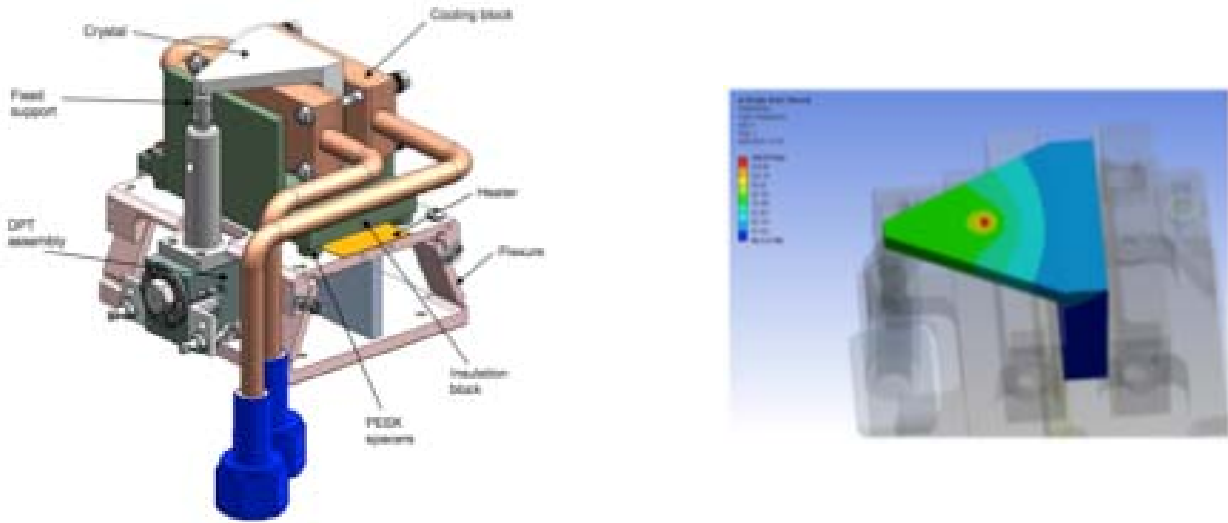


Figure 7-7. Tangential bending mechanism with indirect cooling and associated FEA.

The original bending concept cooled the 1st crystal indirectly via liquid-N₂ cooled OFHC copper plates. Extensive FEA produce marginal cooling given the power level of a standard IVU such as the X25 device; however, when the increased power load of the SAGU was considered, the indirectly cooled cantilevered concept was shown to have an unacceptable thermal bump. To mitigate thermal bump the first action was to reduce the incident power on the 1st crystal to 336 watts. This was done by carefully matching the size of the power-limiting mask upstream of the DCM to the beam distribution of the SAGU and also by adding a filter to attenuate the unused low energy x-rays. In addition to limiting the power delivered to DCM, a tangential bending mechanism with direct cooling channels was developed. The new design, shown in Figure 7-8, utilizes a U-shaped crystal.

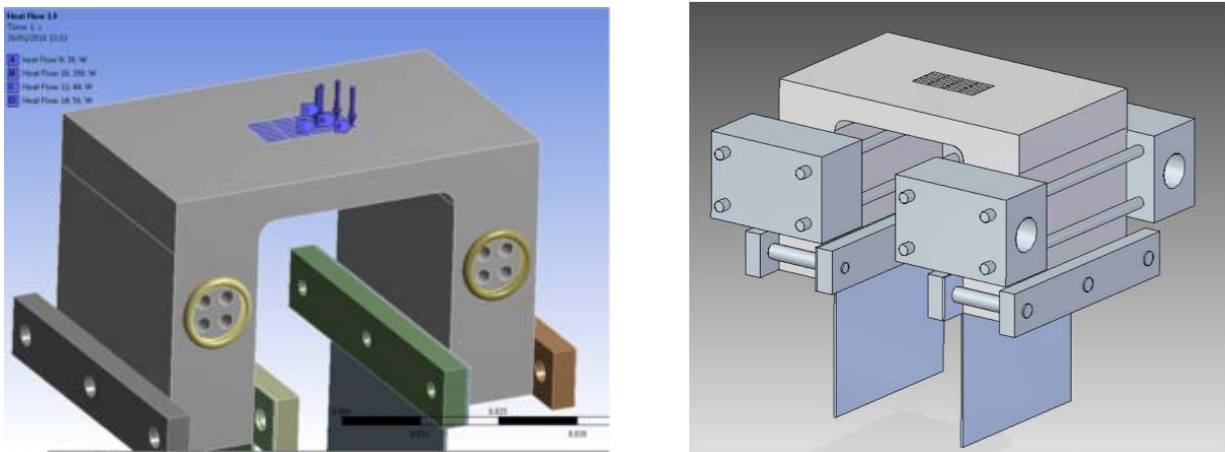


Figure 7-8. Tangential bending mechanism with direct cooling channels.

The U-shaped crystal has the advantage of being symmetric, which improves stability as well as providing two paths for heat flow. As confirmed by the initial FEA results, the U-shaped crystal with direct cooling channels minimizes the thermal bump and stability given the beam power of either the X25 or SAGU; therefore, this is the design that is being finalized for the 1st crystal-bending mechanism.

7.2.4 Sagittal Bending for Horizontal Focusing

The 2nd crystal is sagittally bent and the NYX DCM will use the design previously demonstrated at Soleil on the PSICHÉ beamline. This 2nd crystal sagittal bender design previously manufactured by FMB-Oxford and implemented in the PSICHÉ beamline at Soleil is shown in Figure 7-9.

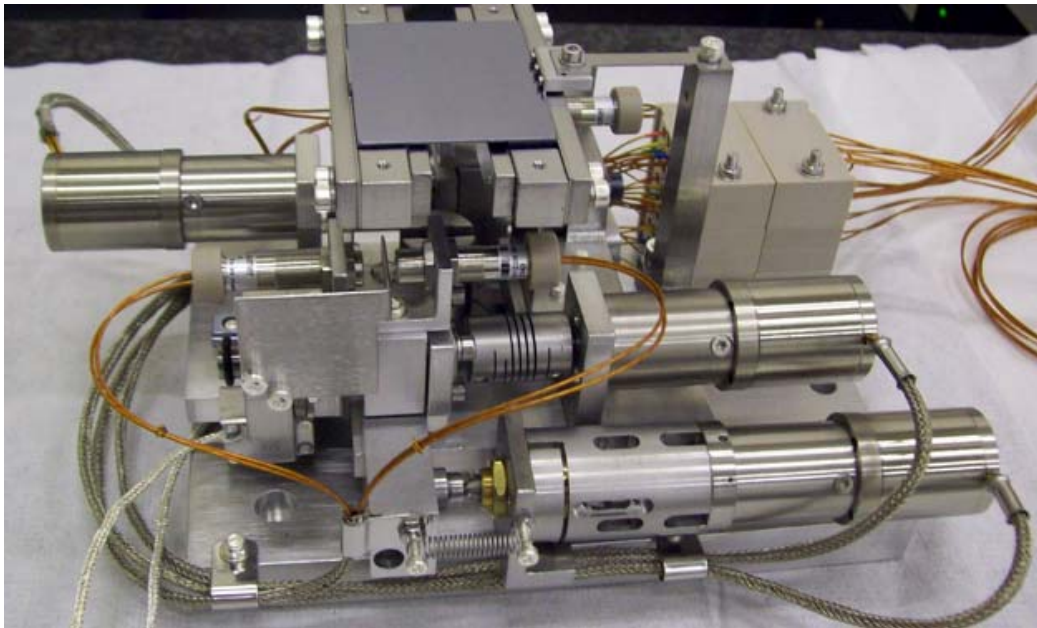


Figure 7-9. 2nd crystal sagittal bender mechanism.

The 2nd crystal is mounted in a sagittal bender to provide micro focussing in the horizontal plane. The sagittal radii required for the various operational energies are listed in Table 7-4. The design is based upon a standard design using leaf springs to provide the moment bending. The shape of the crystal is optimized to minimize antielastic bending and to inhibit twisting of the crystal during the bending. The actuators are prevented from over-travel via limit switches and the bending moment applied to each leg of the crystal monitored using encoders on each leg. The overall size of the unit is 110mm wide x 80mm long x 75mm high.

7.2.5 Cryogenic Cooling System

The 1st crystal in the NYX DCM will be directly cooled and connected with flexible lines to a closed-loop LN2 cryo-cooler systems provided by RI Research Instruments GmbH which was formerly a product of Bruker ASC. The Bruker ASC cryo-cooler has a proven track record of performance at many of the synchrotron light sources in the world was therefore chosen for the the NYX beamline. The sysyem is shown in Figure 7-10 and is known for its superior pressure stability and user friendly operation and handling, the cryo-coolers has been used to cool many double crystal monochromators.

The cryogenics will be automatically controlled and equipped with safety interlocks and pressure relief valves to make sure that all the failure conditions are covered safely. The systems are able to absorb heat loads of up to 2.5 KW at temperature levels of 77 K and above. Full remote operation is implemented into our control system, which is included into the cryo-cooler delivery package. The control system monitors signals and alarm conditions and is equipped with a touch screen panel with a TCP / IP interface. The system communicates with a remote client, e.g. via WebClient, EPICS or TANGO, for data logging and/or for additional settings of parameters or control functions of the system.

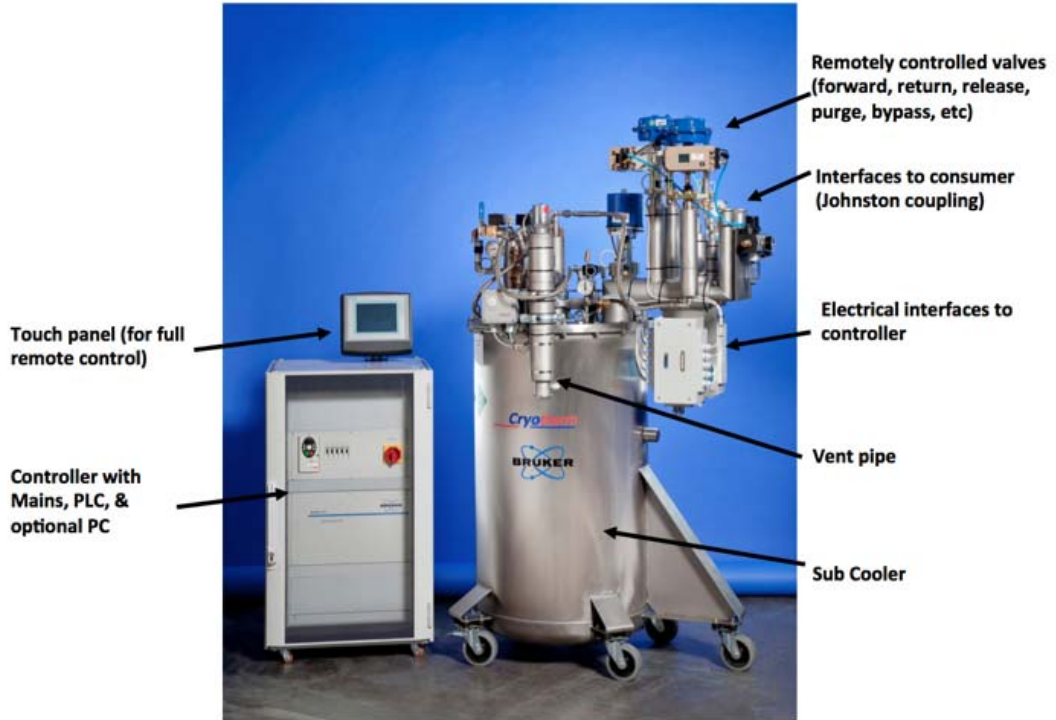


Figure 7-10. **Bruker ASC cryo-cooler**

7.3 Vertical Focusing Mirror (VFM)

The downstream focal point in the vertical plane, due to the 1st tangentially bent asymmetric crystal, is constrained by the Rowland condition and produces a focus at an energy-dependent intermediate conjugate distance listed in Table 7-3. The asymmetric factors also listed further shift this conjugate distance downstream; therefore, an additional vertical mirror is required for practical positioning of the focus. This grazing incident mirror is also needed for rejection of the unwanted high order harmonics diffracted by the monochromator, notably Si(333). The NYX beamline configuration shown in Figure 7-1, has total source-to-focus distance of 6044cm. Given these long distances, the length of a grazing incident mirror becomes long due to the finite beam divergence of the source. One of the added benefits of using bent asymmetric crystals in the geometry described above is the transition from a divergent beam to a converging one, allowing the vertical mirror to be kept to a minimum. The vertical focus mirror parameters are summarized in Table 7-5.

Table 7-5. VFM Parameters at Selected Relevant Energies

Energy (eV)	Distance Source-VFM (cm)	Bend-radius Cylindrical Tangential Plane (cm)	Distance VFM-Focus (cm)
4000	5644	149411	400
12658	5644	213444	400
17500	5644	213444	400

7.3.1 Mirror Specifications and Metrology

IRELEC has designed, manufactured and delivered the Vertically Focusing Mirror (VFM) system for the NSLS-II 19-ID-NYX beamline. The system as installed in hutch 19-ID-C is shown in Figure 7-11. The IRELEC design has proven its performances and similar systems are operated on the BM02 beamline at the ESRF (M1 and M2), and on the ROCK beamline at SOLEIL (M2a and M2b).



Figure 7-11. IRELEC vertical mirror system as installed in hutch 19-ID-C.

The adjustments of mirror pitch and roll are performed using a double-axis goniometric cradle, with a high stiffness and no crosstalk. Two translation stages allow the mirror adjustment into the beampath and the selection of the coating stripe. An additional integrated rotation stage around the vertical axis is proposed as an option for adjusting the mirror yaw motion. It has to be noticed that the management of the mirror yaw alignment by manual adjustments would improve the system global stiffness (and consequently stability). The position motions are located outside the vacuum chamber; the movement is transmitted to the mirror through welded bellows. The mirror substrate was manufactured by InSync, Inc. and the achieved mirror specifications are listed in Table 7-6.

The mirror reflectivity for blank silicon substrate at 3.5keV is shown in Figures 7-12A. The reflectivity is 90% at a 3.5mrad grazing angle. The mirror reflectivity for rhodium coating at 17.5keV is shown in Figures 7-12B. The reflectivity is 90% at a 3.5mrad grazing angle.

The vertical beam divergence of $50\mu\text{rad}$ was used to estimate the length of the NYX mirror. Given that the mirror is positioned 5644cm from the source the minimum length required is 80.6cm at a 3.5mrad grazing angle.

Table 7-6. Mirror Specifications and Metrology

Characteristic	Specified	Achieved
Tangential Slope Error:	$\leq 0.6 \mu\text{ rad RMS}$ in CA (with $\geq 20 \text{ km}$ removed)	$0.31 \mu\text{ rad RMS}$ ($\approx 210 \text{ km CV}$ removed)
Sagittal Slope Error:	$\leq 5.0 \mu\text{ rad RMS}$ in CA (with $\geq 10 \text{ km}$ removed)	$0.91 \mu\text{ rad RMS}$ (no power removed)
Surface Roughness:	$\leq 3.0 \text{ \AA}$ 40X objective	1.8 \AA RMS average
Clear Aperture:	1200mm X 32 mm	
Shape:	Trapezoidal	
Material:		Single crystal silicon
Coating:	2 stripes: rhodium & bare Thickness= $50 \pm 5 \text{ nm}$ Density > 95% of bulk material	
Physical Dimensions:	1340 mm ± 0.5 (L) 55 mm ± 0.1 (W) 91.2 mm ± 0.1 (W) 40 mm ± 0.5 (T)	1340.03 mm (L) 55.02 mm (W) 91.14 mm (W) 39.71 mm (T)

The above optic was manufactured by InSync, Inc.

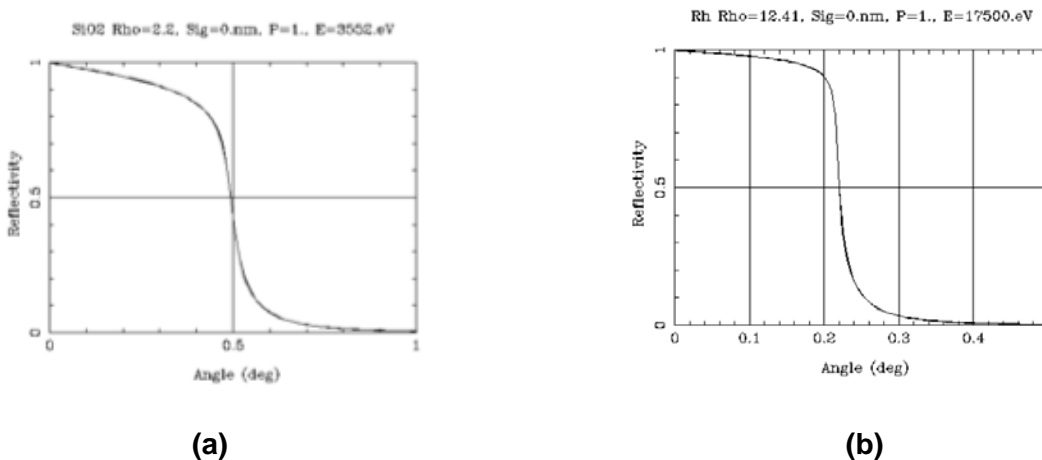


Figure 7-12. Mirror reflectivities at 3.5 keV for blank silicon (a) and at 17.5 keV for rhodium (b).

7.3.2 Mirror Bending System

The mirror figure is a dynamically adjustable using a mechanical bending system developed by IRELC following theory and practice of elliptically bent x-ray mirrors described in the below reference (Howells, MR).

Howells MR, Cambie D, Duarte RM, et al; Theory and practice of elliptically bent x-ray mirrors. *Opt. Eng.* 0001;39(10):2748-2762.

The design developed by IRELEC is mature with more than 20 systems delivered to many of the synchrotron light sources in the world. Most recently the bending system performance is described in the following reference (Nicolas, J.).

Nicolas, J., et al. "Focusing and defocusing using mechanically corrected mirrors at the MX beamline at Alba." *Journal of Physics: Conference Series*. Vol. 425. No. 5. IOP Publishing, 2013.

The bending system uses a trapezoidal mirror substrate to match the elliptical requirements. The mirror substrate mechanically bent with two independent bending moments where the bending strengths are directly controlled by strain gauges. The VFM bending system is shown in Figure 7-13.

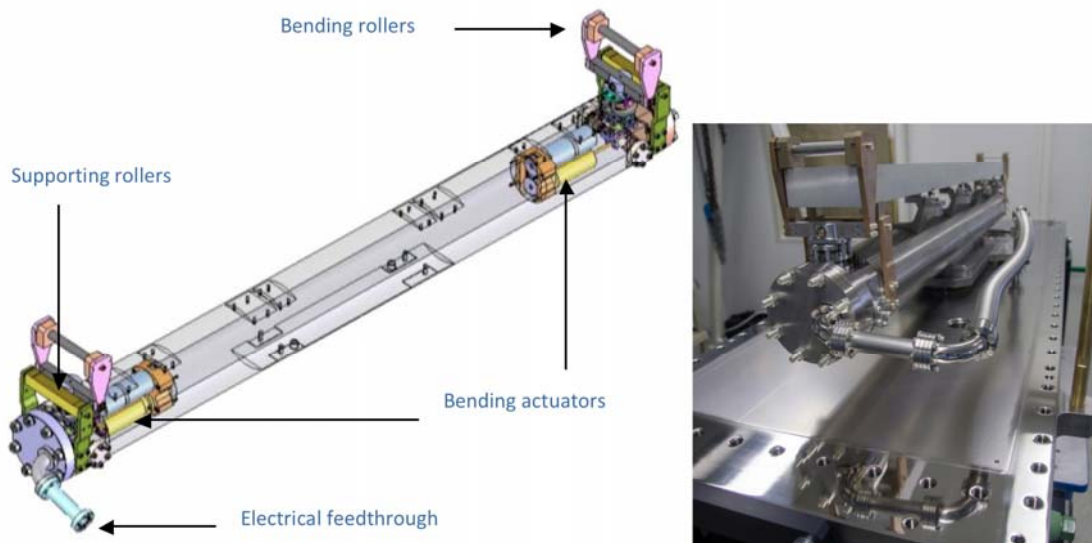


Figure 7-13. VFM bending system

A strain gauge offers better accuracy than an encoder as it directly indicates the force applied to the mirror. This measure does not depend on external parameters, such as mirror curvature, mirror temperature, beam variations, vibrations and mechanical conversion of actuator displacement into force. On the contrary, even if an encoder indicates motors displacements with a high accuracy, this indication is not reliable to estimate mirror bending for the reasons given above. The strain gauge is connected to a digital display with two set points for low and high thresholds. For security reasons, these thresholds can be read by the command control. The strain gauge is used for bender calibration and curvature fast adjustment during operation. Curvature accuracy has been controlled with LTP (ESRF, SOLEIL) and NOM (DLS, ALBA). It is better than 0.5%, with calibrated bender. This accuracy cannot be reached with encoders. Additionally, once the direct measurement of the bending strengths are correlated with metrology, the engineering model can be validated to deterministically predict the bending strengths to produce a desired elliptical figure.

7.4 Beamlne Analysis

7.4.1 Ray Tracing

The synchrotron optics program SHADOW (Lai & Cerrina, 1986) has been used to simulate the over all performance of the proposed beamline. The source parameters used in the computer model were computed from the actual electron beam parameters in a low- β straight section at NSLS-II (electron beam sizes $\sigma_x=31.46\mu\text{m}$ and $\sigma_y=2.97\mu\text{m}$; electron beam divergences $\sigma'_x=19\mu\text{rad}$ and $\sigma'_y=3.2\mu\text{rad}$). The x-ray source characteristics are derived from undulator parameters in NSLS-II source documents. Based on these parameters, we obtain $B = 0.63\text{T}$ at a gap = 7.8mm ($K=1.18$) from which radiation from the 5th harmonic for the Se K-edge (12658eV) yields a flux of 2.2×10^{14} (photons/sec/0.1%BW), a brightness of 1.5×10^{20} (photons/sec/mm²/mr²/0.1%BW), and photon beam horizontal and vertical divergences of $\sigma'_H = 19.3 \mu\text{rad}$ $\sigma'_V = 8.5 \mu\text{rad}$. This flux estimate is in-between the flux expected from the X25 and SAGU devices and can be scaled for comaprison. We have propagated ray tracing analysis for relevant operating energies and in particular show results at the Se K-edge in Figure 7-14.

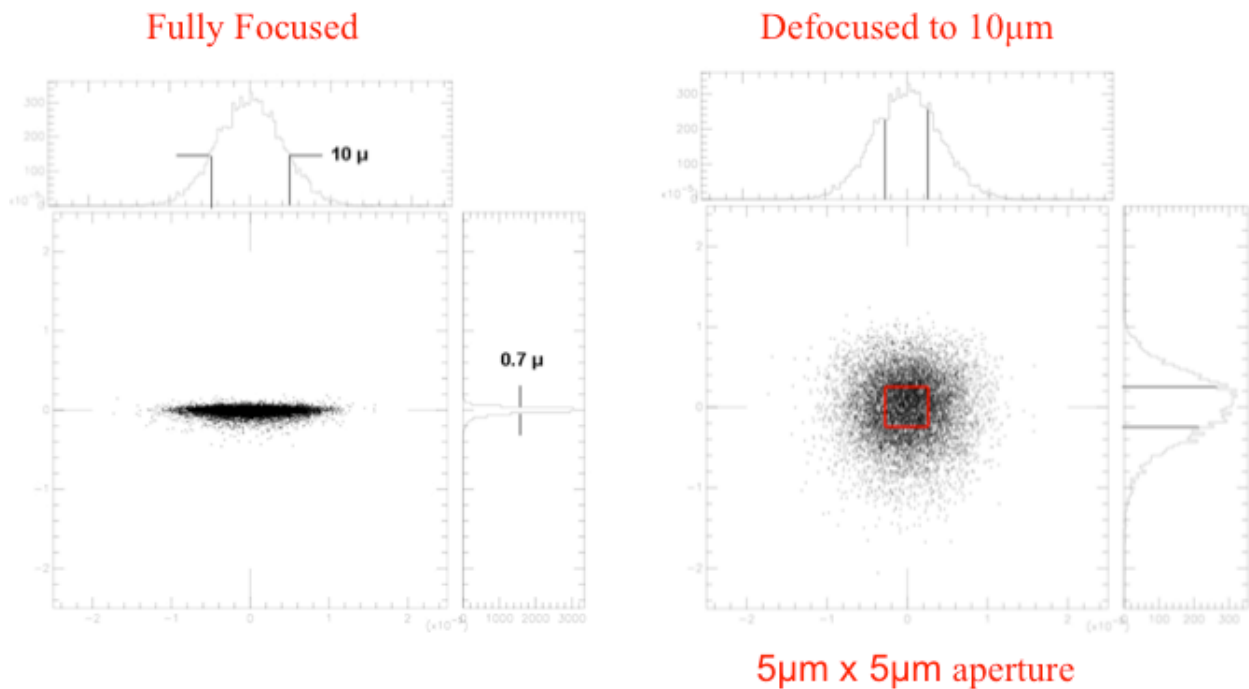


Figure 7-14. Ray tracings for NYX undulator beams at the Se K-edge energy.

The left side of Figure 7-14 shows the minimum focus given the 1st crystal is tangentially bent to meet the Rowland condition at 12658 eV for asymmetric cut of $\alpha=6^\circ$; the vertical mirror is elliptically bent to complete the resulting focus at the sample and the 2nd crystal is bent sagittally for focus at the sample postion. The right side of Figure 7-14 shows the symmetric spot produced by adjusting the VFM to shift the focus downstream of the sample postion, thereby expaning the beam at the sample position. In the event that a larger beam would be desired, curvatures of the VFM and sagittal crystal would be adjusted while maintaining the Rowland condition in the 1st crystal for optimal energy resolution.

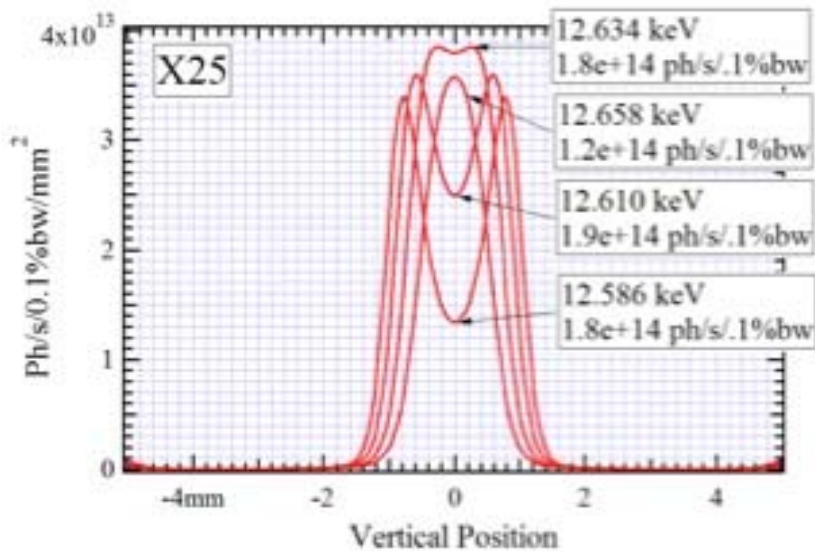


Figure 7-15a. Vertical cut from the X25 source at 5066cm ($Z=2.2\text{mm FWHM}$, $Z'=43\mu\text{rad}$)

The vertical divergence of the source incident to the 1st crystal can be determined from the vertical cut at 5066cm shown in Figure 7-15a. The 2.2mm cut corresponds to a source divergence of $43\mu\text{rad}$ FWHM. SHADOW is used to trace the phase-space in the vertical plane before and after diffraction off the 1st crystal having a 6° asymmetric cut. The phase-space plot shown in Figures 15b, 15c, 15d and 15e demonstrate the preservation of the source divergence only when the crystal is bent to achieve the Rowland condition. Firstly, Figure 15b shows the starting phase space in the vertical plane at the source, which is simply the initial condition of $5.94\mu\text{m} \times 43\mu\text{rad}$. The second phase space plot shown in Figure 7-15c traces the beam as it drifts over a distance of 5333cm, resulting in the beam expanding to 2.29mm given a divergence of $43\mu\text{rad}$. Note that the divergence has not changed in this phase-space plot since it has not yet interacted with the crystal. The last 2 phase space plots compares an asymmetric flat crystal with the same asymmetric crystal bent to satisfy the Rowland condition. The phase-space plotted for the beam diffracted off the flat crystal is shown in Figure 7-15d, where the vertical scale needed to be increase to accommodate the factor of 5 increase in the beam divergence to $215\mu\text{rad}$. The increase in beam divergence scales with the asymmetric factor which is defined as the ratio of the sines for the incident and reflected beams. Also shown in Figure 7-16d is the decrease of the beam size, which also scales by the same asymmetric factor to 0.458mm. The final phase-space plot, Figure 16e, is shown for the crystal bent to satisfy the Rowland condition, which clearly demonstrates that the reflected beam is now converging at the same $43\mu\text{rad}$ angle that was incident to the crystal. Finally, Figure 7-16 shows the rocking curve for the 2nd crystal with a -6° , which has a full width of $46.79\mu\text{rad}$ demonstrating 100% angular acceptance of the 2nd crystal. It is worth noting that this is only true when the 1st crystal is bent to the Rowland condition and is not true for the flat case.

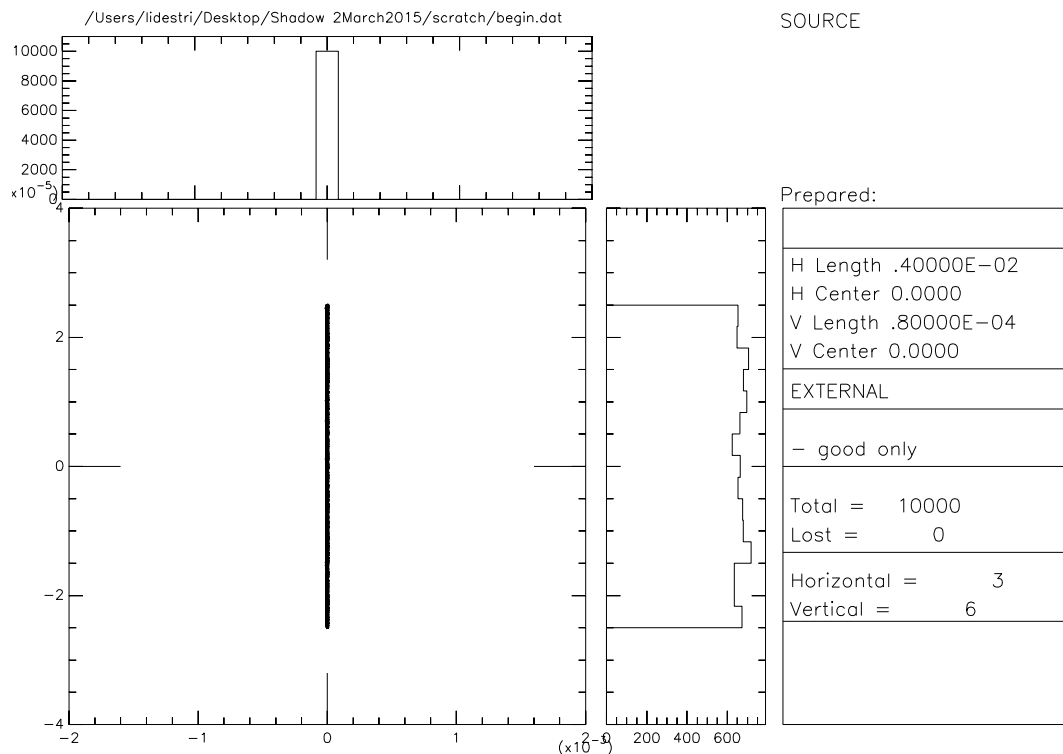


Figure 7-15b. Phase-space at source ($\leftarrow Z=5.94\mu\text{m} \rightarrow$ $\uparrow Z'=43\mu\text{rad} \downarrow$)

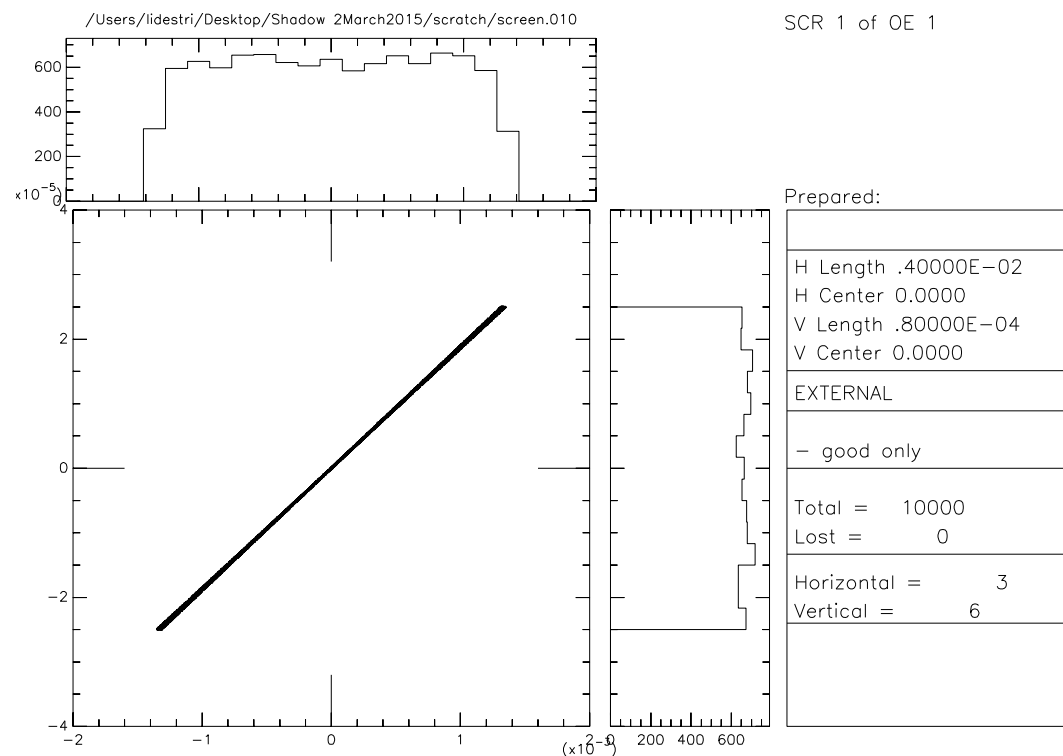


Figure 7-15c. Phase-space at 5333 cm before 1st xtl ($\leftarrow Z=2.29\text{mm} \rightarrow$ $\uparrow Z'=43\mu\text{rad} \downarrow$)

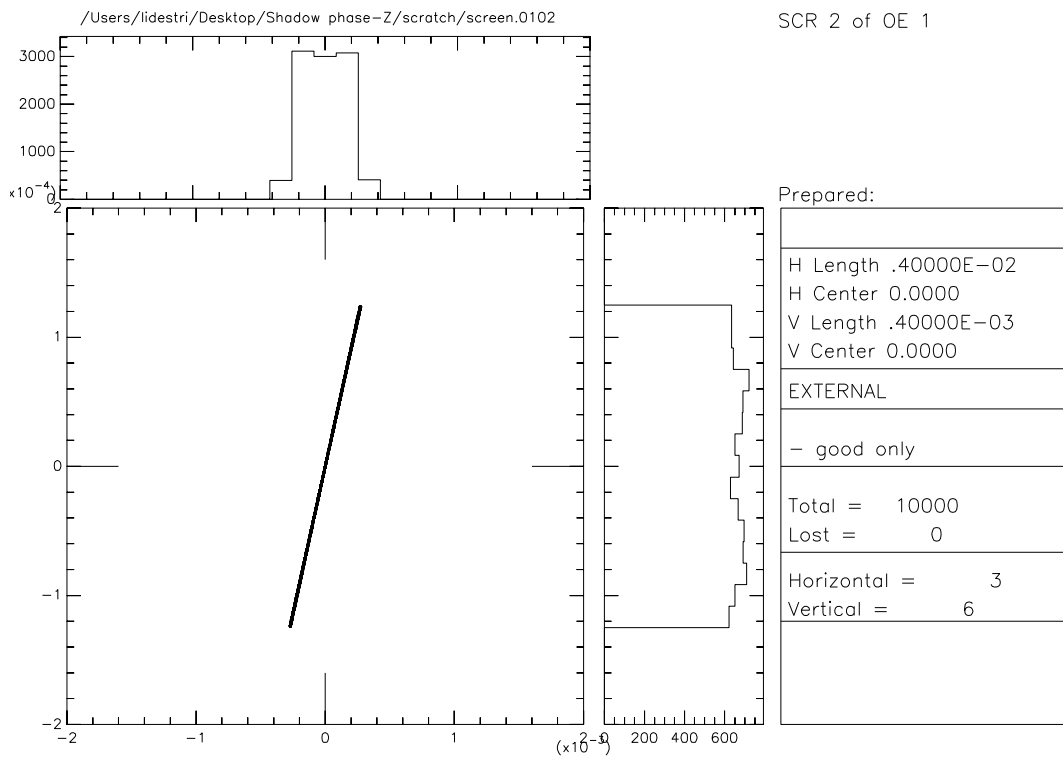


Figure 7-15d. Phase-Space at 5333 cm after 1st xtl-flat ASC=6° ($\leftarrow Z=0.458\text{mm} \rightarrow \uparrow Z'=215\mu\text{rad} \downarrow$)

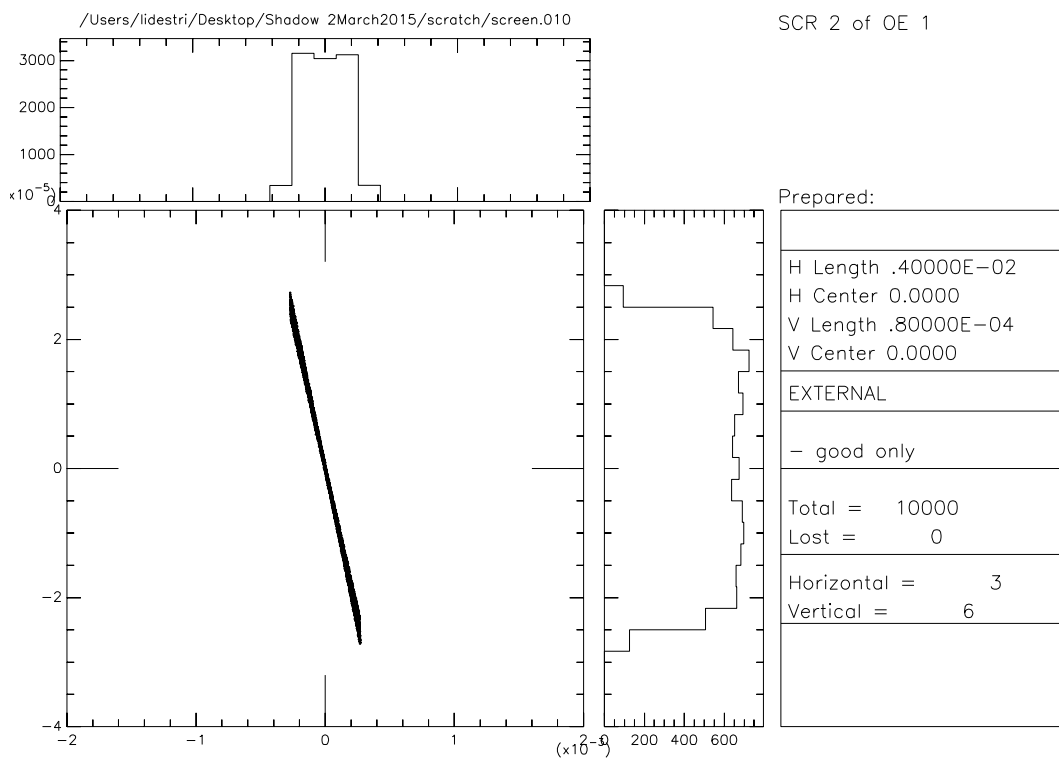


Figure7-16e. Phase-Space at 5333cm after 1st xtl-bent ASC=6°($\leftarrow Z=0.458\text{mm} \rightarrow \uparrow Z'=43\mu\text{rad} \downarrow$)

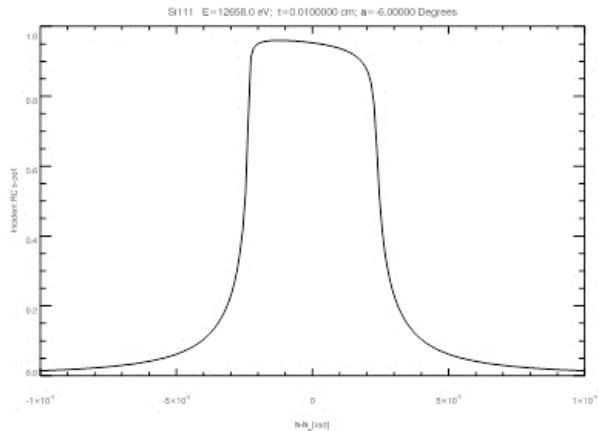


Figure 7-16. Incident rocking curve of 2nd crystal (full width = 46.79 μ rads)

7.4.2 Heat Load Estimates

The primary technical challenge to be addressed in realizing the increased energy resolution of the NYX monochromator Table 7-1 is reduction of the thermal bump by minimizing the effects of local heating of the crystal surface. It has been shown (Zaeper et al., 2001) that crystal bending is effective in compensating for the broadening of a rocking width from the thermal bump induced from local beam heating (Zaeper et al., 2001), which could be an ancillary benefit of our bending the 1st crystal; however, cryocooling of the crystal is the primary method in managing the power load. Power-density plots at a distance 50.66m from the straight-section center are shown in Figure 7-17, with vertical and horizontal cuts, and can be used to estimate the power incident on the 1st crystal of the DCM.

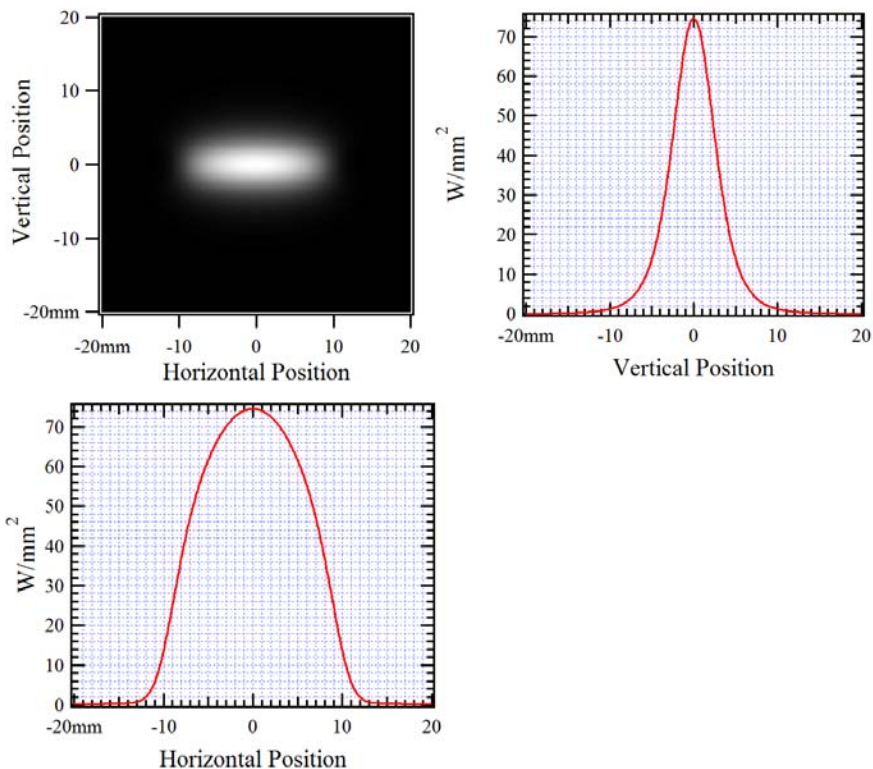


Figure 7-17. Power-density plots at a distance 50.66 m from straight section center.

Monochromator development work at the APS (Mills, 1996) has demonstrated that intrinsic Darwin widths of silicon can be maintained by cryogenic cooling at power loads as high as 3.8kW with an associated power density of 140W/mm² @ 8KeV (APS undulator A). The total power produced by the X25 undulator is 2.43kW with a corresponding on-axis power density of 22.6kW/mr². The total power produced by the SAGU is 7.6kW with a corresponding on-axis power density of 55kW/mr²

The power limiting mask upstream of the DCM is sized at 4x8mm and positioned 50.66m from the straight-section center. This corresponds to an angular horizontal acceptance of 154.8μrad and an angular vertical acceptance of 77.4μrad. Therefore, total angular acceptance is 1.198x10⁻² mr². The corresponding on-axis power for the X25 undulator is 270 watts and the corresponding on-axis power for the SAGU is 659 watts. To reduce the total power incident on the 1st crystal to 336 watts, a filter will permanently be positioned upstream of the power limiting to attenuate the unused low energy x-rays.

7.4.3 Beamline Efficiency Estimates

The flux estimates given in Table 7-3 for various ID and monochromator options are for perfect monochromator crystals, not considering reflectivity and absorption, and they do not consider losses that may occur in the mirror and other elements in the beamline. We have estimated efficiency factors for the various NYX beamline elements, and these are shown for the Se K-edge energy in Table 7-7. Thus, as implemented initially with the X25 undulator, we estimate that intrinsic characteristics of the beamline elements will reduce bandpass-limited flux by 68% from 1.5×10^{13} ph/sec to 1.0×10^{13} ph/sec. For the eventual SAGU, the actual bandpass-limited flux will be reduced from 5.1×10^{13} ph/sec to 3.5×10^{13} ph/sec. Further losses will occur due to endstation elements, including BPMs, air paths, collimators, and also filters that may be included to attenuate the beam intentionally.

Table 7-7. Efficiency of NYX Beamline Elements at 12.658 keV

Characteristic	Preserved Fraction
Monochromator reflectivity and transmission, crystal 1	97%
Monochromator reflectivity and transmission, crystal 2	97%
Monochromator angular acceptance	100%
Mirror reflectivity	90%
Mirror angular acceptance	100%
BPM transmissivity (3 at 30 μm each; 0.98 ³)	94%
Beryllium windows (4 at 0.5mm each; 0.96 ⁴)	85%
Entire photon delivery system	68%

In addition to losses due to absorption and reflectivity considerations, we can expect that beam profiles may be degraded from those given by the Shadow calculations shown in Figure 7-17, which do not consider slope errors in the mirror surface. The measured slope errors (Table 7-6) assure that these defects will not be devastating. As discussed above in our consideration of heat loads (Section 7.4.2), our designs are evaluated with finite element analyses to assure that thermal bumps are within manageable limits with respect to monochromator performance. We also expect that bending of the 1st monochromator crystal will serve to help mitigate thermal bumps.

7.5 Diamond Detector Beam Position Monitors

Beam position monitors (BPMs) employed on NSLS-II 19-ID-NYX beamline are based on chemical vapor deposition (CVD) diamond detectors developed by John Smedley & Erik M. Muller of the BNL instrumentation group. NYSBC additionally developed a BPM detector housing with a Beryllia PCB to optimize the thermal stability of the CVD diamond detectors. The diamonds are grown by Element 6 (London, UK), screened for imperfections, and then bread cut and polished. The first NYSBC detectors are shown in Figure 7-18.

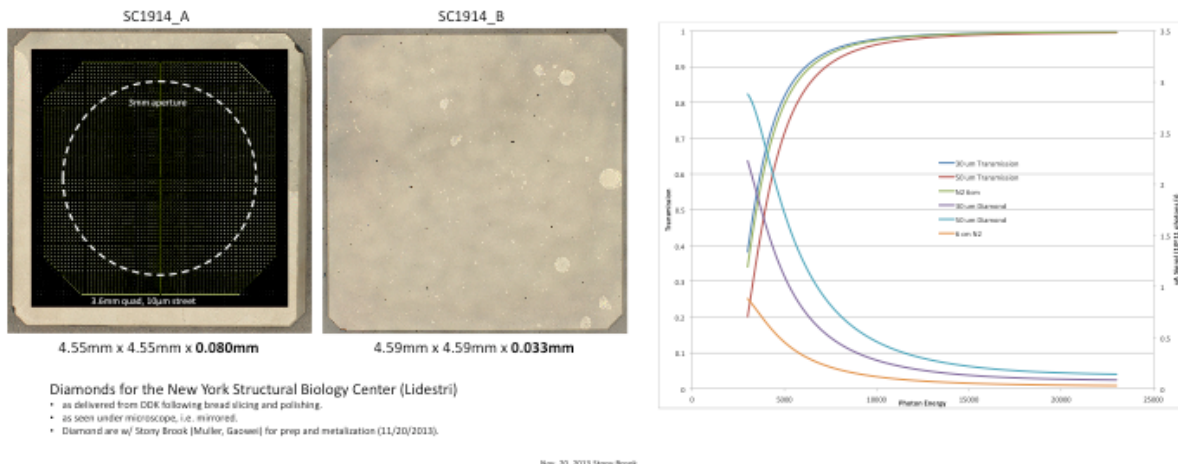


Figure 7-18. CVD diamonds detectors on right & x-ray response on left.

The metal quadrants and pads are deposited on the diamonds and then bonded to the Beryllia PCB and finally mounted into the copper housing shown in Figure 7-19 creating a complete BPM package. NSLS-II 19-ID-NYX beamline will use Libera Photon electronics developed by Instrumentation Technologies to digitally readout the BPM signals.

The beamline design for 19-ID-NYX at NSLS-II incorporates three BPMs in the photon delivery system before the endstation. One white BPM will be installed before the monochromator and two monochromatic BPMs will be installed, one downstream of each optical element. Finally, two BPMs have been integrated into the microdiffractometer. The first set of BPMs designated for use in the microdiffractometer were installed and tested on the X4A beamline prior to the NSLS shutdown. The tests included integration and testing of the Libera Photon digital readout. The test at NSLS beamline X4A demonstrated sub micrometer resolution.



Figure 7-19. NYSBC BPM housing design & Libera Photon digital readout.

8. End Station Instrumentation

The end station will feature a precision six-axis table and an air-bearing goniometer system. A dual integrating and counting pixel-array detector will be implemented to cope with exceptionally high count-rate densities at low angles from microdiffraction at NSLS-II while assuring accurate measurement of the weak high-angle data.

8.1 Microdiffractometer System

The microcrystal diffractometer system for the NSLS-II 19-ID-NYX was codeveloped with NYSBC and Charles E. Strouse of Crystal Logic Inc., Los Angeles, CA. This development involved prototyping a robotic sample changer that was integrated into BLUICE control software and included installation and testing at beamline X4A prior to NSLS shutdown.

The 19-ID-NYX microcrystal diffractometer (Figure 8-1) consists of three components—a high-precision goniometer, a six-axis detector table, and a robotic sample server. A unique feature of this system is the use of position-sensitive diamond detectors in the beampath that allow the instrument to dynamically track the beam.

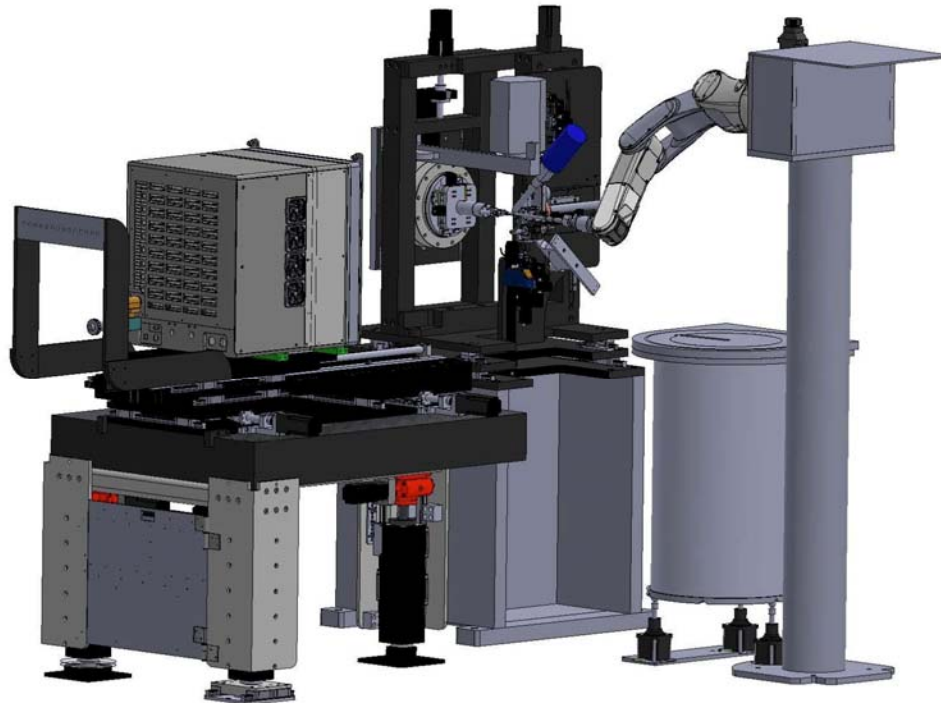


Figure 8-1. Integrated endstation assembly (microdiffractometer, robotic sample changer and pixel area detector)

8.1.1 Goniometer

The goniometer (Figure 8-2) sits on a massive aluminum base that can be anchored to the floor. This base also provides two electronics bays. All the motion control components are mounted in the rear bay. The front bay can be used for user supplied components. Above the base is a translation stage for horizontal motion perpendicular to the beam and a yaw stage. The yaw rotation is centered on the downstream diamond detector in the beampath.

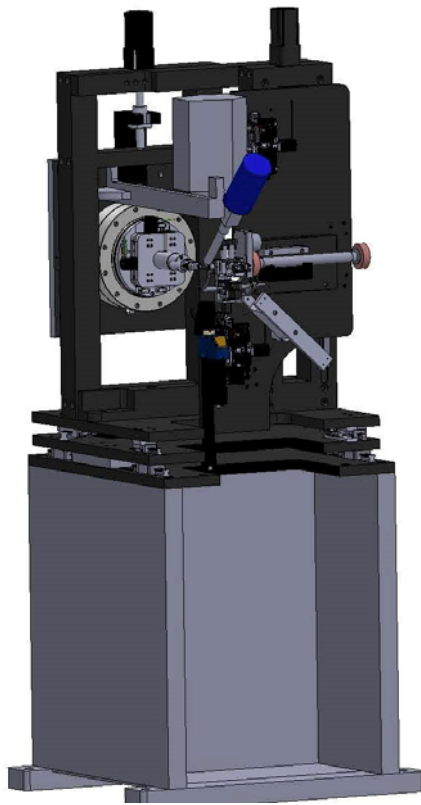


Figure 8-2. Goniometer system and base.

On top of the yaw stage is a double tower that supports two components with independent vertical translations. One component includes a 200mm air-bearing phi stage and a mount for a cryogenic cooler. The phi stage is based on a high-precision direct-drive servo motor with a dual readhead 3.6 million step encoder. On an independent vertical translation stage is the optics stage which contains all the sample visualization and beam conditioning components. The optics stage rotates in pitch about the downstream diamond detector. Also mounted on the optics stage is a pneumatic translation stage that can move a user supplied fluorescence detector into the beam.

Sample Positioner. A minikappa head is mounted on the phi stage integrated with a three-axis sample positioner (Figure 8-3). The phi stage motor attached to the vertical translation stage on top of which is a mount for a Cryostream sample cooler.

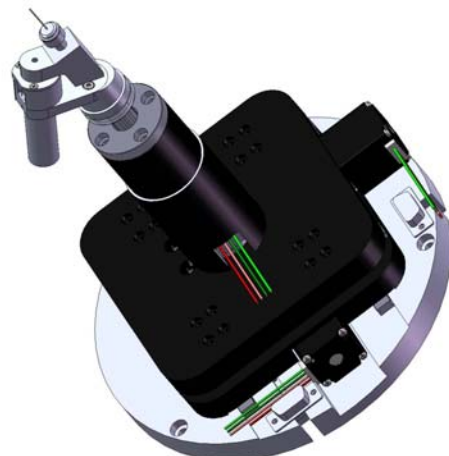


Figure 8-3. Phi motor stage with minikappa head and vertical translation stage.

The Cryostream mount contains a pneumatic actuator to retract the Cryostream for robot sample mounting. The position of the phi tower with respect to the optics tower along the beam direction is manually adjustable.

8.1.2 Beampath

The vacuum beampath (Figure 8-4) consists of a diamond position sensitive detector, a beampipe, a second diamond detector, a shutter, a four-blade slit system, and a beryllium window. These components are joined by NW25 flanges. At the exit of the four-blade slit is an ionization detector, a 750 micron scatter guard aperture and a 45 degree mirror with a hole through which the beam passes. The scatter guard and 45 degree mirror are mounted on a manually adjustable xy stage. Also attached to the four-blade slit component is a motorized beamstop. It is desirable to position the downstream diamond detector at the intersection of the pitch and yaw axes in the center of the goniometer. The position of the sample with respect to the end of the beampipe can be adjusted manually by moving the downstream vertical stage.

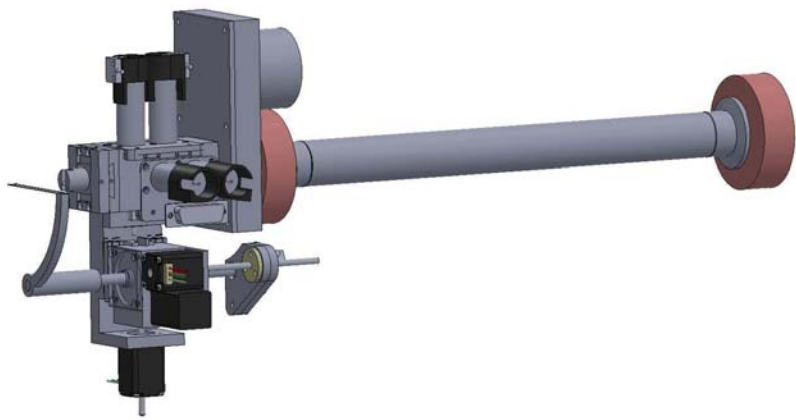


Figure 8-4. Diamond detectors integrated in beampath assembly.

8.1.2.1 Diamond Detectors

The diamond detector housings were developed by NYSBC as described in section 7 and supplied by Crystal Logic. They are mounted on a stainless steel beampipe. As delivered, the separation between the two detectors is 368 mm. It is relatively easy to shorten this distance if for some reason that is desirable. The stainless steel tubes mount in a cradle on the goniometer in such a way that it can be removed and replaced very reproducibly. By changing the position of a locator plate, it is possible to adjust the position of the beampath along the beam direction. As delivered the downstream diamond detector is located very close to the intersection of the pitch and yaw axes in the center of the goniometer, and the upstream detector is 380 mm upstream from that intersection. In this configuration the Y and optics Z motions of the goniometer are used to center the downstream detector on the beam, and the pitch and yaw are used to position the upstream detector.

8.1.2.2 4-Blade Slits

The blocking elements in the rotary slits are 2mm tungsten carbide rods mounted 2mm off center in stainless steel rods. These rods are concentric with the shafts of zero-backlash gearmotors. One pair of blades is represented below in the open and closed positions (Figure 8-5).

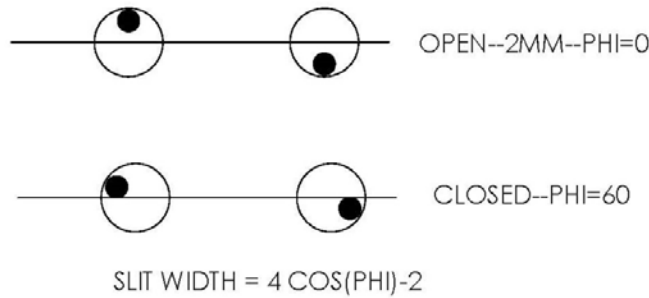


Figure 8-5. Rotary slit concept.

Each of the motors has a home sensor that is tripped when the blade is in approximately the orientation of the blade in the upper left corner of the drawing above. To get to the nominal open configuration indicated above, one of the blades in each pair must be rotated by 180 degrees. One needs, however, to establish a more accurate home position that corrects for inaccuracies in the home sensors and that reflects the actual beam position in the slit assembly.

The x-ray beam can be used to obtain a more accurate home position. With the beam centered in the diamond detectors one can rotate each blade in both directions to determine the positions at which the beam intensity is cut in half. This should require a rotation of approximately 60 degrees in either direction. The midpoint between these two positions should correspond to a more accurate home position for that blade.

8.1.3 Motorized Beamstop

The motorized beamstop shown in Figure 8-5 has a number of useful features. It provides precise three-axis positioning, the beamstop support arm swings out of the way for convenient manual mounting, a YAG crystal can be mounted on the support arm for beam visualization, and the arm is spring loaded in the axial direction to prevent detector damage should the detector be driven into the beamstop.

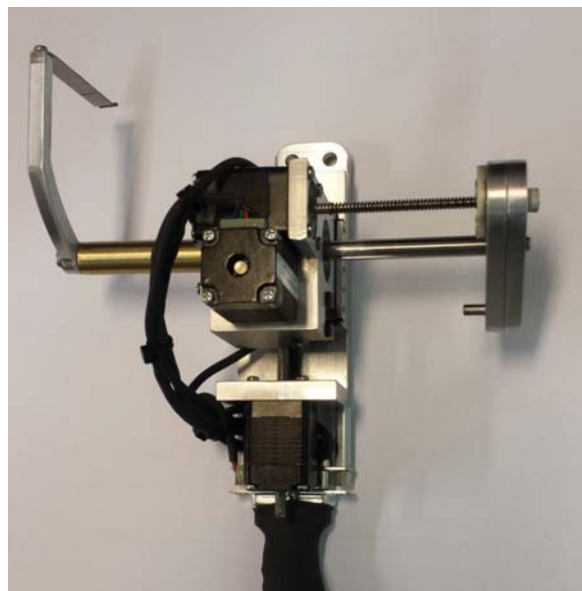


Figure 8-5. Motorized beamstop.

8.1.4 Sample Visualization

The sample visualization components include two viewers, one mounted above and one below the sample. One of the viewers can be configured to view the sample through a 45 degree mirror to provide an inline view. The top viewer is a Questar camera with UV capability. The bottom viewer is based on a dual magnification Qioptiq lens system. Both these viewers are mounted on motorized xy stages and have provision for motorized focus.



Figure 8-6. UV capable telescope.

8.1.5 Motion Control

The control system of the goniometer portion of the instrument is based on three Galil DMC 4080 controllers located in the rear electronics chassis under the goniometer.

8.1.6 Detector Table

The detector table (Figure 8-7) is of conventional design. It has a 91 cm x 122 cm granite top supported on three motorized legs. Each leg contains a jack with a 900 kg capacity. On top of the table is a three-axis detector positioner. The six axes are all driven with Oriental Motors Alpha-Step steppers and controlled by a Galil DMC 4060 controller. Each motor package consists of an integrated motor, encoder, gearhead and brake. Each axis is equipped with homes and limits. A chassis containing the controller and motor drivers is mounted on between the rear legs. The table is built in such a way that it can be shipped as three separate components and easily reassembled on site.

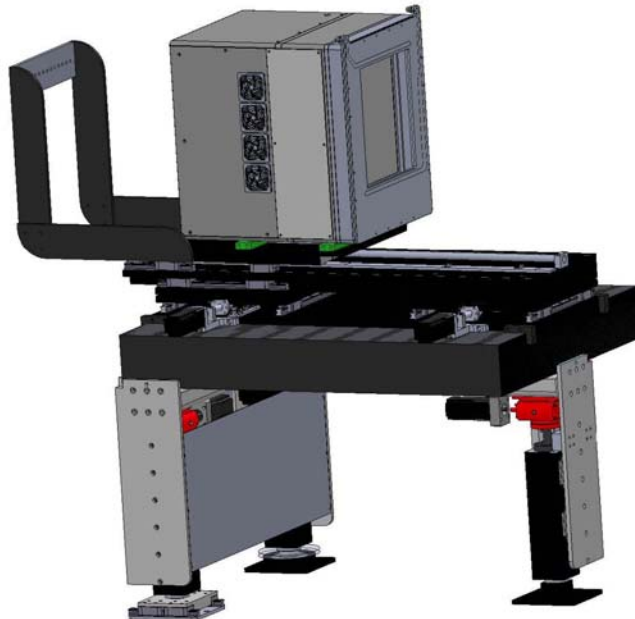


Figure 8-7. Detector and independent kinematic table.

8.2 Robotic Sample Changing

8.2.1 Sample Server

The 19-ID-NYX Sample Server (Figures 8-8 and 8-9) is a standalone device consisting of a Denso six-axis robot on a floor mounted pylon, and a Dewar system that holds 16 Unipucks. The dewar sits on a kinematic mount attached to the floor, allowing easy manual dewar exchange. Provision is also made for an upgrade to a system with automated dewar exchange.

A chassis on top of the robot pylon contains the control electronics and a ethernet switch that provides communications to the goniostat, the detector table, and the beamline computer. The robot controller acts as a network server which mounts and dismounts specified samples based on commands sent from the beamline computer. It also coordinates the robot motion with motions of the goniometer and the dewar lid. A graphical user interface on the robot controller pendent is useful for troubleshooting and serves as a template for a GUI on the beamline computer.

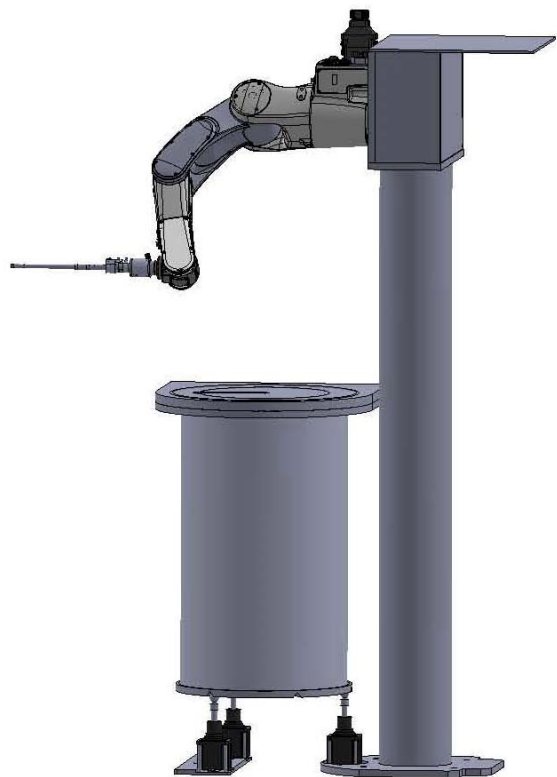


Figure 8-8. Sample server (robotic arm and Dewar system)

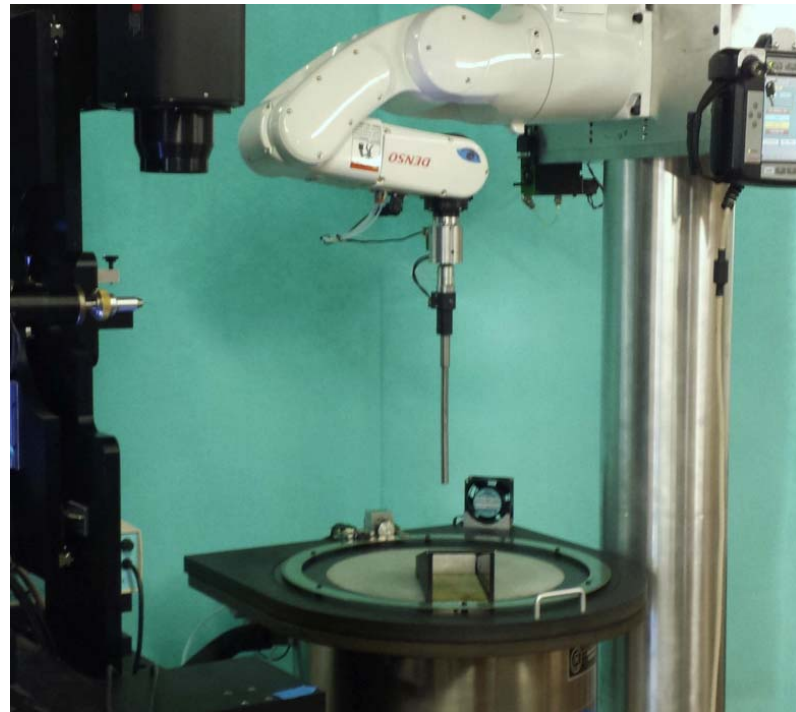


Figure 8-9. Photograph of robotic sample changer integrated with goniometer.

8.2.2 Sample Gripper/Grabber

The sample gripper (Figure 8-10) is based on a custom magnet designed to accommodate a variety of commonly used sample bases. The magnet is extended and retracted by a pneumatic actuator. The grabber is equipped with three axis collision switches which stop the robot if any unplanned contact is made.



Figure 8-10. Sample gripper assembly.

The sample gripper is specifically designed to transport crystals on ferromagnetic bases between the dewar and the goniometer. Built into this device are four trip switches that stop the robot if the gripper collides with anything in its environment. Three of these switches are associated with a round plate with a tapered edge that is spring loaded against a matching cup. This plate holds the probe that extends into the dewar to pick up the sample. If a collision causes the plate to be displaced from its support, one or more of these switches will be actuated. The probe consists of two telescoping stainless steel tubes that are spring loaded in the extended position. If the probe encounters a solid object while moving axially, the inner tube compresses the spring and moves toward the robot flange. After a small amount of travel, this motion trips a Hall sensor, that is wired in parallel with the other mechanical trip switches. This arrangement provides some flexibility in the axial positioning of the probe. The telescoping tubes that make up the probe contain a key that prevents the inner tube from rotating with respect to the outer tube. If the tubes are forcibly rotated with respect to one another, this key could be broken.

The cup in the bottom of the trip switch housing has a provision for the adjustment of the probe alignment. It is connected to the bottom of the housing through three sets of opposing screws. The easiest way to align the probe is to mount the gripper in a lathe with a dial indicator indicating the end of the probe. One rotates the lathe chuck by hand and adjusts the three sets of screws with the 1.5mm hex wrench provided to minimize wobble. One can easily center the probe to a few tenths of a mm. This alignment is not critical to the operation of the system since the calibration routine measures the displacement of the probe tip from the axis of rotation and applies appropriate corrections. If, however, this displacement is too large, it can cause problems with the drying operation.

The mechanism that actually picks up the sample is a small brass can with a specially designed ring magnet mounted on the open end. The magnet design allows it to be used with a variety of commercially available sample bases. The can is driven up and down the gripper tube by a pneumatic actuator which resides at the warm end of the device. The lower tube of the gripper has an inner diameter that allows it to slip over the end of a sample holder. As the tube approaches the sample holder axially, with the magnet extended, the magnet contacts the sample holder just before the tube contacts the shoulder of the sample holder. The strong gripper magnet overcomes the weaker magnets on the goniometer or the puck, allowing the sample to be transported from one location to the other. To release the sample, the gripper is moved to the target location and the can is retracted. This is done in two stages. First 15 psi air is fed to the actuator. This is insufficient to pull the magnet away from the sample holder. Thus if the actuator retracts, this indicates that no sample is present. A second Hall sensor is used to detect whether the magnet is in the retracted position. If the can does not retract, indicating that a sample is present, 60 psi air is supplied to the actuator. This releases the sample and the Hall sensor is actuated. One can use a similar process when picking up a sample, to determine whether or not a sample is present at the pickup point.

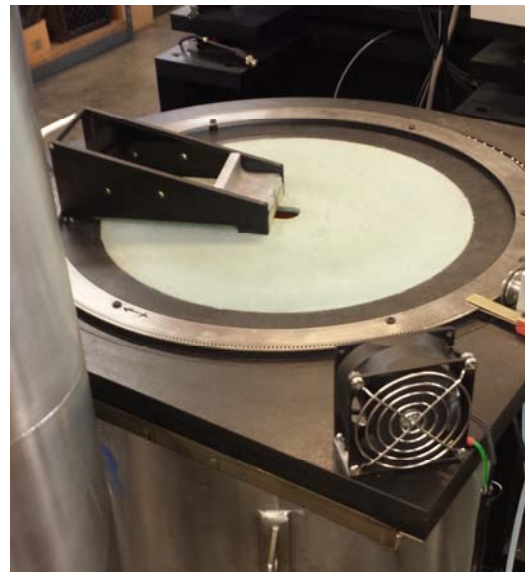
In addition to the two air lines going to the pneumatic actuator, a third line allows dry air or nitrogen to be delivered to the inside of the gripper during the drying operation. The purge flow is controlled by a solenoid valve driven by the robot's IO68 line.

8.2.3 Dewar System

Figure 8-11a shows a pan with provision for 16 Unipucks sits on a kinematic mount inside a custom 76 liter dewar. Below the pan is a tank that is used to periodically pump liquid nitrogen into the pan. This function is controlled by a Galil DMC 30000 series controller which also controls the rotary lid shown in Figure 8-11b.



a



b

Figure 8-11. (a) Open Dewar pan showing 16 Unipucks. (b) Closed Dewar showing the rotary lid with entry slot.

8.2.4 Automated Dewar Exchange

The base scope design for the 19-ID-D hutch includes a vestibule for easy add-on at later date to facilitate automated dewar exchange (Figure 8-12). The hutch design includes internal sliding door and a swing door and two PPS interlocks. Continuous data collection would be accomplished in a Round-robin cyclic loop using a 2 Dewar lift-spinner with 256 samples per Dewar. The ultimate number of Dewars in cyclic loop is only limited by practical floor space.

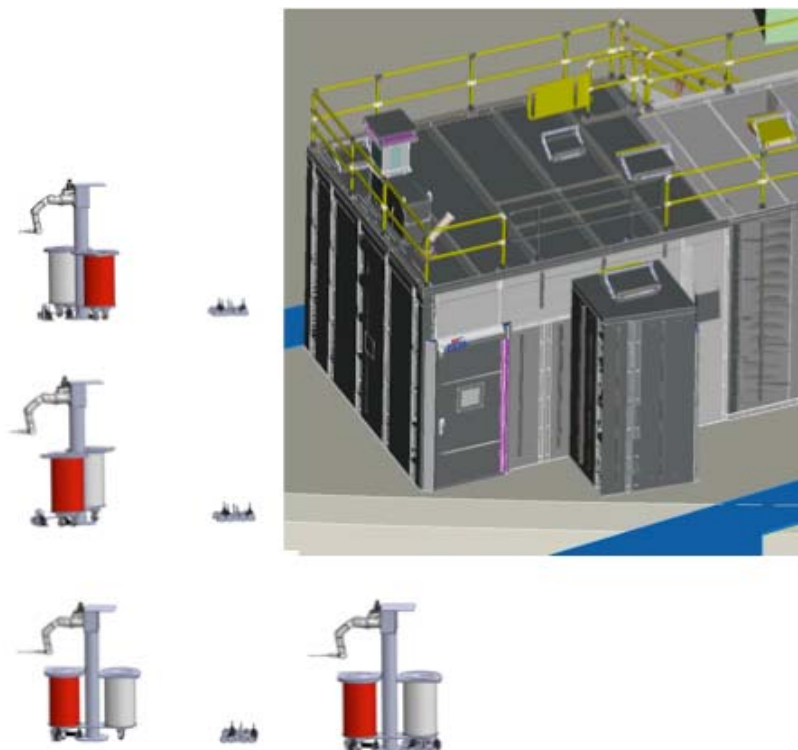


Figure 8-12. Automated dewar exchanger concept with integrated with hutch vestibule.

8.3 Pixel Array Detector System

8.3.1 Introduction to Pixel Array Detector Technology

Large Pixel Array Detectors (> 400mm sq.) were introduced for macromolecular X-ray crystallography in 2005 at the Swiss Light Source. This revolutionary technology features fast readout, shutterless data acquisition, statistically independent pixels with single-pixel point spread, low noise, and high dynamic range. It was superior in almost all respects to the CCD detector technology then used for macromolecular crystallography experiments done at synchrotrons.

The pixel array detector (PAD) introduced at the Swiss Light Source, and subsequently manufactured by Dectris Ltd., consisted of a pixel design that counts individual photons. The type of analysis done on the signal from an incoming X-ray photon is determined by an Application Specific Integrated Circuit (ASIC) and is not limited to photon counting. ASICs have also been designed that accumulate charge in a capacitor in each pixel (detector at the SLAC LCLS), and a joint design by ADSC and Cornell University in which charge from an incoming X-ray photon charges a capacitor holding approximately 50 12Kev photons and the pixel counts the number of these “charge ramps” and digitizes the remaining charge ramp on readout. This “charge ramp counting” design was referred to in the literature as the “MMPAD”.

An overview of Pixel Array Detector technology was given in a Power Point presentation, which also contains a detailed description of the charge ramp counting pixel. In this presentation, it was postulated that the lower resolution, higher intensity data would be of higher quality when collected in the charge ramp counting mode, and that the higher resolution, lower intensity data would be of higher quality when collected in the photon counting mode.

8.3.2 Development of a Dual Mode Pixel Array Detector for NYX

The Pixel Array Detector (PAD) system for the NSLS-II 19-ID-NYX was codeveloped by Area Detector Systems Corporation (ADSC) under contract to NYSBC with funding granted by Defense Threat Reduction Agency, Army Research Office of the Department of Defense (DTRA-ARO-DOD) (grant # W911NF-10-1-0532). This development involved prototyping the HF-262K Dual Mode Pixel Array Detector (DMPAD) and the HF-4M DMPAD. The HF-262K DMPAD was integrated into Blu-Ice control software, installed and tested at beamline X4A prior to NSLS shutdown.

In late 2010 discussions between ADSC and NYSBC began on a design of a pixel array detector for the NYSBC beamline NSLS-II 19-ID-NYX. A Dual Mode PAD design was presented by ADSC to NYSBC and discussions to contract a design and produce a Dual Mode Pixel Array Detector began. In February 2011 the Contract was signed to design and produce a Dual Mode Pixel Array Detector (DMPAD).

Previous MMPAD ASIC Design. As part of an SBIR grant funded by the National Institutes of Health, ADSC developed a pixel array detector design, called the MMPAD (“Mixed Mode Pixel Array Detector”). This design (“AE207”) implements a charge ramp counting pixel design, and was the starting point for the first “mode” of the Dual Model Pixel Array design. The charge ramp counting mode is quite complex, and having a working version of this mode in a prior ASIC design was a significant advantage in creating the new Dual Mode design.

8.3.3 Silicon Design for the DMPAD

In preparation for testing of the Dual Mode design, a testing interface called a “Jaguar” board was developed for testing ASICs. A 128 x 128 pixel MMPAD ASIC with bump-bonded silicon diode sensor

was attached to a Jaguar “socket board” for testing. This allowed testing electronics and software to be developed for one of the two “modes” of the Dual Mode design.

In addition to implementing the two modes of operation for each pixel, charge ramp counting mode and pulse, or photon counting mode, we identified an additional feature that would distinguish our ASIC design from others being used in synchrotron applications: the overlap of data acquisition and data readout. Other ASIC designs by us and competitors required data acquisition to be halted while the ASIC was read out, causing loss of data for 1.0ms to 2.5ms, depending on design. Elimination of this “readout dead time” was added to the ASIC design.

The MMPAD pixel size was 150 microns square, using a 0.25 feature size. We kept the same pixel size of 150 μ m for the DMPAD but reduced the feature size of 0.25 to 0.18 to accommodate the additional circuitry required for the additional photon counting mode.

Design and Fabrication of a 16 x 128 pixel ASIC. In June 2011, a silicon designer was hired to begin work on the Dual Mode ASIC design. Due to the high cost of the layout and production of an ASIC design, and the 180 μ m silicon feature size it was decided that the first prototype ASIC to be produced should be a single “slice”, consisting of 16 columns containing 128 rows each of pixels. Based on a successful completion and verification of this single slice design, a full 128 x 128 pixel ASIC can be constructed as 8 copies of this single slice.

In December, 2011, this single slice ASIC design was submitted to MOSIS, a silicon fabrication consolidation service, for production. The process took about 10 weeks to complete. By March 2012, the ASICs were received, hybridized (diodes attached to the ASIC via a process called “stud bumping”) and mounted onto a “socket board” for testing using our Jaguar testing interface.

Testing and Conclusions for the 16 x 128 Pixel ASIC Design. Testing of the 16 x 128 pixel design demonstrated several problems with the initial silicon design. There were two major design improvements needed as a result of this testing: the need for 6 bits of pulse mode threshold “trim” rather than 5 bits, and better shielding and routing of the digital signal lines.

8.3.3 Final Design and Fabrication of a 128 x 128 Pixel ASIC

The improvements from testing the 16 x 128 pixel ASIC design were incorporated into a final 128 x 128 pixel ASIC design and submitted via MOSIS in September, 2012. A set of 11 wafers with a revised 128 x 128 ASIC design were received in December, 2012, and half of the wafers were sent to have solder bumps applied to each pixel, a process necessary to bump-bond diodes to the ASICs.

Testing and Conclusions. A single ASIC was bump-bonded to a diode sensor and mounted onto Jaguar socket boards for testing and data taken. The most complex part of the Dual Mode pixel design to calibrate is the pulse, or photon counting, mode. The pulse mode threshold “trim” bits in each pixel are used to set the counting threshold of the pixel for a given incident energy. Multiple energies from 8Kev to 17.5Kev are calibrated, or “trimmed”, with interpolation used for intermediate energies. The calibration software infrastructure needed for the 512 x 512 pixel prototype detector, and later the HF-4M detector, was developed using these single ASIC hybrids. Calibration software for the charge ramp counting mode had been previously developed for the AE207 “Mixed Mode” pixel array design.

Not every problem in this “final” ASIC design was completely solved. In particular for the pulse, or photon counting mode, there were still extra counts recorded when the readout circuitry was active and data acquisition is enabled. This means that the overlap of readout and data acquisition mode of data collection cannot be used in for pulse mode data collection. However, there are no problems with overlapping data acquisition and readout in the charge ramp counting mode. When a detector uses a mixture of pulse and charge ramp counting modes, the overlap of data acquisition and readout must not be used. This limits the performance of the detector in a true Dual Mode.

8.3.4 Final 512 x 512 Prototype DMPAD Detector (HF-262K)

The purpose of the intermediate HF-262K detector: First, to develop the building blocks needed for the large HF-4M detector and second, to demonstrate that the DMPAD technology works as intended at a synchrotron beam line.

Detector Design Requirements. Since charge ramp counting mode is an integrating mode, the detector needs to be run at low temperature ($\sim -30\text{C}$) in order to minimize the noise from dark charge. (Pulse mode does not require low temperature operation.) This requires a method of cooling the modules and that the modules be run in a vacuum in order to ensure thermal isolation from the rest of the detector. The detector system must include a vacuum pump and water chiller. A sturdy vacuum enclosure and window capable of withstanding vacuum forces is required.

The active area of the HF-262K DMPAD detector is approximately 80mm sq. For this area, a carbon fiber window may be used. Peltier cooling of the modules was chosen for its simplicity and ability to cool the modules to the required temperature.

A photograph of a completed HF-262K detector is shown in Figure 8-13.



Figure 8-13. HF-262K

Module Design. The basic detector element for both the 512 x 512 prototype DMPAD (HF-262K) detector and the larger HF-4M detector is the module. A module consists of four ASICs bump-bonded to a single diode sensor giving 128 rows by 512 columns of pixels (Figure 8-14).

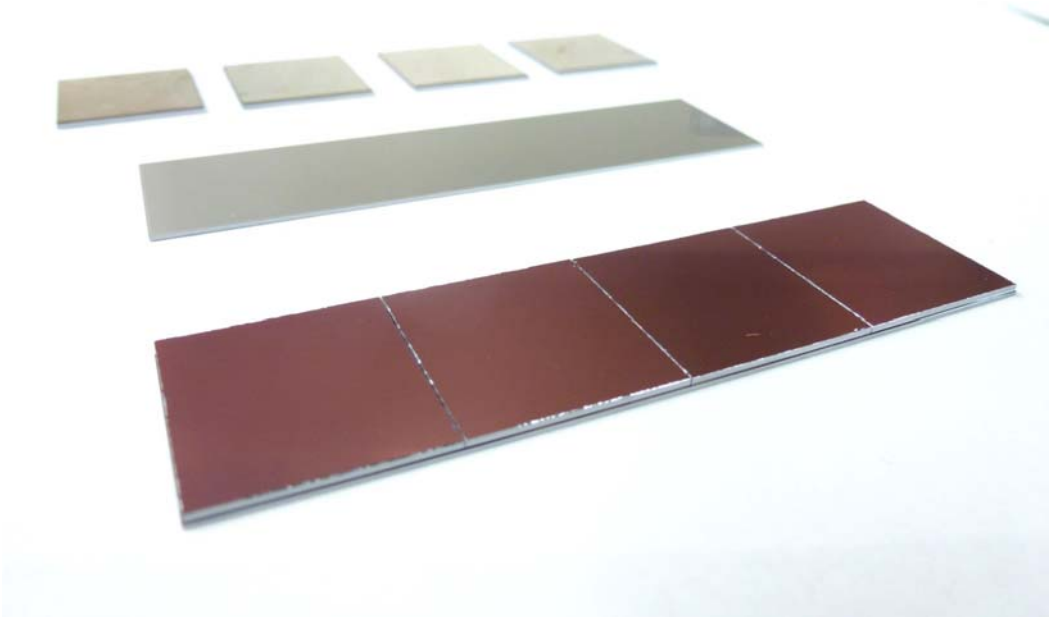


Figure 8-14. Photograph of 4 ASICs, a diode, and the resulting bump-bonded “hybrid”.

The bump-bonded “hybrid” is glued to a Molybdenum heat sink which is in turn is glued to a PCB called an ASIC Adaptor board. The signal pads from the 4 ASICs are wire bonded to the edge of the ASIC Adaptor board. The ASIC Adaptor board carries the control and data signals from the ASICs to a feed through in the detector vacuum wall. A photograph of a completed module is shown in Figure 8-15.

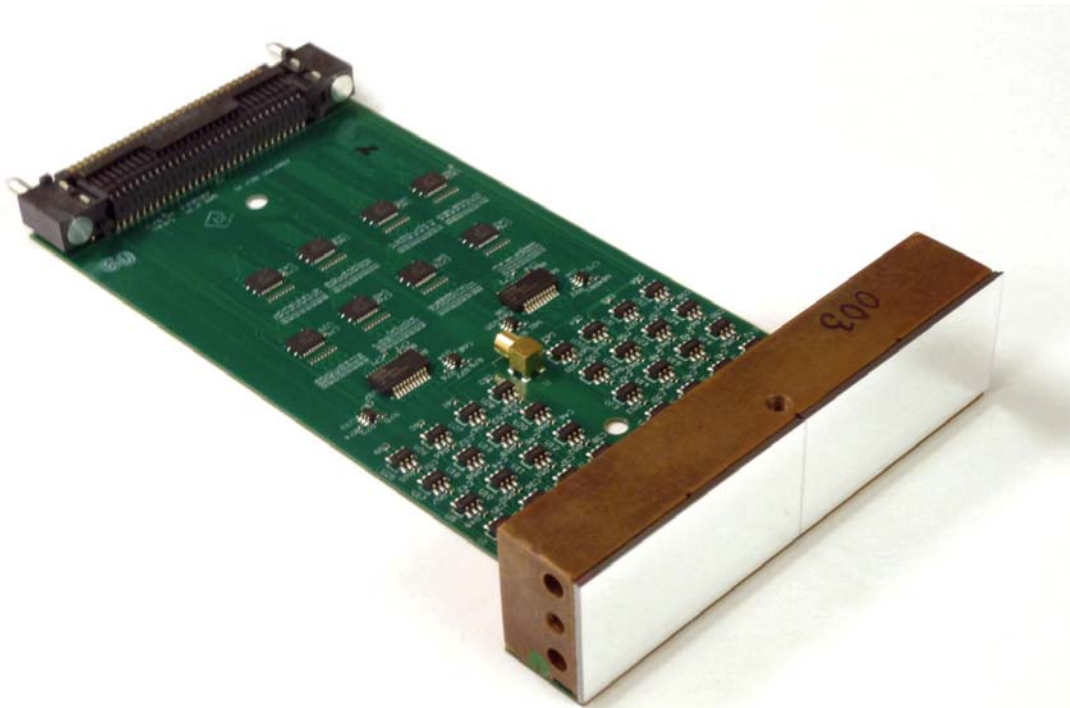


Figure 8-15. Photograph of a completed module.

Supporting Electronics. While testing a single 128 x 128 pixel ASIC detector described above was in progress, three principal electronic boards were being developed for use with the 512 x 128 modules. In addition to the ASIC Adaptor board, a Module Controller and Data Concentrator were developed. The Module Controller controls and reads out the module using a Xilinx Spartan 6 FPGA. The Data Concentrator, using a Xilinx Virtex 6 FPGA, combines the data from up to 4 Module Controllers and sends the data to a Xilinx ML605 PCIe computer interface board. These boards provided the necessary electronics required to build the HF-262K detector.

8.3.5 HF-262K Detector System

The HF-262K detector system consists of a detector enclosure for the 4 512 x 128 pixel modules, a carbon fiber window, a vacuum pump, a water chiller, and computer.

Detector Calibration Software developed for calibration of the charge ramp counting and pulse modes during the initial single ASIC testing was improved and applied to the calibration of the 512 x 512 detector. The number of energies used in the pulse mode calibration was increased from three to five, improving the interpolation of pulse mode threshold trim values for intermediate energies.

Installation of the HF-262K DMPAD Prototype at NSLS X4A. The HF-262K DMPAD detector was delivered to NSLS beam line X4A in early July 2013. First tests involved collecting data in both charge ramp counting mode and photon counting mode. Software was developed during this time to interface the detector to the X4A Blu-Ice data collection control system which will ultimately be used at the NYSBC beam line at NSLS-II. Photographs of the HF-262K detector installed at X4A is shown below in Figures 8-16 and 8-17.

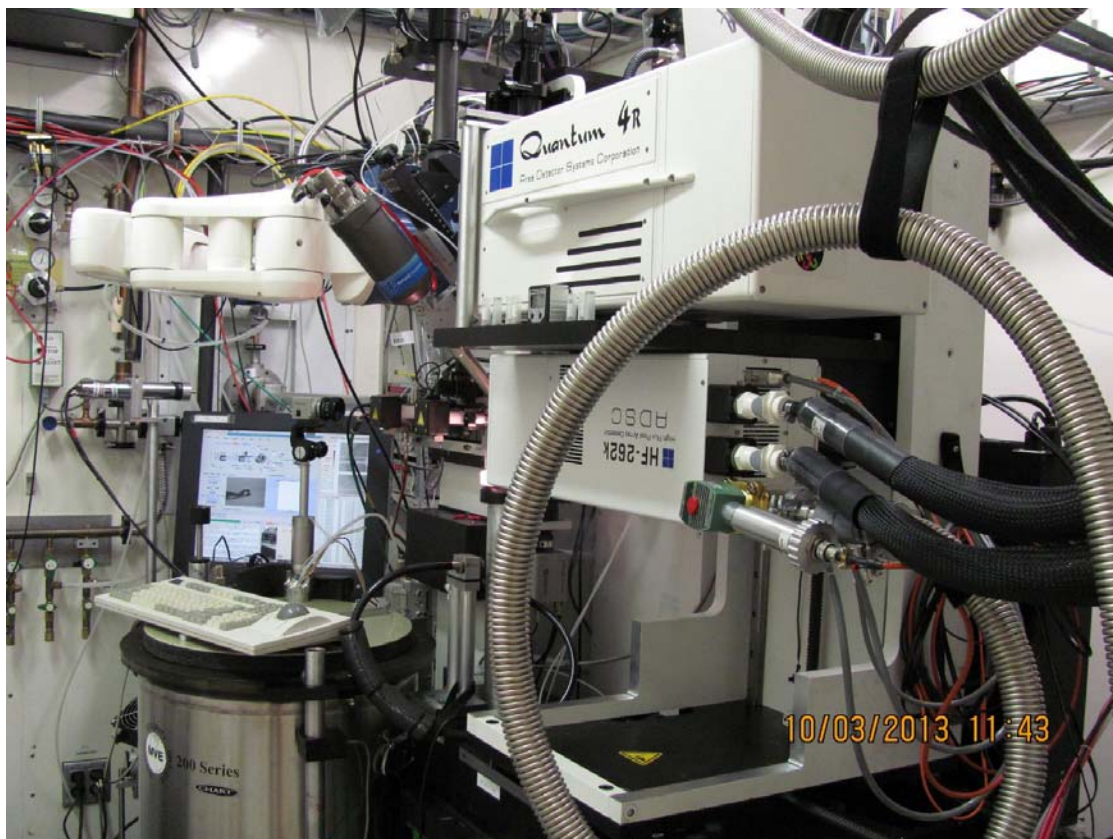


Figure 8-16. Photograph of HF-262K at Beam line X4A at NSLS.



Figure 8-17. Photograph of HF-262K mounted under the Quantum 4 CCD at Beam line X4A at NSLS.

Schedule Performance. From the start of the silicon design to installation of the 512 x 512 prototype detector at X4A was 24 months or 104 weeks, versus 80 weeks for this milestone as specified in the contract.

Detector Testing. After the HF-262K detector was installed and integrated with the beam line control software in July 2013, the first major test of data quality was performed in September 2013. We obtained Sulfur-SAD structure solutions of Lysozyme and Insulin. These results are quite good for a detector with a small active area of 80mm x 80mm. The statistics are given in Table 8-1, and an electron density map of the insulin alpha helix is shown in Figure 8-18.

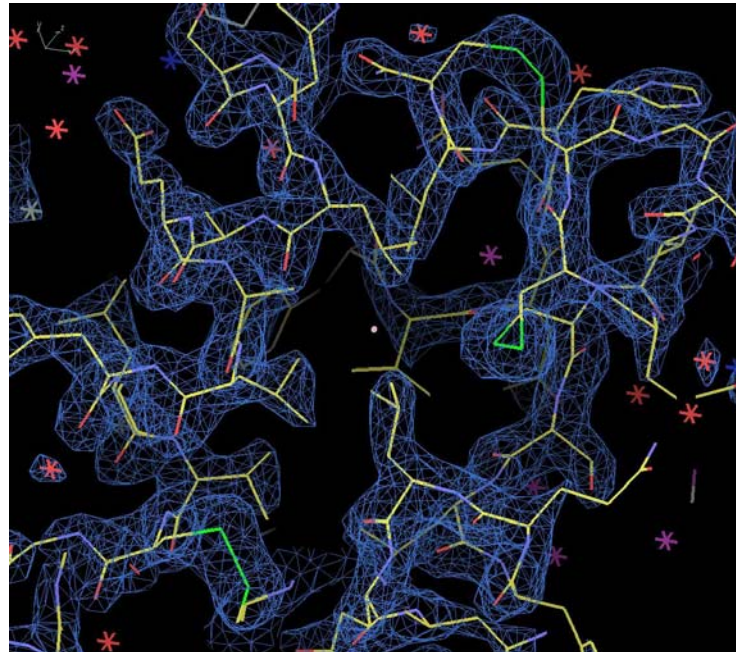


Figure 8-18. Electron density map of the insulin alpha helix showing two disulfide bonds (green). Contouring is at 2.5σ .

Table 8-1. Crystallographic results for the HF-262K at X4A

	Lysozyme	Insulin
Data collection		
Space group	P4 ₃ 212	I2 ₁ 3
Cell dimensions		
<i>a, b, c</i> (Å)	77.66, 77.66, 38.25	78.0, 78.0, 78.0
Resolution (Å)	20.0-2.0 (2.1-2.0)*	20.0-2.0 (2.1-2.0)
R_{sym} or R_{merge}	3.0 (8.8)	3.2 (20.5)
I/σ	68.9 (14.1)	33.4 (3.6)
Completeness (%)	90.0 (62.0)	96.1 (77.8)
Redundancy	18.0 (9.0)	6.5 (3.0)
Refinement		
Resolution (Å)	20.0-2.0	20.0-2.0)
No. of Reflections	7282	4820
$R_{\text{work}} / R_{\text{free}}$	17.5 / 21.9	18.3 / 19.9
No. of atoms	1111	416
Protein	992	394
Solvent	8	22
<i>B</i> -factors		
Protein	15.5	43.5
Solvent	22.6	51.4
R.m.s. deviations		
Bond lengths (Å)	0.008	0.007
Bond angles (°)	1.113	1.033

Since a comparison of the charge ramp counting mode and photon counting mode data quality is an important test to be done on the Dual Mode detector, a lysozyme data set was taken in both modes. Data were measured at 14 keV at NSLS in both modes at beamline X4A, and the the structures were refined based on molecular replacement from the known lysozyme structure. The results of these tests are summarized below in Table 8-2.

Table 8-2. Crystallographic results from the HF-262K at X4A.

	Lysozyme (Charge Ramp Counting Mode)	Lysozyme (Photon Counting Mode)
Data collection		
Space group	P4 ₃ 2 ₁ 2	P4 ₃ 2 ₁ 2
Cell dimensions		
a, b, c (Å)	77.65, 77.65, 38.32	77.76, 77.76, 38.38
Resolution (Å)	20.0-1.5 (1.6-1.5)*	20.0-1.5(1.6-1.5)
R _{sym} or R _{merge}	4.0 (57.3)	4.3 (65.15)
I / σ	26.6 (0.8)	24.2 (2.4)
Completeness (%)	90.4 (47.6)	89.7 (46.9)
Redundancy	6.4 (1.4)	6.3 (1.3)
Refinement		
Resolution (Å)	20.0-1.5	20.0-1.5
No. of Reflections	17711	17530
R _{work} / R _{free}	16.3/21.1	16.2/21.0
No. of atoms	1184	1183
Protein	1012	1012
Solvent	172	171
B-factors		
Protein	19.8	17.9
Solvent	32.0	29.1
R.m.s. deviations		
Bond lengths (Å)	0.006	0.010
Bond angles (°)	0.98	0.983

NOTES: Same crystal was used for both structures. (Values in parentheses are for highest-resolution shell).

Milestone. Based on the detector testing at NSLS beam line X4A reported in Tables 8-1 and 8-2 which yielded not only high quality data as measured by R-factors but several aulfur-SAD structure solutions, the prototyping milestone was met and ADSC proceeded to build the HF-4M detector.

8.3.5 HF-4M 2K x 2K Pixel DMPAD Detector

Scaling up the 512 x 512 detector design to a 2K x 2K design. An important decision that had to be made was which components and electronic boards developed for the 512 x 512 prototype DMPAD detector can be used in the 2K x 2K DMPAD detector, called the HF-4M. The module design, with ASIC adaptor board, together with the module controller could be used in the larger detector. However, due to the number of modules (64) in this detector, and detector dimension constraints, data concentrators combining the data from 8 modules rather than 4 modules needed to be developed. A new PCIe interface, called a LynxM board, needed to be developed to receive the data from a group of four 8-module data concentrators over fiber optic cables. The detector uses two LynxM interface boards.

The 512 x 512 DMPAD detector's modules were cooled by Peltier cooling devices. Due to power and cabling constraints it is not possible to scale this cooling method to the size of the HF-4M detector. For this size detector a direct refrigeration system that cools a large copper plate (Figure 8-19) that in turn cools the detector modules is needed.

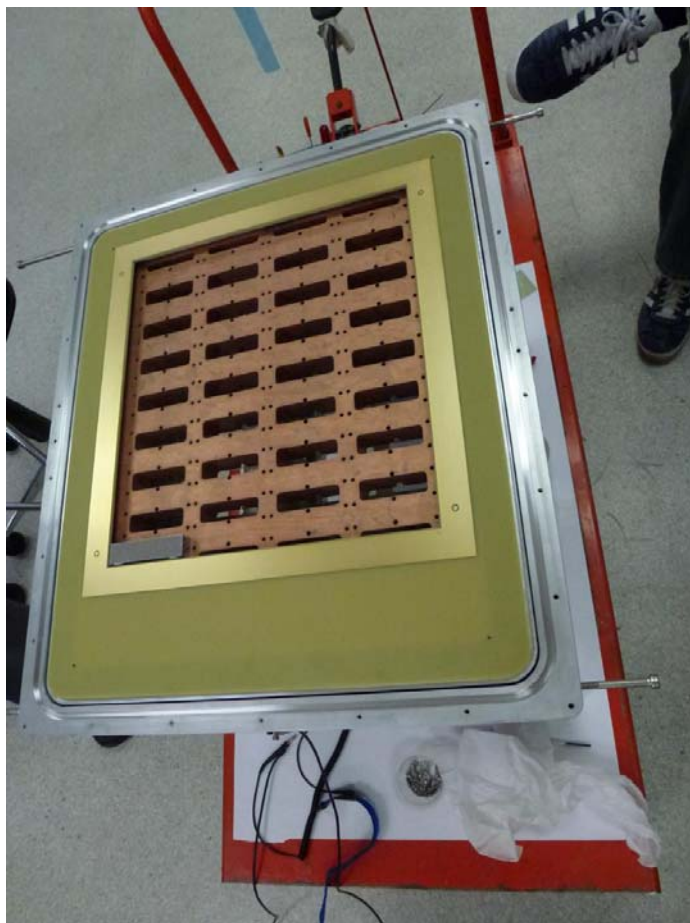
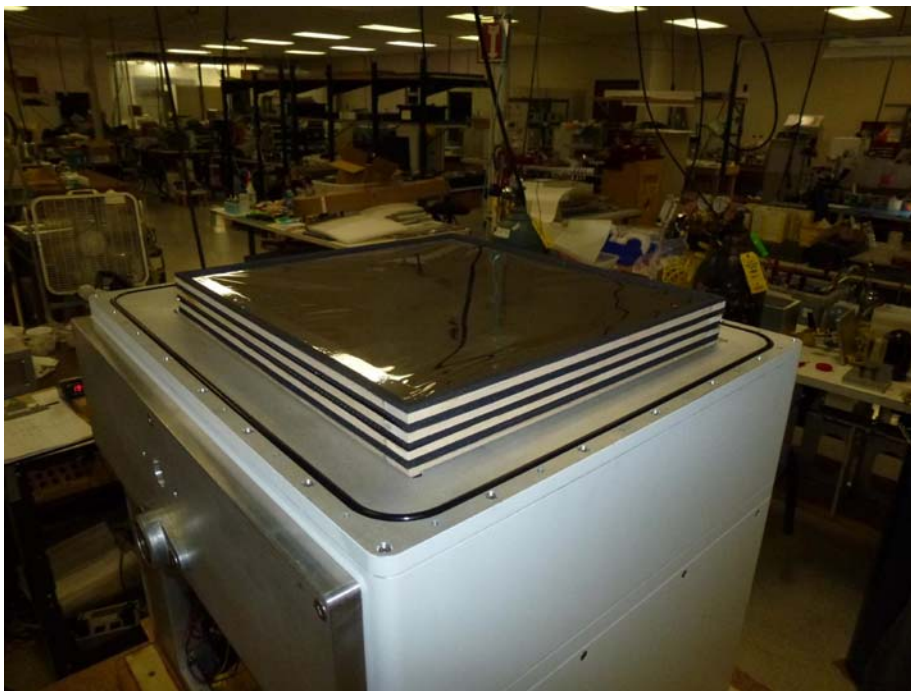


Figure 8-19. Copper refrigeration plate with one module inserted (lower left).

The HF-262K detector used a carbon fiber window. For a detector of the size of the HF-4M, a carbon fiber window cannot be used as it cannot withstand the forces of the vacuum. A completely new window design had to be created, one with 6 separate windows. The first window is made from aluminized Mylar serves two purposes: the aluminum side supplies bias voltage for the diode sensors and the window is pulled against the modules allowing a vacuum to be established in the detector. If the modules are refrigerated to -30C and this window is exposed to room temperature air, ice will

necessarily form on the outside of this window. Four more windows of thin Mylar are used to isolate the vacuum window from the outside by creating small spaces filled with circulating air. A final aluminized Mylar window is installed on the front providing a final moisture barrier. No ice forms using this multi-window design. A photograph below (Figure 8-20) shows the “window stack”, and another photograph (Figure 8-21) shows the detector front window made of aluminized Mylar being pulled against the



modules by the detector enclosure vacuum.

Figure 8-20. Detector front “window stack”.

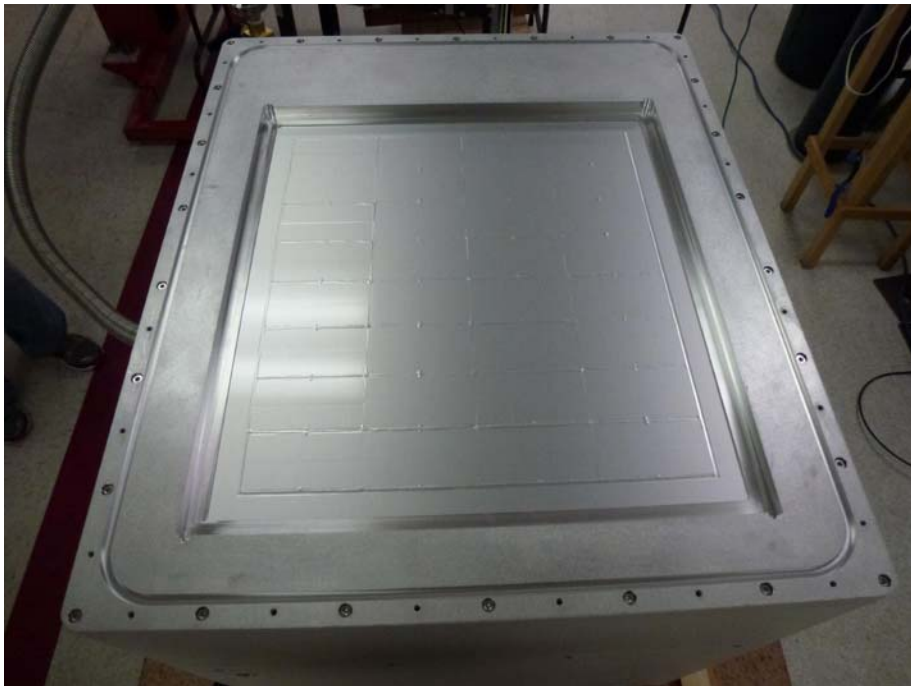


Figure 8-21. Aluminized Mylar pulled against the detector modules by vacuum.

Module production and calibration. From January until July of 2014, more than 64 modules were produced. Each module took approximately two weeks to produce using about 30 man hours of labor. To produce a module, four ASICs one diode sensor must be bump-bonded, this “hybrid” then glued to a Molybdenum heat sink in turn glued to an ASIC Adaptor board. The ASIC signal pads are then wire-bonded to the ASIC Adaptor board edge by a local wire-bonding specialist. The completed modules are then bench tested and the module accepted, remediated, or rejected. The accepted modules are calibrated four at a time. A photograph of the assemblage of HF-4M modules is shown in Figure 8-22.



Figure 8-22. Module controllers installed in the back of the detector.

Overall Detector Calibration. Fluorescent radiation is used to calibrate threshold settings for the pulse mode. This only works well for ‘small’ detectors such as the 512 x 512 pixel detector. A method needed to be found to calibrate modules in the pulse mode for the HF-4M detector at the detector’s operating temperature (~ -30C). The logical solution was to calibrate the modules four at a time using an HF-262K detector, and three HF-262K detectors were fabricated for this purpose.

For pulse mode, the threshold trim calibrations determined in groups of four modules using the HF-262K detectors could be used when assembled into a large array. The placement of the modules in the array does not matter. For the charge ramp counting mode, a uniform flood field in our X-ray calibration facility was used. The uniformity of this flood field is independently adjusted and verified using our flood field calibration procedure. This same procedure was used to verify the flood field calibration for all of our CCD detectors.

Flood Field Laboratory Testing. After detector assembly, testing commenced in our flood field facility (Figure 8-23). Several defective modules and electronics boards were replaced and final firmware for controlling and reading out of the detector was completed.



Figure 8-23. The detector on a cart in flood field laboratory.

8.3.6 Installation and Testing at APS Beam Line 24-ID-E

The detector system was installed at APS beam line 24-ID-E on 9 December 2014, a day without X-rays, temporarily replacing the ADSC Q315 detector for this day (Figures 8-24 and 8-25). The plan was to reinstall the Q315 detector on 10 December and run the normal user program until the last day of the run, 15 December. On 10 December, prior to the removal of the HF-4M, two thaumatin data sets were collected as a final system check. The data were of good quality and demonstrated that the detector system was ready to use on the 15th. However, a refrigeration failure occurred on 13 December that required the detector tests scheduled for 15 December to be scrubbed and the detector shipped back to ADSC.

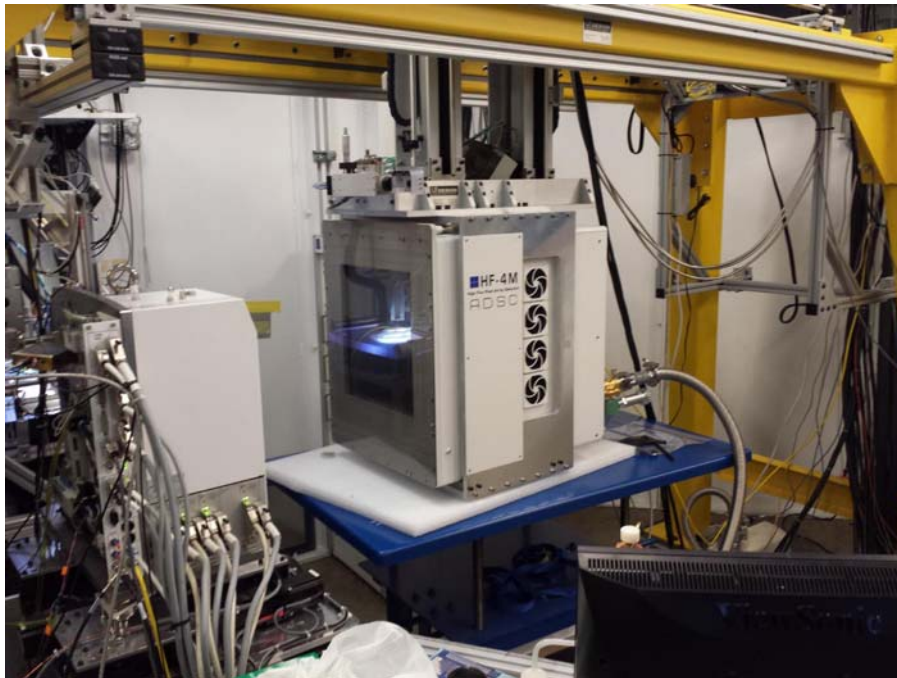


Figure 8-24. HF-4M detector suspended from APS NECAT 24-ID-E A-frame.

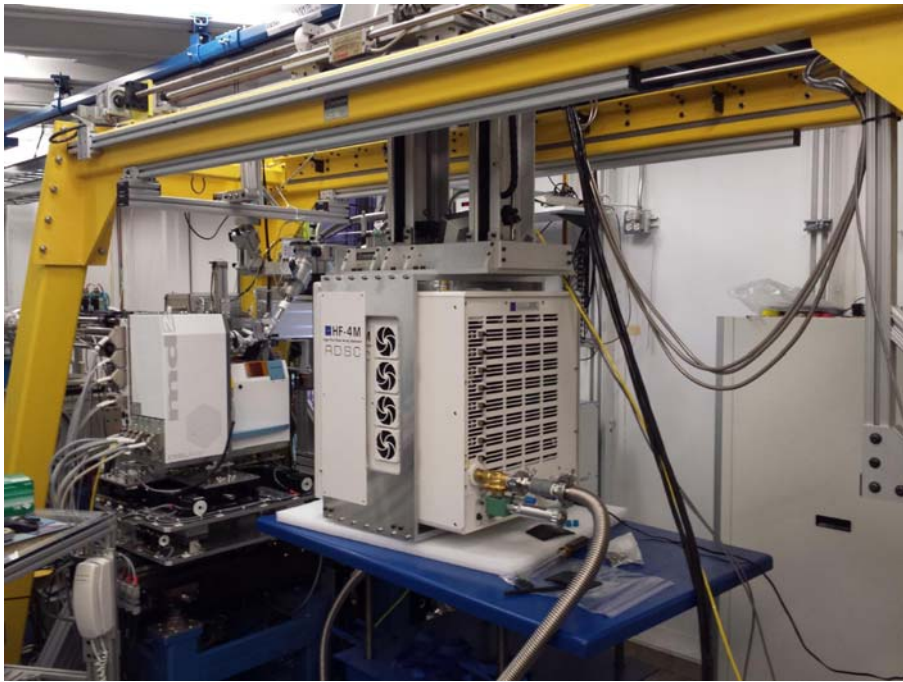


Figure 8-25. HF-4M detector viewed from the back at APS NE-CAT 24-ID-E.

HF-4M tests in December 2014 and February 2015. The two thaumatin data sets collected on 10 December before returning the detector to ADSC were processed with XDS. The resulting data set showed a completeness of 97% to 1.34Å Bragg spacings with an overall R-sym of 5.9% and an R-sym of 2.7% in the lowest resolution shell.

After repair of the refrigeration problem, the detector was returned and reinstalled at 24-ID-E, and further tests were completed. These included further thaumatin data sets and the collection of a number of data sets from selenomethionyl (SeMet) proteins. Uniformly, the resolution limits and data quality from the HF-4M PAD detector were markedly superior to those from the Q315 CCD detector. The SeMet structures were readily solved from these data and thaumatin maps and models achieved by molecular replacement were excellent. Although one expects the anomalous scattering signal from sulfur atoms to be very small at the Se K-edge ($S f'' = 0.24e$), we were hopeful that they might suffice for structure determination with the DMPAD; however, we did not succeed in obtaining SHELX solutions for the sulfur substructure.

The detector was then put into operation for NE-CAT users. After about a month of normal NE-CAT operation, shadows were observed on the detector surface. These shadows were deduced as coming from ice formations on window layers. The detector was then taken offline and the window assembly and dry nitrogen purging system was redesigned.

Detector front window revision. The primary problem in obtaining good test and evaluation data in February 2015 was traced to the formation of ice on the detector front window layers. Since the detector runs at -35C, any moisture that condenses on any of the multiple window layers will form ice, and this will adversely affect data quality. This problem was addressed by a change of material in the window frames so that no moisture would outgas during operation, while very dry nitrogen is flowed through the window layers. A meter was attached to the nitrogen output stream so the dew point could be monitored. The dew point of this output stream is now close to -70C, far below the detector

operating temperature of -35C. Flood field scattering tests performed on the detector after continuous cold temperature operation for over10 weeks showed no ice formation on the detector front window.

HF-4M tests in December 2015 and February 2016. Testing of the detector with diffraction data was performed in December 2015 and February 2016 at the NECAT beam line, 24IDE, at the APS. Thaumatin data was collected for the analysis of difference maps on both the HF-4M and the Q315. Data analysis showed that the HF-4M consistently produced higher resolution diffraction data, and better quality maps. Several data sets were collected with very low beam transmission and a sulfur SAD structure solution was obtained. In February 2016 additional diffraction data was collected resulting in two SeMet structure solutions and also a novel structure analyzed by molecular replacement. A representative diffraction pattern is shown in Figure 8-26.

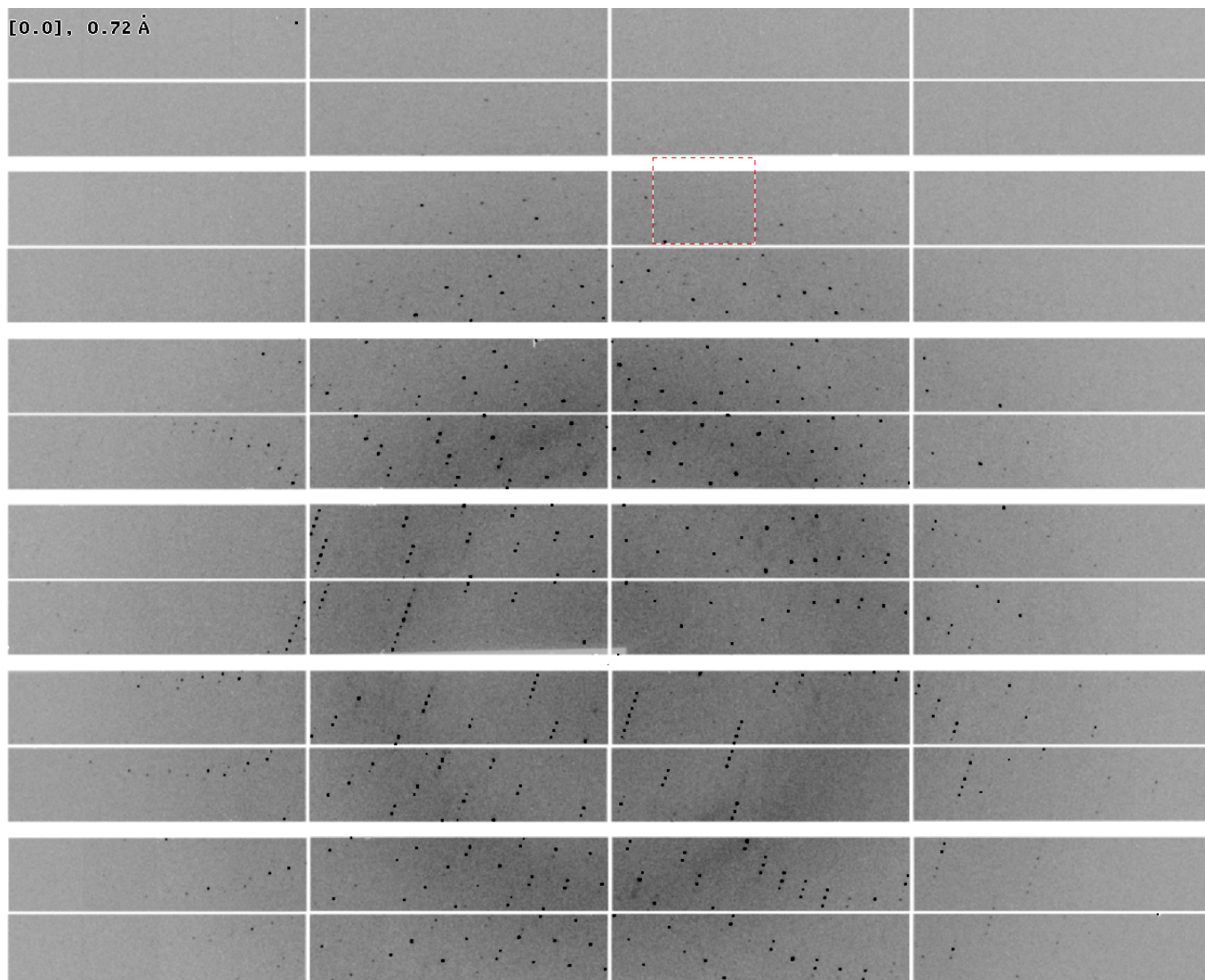


Figure 8-27. Thaumatin diffraction image from HF-4M collected at APS NECAT 24-ID-E. This image is truncated at the bottom whereby 16 modules are left out.

Data measured from a crystal of an NYSBC SeMet protein (phopho-2-dehydro-3-deoxyheptonate aldolase from *Francisella tularensis*) showed excellent statistics to 1.8Å spacings as processed by XDS (Table 8-3). The structure was solved using ShelX for substructure determination and density modification as illustrated in Figure 8-28. The resulting structure was appreciably superior to that previously determined at 2.3 Å resolution from data measured at X4C with a CCD detector.

Table 8-3. Diffraction data for an NYSBC SeMet protein from the HF-4M at 24-ID-E.

Shell	Lower	Upper	Average	Average	Norm.	Linear	Square					
limit	Angstrom	I	error	stat.	Chi**2	R-fac	R-Fac	Rmeas	Rpm	CC1/2	CC*	
50.00	4.75	151.8	4.2	3.8	0.715	0.040	0.047	0.043	0.016	0.999	1.000	
4.75	3.77	173.8	4.4	3.9	0.905	0.048	0.054	0.051	0.018	0.998	1.000	
3.77	3.29	112.3	3.2	2.9	1.020	0.062	0.069	0.066	0.023	0.998	0.999	
3.29	2.99	60.5	2.2	2.1	0.955	0.078	0.084	0.083	0.029	0.997	0.999	
2.99	2.78	35.3	1.9	1.8	0.949	0.101	0.106	0.109	0.042	0.992	0.998	
2.78	2.61	23.8	1.6	1.6	0.848	0.130	0.137	0.141	0.053	0.989	0.997	
2.61	2.48	17.8	1.5	1.4	0.738	0.161	0.167	0.173	0.062	0.987	0.997	
2.48	2.38	15.8	1.5	1.5	0.783	0.195	0.211	0.208	0.074	0.984	0.996	
2.38	2.28	12.8	1.5	1.4	0.805	0.247	0.289	0.264	0.093	0.972	0.993	
2.28	2.20	10.3	1.4	1.4	0.738	0.290	0.317	0.309	0.107	0.967	0.992	
2.20	2.14	8.7	1.4	1.4	0.690	0.333	0.368	0.355	0.121	0.958	0.989	
2.14	2.07	6.9	1.5	1.5	0.659	0.400	0.438	0.428	0.152	0.933	0.983	
2.07	2.02	5.6	1.6	1.6	0.640	0.464	0.525	0.503	0.190	0.887	0.970	
2.02	1.97	4.3	1.6	1.6	0.594	0.577	0.635	0.628	0.246	0.822	0.950	
1.97	1.93	3.4	1.6	1.6	0.555	0.716	0.827	0.777	0.300	0.754	0.927	
1.93	1.89	2.6	1.5	1.5	0.529	0.937	1.097	1.008	0.369	0.642	0.884	
1.89	1.85	2.0	1.5	1.5	0.495	1.158	1.281	1.244	0.450	0.555	0.845	
1.85	1.81	1.6	1.5	1.5	0.480	1.484	1.719	1.599	0.590	0.431	0.776	
1.81	1.78	1.3	1.6	1.6	0.471	1.648	1.885	1.791	0.695	0.320	0.696	
1.78	1.75	1.2	1.8	1.8	0.515	2.000	2.257	2.223	0.954	0.156	0.520	
All reflections		32.6	2.0	1.9	0.715	0.104	0.069	0.112	0.040			

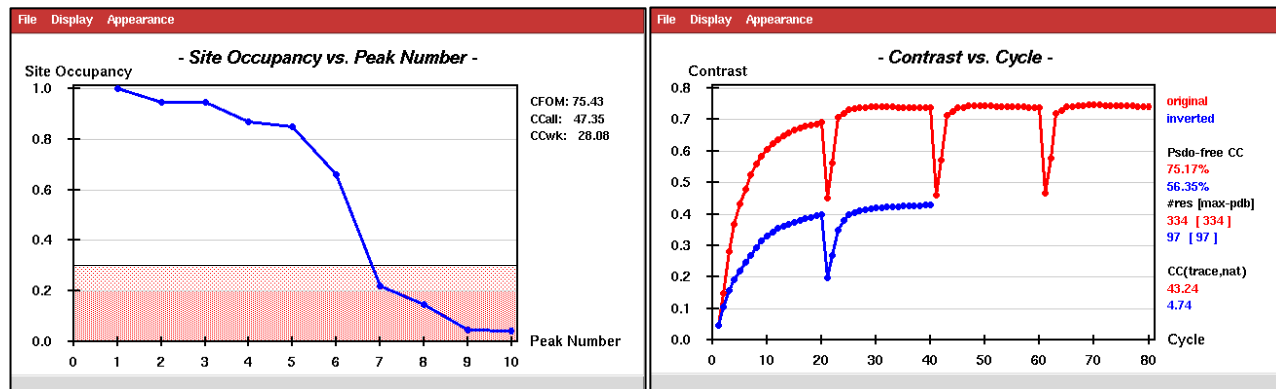


Figure 8-28. Aspects of SeMet structure determination by ShelX. (Left) Substructure determination. (Right) Density modification.

The data for thaumatin were obtained from two crystals (~150-200 μ bipyramids) yielding three data sets (left and right tips of the bigger crystal). Each data set has 1440 frames with 0.5° rotation and exposure times of 0.25-0.50 sec with either 5% or 2% flux. Data were integrated using XDS, and scaled and merged using PHENIX. A search for 14 sulfur sites, phasing, and automated model building was done by PHENIX using default parameters. Out of 207 thaumatin residues, 186 were built and 167 side chains were placed correctly. The final overall model-map correlation is 0.83 and the R/R_{free} values are 0.21/0.23. An image from the resulting map at 1.3 Å resolution is shown in Figure 8-29. The result now provides validation for effectiveness of the HF-4M detector.

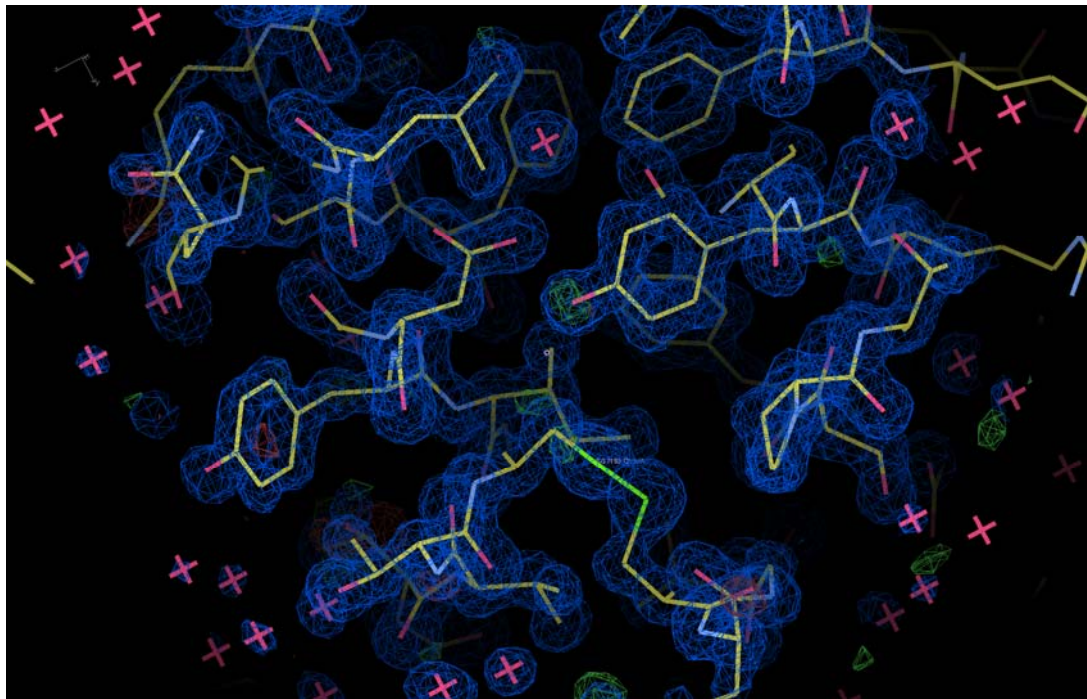


Figure 8-29. Portion of the electron-density distribution at 1.3 \AA resolution from the sulfur-SAD structure of thaumatin as analyzed from HF-4M data collected on APS 24-ID-E at 12.667 keV, far away from the sulfur edge.

8.4 DATA ACQUISITION SYSTEM AND COMPUTING

Beamline 19-ID-NYX will start up with a 10GigE network switch compliant with NSLS-II and will provide data transfer appropriate for the following computing infrastructure:

Data storage:

The network storage system for Beamline 19-ID-NYX will be distributed over a fiber-optic network with capacity of 150 TB of storage space in addition to 5 TB of a fast buffer storage as implemented with the IBM GPFS file system.

Computational Software:

The following crystallographic software will be available to users -

Data Processing: mosflm, XDS, HKL2000, DIALS and Xia2

Phasing and Refinement: SHELX, Solve/Resolve, Refmac, Phenix, CCP4, SnB, AutoSHARP, CNS and Phaser

Model Building: Coot

Molecular Graphics: PyMol

Computing cluster:

A multi-core computer cluster (6 nodes for a total of 120 cores and 3 TB RAM) will be optimized for the above software to enable data processing on a similar time scale as data collection. This will be available so to users to evaluate data quality during collection.

Automated data collection & processing pipeline:

The shutterless capability of the HF-4M DMPAD will be used to strategically adjust the frame rate to provide an optimized data collection strategy.

Web-Ice: To view diffraction images, screening, auto indexing. This can be used to remotely and locally control data collection.

AutoPROC: Automatic data processing.

Remote Data Collection:

Beamline 19-ID-NYX will utilize NoMachine client-server and RSA SecurID token to enable encrypted remote terminal access for data collection and computing.

9. Beamline Controls

9.1 General Description

9.1.1 Hardware Configuration

NYX uses Galil DMC-4080 advanced motion controllers to control NYX the beamline photon delivery system and the experimental station. It takes care of all the motion controls, most I/Os, temperature monitoring and analog input. The Galil motor amplifiers are built into the controller. We embedded the Galil controllers in custom-built control cabinets located near each of the major beamline and endstation components. The advantage of such a configuration is that it eliminates long motor and encoder cables to the motor amplifier and controllers. The main control PC communicates to the Galil controller through ethernet.

9.1.2 Software Plan

Blu-Ice is a graphical interface to a Distributed Control System (DCS) for crystallographic data collection at synchrotrons. It was designed and developed by SSRL, and it is used at crystallography beamlines worldwide. It is proven and has the reputation of being elegant and user friendly.

NYSBC used Blu-Ice at NSLS beamline X4 in the last five years of its operation. It controlled all major components of the X4 endstation. Our experience with Blu-Ice can be summarized as follows:

1. User friendly. Blu-Ice is easy to use. The GUI is self-explanatory. The user can master beamline control and data collection in a very short time. Our users love it.
2. Central control. All the beamline control and data collection is under one GUI, unlike much beamline software, where the user needs to open multiple windows. It's less confusing.
3. Multi-user. It controls or monitors the data collection both locally and remotely. Blu-Ice can be accessed by many users at the same time to monitor their experiments. Users are able to view all processes of the experiments, but only one user is allowed to control the experiments.
4. Security. The authentication server takes care of the user login security. Each user can have their own user name and password to access the software and collect their data securely.
5. Reliability. We have had very smooth operating experience since using Blu-Ice, and there is rarely a need to reboot or restart, unlike with our previous control softwares.
6. Efficiency. The experimental processes are standardized. The user can simply use data collection number tabs to setup multiple data collections and run them continuously.
7. Many experimental procedures and scripts have already been developed for beamline control; we can easily use them or modify them. This saves us a lot of time in development.
8. Easy to expand and upgrade. New hardware can be easily added into the system. SSRL provides many useful templates. We also have full access to the Blu-Ice repository so that we can upgrade to the newer version of the Blu-Ice whenever it's available.
9. Excellent support from SSRL. The people in the SSRL control group have been extremely supportive over the last five years, making themselves available for us if we need help.

Blu-Ice References

- [1] T.M. McPhillips, S.E. McPhillips, H.-J. Chiu, A.E. Cohen, A.M. Deacon, P.J. Ellis, E. Garman, A. Gonzalez, N.K. Sauter, R. P. Phizackerley, S.M. Soltis and P. Kuhn Blu-Ice and the Distributed Control System: software for data acquisition and instrument control at macromolecular crystallography beamlines. *J. Synchrotron. Radiation* **9**, 401-406 (2002).
- [2] A. González, P. Moorhead, S.E. McPhillips, J. Song, K. Sharp, J. R. Taylor, P.D. Adams, N.K. Sauter and S.M. Soltis. Web-Ice: integrated data collection and analysis for macromolecular crystallography. *J. Appl. Cryst.* **41**, 176-184 (2008).

[3] Y. Tsai, S.E. McPhillips, A. Gonzalez, T.M. McPhillips, D. Zinn, A.E. Cohen, M.D. Feese, D. Bushnell, T. Tiefenbrunn, C. D. Stout, B. Ludaescher, B. Hedman, K.O. Hodgson and S.M. Soltis. AutoDrug: fully automated macromolecular crystallography workflows for fragment-based drug discovery. *Acta Cryst. D* **69**, 796–803 (2013).

9.2 Major Hardware Components

9.2.1 Components and Controlling Connections

End Station

- Diffractometer Crystal Logic
- Auto Mounter Robot Crystal Logic
- Dual Mode detector ADSC
- Camera Server Axis
- BPM System BNL/Libera

Optics

- Monochromator Oxford FMB
- Mirror Irelec

Insertion Device

- Undulator X25-NSLS

Control Computer

- Intel based PC

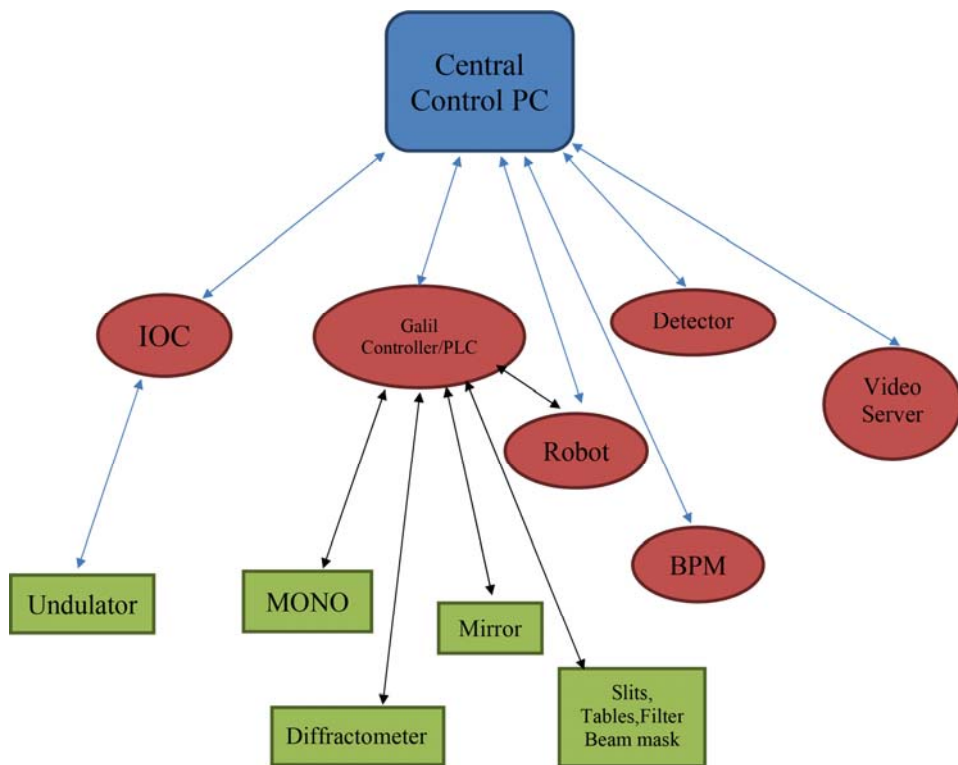


Figure 9-1. Connection schematics

9.2.2 Device and Interface List

Device Name	Function	Specification	controlled by	Interface	Protocol Name
GUI PC	User interface to control experiment	Intel Processor base PC	-	-	-
Galil Motor Controller	Control motors and encoders		GUI PC	eth	proprietary
Galil Pocket PLC	Analog Input Timer and Counter		GUI PC	eth	proprietary
Mean Well	Power Supply	24V-48V		eth	
Galil SCB 48316	K thermal card for reading motor temperature sensor	Galil	Galil	eth	analog
Renishaw	Encoder		Galil		quadrature
MicroE Mercury2000-MV	Encoder		Galil		quadrature
Phtron	Vacumm Motors		Galil		
PM170	McLennan servo driver		Galil	-	-
M543E	McLennan Servo Motor for Phi		Galil		
Stogra SM56.2.18.J3	Steppers for Mirror		Galil		
VEXTA PK266M-03A	NSLS2 Stage		Galil		
Nanotec 2 phase	Stepper for 4 Jaw slits		Galil		
NEMA 17-4018	Stepper for Beam mask		Galil		
HaydonKerk 57H4A 3.25	Steppers for Crystal logic		Galil		

050 ENG 0716	diffractometer				
Oriental Motor AR66MA-N10-3	Stepper for Crystal logic table		Galil		
Lin WO-211-18-02D	Steppers for camera and sample stage		Galil		
FaulhaberAM1 5A0046	Steppers for Slits		Galil		
McLennan 23HSX206	Stepper for filter		Galil		
LS	Limit switches for motion	-	Galil	5v DIO	TRUE/FALSE
Physik Instrument P-841-30	Stain gauge for Mono Benders		Galil	0-10V	
PI E-500 Modular Piezo controller	Control Piezo		Galil	0-10V	
Infinity Strain Meter	Mirror bending force reader		Galil	0-10V	
IOC	Hosts PVs, integrates connected devices	NSLS2 compliant	GUI PC	eth	CA
PLC	Read temperature, implement Interlock logic	Allen Bradley Compact Logix	IOC	eth	EtherIP
GB	DeltaTau Geobrick IMS 2 Motion controller	BNL compliant	IOC	eth	DeltaTau proprietary

9.3 NYX Beamline Control System

The NYX control system has three components: the general user interface (GUI), the distributed control system server (DCSS) and the the distributed hardware server (DHS).

Blu-Ice provides the GUI for NYX beamline controls and it thereby interfaces with the DCSS and on to hardware elements through the DHS/EPICS Gateway (Figure 9-2).

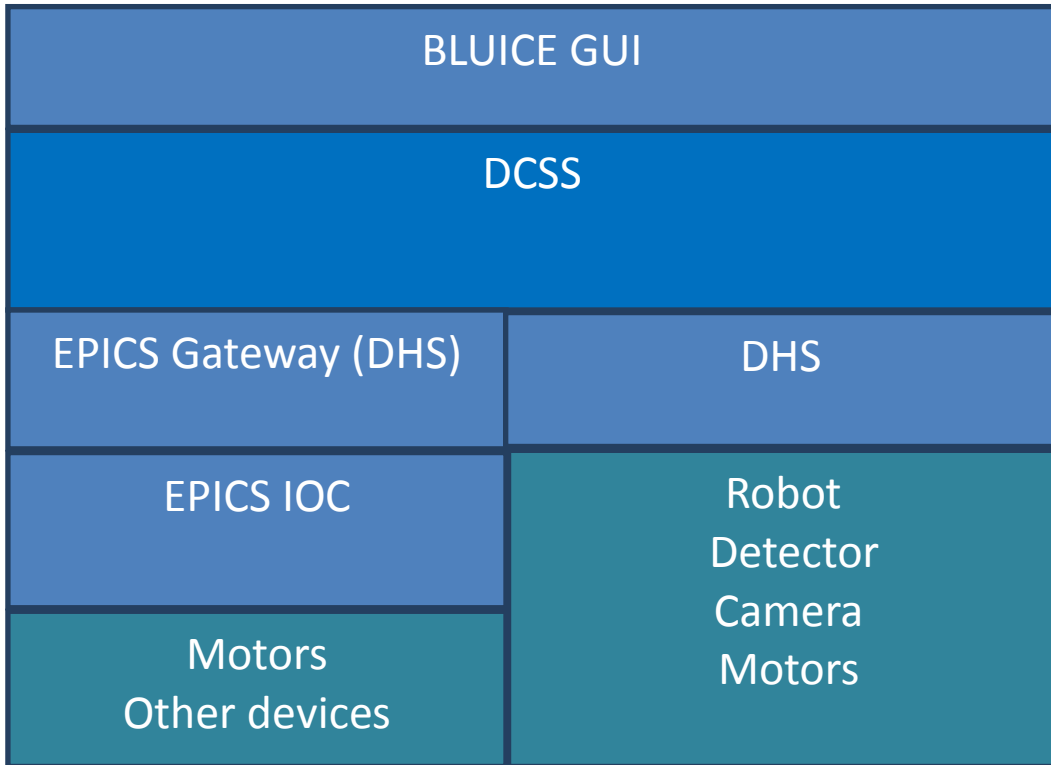


Figure 9-2. Blu-Ice Control Block Diagram

9.3.1 DCSS

Distributed Control System Server (DCSS) is a centralized sever. It handles the communications between GUI and DHS. It has two basic functions:

1. Message handler:

It delivers messages from Blu-ice GUI to DHS to control the devices and broadcast messages from DHS to all the GUI

GUI ↔ DCSS ↔ DHS ↔ Device

2. Script Engine:

It also is a special Client called “self” for both DCSS and Blu-Ice GUI. It can receive all the messages from DHS and access all the DHS. It can execute the user defined scripts which controls devices.

The DCSS is running in the Central Control PC.

9.3.2 DHS

Distributed Hardware Server is a program which talks directly to devices. It accept DCS messages and controls a piece of hardware directly. It reports the status of the device to the DCS.

9.3.3 Blu-Ice DCS Framework

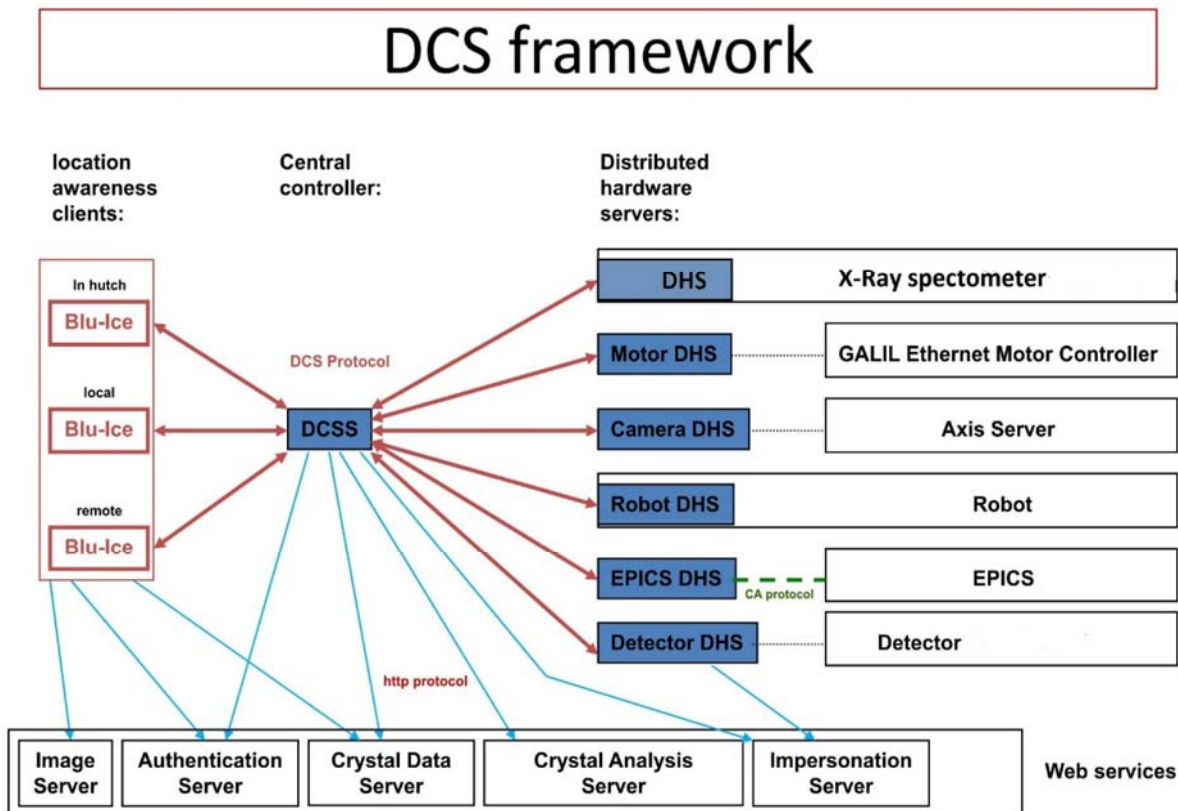


Figure 9-3. DCS Framework. This figure is courtesy of SSRL

Features of the framework include the following:

- **Central Control**
- **Security**
 - **Authentication Server**
 - **Impersonation Server**
- **Web-Ice service [Reference 2]**
 - **Crystal Information Server**
 - **Crystal Analyze Server**

9.3.4 Blu-Ice GUI

9.3.4.1 Hutch Tab

The **Hutch Tab** (Figure 9-4) allows the users to adjust various parameters for data collection.

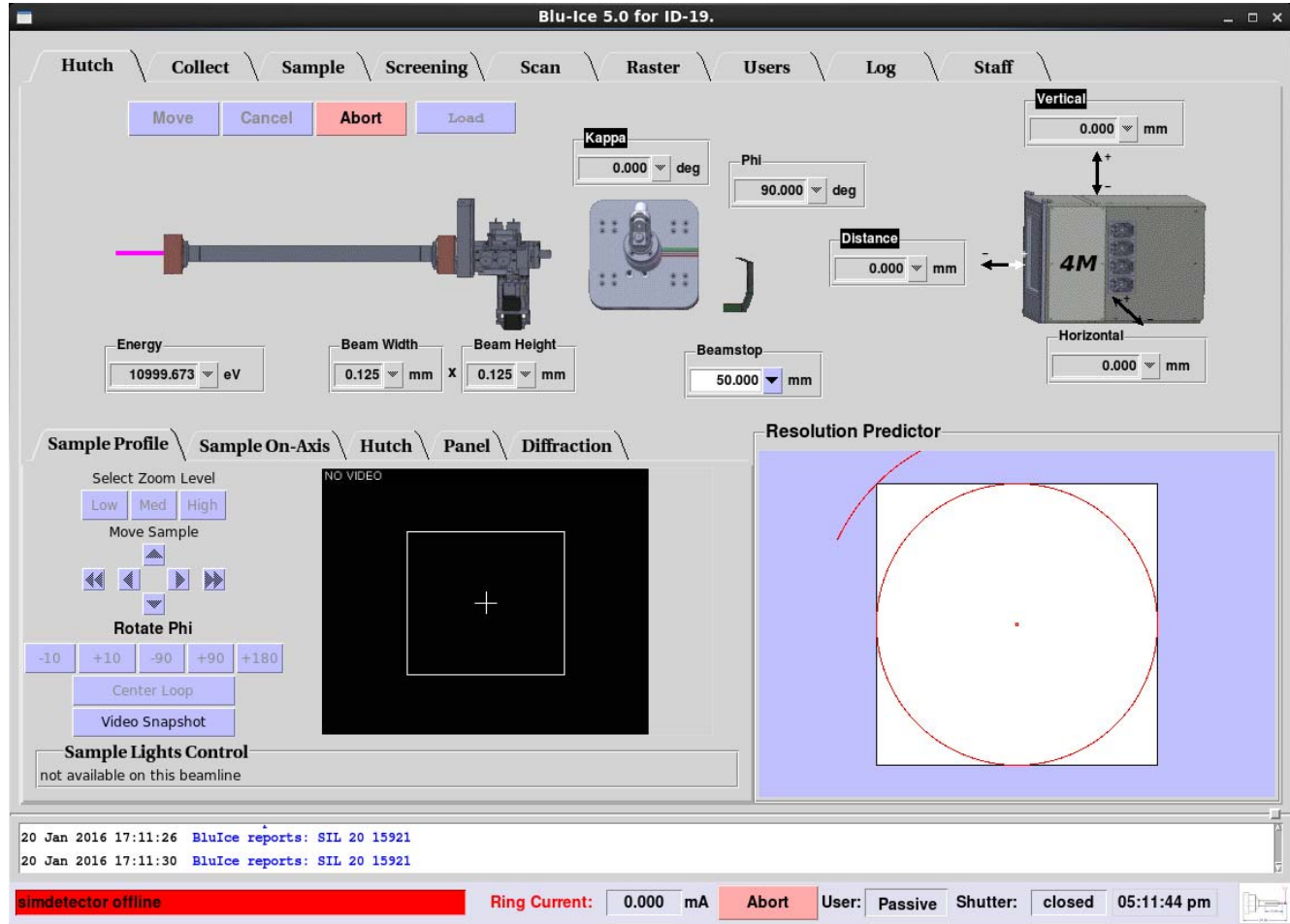


Figure 9-4. Hutch Tab

9.3.4.2 Data Collection Tab

The **Collect Tab** (Figure 9-5) is used for collecting test images and complete monochromatic, SAD and MAD data sets. Multiple run windows can be set up by creating additional Run Tabs.

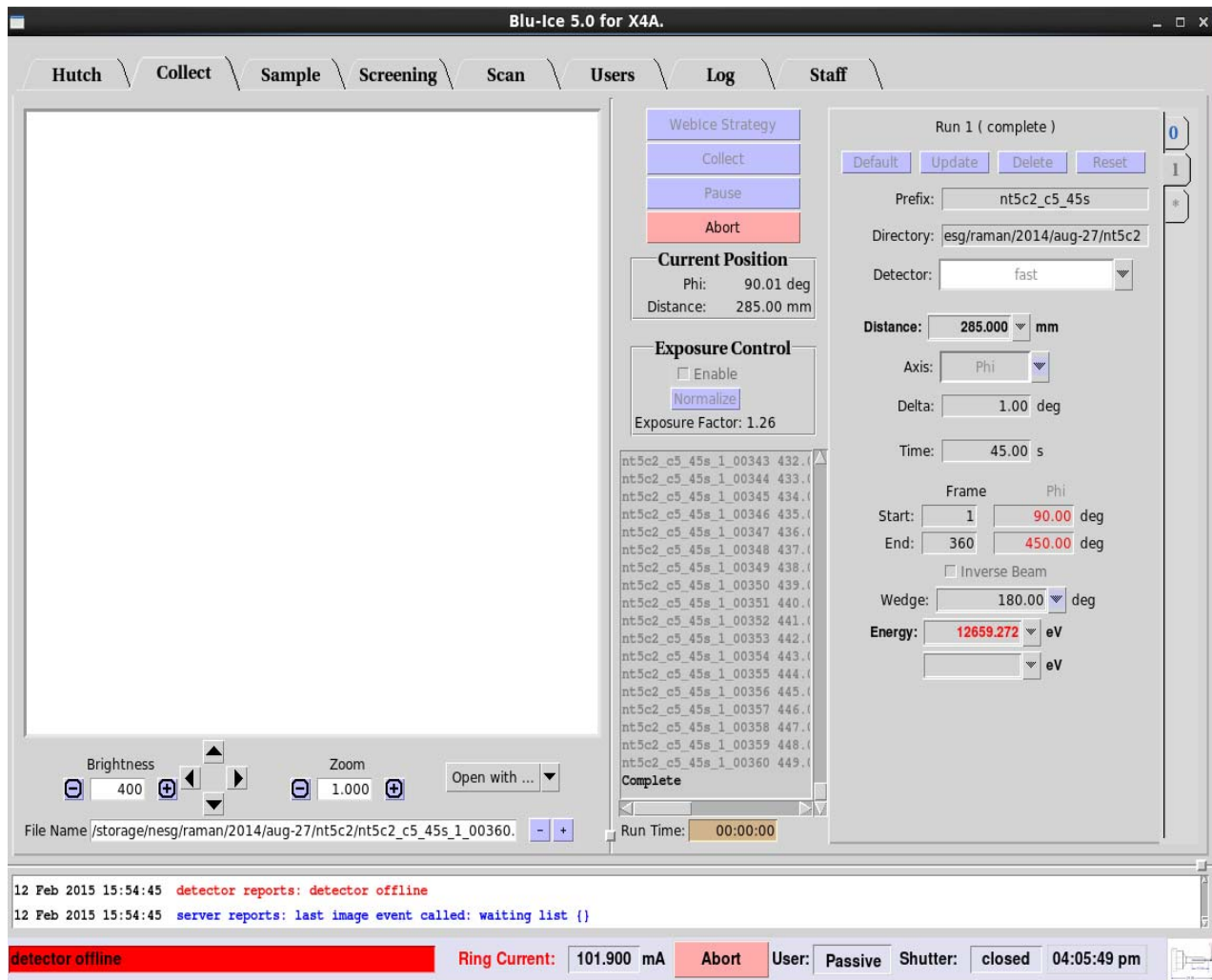


Figure 9-5. Data Collect Tab

9.3.4.3 Sample Tab

The **Sample Tab** (Figure 9-6) allows the user to prepare the sample for data collection: The user can change the sample camera zoom and adjust the sample position, change the beam size, mount and dismount additional samples with the robot, remove ice, and anneal the crystal.

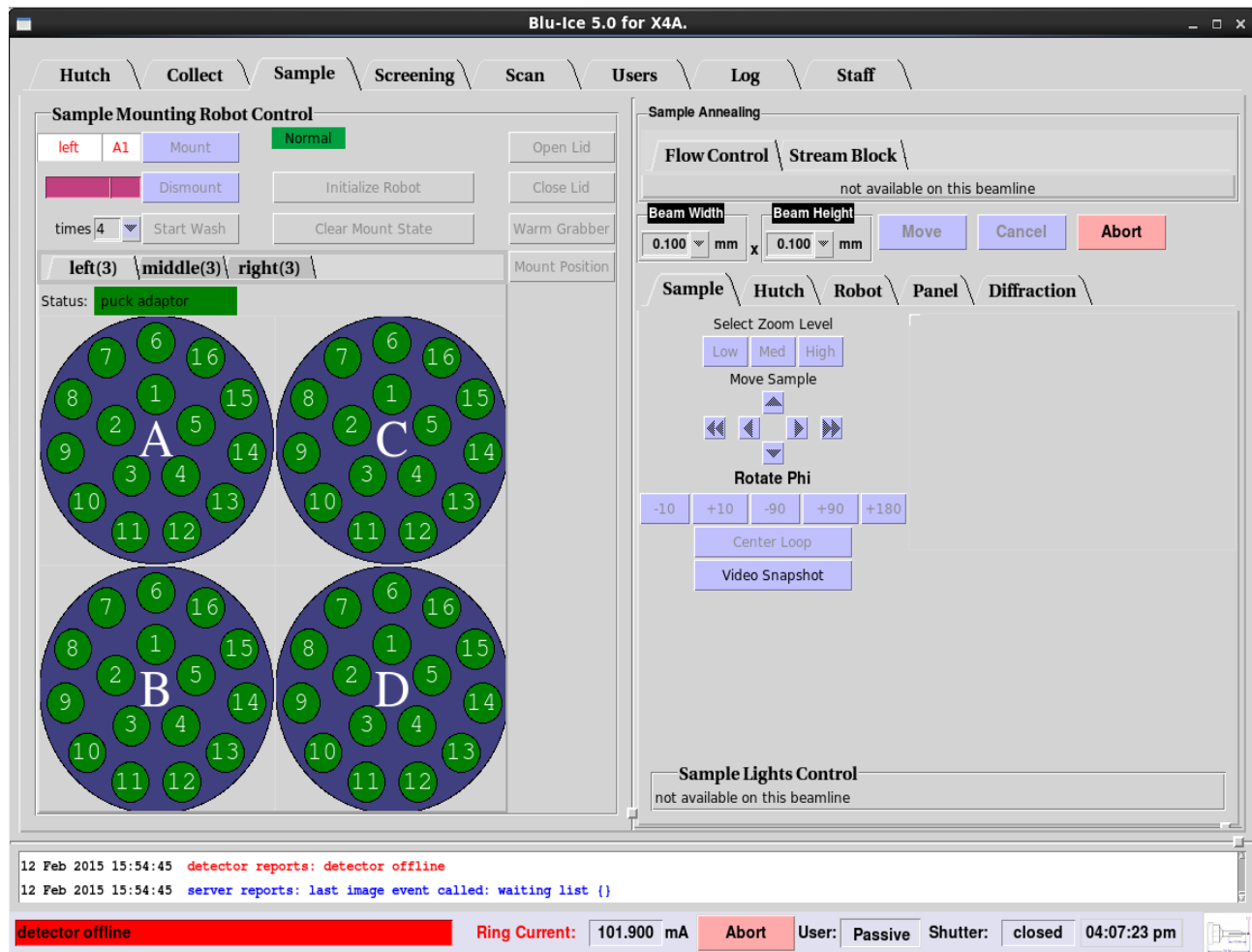


Figure 9-6. Sample Tab

9.3.4.4 Screening Tab

The **Screening Tab** (Figure 9-7) provides an interface for automatically screening samples. With this interface, the user selects multiple samples of interest from an embedded spreadsheet and defines the actions to be performed on each sample. Once started, the interface can run with minimal supervision until all of the samples have been screened identically.

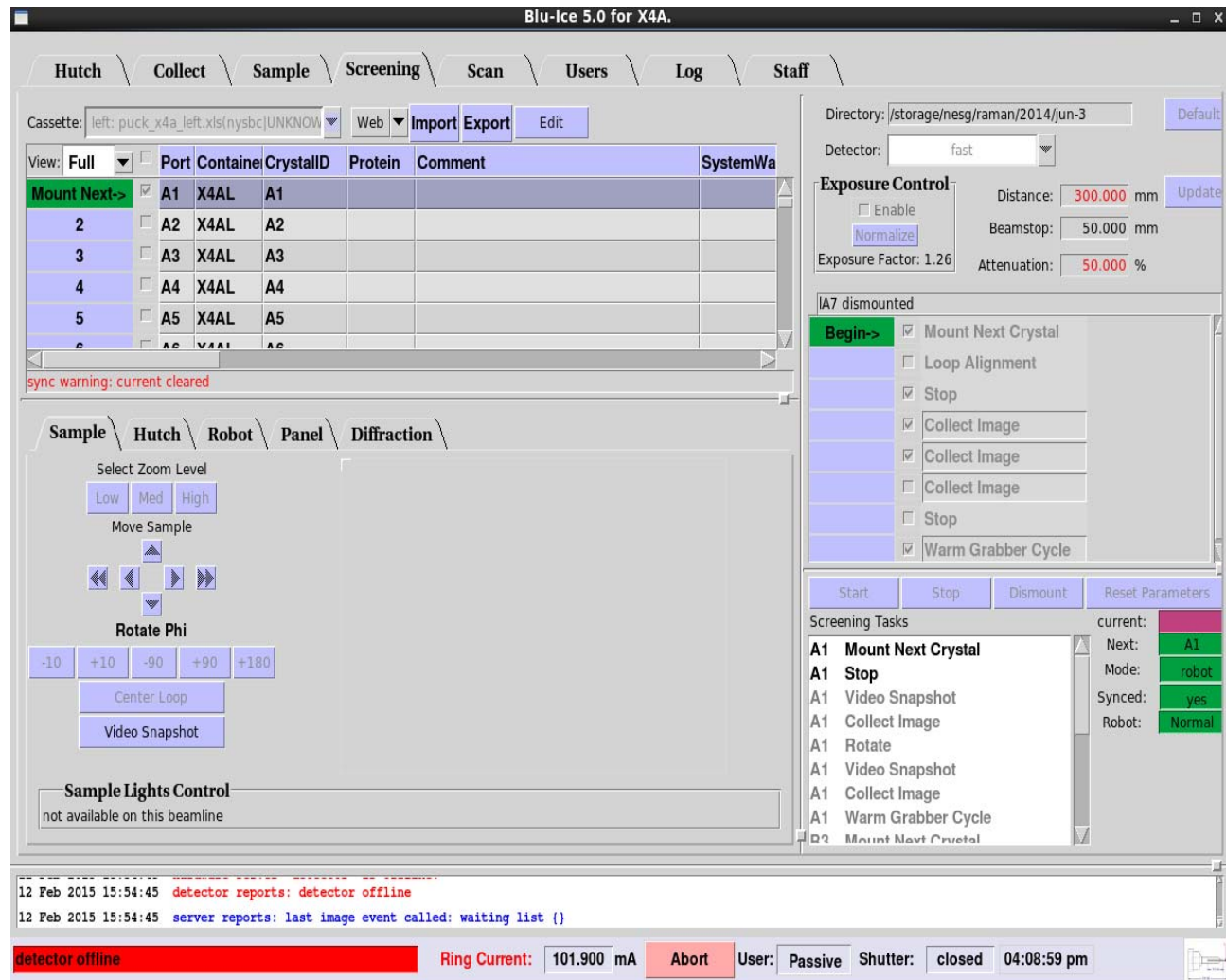


Figure 9-7. Screening Tab

9.3.4.5 Scan Tab

The **Scan Tab** (Figure 9-8) is used for energy and excitation scans. The energy (MAD) scans are used to select the appropriate wavelengths for anomalous dispersion experiments (optimized SAD and MAD). The excitation scan is useful to identify and verify the presence of anomalous scatterers in the sample.

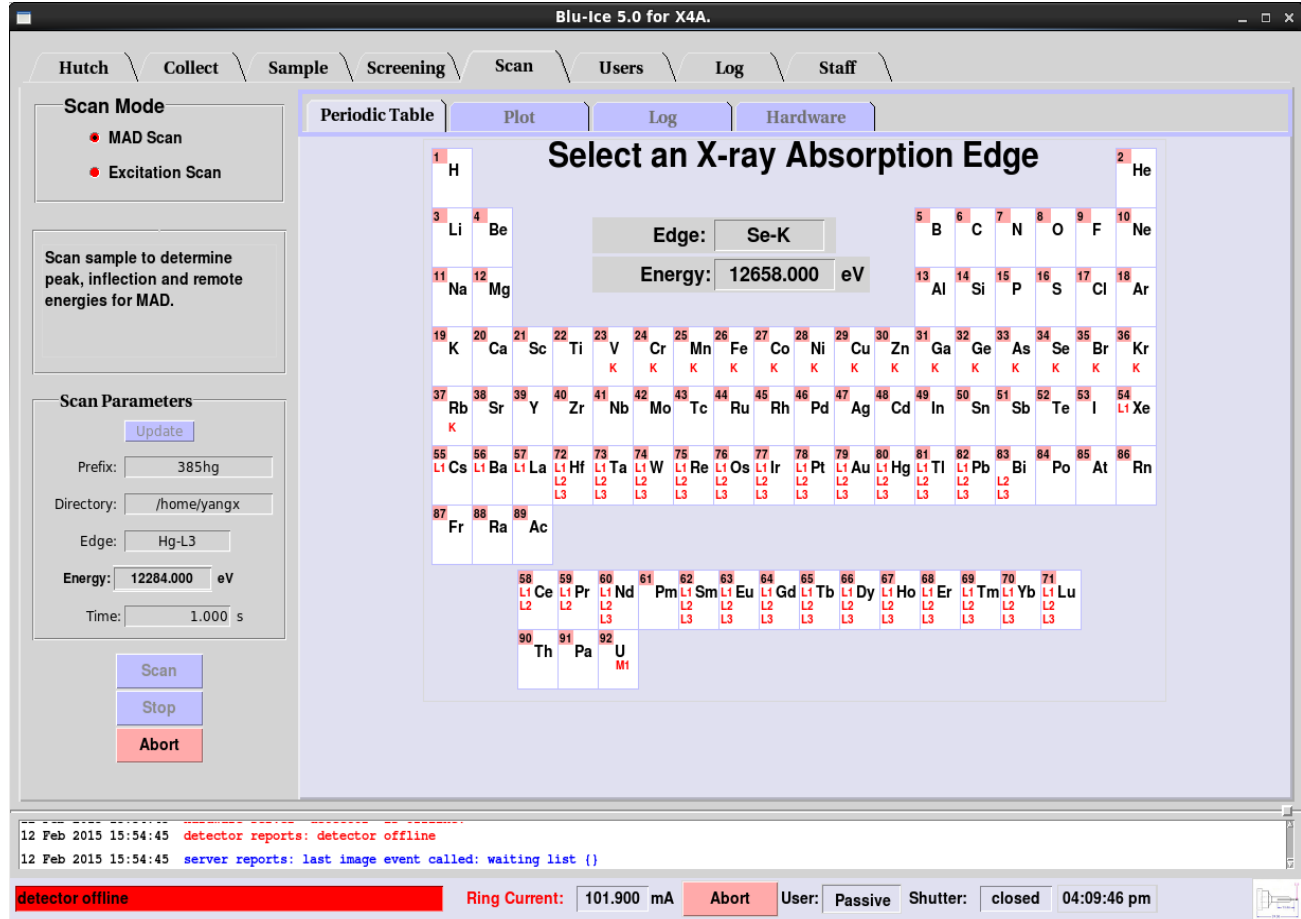


Figure 9-8. Scan Tab

9.3.4.6 Raster Tab

The **Raster Tab** (Figure 9-9) allows the user to search for and align crystals based on low level diffraction. This is carried out by defining a 3-dimensional raster, recording low level diffraction images, and then processing them with "Spotfinder" using a specialized input file tailored for weak low resolution spots and detector characteristics.

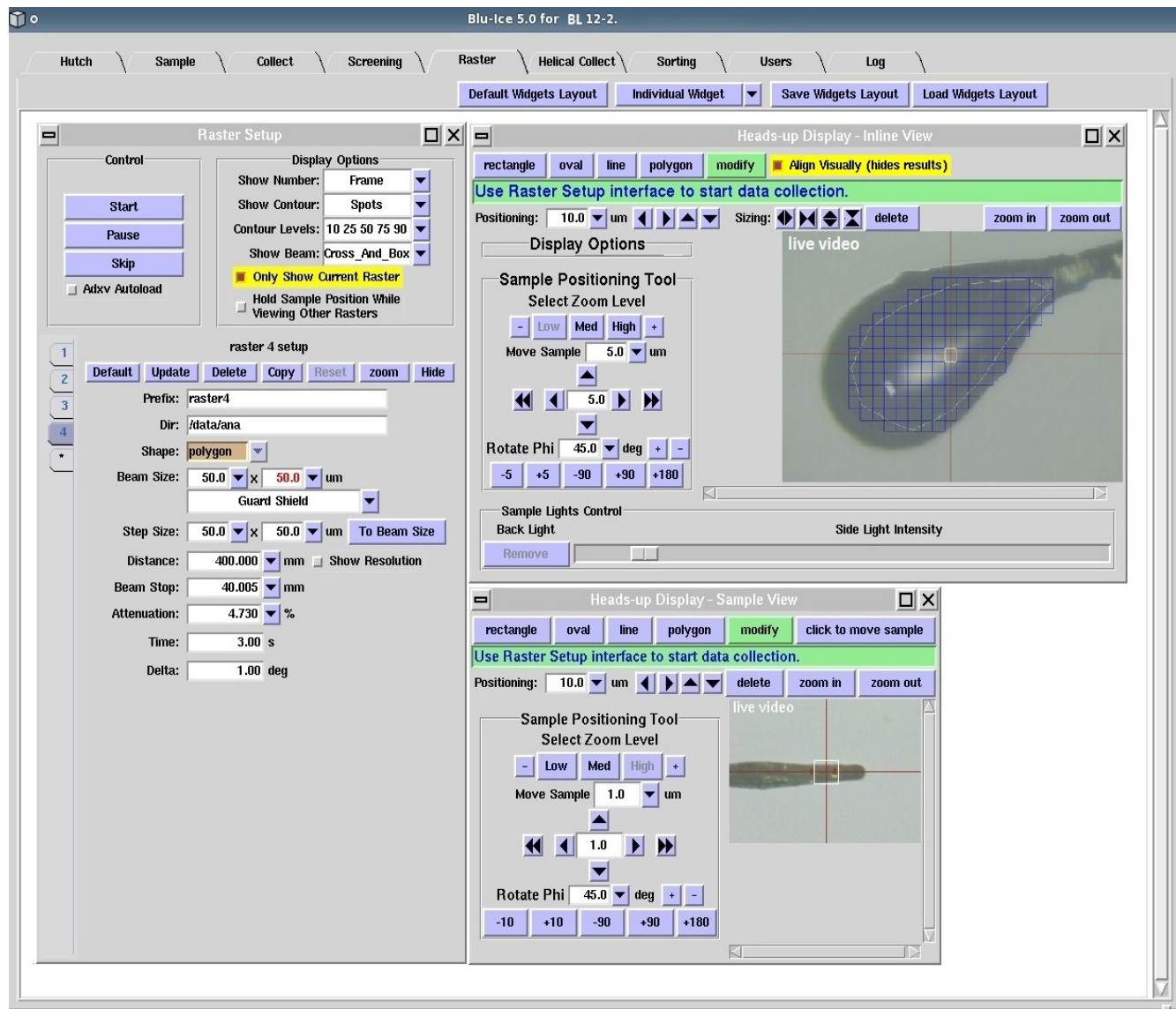


Figure 9-9. Raster Tab. This figure is courtesy of SSRL

9.3.4.7 Helical Collection Tab

The **Helical Tab** (Figure 9-10) allows collection of oscillation data while translating the crystal along the spindle axis: The software collects one oscillation image before moving the crystal to a new position and collecting a new image, with the new oscillation starting where the previous one ended.

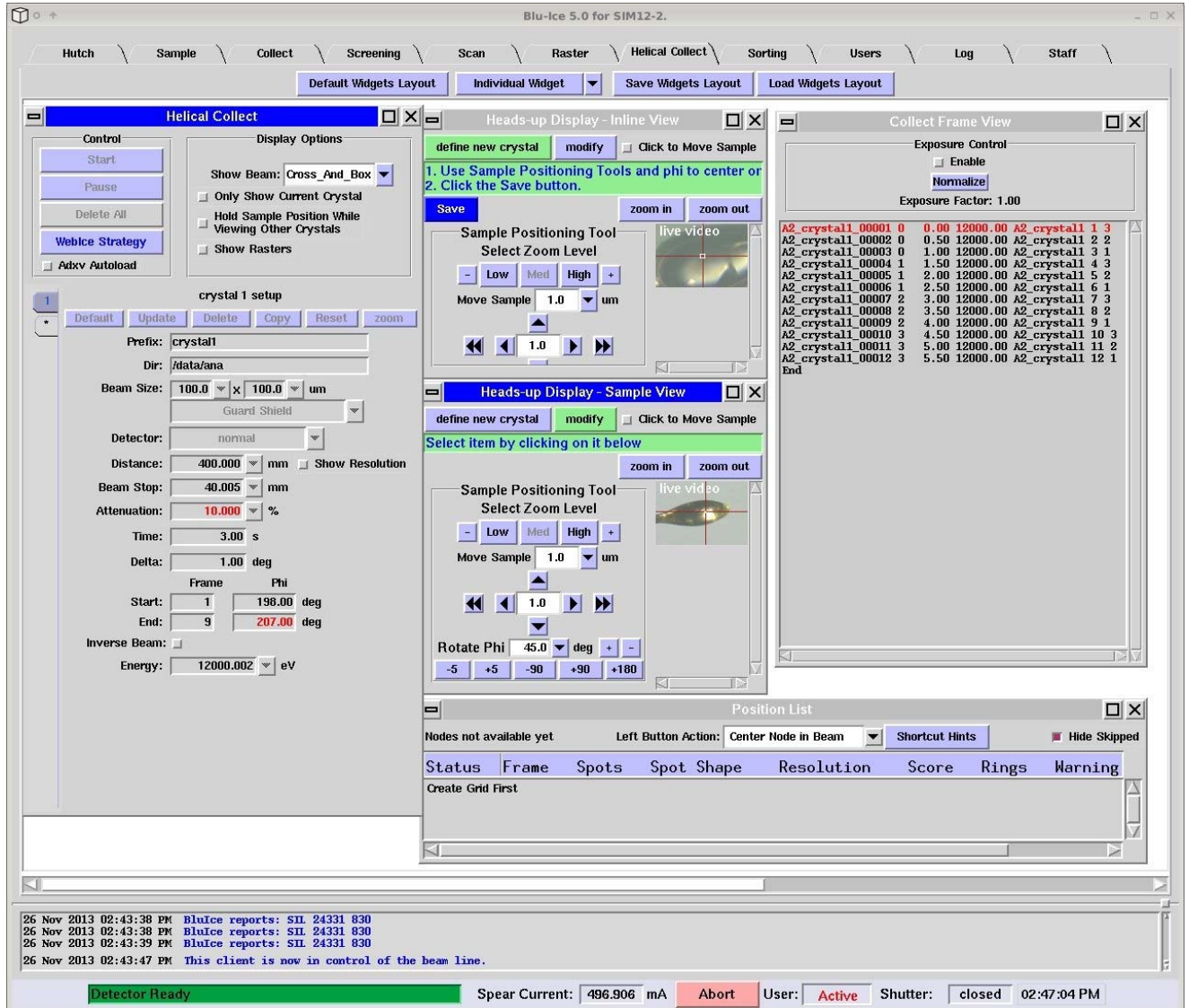


Figure 9-10. Helical Collection Tab. This figure is courtesy of SSRL

9.3.4 Summary on Blu-Ice

- Least risk (transition from X4 to NYX); Easy to manage for a small group with limited resource.
- Minimal development work required.
- Good support from SSRL.
- Takes advantages of other software associated with Blu-Ice like Web-Ice [Reference 2] and Autodrug [Reference 3].

9.4 Local Control Cabinets

There are four local control cabinets designated for the NYX beamline. There is an additional local control cabinet for the LAX line.

Each local control cabinet, as shown in Figure 9-11, contains motor controllers with drivers and ancillary components for up to 12 motions. Each cabinet will be mounted near the motors it drives, so motor and encoder cables will be kept short, as well as any other cables such as thermocouple. Each cabinet has its own internal DC power supplies, so the cabinet will need only a single AC cord for power, and an ethernet line for communications.

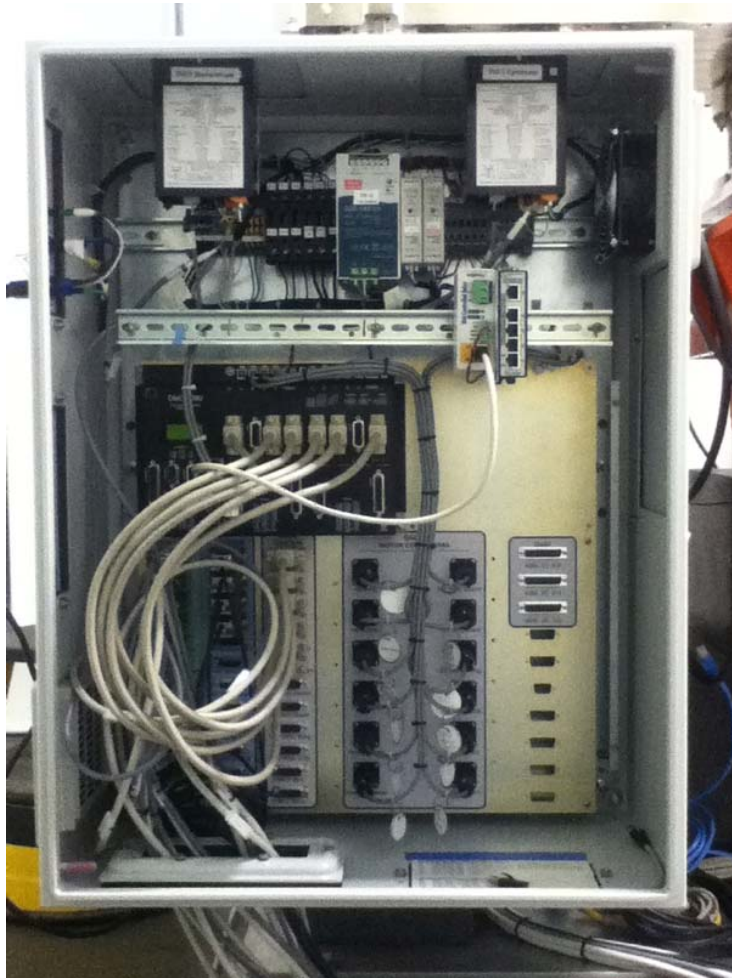


Figure 9-11. An NYX Local Control Cabinet

Locations:

For the NYX line, there are four designated cabinets: LCC2, LCC3, LCC4, and LCC5.

LCC2 will be mounted on the upstream C-hutch wall and will control beam position monitor 1, an aperture, and filters.

LCC3 will be mounted in the C-hutch on the monochromator plinth and control the monochromator motions as well as beam position monitor 2.

LCC4 will be mounted in the C-hutch on the mirror plinth, and will control the motions of the mirror as well as the 4-jaw slits and beam position monitor 3.

LCC5 will be mounted in the D-hutch on the pathway stand, and will control the four motions of the pathway.

The control cabinets are 600mm x 800mm x 300mm, and are manufactured by Hoffman. They are sealed with high-density foam gasketing on all removable panels and the door, and use Roxtec glands for cable entry. There is a fan and a passive vent.

The contents of each cabinet are arranged around a large aluminum patch panel, which serves to mount the Galil motor drivers, as well as all the connectors needed to interface the Galils with the motors. In addition, each cabinet has two DIN rails to mount DIN components.

The large aluminum panel on which the Galil drivers are mounted acts as an additional heat sink. Then, forced air cooling removes the heat from the cabinet. There is a passive vent on the lower right of the cabinet, and a five inch fan blowing air out on the upper right of the cabinet, drawing air across the Galils.

The electronic components common to every LCC are:

Galil DCM-4080 – 8-motion controller/driver

Galil DCM-4040 – 4-motion controller/driver

Meanwell SDR-240-24 - 10amp 24vdc power supply – for Galil and motor power

(2) Meanwell MDR-20-24 - 1 amp 24vdc power supplies – for Netswitch and Web-relay

Stride Netswitch SE-SW5U-WT - to distribute ethernet within the cabinet

Xytronix WebRelay X-WR-1R12-1I5-I to enable a remote shutdown function

Location-specific components:

Also, there are a few location-specific components, such as the readouts for the strain gauges on the mirror (LCC4), and the crystal heater with its power supply for the monochromator (LCC3).

Components specific to the monochromator cabinet, LCC3, are:

Jumo Ctron crystal heater and power supply

Components specific to the mirror cabinet, LCC4, are:

(2) Rockport INFS strain gauge readouts for the mirror bender

In each cabinet there is a power distribution harness for AC and DC which uses DIN terminal blocks and fuses. The cabinet has a main fuse, and each AC powered device within the cabinet has its own fuse, this includes the DC power supplies as well as the fan. In addition, each DC powered item has its own fuse, this includes each Galil drivers as well as the DIN components such as the Netswitch.

The patch panel:

In brief, the Galil groups its motor output on one connector (per motion), and its limit and encoder together on a second connector, whereas we need a different grouping: we use the motor and limit signals grouped together on one connector (per motion), and the encoder on a second connector. So, the panel's main patch function is to provide this regrouping for twelve motions.

9.5 Equipment Racks

There are eight equipment racks distributed along the NYX beamlines. The configuration adopted by NYX consist of commercially available NEMA-12 racks integrated with industry standard pannel mounted heat exchangers (Figure 9-12). This configuration is similar to what was implemented by the NSLS-II accelerator group for more than 800 racks used to enclose accelerator power supplies and instruments. The panel mounted heat exchangers are attached to the side of each group of racks avoiding over head water connections and eliminating equipment damage due to water leaks. Conforming to NEMA-12 restricts air infiltration which provides automatic fire saftey by oxygen starvation in the event of equipment failure. To manage the loss of the cooling supply water while the equipment contained in the racks are actively rejecting heat, the electrical power will be latched with power relays activaed by passive temperture alarm in each heat exchanger. The following is the distribution of rack on NYX. One is near the A-hutch and reserved for the LAX beamline. The remaining seven are dedicated to the NYX beamline. All the racks are identical and connected in groups of two and three. Each rack has both UPS power and unconditioned power.

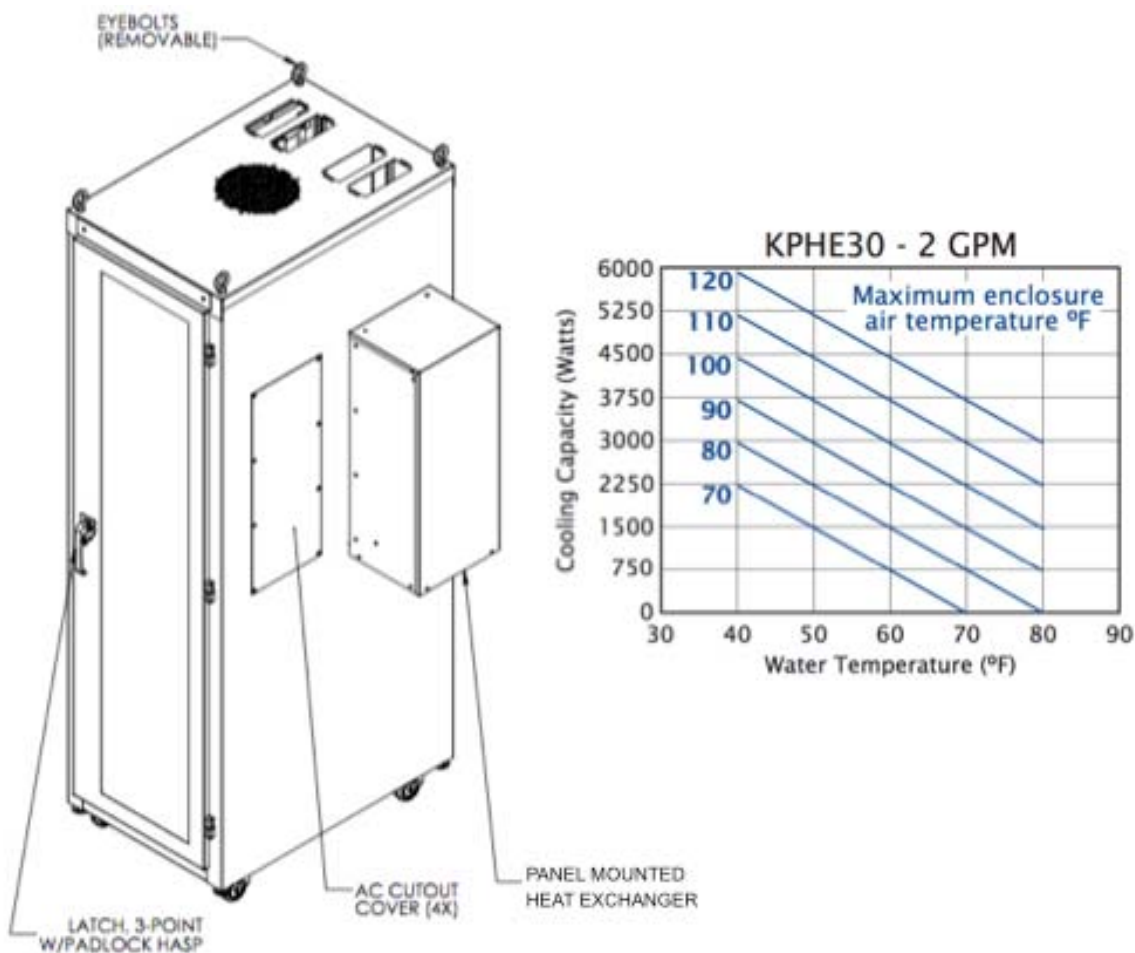


Figure 9-12. NYX Equipment Rack

NYX Rack Locations:

The racks will be distributed along the NYX beamline as shown in Figure 9-13.

There is a group of two racks on the outside end of the D-hutch that will be used for control and data collection systems and computers.

There is a group of two racks on the roof of the D-hutch that will be used for Ion pump controllers, gauging controllers, and any diamond detector equipment which cannot fit inside the D-hutch.

There is a group of three racks on top of the C-hutch that will be used for Ion pump controllers, gauging controllers, and any other support equipment for the C-hutch.

There will be space available in all racks for EPS units, so they can be placed where needed.

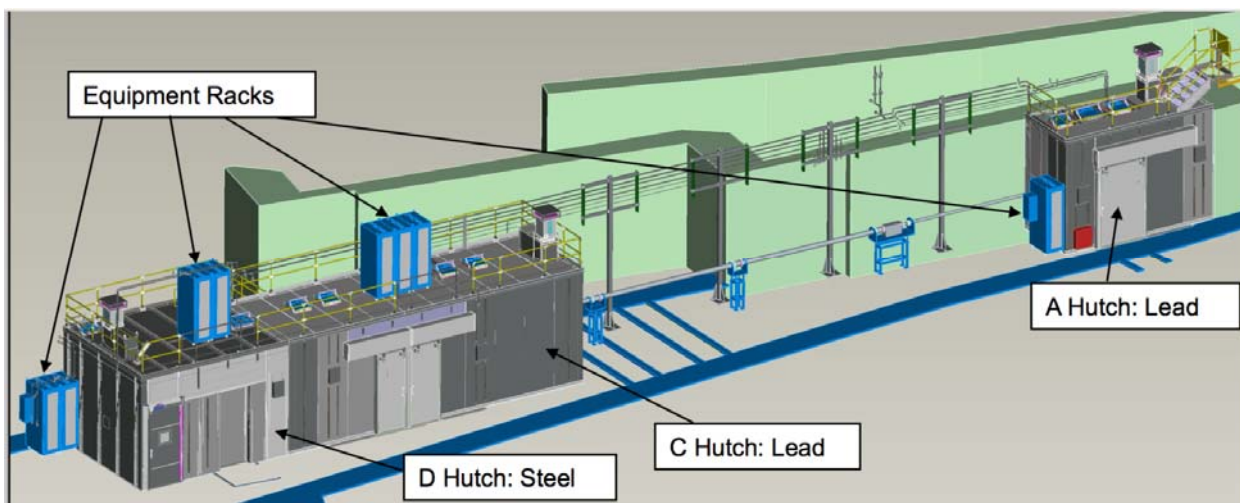


Figure 9-13. Distribution of NYX Equipment Racks

9.6 Cables and Interconnectivity

Most of the electronic control system cabling, motor, limit, and encoder, will be provided by the vendors who supply the connected equipment: Irelec for the Mirror, and Oxford for the Monochromator, Slits, Filters, and Apertures. These cables will run directly from the respective unit to the assigned local control cabinet, and will not run in cable trays.

We will be making the motor, limit, and encoder cables for the Beam Position Monitors, and for the D-hutch pathway. Cables will be constructed of PVC multi-conductor cable, with motor/limit cables being terminated at the motor side with 12 pin metal Trim-Trio connectors, and at the control cabinet/patch panel side with fifteen-pin D-sub connectors.

The local control cabinets are connected to the beamline control computer by ethernet cables. These cables will run through hutch walls and in cable trays, so will have to be LSZH.

10. Beamline Safety Systems

ACRONYMS

APPSS	Accelerator Personnel Protection System
EPS	Equipment Protection System
ESD	Emergency Shutdown
FOE	First Optics Enclosure
HMI	Human Interface
LAN	Local Access Network
PLC	Programmable Logic Controller
PPS	Personnel Protection System

CONTENTS

10.1 PERSONNEL PROTECTION SYSTEM (PPS)

- 10.1.1 BEAMLINE AREA PPS
- 10.1.2 FUNCTIONALITY
- 10.1.3 DESIGN SPECIFICATIONS
- 10.1.4 INTERFACE

X.4 EQUIPMENT PROTECTION SYSTEM

- 10.2.1 FUNCTIONALITY
- 10.2.2 DESIGN SPECIFICATION
- 10.2.3 INTERFACE

FIGURES

- X-14 Typical PPS configuration for a FOE and two experimental stations
- X-14 Preliminary PPS Requirements Development for FMX & AMX Beamlines

10.1 Personnel Protection System (PPS)

10.1.1 Beamlne Area PPS

NSLS-II will produce intense light from IR, UV, and hard x-rays. Beamlines are designed to use either the bending magnet radiation or the radiation from insertion devices located in the straight sections of the storage ring. Beamlines may have more than one station along the beamline. These stations are expected to work in parallel or sequentially. The PPS is an engineered system that provides a means to ensure that personnel are not exposed to the radiation in the beamline. At NSLS-II, the role of the PPS is specifically to protect personnel from radiation that is present only when there are stored electrons in the storage ring. The PPS is expected to monitor the various devices installed in the beamline for personnel safety and to provide emergency shutdown in case of any breach of the interlock. The PPS system, along with the required shielding in the beamlines, is expected to provide complete personnel safety during routine operation of the facility and provide protection during abnormal conditions. The following figure shows a typical system configuration, in this case for an FOE and two experimental stations, although this is designed to be easily configured to the required number of stations and beamline operating modes.

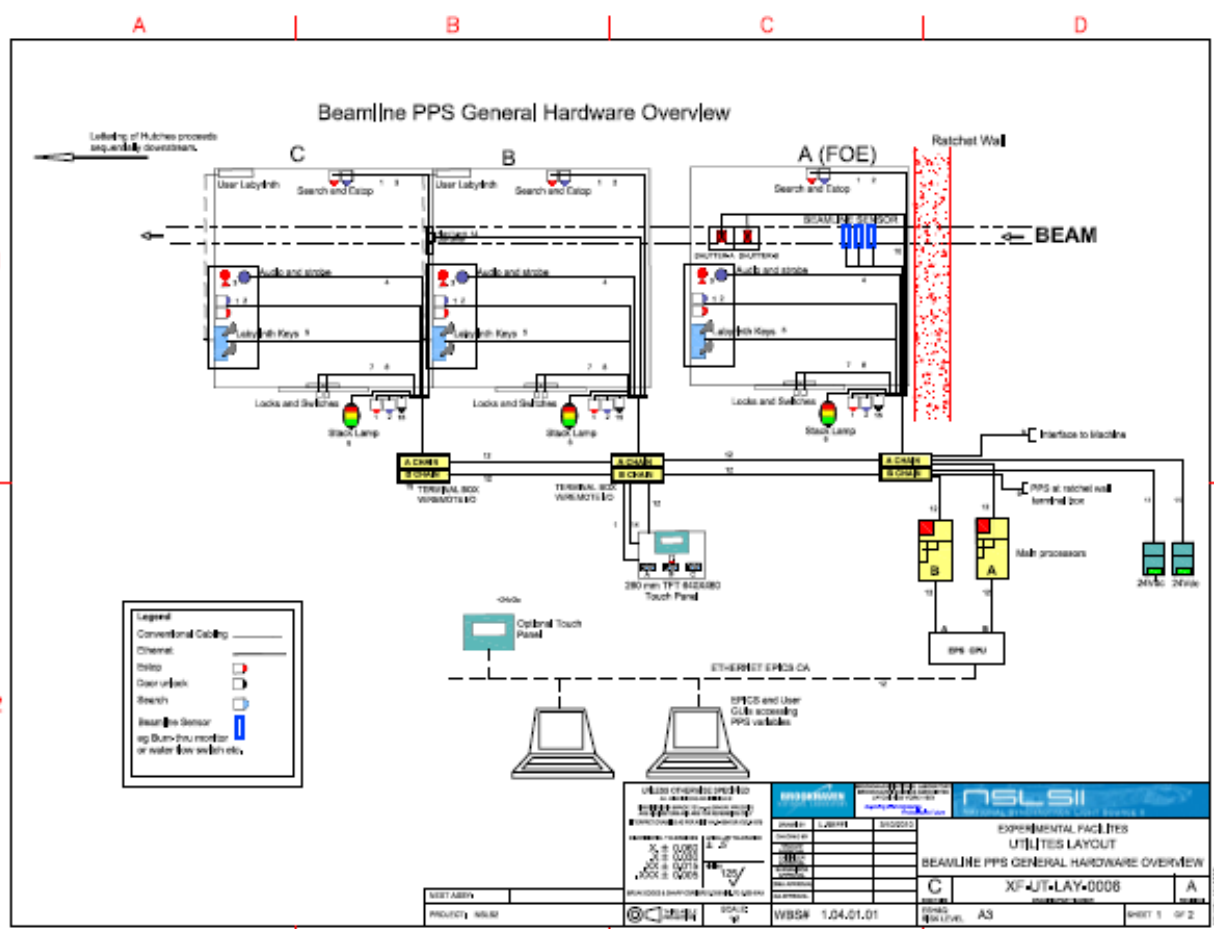


Figure 10-1. Typical system configuration for an FOE and two experimental stations.

10.1.2 Functionality

Beamlines will consist of stations where synchrotron radiation is expected to be admitted. The beamline stations are expected to be made of lead-lined walls and roof, as appropriate for the particular radiation characteristics. These stations will house beamline optical components or beamline experimental equipment. The stations are expected to be large enough for personnel to work with the equipment inside. The beamlines will have one or

more shutters based on the particular layout, which is expected to vary from beamline to beamline. However, the functionality of the shutters, from the PPS perspective, is expected to be the same and they will be monitored by the PPS. All x-ray beamlines will have shutters in the front-end area inside the storage ring shield wall. The bremsstrahlung radiation emitted by the synchrotron can only be stopped by heavy metal elements such as tungsten or lead. The heavy metal device that stops the bremsstrahlung radiation is referred to as the safety shutter. This is a dual shutter for redundancy. The synchrotron radiation beam, consisting of very high total power and power density, will be stopped by a device that is water cooled, made of copper or alloys of copper, and referred to as the photon shutter. These three devices, the two safety shutters and the photon shutter, will form a shutter cluster; their states (open, closed, or undefined) are monitored by the PPS. Along the beamline are beamline optical elements that will condition the beam, including, for example, monochromators and mirrors. These devices change the characteristics of the synchrotron radiation. The radiation passing through the monochromator will, in most cases, be displaced in either the vertical plane or the horizontal plane from the incident radiation and only a small fraction of the incident radiation with a band pass (of about 0.01% or less) will be passed, with little or no power. In such cases the shutters, located downstream of the monochromator, are known as monochromatic shutters. They will be made of heavy metal and will be much shorter than the safety shutters. Once again, these monochromatic shutters are fully redundant for safety and will be monitored by the PPS.

A major role for the PPS will be to provide a means of ensuring that no personnel are inside beamline stations when the station is opened to synchrotron radiation. Prior to admitting the synchrotron radiation inside these stations, a search of the area has to be performed by a person. It is expected that the station search will be performed by one person only. There will be PPS devices called “search boxes” inside the station which must be visited as part of the search. Search boxes are strategically placed to ensure that during the search all parts of the station are either visible or visited by the search personnel and no person is left behind inside the station. The search is completed when the station door is closed. The PPS will then lock the door. Once the search process is started the PPS will start a beacon and audio signal inside the station, warning all personnel to exit. This signal is expected to last for some time, on the order about 20 to 30 seconds after the station door is closed. The function of the beacon and audio signal is to warn any personnel overlooked by the search person of impending danger. There will be very distinct emergency shutdown buttons placed inside the station which, when pressed, will instantly remove the presence of the prompt synchrotron radiation hazard. In addition, there will be also emergency egress buttons inside the station to unlock and open the door.

10.1.3 Design Specifications

The PPS will be designed to be robust and provide the emergency shutdown functionality to provide personnel safety from prompt radiation. Like the EPS, the PPS is expected to be based on programmable logic controllers. PLCs have numerous advantages over the relay logic scheme of interlocks. They can be reprogrammed to reflect changes in configurations and also have numerous diagnostics. The use of PLCs in safety systems is now very common. All devices attached to the PPS are expected to be designed to be fail-safe—that is, in case of failure the device will fail in such a manner as to either remove the hazard or remove the permit to generate or maintain the hazard. Every beamline PPS will be designed under the same guidelines. The PPS will consist of two PLCs, referred to as chains A and B. The two PLCs will provide redundancy and will independently monitor all the devices. All shutters will have two switches, one for chain A and one for chain B. There will be switches to monitor the closed and open positions. Similarly, all station doors will be monitored with two switches, one each for chains A and B. At beamlines, there will be circumstances when a device such as a mask or photon beam stop is provided to absorb the power of the beam, while the radiation safety is provided by lead shielding in the form of collimators or radiation stops. In such cases, the integrity of the masks and beam stops cannot be compromised, as they, in turn, protect the lead shielding which provides the personnel safety. In these cases, the mask or beam stop will be monitored by the PPS to ensure that it is not compromised. In most cases, a burn-through monitor will be fitted and the water flow to these components will be monitored independently by chains A and B of the PPS. All PPS equipment will be clearly identified, and secured in locked cabinets. Cabling for the PPS equipment to field devices will be on separate closed conduits, which will be used exclusively for the PPS. All power to the PPS will be provided by uninterruptible power supplies, which will be backed up by generators.

10.1.4 Interface

The PPS must interface with numerous systems. The primary functionality of the PPS is to monitor and provide emergency shutdown. To provide emergency shutdown, the PPS interfaces to the Accelerator Personnel Protection System (APPS). The PPS will remove a permit to the APPS to operate the storage ring. In the event of the removal of the permit by the PPS, it is the responsibility of the APPS to remove the hazard by dropping the dipole power supply and the RF to the storage ring systems. The APPS will monitor the positions of the front-end shutters located inside the storage ring shield wall. The APPS will fan-out the status of the shutters to the PPS. There will be a provision in the APPS to remove the PPS interactions for a specific beamline. This is expected to be in the form of a Kirk Key in an interface box between the PPS and APPS for each beamline. The APPS will monitor the closed positions of the front end shutters when the PPS is not available and will remove the storage ring permit if it experiences any “not closed” activity. When the PPS is available, the APPS will ignore the status of the shutters. This scheme will allow installation, maintenance, and validation of the PPS to take place while the machine is in operation. All PPS functions will be monitored and data archived using the control system at NSLS-II. It is expected that EPICS will interface to the PPS PLCs to monitor their functionality. The EPICS interface will be read-only; there will be no writing to PLCs from the EPICS interface. Changes to the PLC operating codes will be possible from the field devices or when the PLC software is downloaded to the PLCs during routine validation of the system. All command and control functionality for the PPS will reside with the Equipment Protection System (EPS) for the beamlines and front ends. The EPS will interface to the PPS and will receive signals from the PPS prior to operation of the shutter. In the event the EPS malfunctions, the emergency shutdown (ESD) procedure of the PPS will activate and will remove the permit for the machine to operate. The PPS will only provide the ESD functionality; hence it is expected to be simple and easy to maintain and validate.

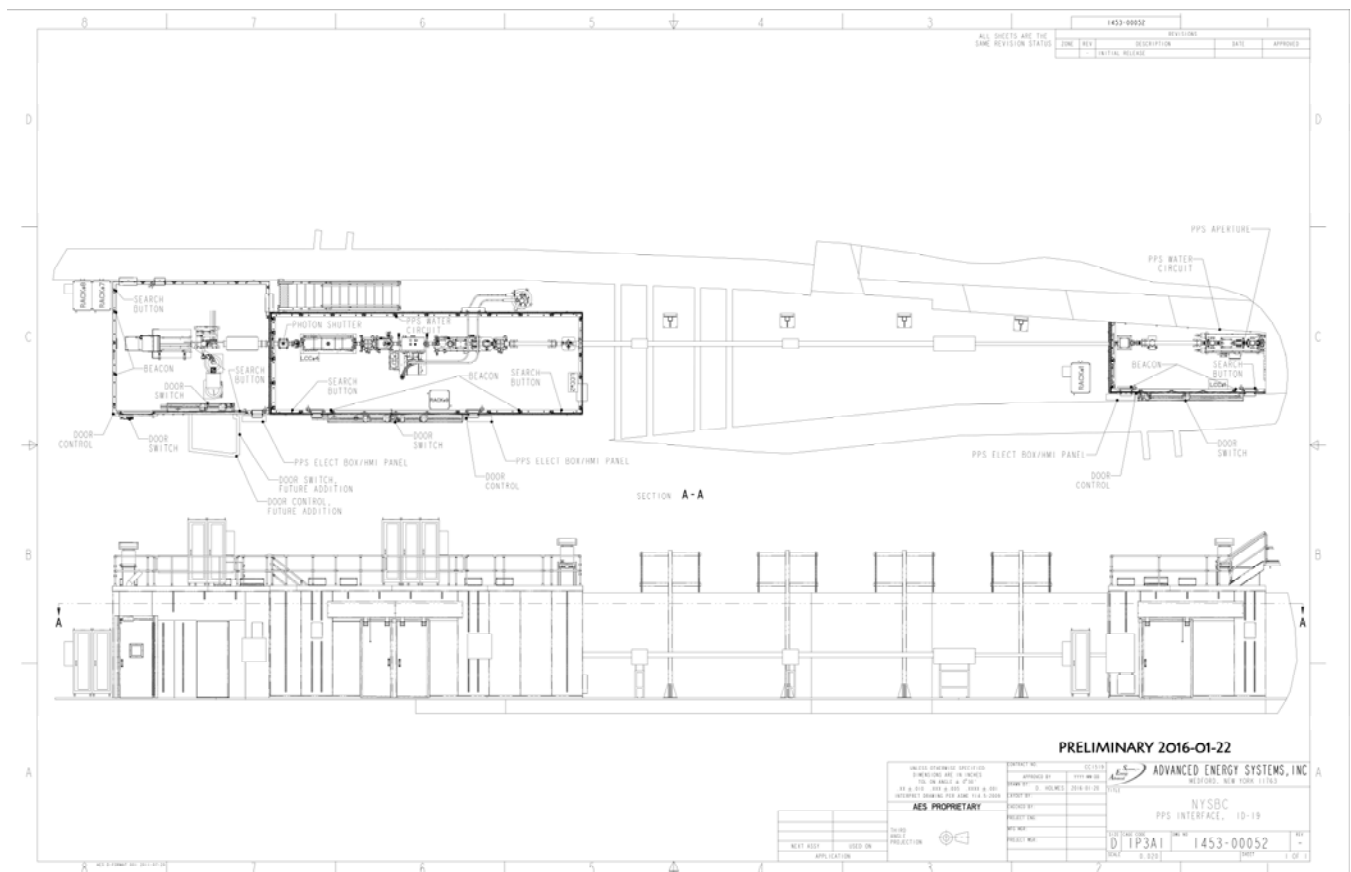


Figure 10-2. NYX PPS Interface

10.2 Equipment Protection System (EPS)

The beamlines at NSLS-II are expected to handle x-ray beams with very high power and power densities. Therefore, care must be taken to design the beamline with components that can handle these power loads. Any component that will handle these high levels of power must be monitored. The beamline Equipment Protection System provides a means of monitoring the components which, when jeopardized, can cause component failure. The EPS has the responsibility to act on alarm conditions by mitigating the situation that has caused the alarms.

10.2.1 Functionality

Every beamline EPS will monitor and interlock the devices in the front end and the beamline. All front ends at NSLS-II are expected to have two safety shutters, one photon shutter, and a few masks. In addition, the front end will also have vacuum inline valves to provide vacuum isolation. The front end is also expected to have a fast valve to provide a conductance limitation during a vacuum accident. Some beamlines will also have an x-ray exit window as part of the front end. These x-ray windows will provide a vacuum isolation but will transmit the x-ray beam. Certain beamlines, such as the soft x-ray beamlines, are expected to share the storage ring vacuum with the front end providing the interface. In such cases, the fast valve, along with the rest of the inline vacuum valves, provides the isolation needed in case of accidents. Due to the large power loads, all components in the front end that intercept the beam will have water cooling. These components are typically the fixed mask, photon shutter, and exit windows. The water flow will be monitored by flow meters and the signals will be fed to the EPS. All vacuum valves will be pneumatically operated. All vacuum valves will be operated by the EPS and have their positions monitored. Most beamlines are expected to have some beam conditioning optics upstream of their monochromator. The beam conditioning optics will see the large power of the beam and as such will be interlocked by the EPS. Beamlines are also expected to have vacuum valves, which will also be controlled by the EPS. The beamline portion of the EPS system will be customized to suit the condition of the specific beamlines.

10.2.2 Design Specification

The design of the EPS is expected to be robust. The system will be based on programmable logic controllers (PLCs), which provide excellent customization capability and also extensive diagnostics. The hardware used will be the same as used in the beamline PPS and the APPS. Each beamline will have its own EPS system, with the sole function being to provide protection from damage of equipment due to synchrotron radiation. As such, the EPS will consist of only one PLC per beamline. The EPS system will consist of three parts: front-end EPS, beamline-specific EPS, and command/control of PPS components such as shutters and station doors. The front-end portion of the EPS is expected to be similar on most beamlines, while the beamline portion of the EPS will be customized to each beamline. Similarly, for the command/control of PPS components, the front-end shutters will be identical in all beamlines; however, additional shutters on the beamline will be beamline specific. All front-end components that intercept the synchrotron beam will have water cooling of the components. The water flow of the components will be monitored by the EPS via flow meters. The EPS will be in alarm state if the flow drops below a specified set point for more than a defined short duration. Depending on the location of the component an EPS monitors, it will command the photon shutter to close and—for cases where the flow is upstream of the photon shutter—it will request the stored beam to be dumped. All vacuum valves in the front end will also be controlled by the EPS. Set points from vacuum controllers that are provided to the EPS will be used to determine when it is permissible to allow opening of the valves. The EPS will determine when it is necessary to close a valve, and will do so if it senses a vacuum alarm, based on the vacuum set-point of the system.

For specific beamlines, the EPS will be customized based on the user requirements for that beamline. Besides monitoring the water flow and controlling the vacuum valves, the EPS system may be used on beamlines to monitor other variables, such as temperature, position, and so forth. The EPS will be used to control the actuation of the shutters. It will monitor the status of the PPS for each shutter and, when a permit is available, it will accept requests to open the shutters. The EPS will be responsible for sequencing the shutters in cases that involve a combination of photon shutters and safety shutters. Any station doors that are automated (none are planned at this stage) will also be operated by the EPS.

(Insert EPS interface design drawing)

10.2.3 Interface

The EPS will have human interfaces (HMI) located at the main location of the hardware, which is expected to be directly above the front end on top of the storage ring tunnel. In addition, there will be a minimum of one HMI per beamline at the beamline stations. The EPS provides the command and control functionality for the beamline PPS. It receives the status information of the PPS and, based on that, can operate the shutters. The PPS, in addition, can request the shutter to close and the EPS will then command the shutter to close. In the event the shutter does not close within a specified time, as determined by the PPS, the PPS will initiate an emergency shutdown (ESD) situation. The EPS will have an EPICS interface to the control system. The EPICS interface will provide both the main control room and the beamlines a complete overview of the status of each beamline. The data from the EPICS interface will also be logged and archived by the central computing systems. The EPICS interface to the EPS will be both read and write. The write functionality will be controlled by the EPICS Channel Access Security. This is essential, to isolate the possibility of accidental control of the wrong beamline EPS via the control system.

11. Utilities

The utility systems for NSLS-II beamlines comprise the following services in a standardized (but tailored) “utility pack”:

- Mains electrical distribution: 30 kVA total, with separate UPS circuits where needed.
- Chilled water for electrical racks and user equipment
- De-ionized (DI) water for beamline optical components
- Compressed air, experimental gases, gaseous nitrogen, and liquid nitrogen
- PPS wiring and conduits

11.1 Mechanical Utilities

The design approach includes the supply of air and water in modules (stainless steel for water, copper for air) utilizing purchased standard manifolds, these modules may be added or subtracted as needed by a specific beamline. Flow measuring or flow alarms will be used on the water return circuits where required.

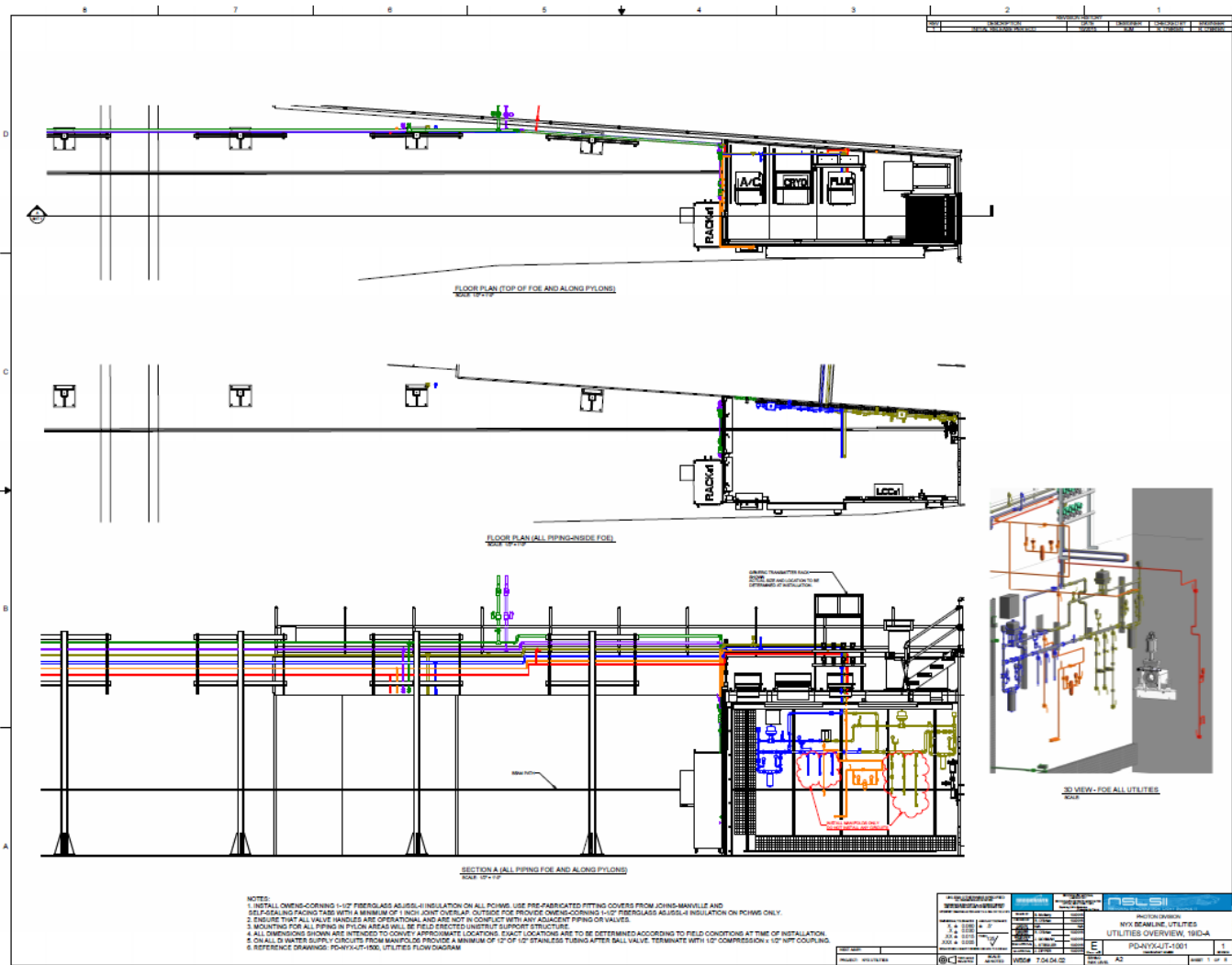


Figure 11-1. Mechanical Utilities Requirements installation for NYX FOE (19-ID-A)

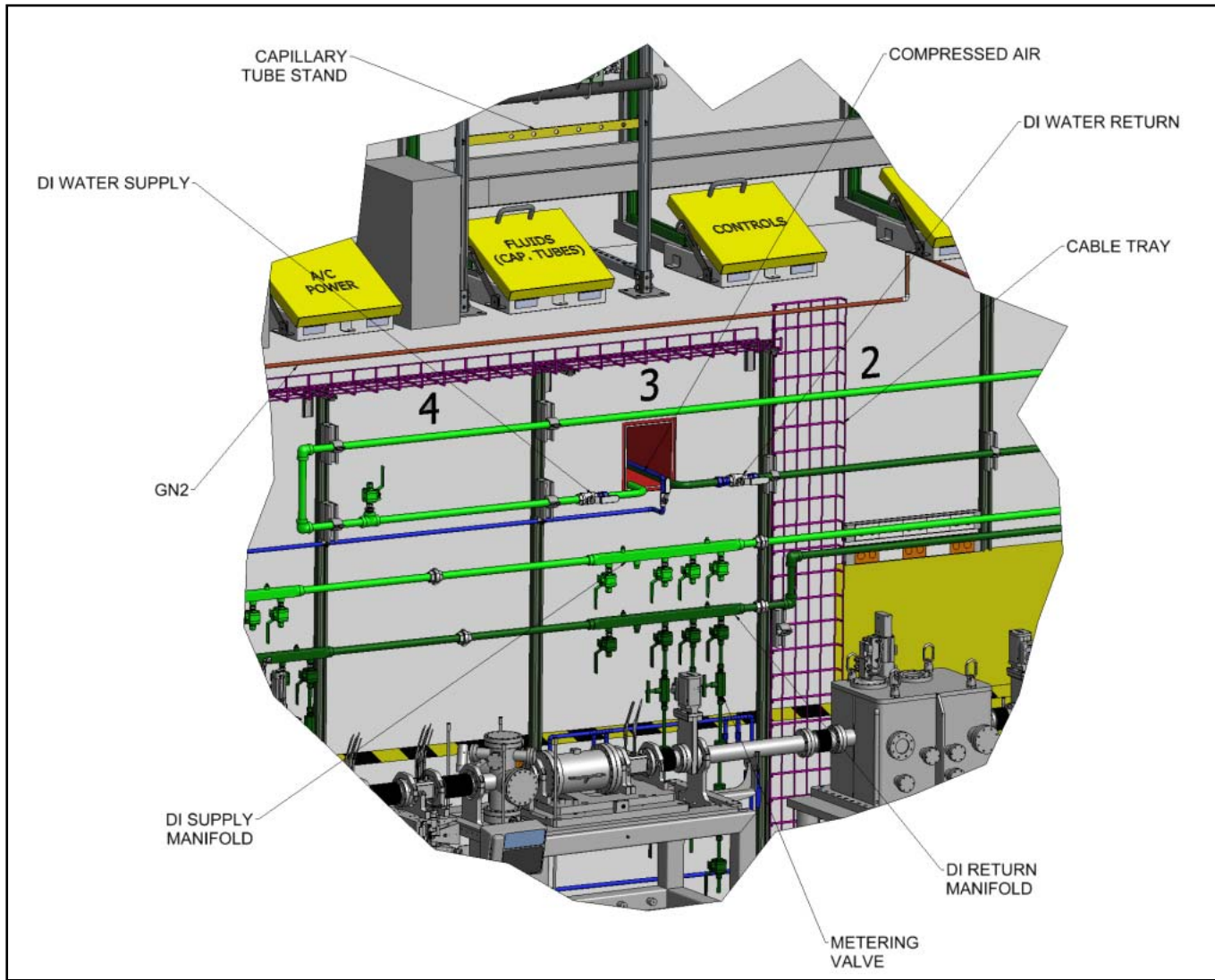


Figure 11-2. Utility layout showing the DI water and compressed air passing through the ratchet wall into the FOE, and the pipework distribution, along with labyrinth designations.

11.2 Electrical Utilities

The AC power sockets and the water connections will be located in alternating 1 m “bays” for improved electrical safety. The two supply transformers provide power for sensitive and non-sensitive applications. Outlets inside the enclosure are supported within a Wiremold product designed for such applications.

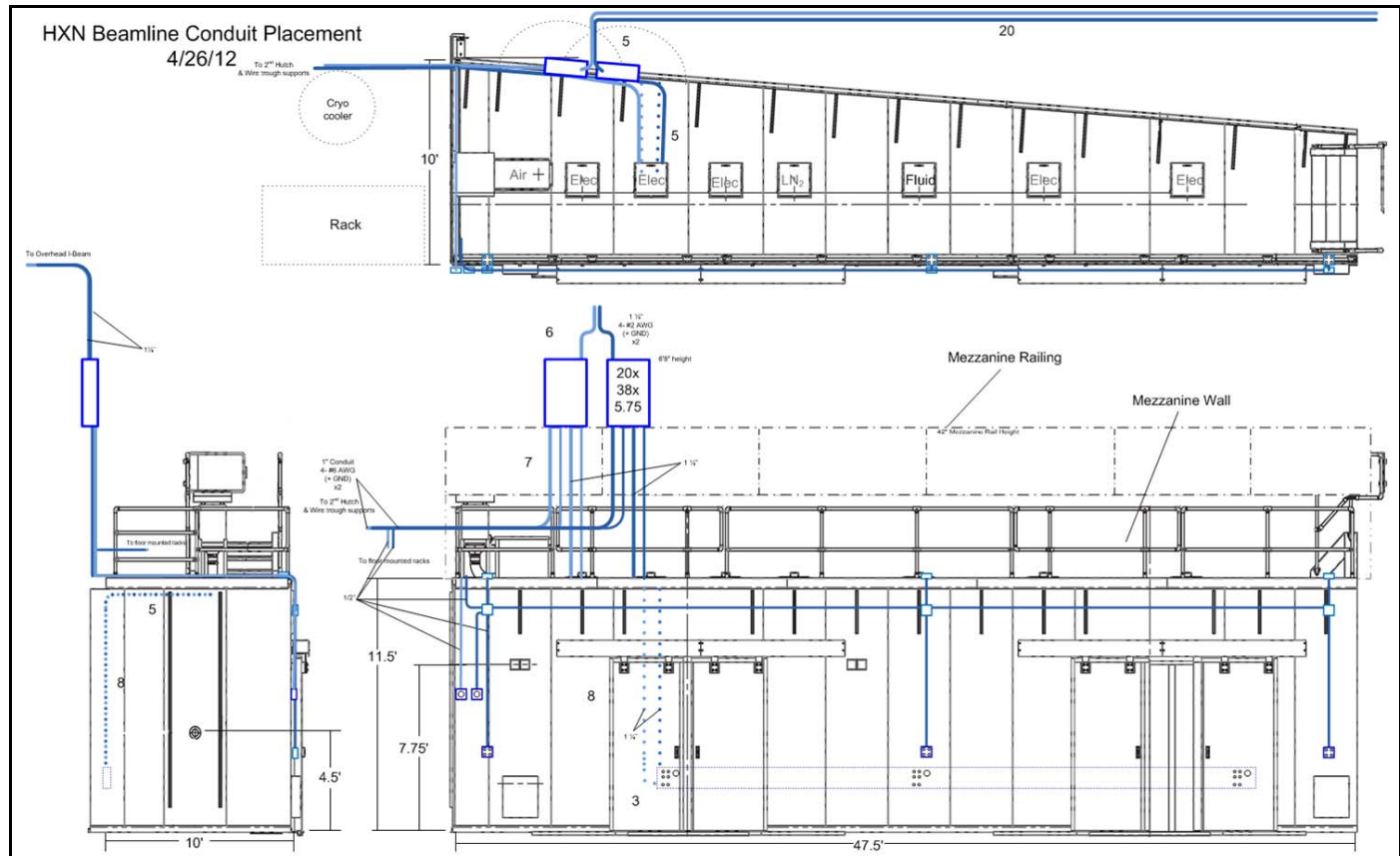


Figure 11-3. A typical provisional layout for the electrical mains distribution.

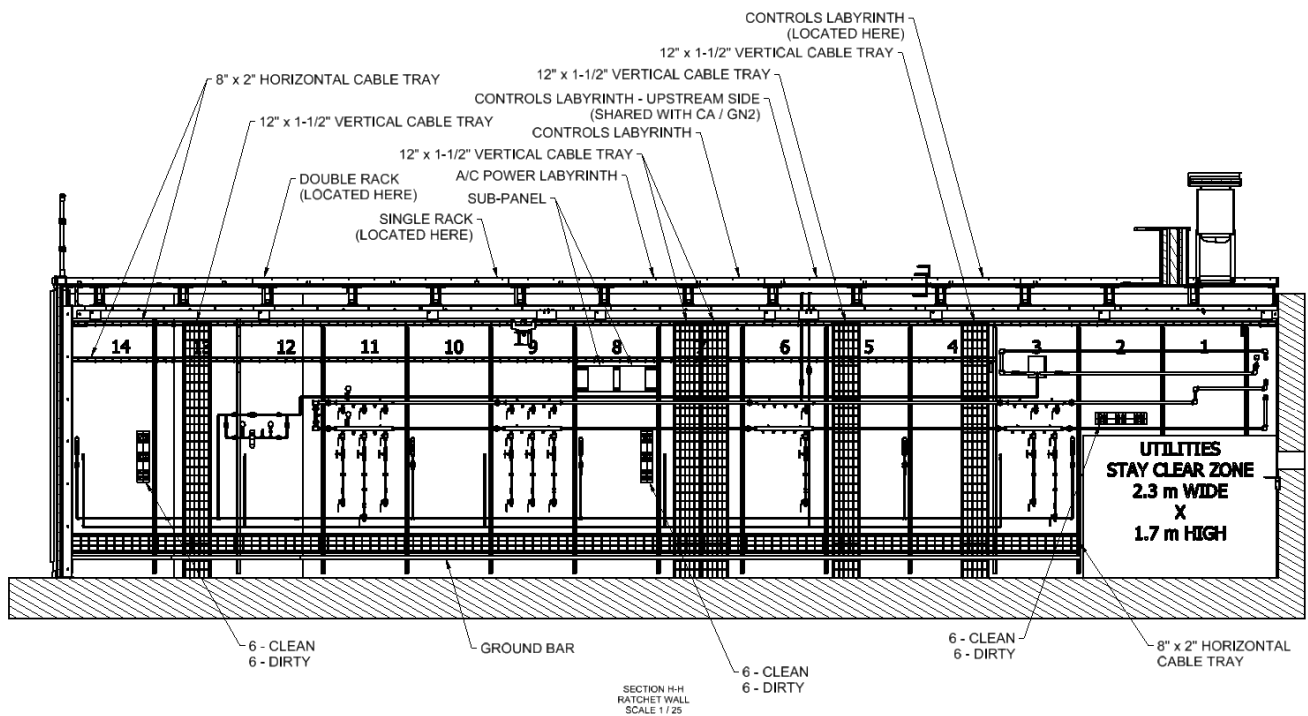


Figure 11-4. A typical preliminary layout for the electrical distribution within an FOE

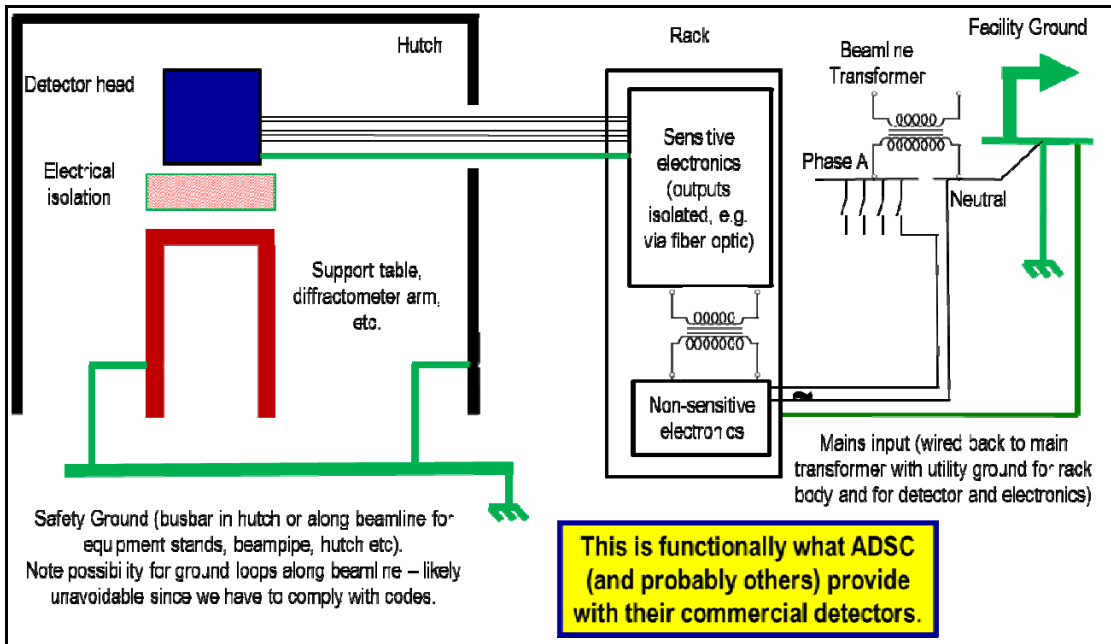


Figure 11-5. Schematic for the mains grounding, commensurate with both low-noise detectors AND a high level of electrical safety.